Hydroblasting & Coating of Steel Structures

Andreas Momber

ELSEVIER

Hydroblasting and Coating of Steel Structures

Hydroblasting and Coating of Steel Structures

Andreas W. Momber
Privatdozent, Department of Mining,
Metallurgy and Earth Sciences,
RWTH Aachen Germany

ELSEVIER

UK Elsevier Ltd, The Boulevard, Langford Lane, Kidlington, Oxford OX5 1GB, UK
USA Elsevier Inc, 360 Park Avenue South, New York, NY 10010-1710, USA
JAPAN Elsevier Japan, Tsunashima Building Annex, 3-20-12 Yushima, Bunkyo-ku, Tokyo 113, Japan

Cover illustration: Courtesy of Mühlhan Surface Protection International GmbH, Hamburg, Germany

British Library Cataloguing in Publication Data
Momber, Andreas W., 1959–
Hydroblasting and coating of steel structures
1.Water jet cutting 2.Steel, Structural – Cleaning
3.Building, Iron and steel – Cleaning
I.Title
620.1'06

ISBN 185617395X

Library of Congress Cataloging-in-Publication Data
Momber, Andreas W., 1959–
Hydroblasting and coating of steel structures / Andreas W. Momber
p. cm.
Includes bibliographical references and index.
ISBN 1-85617-395-X (hardcover)
1. Steel, Structural – Corrosion. 2. Corrosion and anti-corrosives.
I. Title.

TA467 .M545 2002
620.1'723–dc21 2002040768

Published by
Elsevier Advanced Technology,
The Boulevard, Langford Lane, Kidlington, Oxford OX5 1GB, UK
Tel: +44(0) 1865 843000
Fax: +44(0) 1865 843971

Typeset by Newgen Imaging Systems (P) Ltd, Chennai, India
Printed and bound in Great Britain by Biddles Ltd, Guildford and King's Lynn

Contents

List of Symbols and Abbreviations Used

A	model parameter
A^*	jet structure parameter
A_C	cleaned surface
$\dot{A}_C$	cleaning rate
A_N	nozzle (orifice) cross section
A_P	plunger cross section
B^*	jet structure parameter
b_C	fatigue parameter
C_E	cleaning energy flux
c_F	speed of sound water
C_L	constant
c_M	speed of sound target
C_P	paint consumption
C_X	jet spreading coefficient
D	paint degradation rate
d_D	drop diameter
d_{Dmax}	maximum drop diameter
d_{DS}	Sauter diameter (water drop)
DFT	dry film thickness
d_H	hose diameter
d_J	jet diameter
d_N	nozzle (orifice) diameter
d_P	plunger diameter
d_T	threshold nozzle diameter
e_A	cleaning effectiveness
E_A	kinetic energy hydro-abrasive jet
E_C	cleaning efficiency
E_J	kinetic energy water jet
E_M	Young's modulus
E_P	kinetic energy abrasive particle
E_S	specific energy
f_d	frequency pulsating liquid jet

F_P plunger rod force
F_R reaction force
g acceleration due to gravity
h erosion depth
$\dot{h}$ erosion rate
H geodetic height
h_C coating thickness
H_M micro hardness
H_S stroke
I_J erosion intensity
$\dot{I}_J$ jet impulse flow
k internal roughness
k^* damage accumulation parameter
l_H hose length
L_R coating performance life
$\dot{m}_A$ abrasive mass flow rate
$\dot{m}_C$ coating mass loss rate
m_C mass loss coating material
m_D model parameter
m_S solid mass
$\dot{m}_W$ water mass flow rate
N_1 life cycle (fatigue) number
n_C crank-shaft speed
N_D drop number
N_P plunger number
n_S cleaning steps
Oh Ohnesorge number
p pressure
p_A atmospheric pressure
P_D power density water jet
P_H hydraulic power
p_J cavitation pressure
P_J jet power
p_O optimum pressure
p_S stagnation pressure
P_T theoretical hydraulic power
p_T threshold pressure
p_V pressure loss
$\dot{Q}_A$ actual volumetric flow rate
$\dot{Q}_L$ loss in volumetric flow rate
$\dot{Q}_N$ nominal volumetric flow rate
$\dot{Q}_W$ volumetric flow rate water
R_C erosion resistance parameter
R_D rust rate
R_S specific disposal rate
Re Reynolds number

RG rust grade
R_M mixing ratio
R_P pressure ratio
r_R substrate roughness factor
r_T radial distance nozzle–rotational centre
S_{10} paint lifetime parameter
S_C erosion strength
S_d Strouhal number
SP surface preparation parameter
S_V solid by volume (paint)
S_{VJ} water jet velocity standard deviation
t_E exposure time
t_B blasting time
t_D nozzle down time
T_I interface fracture energy
t_P impact duration
T_U turbulence
t_W working time
v_0 theoretical jet velocity
v_A abrasive particle velocity
v_C crank-shaft circumferential velocity
v_D drop velocity
v_F flow velocity
v_J jet velocity
$\bar{v}_J$ average jet velocity
v_N nozzle (orifice) flow velocity
v_P average plunger speed
v_T traverse rate
W water consumption
w_C cleaning width
We Weber number
x jet length; stand-off distance
x^* critical stand-off distance
x_C water jet core length
x_{TR} water jet transition zone length
z traverse parameter
Z_C acoustic impedance coating
Z_F acoustic impedance water
Z_S acoustic impedance substrate
Δp hose pressure loss
ΔP power loss
Ω coating thickness parameter
Ψ impedance ratio
α nozzle (orifice) flow parameter
α^* erosion response parameter
α_A abrasive mixing efficiency parameter

α_C crank-shaft angle
α_G gas content
β_L model parameter
χ_C paint loss correction factor
χ_L DFT conditioning factor
ε efficiency parameter
ϕ impact angle
γ_L model parameter
η_0 pump efficiency
η_F kinematic viscosity water
η_h hydraulic efficiency
η_M mechanical efficiency
η_T transmission efficiency
φ_D model parameter
κ_D model parameter
λ stress coefficient
λ_D model parameter
μ nozzle (orifice) efficiency parameter
ν_C Poisson's ratio coating
ν_F dynamic viscosity water
θ contact angle
θ_D model parameter
θ_R nozzle (orifice) angle
ρ_C coating density
ρ_L density air
ρ_M density target
ρ_W density liquid
σ_C average surface stress
σ_D impact stress (water hammer pressure)
σ_F surface tension water
σ_I endurance limit coating material
σ_U ultimate strength
ω_T rotational speed
ξ_C compressibility parameter
ξ_F hose friction number
ξ_L volume loss parameter

CHAPTER 1

Introduction

1.1 Definitions of Surfaces and Preparation Methods

Surface preparation processes affect performance and lifetime of coating systems significantly. Surface preparation is defined in ISO 12944-4 as 'any method of preparing a surface for coating.' Surface preparation is an important part of any steel corrosion protection strategy. This is illustrated in Fig. 1.1 which shows major factors for the selection of a corrosion protection system.

A surface that is prepared for painting or coating is usually denoted 'substrate'. A definition for substrate is: 'The surface to which the coating material is applied or is to be applied.' (ISO 12944-1). Therefore, a substrate is generally generated from an existing surface. A substrate is a prepared or treated surface. Surfaces that are prepared by different methods include the following types (ISO 12944-4):

(i) Uncoated surfaces
Uncoated surfaces consist of bare steel, which may be covered by mill scale or rust and other contaminants. They will be assessed in accordance with ISO 8501-1 (rust grades A, B, C and D).

(ii) Metal-coated surfaces
- surfaces thermally sprayed with zinc, aluminium or their alloys;
- hot-dip-galvanised surfaces;
- zinc-electroplated surfaces;
- sherardised surfaces.

(iii) Surfaces painted with prefabrication primer
Surfaces painted with prefabrication primer consist of automatically blast-cleaned steel to which a prefabrication primer has been applied automatically in a plant.

(iv) Other painted surfaces
Other painted surfaces consist of steel/metal-coated steel which has already been painted.

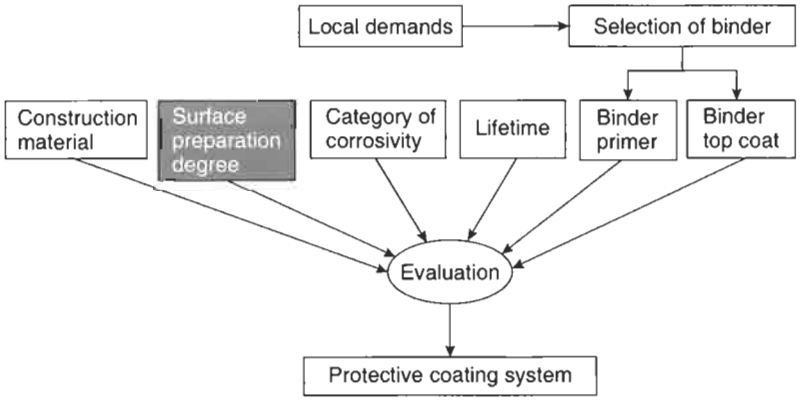

Figure 1.1 Evaluation process for a protective coating system (Pietsch and Kaiser, 2002).

Definitions and subdivisions of steel surface preparation methods are listed in ISO 12944-4 (1998). Basically, the following three principal surface preparation methods can be distinguished:

(i) water, solvent and chemical cleaning;
(ii) mechanical cleaning including blast-cleaning;
(iii) flame cleaning.

Typical cleaning operations performed with these methods are listed in Table 1.1.

Table 1.1 Procedures for removal extraneous layers and foreign matter (ISO 12944-4).

Matter to be removed	Procedure	Remarks[1]
Grease and oil	Water cleaning	Fresh water with addition of detergents. Pressure <70 MPa may be used. Rinse with fresh water.
	Steam cleaning	Fresh water. If detergents are added, rinse with fresh water.
	Emulsion cleaning	Rinse with fresh water.
	Alkaline cleaning	Aluminium, zinc and certain other types of metal coatings may be susceptible to corrosion if strongly alkaline solutions are used. Rinse with fresh water.
	Organic-solvent cleaning	Many organic solvents are hazardous to health. If the cleaning is performed using rags, they will have to be replaced at frequent intervals as otherwise oily and greasy contaminants will not be removed but will be left as a smeared film after the solvent has evaporated.
Water-soluble contaminants, e.g. salt	Water cleaning	Fresh water. Pressure <70 MPa may be used.
	Steam cleaning	Rinse with fresh water.
	Alkaline cleaning	Aluminium, zinc and certain other types of metal coating may be susceptible to corrosion if strongly alkaline solutions are used. Rinse with fresh water.
Mill scale	Acid pickling	The process is normally not performed on site. Rinse with fresh water.
	Dry abrasive blast-cleaning	Shot or grit abrasives. Residuals of dust and loose deposits will have to be removed by blowing off with dry oil-free compressed air or by vacuum cleaning.
	Wet abrasive blast-cleaning	Rinse with fresh water.
	Flame cleaning	Mechanical cleaning will be required to remove residues from the combustion process, followed by removal of dust and loose deposits.
Rust	Same procedures as for mill scale, plus:	
	Power-tool cleaning	Mechanical brushing may be used in areas with loose rust. Grinding may be used for firmly adhering rust. Residuals of dust and loose deposits will have to be removed.

Table 1.1 Continued

Matter to be removed	Procedure	Remarks[1]
	Water blast-cleaning	For removal of loose rust. The surface profile of the steel is not affected.
	Spot blast-cleaning	For localised removal of rust.
Paint coatings	Stripping	Solvent-borne pastes for coatings sensitive to organic solvents. Residues to be removed by rinsing with solvents. Alkaline pastes for saponifiable coatings. Rinse thoroughly with fresh water. Stripping is restricted to small areas.
	Dry abrasive blast-cleaning	Shot or grit abrasives. Residues of dust and loose deposits will have to be removed by blowing off with dry oil-free compressed air by vacuum cleaning.
	Wet abrasive blast-cleaning	Rinse with fresh water.
	Water blast-cleaning	For removal of poorly adhering paint coatings. Ultra-high-pressure (>170 MPa) cleaning may be used for firmly adhering coatings.
	Sweep blast-cleaning	For roughening coatings or removal of the outermost coating layer.
	Spot blast-cleaning	For localised removal of coatings.
Zinc corrosion products	Sweep blast-cleaning	Sweep blast-cleaning on zinc may be performed with aluminium oxide (corundum), silicates or olivine sand.
	Alkaline cleaning	5% (m/m) ammonia solution in combination with a synthetic-fabric pad with embedded abrasives may be used for larger surfaces. At high pH, zinc is susceptible to corrosion.

[1]When rinsing and drying, structures with slots or rivets shall be treated with particular care.

Water, solvent and chemical cleaning includes the following methods:

- water cleaning;
- steam cleaning;
- emulsion cleaning;
- alkaline cleaning;
- organic-solvent cleaning;
- cleaning by means of chemical conversion;
- stripping;
- acid picking.

The methods of mechanical cleaning are given in Fig. 1.2. Blast-cleaning methods are further subdivided in Table 1.2. Hydroblasting is denoted as *water blast-cleaning* (marked in Fig. 1.2) in terms of ISO 12944-4, and is defined as follows: 'This method consists in directing a jet of pressurised clean, fresh water on to the surface to be cleaned. The water pressure depends on the contaminants to be removed, such as water-soluble matter, loose rust and poorly adhering paint coatings.'

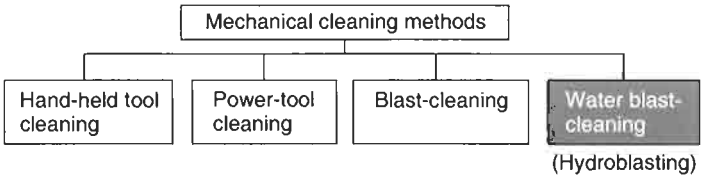

Figure 1.2 Mechanical cleaning methods according to ISO 12944-4, and classification of hydroblasting.

Table 1.2 Blast-cleaning methods according to ISO 12944-4.

Dry abrasive blast-cleaning	Centrifugal abrasive blast-cleaning. Compressed-air abrasive blast-cleaning. Vacuum or suction-head abrasive blast-cleaning.
Moisture-injection abrasive blast-cleaning	(no further subdivision).
Wet abrasive blast-cleaning	Compressed-air wet abrasive blast-cleaning. Slurry blast-cleaning. Pressurised-liquid blast-cleaning.
Particular applications of blast-cleaning	Sweep blast-cleaning. Spot blast-cleaning.

1.2 Importance of Surface Preparation Processes

ISO 8502 states the following: 'The performance of protective coatings of paint and related products applied to steel is significantly affected by the state of the steel surface immediately prior to painting. The principal factors influencing this performance are:

- the presence of rust and mill scale;
- the presence of surface contaminants, including salts, dust, oil and greases;
- the surface profile.'

The importance of surface preparation for coating performance may be illustrated based on a recently introduced coating performance model. Adamson (1998) developed a mathematical model for predicting coating lifetime, and for foreseeing coating degradation rate. This model considers the following parameters:

- total dry film thickness;
- surface preparation methods;
- environmental classification;
- rust grade;
- paint type.

A first approximation of paint degradation rate is obtained using the following equation:

$$D = \frac{5 \cdot (1.04 - \varphi_D \cdot S_{10}) \cdot (0.0075 \cdot R_D + \kappa_D) + 0.47 \cdot (1 + m_D \cdot \lambda_D)}{\mathrm{DFT}^{\beta_D} \cdot \mathrm{SP}^{m_D}} \tag{1.1}$$

The performance life of a coating system in years for a given environment for a designated rust grade of RG = 4.5, can be calculated using the following approach:

$$L_R^{4.5} = \chi_L \cdot [A \cdot \mathrm{DFT} + S_{10} - \mathrm{SP}^{n_L \cdot \alpha_L} + 1 - (\beta_L + R) \cdot \gamma_L]. \tag{1.2}$$

Both equations are rather complex in structure and certain classified information is required to solve them. Most of this information is given in the original work (Adamson, 1998). Of particular interest are the parameters SP, m_D and n_L because their values depend on surface preparation standard and quality. Degradation rate basically depends on surface preparation standard as follows:

$$D \propto 1/\mathrm{SP}^{m_D}. \tag{1.3}$$

Here, the term $(1+m_D)$ is neglected. Lifetime depends on surface preparation standard according to a simplified function:

$$L_R \propto (C_L - \mathrm{SP}^{n_L}), \tag{1.4}$$

where C_L summarises other parameters. Three levels of surface preparation based on SSPC designation are used in the calculations: SP 10 (near white), SP 6 (commercial blast) and SP 3 (power tool cleaning). Note that cleaning intensity increases as the number for 'SP' increases. Exponential indices n_L (for lifetime estimation) and m_D (degradation rate) are assigned according to these quality levels. The relationships are explained in Table 1.3. The power functions included in Eqs. (1.1)–(1.4) are graphically illustrated in Fig. 1.3. From this figure, lifetime increases and degradation rate decreases if surface preparation standard increases. These results of preliminary calculations illustrate the importance of a high-quality surface preparation for coating performance. These model calculations are verified through experimental results presented in Fig. 1.3 where a substantial improvement in corrosion protection performance of two coating systems can be seen if surface

Table 1.3 Surface preparation indices (Adamson, 1998).

Surface preparation	Designation		Indices	
	SSPC-SP/NACE	ISO	n_L	m_D
Near-white blast	SP 10/NACE 2	Sa 2.5	0	0
Commercial blast	SP 6/NACE 3	Sa 2	0.5	−0.07
Power tool	SP 3	St 3	1.35	−0.35

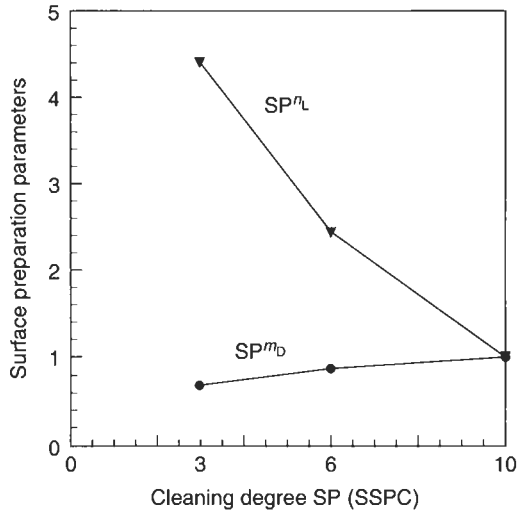

Figure 1.3 Surface preparation parameters for Eqs. (1.1)–(1.4).

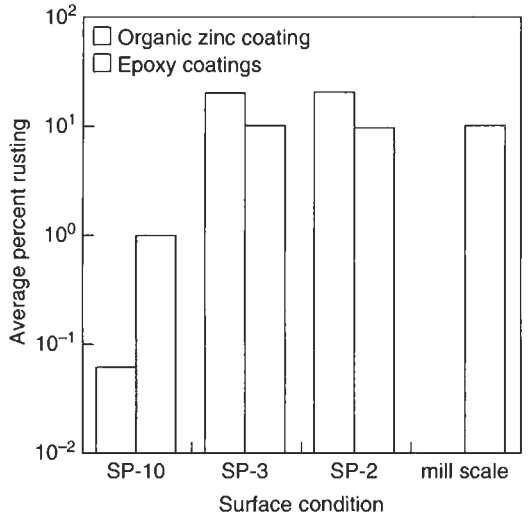

Figure 1.4 Effect of surface quality on corrosion protection (Kogler et al., *1995).*

preparation level increases. Figure 1.4, taken from an independent reference, verifies these results. The average percentage of rusting decreases notably if the quality of surface preparation improves.

Vocational training in the area of corrosion protection spends much attention to surface preparation issues. In Norway, as an example, advanced training courses for surface treatment offer the following topics (Hartland, 2000): corrosion (8%);

surface preparation (20%); application (24%); materials (20%); equipment and machinery (12%); health, safety and environment (8%); specification, control and reporting (8%). The percentage for the educational module 'surface preparation' (20%) illustrates the importance of this particular area.

1.3 Subdivision of Water Jets

1.3.1 Definitions and Pressure Ranges

The tool of any hydroblasting application is a high-speed water jet. Although the speed of the jet is its fundamental physical property, the pressure generated by the pump unit that produces the jet is the most important evaluation parameter in practice. Fundamentals of jet generation are provided in Chapter 3.

According to the Water Jet Technology Association, St Louis, water jet applications can be distinguished according to the level of the applied operational pressure (WJTA, 1994) as follows:

- *Pressure cleaning*: The use of pressurised water, with or without the addition of other liquids or solid particles, to remove unwanted matter from various surfaces, and where the pump pressure is below 340 bar.
- *High-pressure water cleaning*: The use of high-pressure water, with or without the addition of other liquids or solid particles, to remove unwanted matter from various surfaces, and where the pump pressure is between 340 and 2000 bar.
- *Ultra high-pressure water cleaning*: The use of pressurised water, with or without the addition of other liquids or solid particles, to remove unwanted matter from various surfaces, and where the pump pressure exceeds 2000 bar.

However, this designation considers all fields of application and does not distinguish between different applications, such as hydrodemolition, decontamination or hydroblasting. Therefore, a designation that meets the requirements of hydroblasting applications may be applied. Such a designation is given in the standard SSPC-SP 12/NACE No. 5 (2002) as follows:

- *Low-pressure water cleaning (LPWC)*: Water cleaning performed at pressures less than 34 MPa. This is also called 'power washing' or 'pressure washing'.
- *High-pressure water cleaning (HPWC)*: Water cleaning performed at pressures from 34 to 70 MPa.
- *High-pressure water jetting (HPWJ)*: Water jetting performed at pressures from 70 to 210 MPa.
- *Ultrahigh-pressure water jetting (UHPWJ)*: Water jetting performed at pressures above 210 MPa.

Following the above designation, this book deals with HPWJ and UHPWJ. It considers in particular applications with operating pressures in excess of 150 MPa.

1.3.2 Fluid Medium and Loading Regime

According to the liquid medium, the following modifications can be distinguished:

- plain water jets;
- additive water jets: water jets with soluble additives (Howells, 1998);
- abrasive water jets: water jets with non-soluble additives (Momber and Kovacevic, 1998).

Abrasive water jets divide further according to their generation and phase composition into injection-abrasive water jets, and suspension-abrasive water jets. An injection-abrasive water jet consists of water, air and abrasives, and is considered to be a three-phase jet. In contrast, a suspension-abrasive water jet does not contain air and, therefore, is a two-phase jet. Formation, behaviour and applications of abrasive water jets are in detail discussed by Momber and Kovacevic (1998) and Summers (1995). This book, with the exception of Paragraph 7.2, focuses on the application of plain water jets.

Regarding the loading regime, the following types two can be distinguished:

- continuous jets;
- discontinuous jets (Vijay, 1998a).

Wiedemeier (1981) defines a jet as discontinuous, if it generates a discontinuous load at the impact site. But as Momber (1993a) pointed out, every water jet internally contains discontinuous phases resulting from pressure fluctuations, jet vibrations and droplet formation. He suggests that 'discontinuous jets' are formed artificially by external mechanisms, whereas 'continuous jets' are not influenced by external mechanisms. Reviews about the formation, properties and applications of discontinuous water jets are given by Labus (1991), Momber (1993a) and Vijay (1998a). Although aspects of drop impact and jet disintegration are discussed in this book as well (see Paragraph 7.1), it generally addresses continuous water jets.

1.4 Industrial Applications

1.4.1 General Statement

Water jet technology is becoming a state-of-the-art technology not only in the area of surface engineering but is also one of the most flexible techniques available in industrial maintenance. In industry, water jet technology is frequently used in the following areas:

- building sanitation and rehabilitation;
- concrete hydrodemolition;
- decontamination and demilitarisation;
- demolition of technical structures;

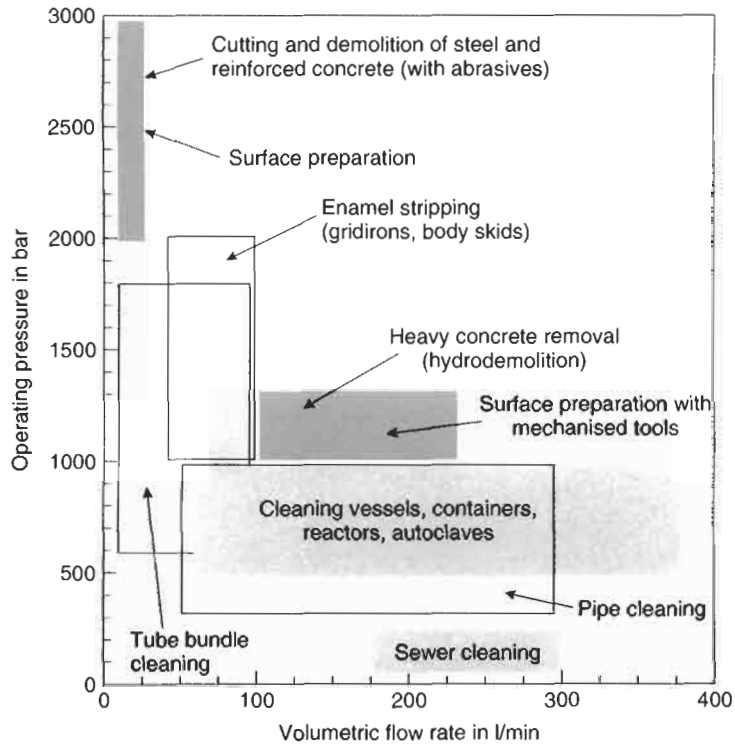

Figure 1.5 Industrial applications of high-speed water jets.

- foundation engineering;
- industrial cleaning;
- jet cutting of ceramics, fibre-reinforced plastics, food, glasses, metals and rocks;
- maintenance of technical structures and equipment;
- mechanical processing of minerals;
- medical applications;
- mining and rock cutting;
- paint and lacquer stripping;
- rock fragmentation;
- sewer channel and pipe cleaning;
- surface preparation for protective coatings (Hydroblasting).

Several of these applications as well as the corresponding major operational parameters are summarised in Fig. 1.5.

1.4.2 Industrial Cleaning

Industrial cleaning is the classical industrial application of the water jet technology. It dates back to the 1920s when it was used for cleaning of moulds and castings

(Lohse, 1929). Later, as reliable high-pressure pumps were developed in the late 1950s, the water jet revolutionised the areas of sewer and pipe cleaning. Today, commercialised water jetting covers the following cleaning applications:

- aircraft cleaning in the aviation industry: removal of paint, grease, dirt (Hofacker, 1993);
- cement kiln and autoclave vessel cleaning in the construction materials industry: removal of cement lips, incrustations, lime, solidified dust (Wood, 1996);
- gridiron and body skid cleaning in the automotive industry: removal of non-hardened, sprayed lacquer (Halbartschlager, 1985);
- pipe cleaning in the municipal and chemical industry: removal of worn protective coatings, incrustations, solidified materials, etc. (Momber, 1997; Momber and Nielsen, 1998);
- reactor, vessel and container cleaning in the chemistry and oil industry: removal of production leftovers, especially resins, latex, adhesives, oils or plastics (Geskin, 1998);
- roller drum cleaning in the printing industry: removal of ink;
- semiconductor frame cleaning in the electronic industry: removal of excess resin (Yasui *et al.*, 1993);
- municipal sewer cleaning: removal of deposits (Lenz and Wielenberg, 1998);
- ship cleaning in the maritime industry: removal of marine growth, loosen paint, dirt and rust;
- sieve and filter cleaning in the process engineering industry: removal of production leftovers, especially solidified agglomerates (Jung and Drucks, 1996);
- steel cleaning in steel mills: removal of weld slag, water scale, mill scale and rust (Raudensky *et al.*, 1999);
- tube bundle cleaning in the process engineering and oil industry: removal of incrustations and residues, especially calcium carbonate, from internal and external tube surfaces (Momber, 2000c).

Some of these applications are shown in Fig. 1.6.

1.4.3 Civil and Construction Engineering

Water jetting is state-of-the-art technology in civil engineering. A recent review given by Momber (1998a) includes an extensive database. Several aspects of civil engineering use are also mentioned by Summers (1995). The applications include the following:

- cleaning of concrete joints prior to concreting (Utsumi *et al.*, 1999);
- cleaning of concrete, stone, masonry and brick surfaces (Lee *et al.*, 1999);
- cleaning of soils (Sondermann, 1998);
- cutting and drilling of natural rocks in quarries (Ciccu and Bortolussi, 1998);
- decontamination of industrial floors;

(a) Aircraft cleaning (WOMA GmbH, Duisburg).

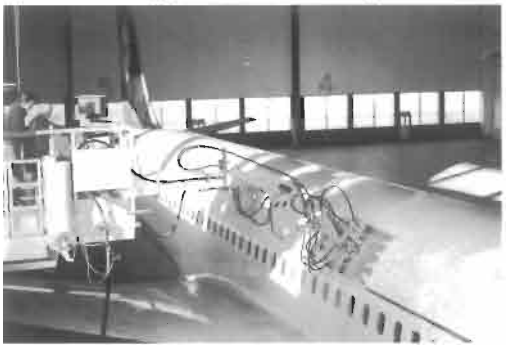

(b) Body skid cleaning (Hammelmann GmbH, Oelde).

(c) Pipe cleaning (Hammelmann GmbH, Oelde).

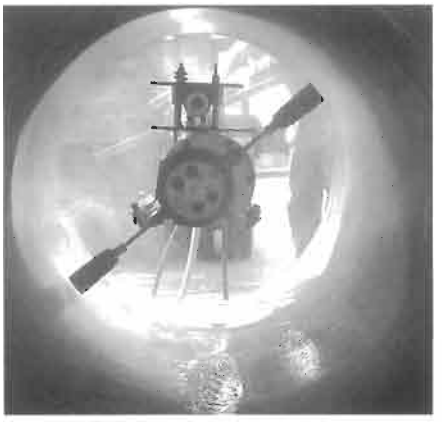

(d) Sewer cleaning (WOMA GmbH, Duisburg).

(e) Ship hull cleaning (WOMA GmbH, Duisburg).

(f) Tube bundle cleaning (Momber, 2000c).

Figure 1.6 Industrial cleaning applications of water jets.

(a) Surface cleaning (WOMA GmbH, Duisburg).

(b) Rock drilling (BGMR, RWTH Aachen, Aachen).

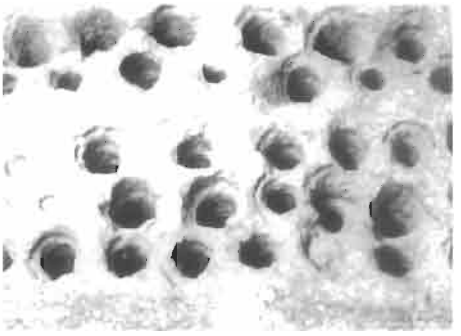

(c) Floor decontamination (Hammelmann GmbH, Oelde).

(e) Hydrodemolition (Aquajet AB, Holysbrunn).

(d) Asphalt removal (WOMA GmbH, Duisburg).

(f) Building demolition (WOMA GmbH, Duisburg).

Figure 1.7 Civil and construction engineering applications of water jets.

- jet cutting of construction materials, such as tiles, natural rocks and glass (Momber and Kovacevic, 1998);
- removal of asphalt and bitumen from road constructions (Momber, 1993b);
- removal of rubber deposits from airport runways (Choo and Teck, 1990);
- removal of traffic marks from roadways;
- selective concrete removal by hydrodemolition (Momber *et al.*, 1995; Hilmersson, 1998; Momber, 1998b, 2003a);
- soil stabilisation and improvement by Jet Grouting (Yonekura *et al.*, 1996; Gross and Wiesinger, 1998a);
- vibration-free demolition by abrasive water jets (Momber, 1998a; Momber *et al.*, 2002c);
- water jet assisted pile driving (Horigushi and Kajihara, 1988).

Some of these applications are illustrated in Fig. 1.7.

1.4.4 Environmental Engineering

The introduction of water jet technology into environmental engineering is one of the most recent developments. Water jets, due to their capability to remove materials selectively, and due to their heat-free performance, are ideally suited for separation processes. A review about typical applications is given by Momber (1995). More recent developments are summarised in Momber's (2000b) book. The technique, among others, is used to solve the following problems:

- decontamination and decommissioning of nuclear power equipment (Lelaidier and Spitz, 1978; Bond and Makai, 1996);
- decontamination of soils (Heimhardt, 1998; Sondermann, 1998);
- demolition of mercury-contaminated constructions;
- dismantling of nuclear power plants (Alba *et al.*, 1999);
- encapsulation of contaminated ground and hazardous waste sites (Carter, 1998);
- removal of explosives from shells (Fossey *et al.*, 1997);
- removal of propellants from rocket motors (Foldyna, 1998);
- removal of PCB-contaminants (Crine, 1988);
- selective carpet recycling (Weiß and Momber, 1998; Momber *et al.*, 2000; Weiß *et al.*, 2003);
- selective separation of automotive interior compounds (Weiß and Momber, 2002);
- aggregate liberation from cement-based composites (Momber, 2003c).

Some of these applications are shown in Fig. 1.8.

(a) Soil decontamination (Keller Grundbau GmbH, Fallingbostel).

(b) Removal of PCB-contaminated plaster (DSW GmbH, Duisburg).

(c) Carpet separation (Weiß *et al.*, 2003).

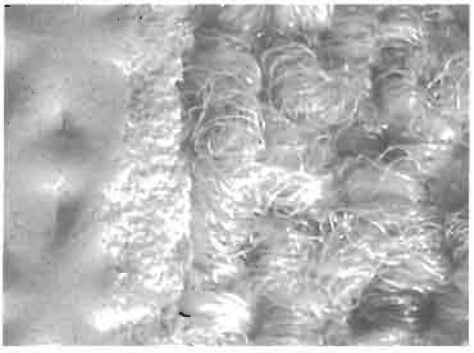

(d) Textile compound separation (Weiß and Momber, 2002).

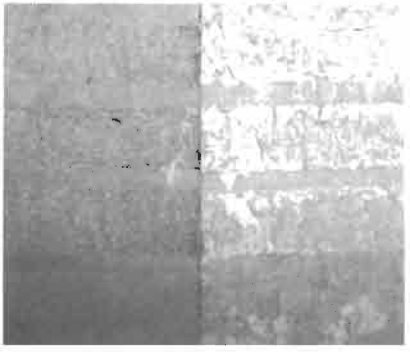

(e) Explosive removal from shells (WOMA GmbH, Duisburg).

(f) Propellant removal from rocket motors (Institute of Geonics, Ostrava).

Figure 1.8 Environmental applications of water jets.

CHAPTER 2

Fundamentals of Hydroblasting

2.1 Properties and Structure of High-Speed Water Jets

2.1.1 Velocity of High-Speed Water Jets

The properties of water are listed in Table 2.1. Numerous properties, namely density, viscosity or compressibility depend on pressure and temperature. Other properties, such as speed of sound are dependent on the conditions of the contact between water and solid.

The acceleration of a given volume of pressurised water in a nozzle generates a high-speed water jet. For that case, Bernoulli's law delivers

$$p_A + \frac{\rho_W}{2} \cdot v_0^2 + \rho_W \cdot g \cdot H_1 = p + \frac{\rho_W}{2} \cdot v_N^2 + \rho_W \cdot g \cdot H_2. \tag{2.1}$$

With $H_1 = H_2$, $p_A \ll p$ and $v_0 \gg v_N$, the approximate theoretical jet exit velocity is

$$v_0 = \left(\frac{2 \cdot p}{\rho_W}\right)^{1/2}. \tag{2.2}$$

Considering friction losses in the nozzle, the real water jet velocity is

$$v_J = \left(\frac{2 \cdot (p - p_V)}{\rho_W}\right)^{1/2} = \left(\frac{2 \cdot p \cdot (1 - p_V/p)}{\rho_W}\right)^{1/2}. \tag{2.3}$$

With $[1 - (p_V/p)]^{1/2} = \mu$, neglecting the compressibility of the water, and applying p in MPa, one obtains

$$v_J = \mu \cdot \left(\frac{2 \cdot p}{\rho_W}\right)^{1/2} \approx \mu \cdot 44.71 \cdot p^{1/2}. \tag{2.4}$$

Table 2.1 Typical water properties (temperature: 20 °C).

Property	Unit	Value
Dynamic viscosity	Pa·s	0.001
Kinematic viscosity	10^{-6} m^2/s	1.004
Density	kg/m^3	997.3
Speed of sound	m/s	1460 (15°C)
Coefficient of extension	1/K	0.00018
Specific heat	cal/g·K	1.0
Melting temperature	°C	0
Specific melting heat	kcal/kg	79.7
Vaporisation heat	kcal/kg	539.1
Surface tension	N/m	0.071
Prandtl-number	–	13.31
Heat conductivity	W/m·K	5.68
Vapour pressure	kPa	2.33
Temperature of ebullation	°C	99.63
Young's modulus	MPa	4070

Table 2.2 Values for the efficiency parameter μ.

Reference	Pump pressure (MPa)	μ-value
Neusen *et al.* (1992)	69–241	0.92
Himmelreich and Riess (1991)	100	0.92
Chen and Geskin (1991)	90–350	0.85–0.90
Neusen *et al.* (1994)	69–310	0.93–0.98

In this equation, v_0 is given in m/s. For $p_V = 0$, $\mu = 1$, the theoretical velocity will be reached. For $p_V = p$, $\mu = 0$, the entire pump pressure is absorbed, which delivers $v_0 = 0$. The certain value of the parameter μ depends on nozzle design, pump pressure and nozzle diameter. Typical values for commercial sapphire nozzles are in the range $0.9 < \mu < 0.95$ (Momber and Kovacevic, 1998). Some results obtained from direct velocity measurements are listed in Table 2.2.

The exit velocity of a water jet generated at a pressure of $p = 250$ MPa in a typical sapphire nozzle ($\mu = 0.95$) is $v_J = 671$ m/s.

2.1.2 Kinetic Energy and Power Density of High-Speed Water Jets

2.1.2.1 Kinetic energy

As the water jet exits the nozzle, its kinetic energy is

$$E_J = 1/2 \cdot \dot{m}_W \cdot v_J^2 \cdot t_E. \tag{2.5}$$

The actual water mass flow rate is

$$\dot{m}_W = \dot{Q}_W \cdot \rho_W = A_N \cdot v_J \cdot \rho_W = \alpha \cdot (\pi/4) \cdot d_N^2 \cdot v_J \cdot \rho_W. \tag{2.6}$$

In this equation, α is a nozzle orifice parameter that considers the reduction in the volumetric flow rate due to the sudden changes in the fluid conditions in a nozzle with a sharp orifice. Basically, for diamond orifices, its value is about $0.65 < \alpha < 0.75$ (Momber and Kovacevic, 1998; Momber, 2001). It depends only weakly on the pump pressure, but more on the nozzle exit diameter. For a nozzle diameter of $d_N = 0.3$ mm, a pump pressure of $p = 250$ MPa and $\alpha = 0.7$, Eq. (2.6) yields a mass flow rate of $\dot{m}_W = 0.033$ kg/s (see Table 2.3).

With Eqs. (2.4), (2.6) and an exposure time of $t_E = d_N/v_T$, the kinetic jet energy is

$$E_J = \frac{\alpha \cdot \pi \cdot \mu^3 \cdot p^{3/2} \cdot d_N^3}{2^{3/2} \cdot \rho_W^{1/2} \cdot v_T}. \tag{2.7}$$

Here, v_T is the traverse speed of the nozzle. If the nozzle is fixed at a rotating nozzle carrier (see Figs. 2.1 and 3.18), the traverse speed is:

$$v_T = \omega_T \cdot r_T. \tag{2.8}$$

Table 2.3 Kinematic parameters of a typical water jet ($p = 250$ MPa, $d_N = 0.3$ mm, $\omega_T = 2000\ min^{-1}$, $\rho_W = 1000\ kg/m^3$).

Parameter	Equation	Value
Velocity	(2.4)	671 m/s
Volumetric flow rate	(3.20)	0.033 l/s
Mass flow rate	(2.6)	0.033 kg/s
Impulse flow (reaction force)	(3.16)	22 N
Power	–	7.43 kW
Kinetic energy	(2.7)	3.33 Ws
Power density	(2.9)	10.5 MW/cm^2

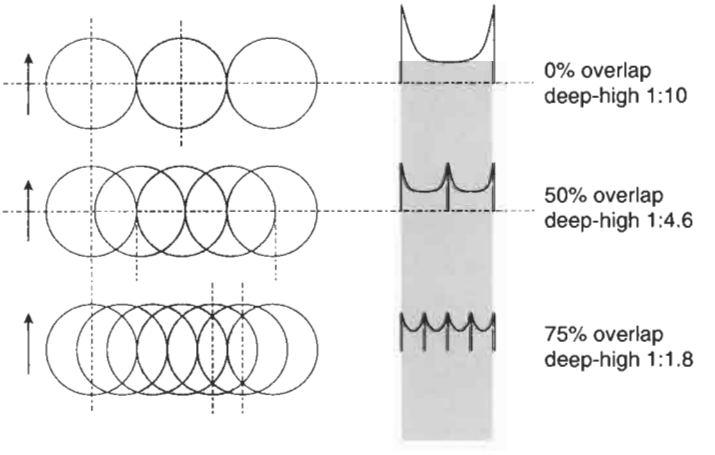

Figure 2.1 Energy distribution for a rotating nozzle carrier (Momber et al., *2000).*

Here, ω_T is the rotational speed, and r_T is the distance between nozzle and rotational centre. For the water jet mentioned with $r_T = 20$ mm and $\omega_T = 2000\ min^{-1}$, the traverse speed is 0.67 m/s, and the exposure time is $t_E = 4.5 \cdot 10^{-4}$ s. All these conditions are typical for hydroblasting tools. The kinetic energy of this water jet is then $E_J = 3.33$ Nm (Ws).

2.1.2.2 Power density

The power density, which is the power acting over a certain time increment on a certain circular cross section, is

$$P_D = \frac{4 \cdot P_J}{\pi \cdot d_J^2} = \frac{2^{1/2} \cdot \alpha \cdot \mu^3 \cdot p^{3/2} \cdot d_N^2}{d_J^2 \cdot \rho_W^{1/2}}. \tag{2.9}$$

If nozzle diameter and jet diameter are assumed to be equal, and the pressure is applied in MPa, Eq. (2.9) gives the power density in MW/mm^2 and simplifies to

$$P_D = \frac{2^{1/2} \cdot \alpha \cdot \mu^3 \cdot p^{3/2}}{\rho_W^{1/2}} = 2.68 \cdot 10^7 \cdot p^{3/2}. \tag{2.10}$$

Note that the power density at the nozzle exit is independent of the nozzle diameter. Any increase in the nozzle diameter will raise both the impacted cross section as well as the volumetric flow rate in a quadratic relationship. For the assumed conditions, the power density is $P_D = 10.5$ MW/cm^2. For comparison, a typical value for a laser used to efficiently strip paint for airplanes, is about 5 MW/cm^2 (US Air Force, 1999).

Equations (2.7) and (2.10) are valid only for the conditions immediately after the nozzle exit. For the specific conditions in a high-speed water jet, some values, such as pressure and water density, must be varied. Also, d_N must be replaced by d_J. Specific power (or energy) is not evenly distributed over the surface; its distribution depends on nozzle configuration and nozzle carrier movement. This is shown in Fig. 2.1. The energy distribution can be smoothed out if a high overlap ratio between the individual cleaning steps is realised. Models of how to estimate power distributions of rotating hydroblasting tools are provided by Blades (1994) and Küfer (1999).

2.1.3 Structure of High-Speed Water Jets

2.1.3.1 Jet core zone

The structure of high-speed water jets escaping into air is described by Thikomirov *et al.* (1992) and Momber and Kovacevic (1998). However, a few relationships may be mentioned here. The general structure of a water jet is shown in Fig. 2.2. In the axial (x-) direction, the jet typically divides into three zones: A core zone, a transition zone and a final zone. In the cone-shaped core zone, the flow properties, such as stagnation pressure and flow velocity, are constant along the jet axis. Usually, the length of this zone, x_C, is related to the nozzle diameter:

$$\frac{x_C}{d_N} = A^*. \tag{2.11}$$

The parameter A^* depends on the Reynolds-Number of the jet flow (up to Re = $450 \cdot 10^3$), on nozzle geometry and quality, and on pump pressure. An average from

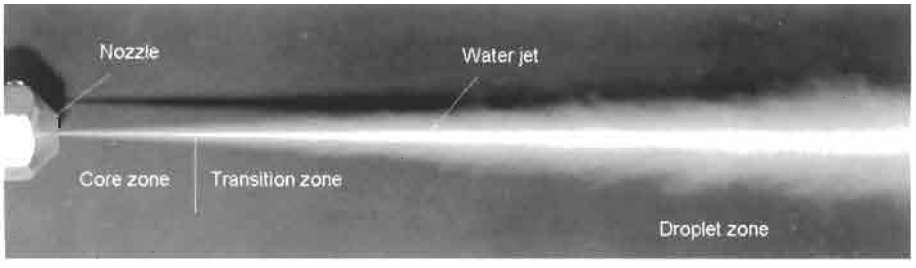

Figure 2.2 Structure of a high-speed water jet (Momber et al., *2002a). (For scaling, nozzle exit diameter: 0.8 mm.)*

values published in the literature (see Momber and Kovacevic, 1998) is $A^* = 100$. An approximation for the core-zone length as a function of the pump pressure can be established based on measurements from Neusen *et al.* (1994). Their results fit very well into a negative power relation

$$\frac{x_C}{d_N} = 1958 \cdot p^{-0.65}. \tag{2.12}$$

In this equation, p is given in MPa. For the assumed pressure of $p = 250$ MPa and the nozzle diameter of $d_N = 0.3$ mm, the length of the core zone is $x_C = 16$ mm.

2.1.3.2 Jet transition zone

In the transition zone, the flow velocity is a function of the jet radius, $v_J = f(r_J)$. This radial velocity profile has a typical bell shape that can mathematically be described by exponential functions. Several examples are published by Momber and Kovacevic (1998). Additionally, the axial flow velocity drops in that region. The length of the transition zone, x_{TR}, relates to the core zone as follows:

$$\frac{x_{TR}}{x_C} = B^*. \tag{2.13}$$

A typical value for the constant is $B^* = 5.33$ (Yanaida, 1974). Thus, for the given example, the transition zone starts at $x_{TR} = 85$ mm. Figure 2.3 shows a notable increase in jet diameter with jet length. A quantitative relationship of this very important aspect is shown in Fig. 2.3. A mathematical relationship is (Yanaida, 1974):

$$\frac{d_J}{d_N} = 0.42 \cdot x^{1/2}. \tag{2.14}$$

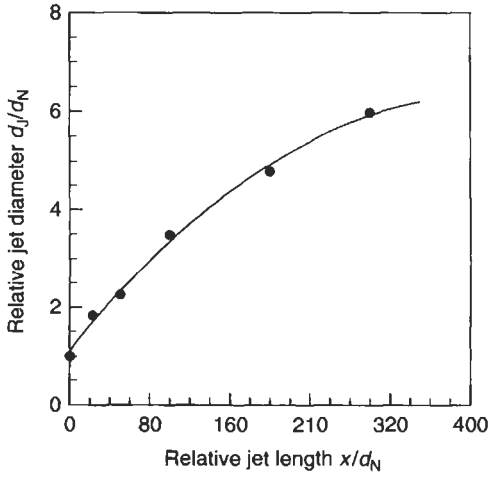

Figure 2.3 Jet diameter as a function of jet length (measurements: Yanaida and Ohashi, 1980).

2.1.3.3 Velocity distribution and turbulence

Himmelreich (1993), Himmelreich and Rieß (1991), and Neusen *et al.* (1991) performed investigations of the structure of plain high-speed water jets. Figure 2.4(a) shows some results from measurements of the velocity distribution of the water in a jet. It can be seen that the velocity has high values at the centre of the jet and decreases as it approximates the rim of the jet. Figure 2.4(b) illustrates the turbulence of a water jet, which is defined as

$$T_U = (S_{VJ}/\bar{v}_j) \cdot 100. \tag{2.15}$$

The turbulence is about 6% with higher values in radial direction. Therefore, water jets have a notable radial velocity component which causes jet disintegration, fluid slag formation and air entrainment. It is evident from Figs 2.4(a) and (b) that turbulence is also the reason for the decrease in the axial velocity of the fluid particles at the rim of the jet.

2.1.4 Water Drop Formation

In the transition zone, water drop formation occurs in the jet due to external friction, air entrainment and internal turbulence. These drops add a highly dynamic component to the jet. The average drop diameter can be approximated by the following equation known from liquid atomisation (Schmidt and Walzel, 1984):

$$d_{DS} = \frac{1 + 3.3 \cdot Oh}{We^{1/2}} \cdot \left(\frac{\rho_L}{\rho_F}\right)^{-1/4} \cdot d_N. \tag{2.16}$$

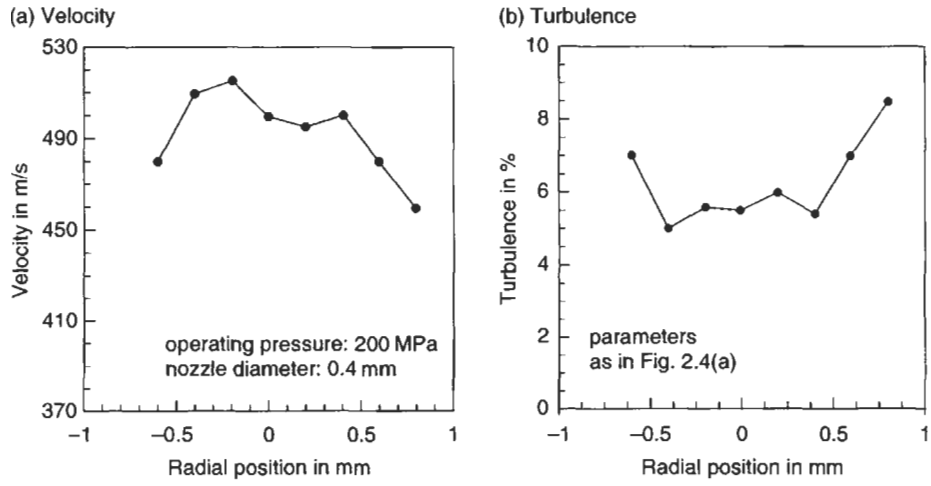

Figure 2.4 Distributions of velocity and turbulence in a water jet (Himmelreich and Rieß, 1991).

The diameter d_{DS} is the 'sauter mean diameter'; this is the diameter of a drop that has the same ratio of volume to surface area as the ratio of total volume to total surface area in a distribution of drops. In Eq. (2.16), Oh is the Ohnesorge number (in Ohnesorge's (1936) original work notated 'Z'); it balances viscous force, surface tension force and inertia force:

$$\mathrm{Oh} = f(\mathrm{Re}) = \mathrm{We}^{1/2}/\mathrm{Re}. \tag{2.17}$$

For friction-less fluids, Oh = 0. The parameter We is the Weber number:

$$\mathrm{We} = \frac{\rho_F \cdot d_N \cdot v_D^2}{\sigma_F}, \tag{2.18}$$

and Re is the Reynolds number:

$$\mathrm{Re} = \frac{v_D \cdot d_N}{\nu_F}. \tag{2.19}$$

From Eqs. (2.16)–(2.19), it follows:

$$d_D \propto v_D^{-1}. \tag{2.20}$$

The higher the drop velocity (jet velocity, respectively), the smaller the average drop diameter. The maximum (stable) drop diameter in a disintegrated fluid jet can be approximated according to a relationship derived by Troesch (1954):

$$\frac{\sigma_F}{\rho_F \cdot v_D^2 \cdot d_{Dmax}} \cdot \left(1 + 10^6 \cdot \frac{\eta_F^2}{\sigma_F \cdot \rho_F \cdot d_{Dmax}}\right)^{1/12} \cdot \left(1 - 0.5 \cdot \frac{\rho_L}{\rho_F}\right) = 4.8 \cdot 10^{-5}. \tag{2.21}$$

The maximum drop diameter can be calculated by an iterative calculation procedure: see Fig. 2.5 for some results of a typical calculation. For a rather high impact, velocity average and maximum drop diameter are equal. Interestingly, the jet velocity of 800 m/s corresponds to an operating pressure of about 300 MPa which may become a standard in the near future for hydroblasting applications.

2.2 Basic Processes of Water Drop Impact

2.2.1 Stresses Due to Impact

Two examples of coating removal due to the impact of water drops are illustrated in Fig. 2.6. It is accepted that liquid drop impact consists of three predominant stages:

(i) compressible impact stage;
(ii) jetting stage;
(iii) stagnation pressure stage.

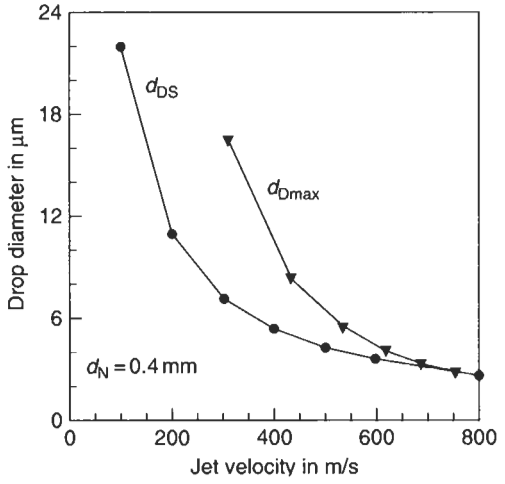

Figure 2.5 Solutions of Eqs. (2.16) and (2.21).

(a) Enamel paint on aluminium.

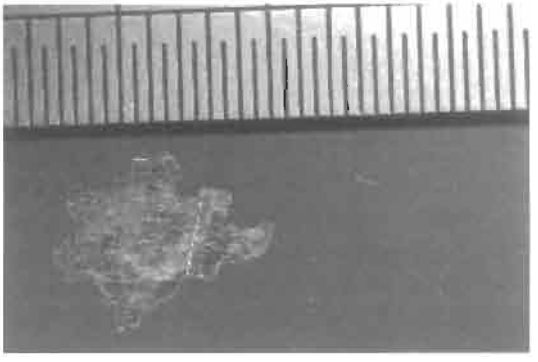

(b) Matt black paint on aluminium.

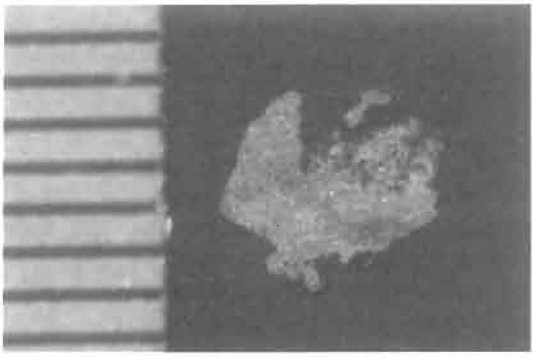

Figure 2.6 Coating removal due to drop impact (Dr C. Kennedy, Cavendish Laboratory, Cambridge). (Scales: mm, paint thickness: ca. 0.2 mm, $v_D = 380$ m/s, $d_D = 2$ mm.)

Stages (i) and (ii) are illustrated in Fig. 2.7. Recent reviews about the phenomena associated with these phases were given by De Botton (1998), Field (1999) and Lesser (1995) who also reported details of loading intensity and duration. As seen in Image 1 of Fig. 2.7, the liquid at the edge of the drop is trapped behind a compressive wave that propagates into the drop. The corresponding high stresses can be approximated by the so-called 'water hammer equation':

$$\sigma_D = \rho_F \cdot c_F \cdot v_D. \tag{2.22}$$

Here, c_F is the speed of sound in the liquid. For water with $c_F = 1500$ m/s, and $v_D = 671$ m/s from the previous example, the generated stress is $\sigma_D \cong 10^9$ N/m^2. A more rigid solution of the stress problem is given in Eq. (2.23) that considers the properties of the target material:

$$\sigma_D = \frac{\rho_F \cdot c_F \cdot v_D}{1 + (\rho_F \cdot c_F / \rho_M \cdot c_M)}. \tag{2.23}$$

The product $\rho \cdot c$ is the acoustic impedance. See Table 2.4 for corresponding values. It can be noted that materials with high acoustic impedance experience lower stresses. Using typical material properties of epoxy, Eq. (2.23) yields for $v_D = 671$ m/s,

Table 2.4 Acoustic parameters for coating components (Columns 2–4 adapted from Springer, 1976).

Material	Density in kg/m^3	Speed of sound in m/s	Acoustic impedance in kg/m$^2 \cdot$ s	Ψ_{SC} Eq. (2.43)	Ψ_{FC}	Γ_1	Γ_2	Γ_3
1	2	3	4	5	6	7	8	9
Acrylic	1220	1943	$2.37 \cdot 10^6$	0.89	−0.24	1.557	0.358	1.215
Epoxy	1770	3531	$6.25 \cdot 10^6$	0.73	−0.63	1.185	0.156	1.457
Polyester	1820	3200	$5.82 \cdot 10^6$	0.74	−0.61	1.199	0.166	1.451
Polyethylene	920	1473	$1.35 \cdot 10^6$	0.93	0.025	1.976	1.976	0.976
Polyamide	1930	3708	$7.16 \cdot 10^6$	0.69	−0.67	1.156	0.135	1.463
Polyurethane	990	274	$0.27 \cdot 10^6$	0.99	0.68	6.089	0.836	0.329
Water[1]	1000	1450	$1.45 \cdot 10^6$	–	–	–	–	–
Steel[2]	7600	5182	$39.38 \cdot 10^6$	–	–	–	–	–

[1] Projectile material.
[2] Substrate material.

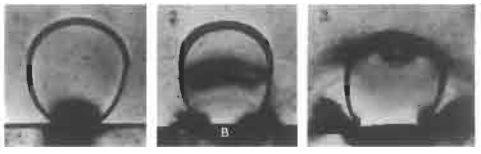

Figure 2.7 Radial jetting during water drop impact (photographs: Camus, 1971).

a peak stress of $\sigma_D = 7.76 \cdot 10^8$ N/m^2. For target materials with very high acoustic impedance, Eq. (2.23) approximates Eq. (2.22).

The duration of the compressible stage can be estimated from geometrical considerations (Erdmann-Jesnitzer and Laschimke, 1966; Lesser and Field, 1983). It is given through the following equation:

$$t_P = \frac{d_D \cdot v_D}{4 \cdot c_F^2}. \tag{2.24}$$

The duration is dependent on the impact velocity (note that this argument applies only to curved liquid slugs). For a drop diameter of 6 μm (for v_D = 671 m/s), Eq. (2.24) delivers $t_P = 4.5 \cdot 10^{-10}$s.

2.2.2 *Stress Wave Effects and Radial Jetting*

Stress wave effects become important if drops impinge on rigid, non-deformable materials: the compression of an impact is transmitted through the thickness of the coating by dilatational waves. These waves are subsequently reflected from the opposite side as tension. Figure 2.8 schematically shows this situation. These aspects are discussed by Field (1999).

Furthermore, so-called radial jetting is observed with spherically shaped water drops. The velocity of the radial flow can be more than twice the speed of the impacting drop (Bourne *et al.*, 1997), and it depends on the impact angle (Shi and Dear, 1992). This phenomenon is illustrated in Fig. 2.7 (Image 3); it generates notable shear stresses in coating systems, and it has been observed that jetting contributes to the removal of coatings due to adhesive failure (Engel, 1973). Image 2 of Fig. 2.7 shows also cavitation occurring in the contact area between drop and target (denoted 'B'). It was in fact proved that cavitation erosion is a very promising method

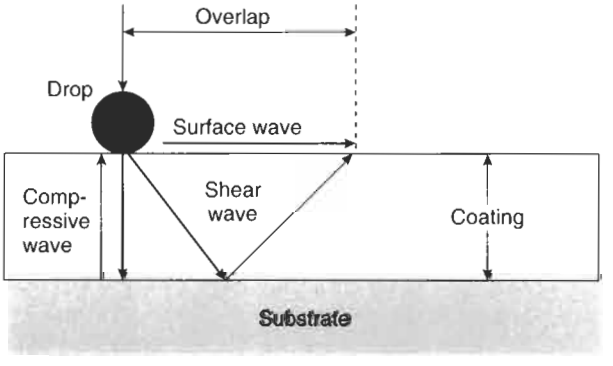

Figure 2.8 Stress wave effects during drop impact (adapted from Schikorr, 1986).

for efficient coating removal (Kaye *et al.*, 1995). The duration of the jetting stage is $t_J = 2 \cdot t_P$ (Field, 1999).

2.2.3 Multiple Drop Impact

The number of impinging water drops is critical to the material removal process. The situation can be generalised by the relationship shown in Fig. 2.9. This function can sufficiently be described by

$$m_C(N_D) = a_1 \cdot (N_D - N_D^*)^{b_1}. \tag{2.25}$$

The following three regions can be distinguished in Fig. 2.9:

- region I ($N_D < N_D^*$): for very small numbers of impinging drops, no material removal occurs; the number of drops is not sufficient to visibly damage the material. The critical drop number N_D^* can be considered to be an incubation number.
- region II ($N_D < N_D^*$, $b_1 = 1$): a linear relationship with a progress of a_1 exists between drop number and removed material. Any additional drop impact removes an equivalent mass of material.
- region III ($N_D < N_D^*$, $0 < b_1 < 1$): the progress of the function drops, and $a_1 = f(N_D)$. The erosion efficiency declines which can be explained by drop break-up due to the roughened surface; also, the impact is no longer normal to the whole of the surface.

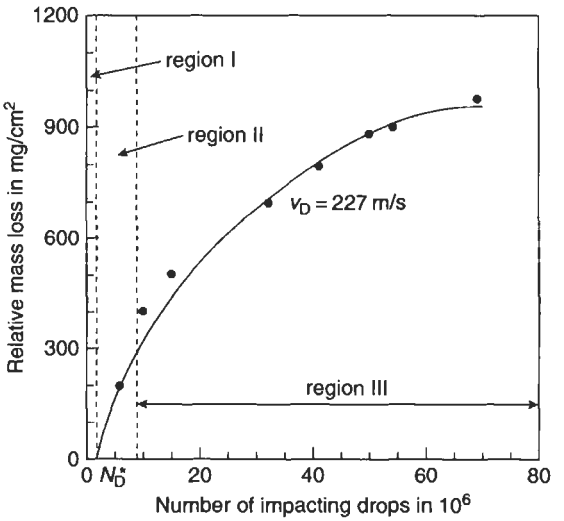

Figure 2.9 Drop number influence on mass loss (measurements: Baker et al., *1966).*

2.3 Parameter Influence on the Coating Removal

2.3.1 Parameter Definition

2.3.1.1 Target parameters for coating removal

Basic target parameters include coating thickness (h_C), mass removal (m_C) and cleaning width (w_C). They are illustrated in Fig. 2.10(a). For the erosion by a stationary water jet, these parameters are related through the following approximation:

$$m_C = (\pi/4) \cdot w_C^2 \cdot h_C \cdot \rho_C. \tag{2.26}$$

For a given cleaning width, a certain coating mass must be removed to completely penetrate the coating with a given thickness. A maximum mass removal is desired. The energy efficiency of the cleaning process is given by the specific energy:

$$E_S = E_I/m_C. \tag{2.27}$$

This parameter should be as low as possible; its physical unit is kJ/kg. The cleaning rate is the area cleaned in a given time period:

$$\dot{A}_C = \frac{\dot{m}_C}{h_C \cdot \rho_C}. \tag{2.28}$$

The thicker the coating and the higher its density, the lower the cleaning rate. The cleaning rate should be maximum; its physical unit is m^2/h. Other target parameters that may focus on the surface quality, such as roughness or cleanliness, are not considered in this paragraph.

2.3.1.2 Process parameters

Process parameters in hydroblasting are shown in Fig. 2.10(b). They can be subdivided into hydraulic parameters and performance parameters. Hydraulic

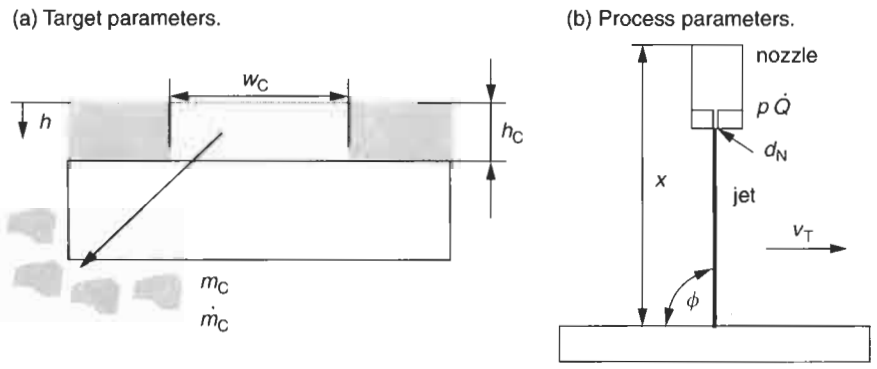

Figure 2.10 Target and process parameters for hydroblasting.

parameters characterise the pump-nozzle-system; they include the following:

- operating pressure (p);
- volumetric flow rate ($\dot{Q}$);
- nozzle diameter (d_N).

Typical relationships between these parameters are described in Section 3.2.3.2 in Chapter 3. Performance parameters are more related to the process performance and include the following:

- stand-off distance (x);
- traverse rate (v_T);
- impact angle (ϕ).

The traverse rate covers additional parameters, such as the number of cleaning steps, n_S, and the exposure time t_E.

2.3.2 Pump Pressure Influence

Figure 2.11(a) shows the relationship between pump pressure and coating mass loss which can be described mathematically as follows:

$$m_C(p) = A_1 \cdot (p - p_T)^{B_1}. \tag{2.29}$$

This function features three parameters: a threshold pressure p_T, a progress parameter A_1, and a power exponent B_1. The threshold pressure has appeared in several experiments (Taylor, 1995; Wu and Kim, 1995; Mabrouki *et al.*, 1998). The meaning of this parameter is illustrated in Fig. 2.12 based on high-speed camera images taken during the removal of a latex-coating from a fibrous substrate. Note from the left image the complete reflection of the impinging jet from the coating surface; no material was removed. This situation counts for $p < p_T$. In the right image material erosion occurred; the jet completely removed the coating and penetrated the fibrous substrate. This situation counts for $p > p_T$. Some typical values for the threshold pressure estimated by numerous authors were bitumen on steel (Schikorr, 1986), 50–120 MPa for epoxy-resins (Mabrouki *et al.*, 1998), 105 MPa for aluminium (Wu and Kim, 1995), 120–140 MPa for alkyd coats (Meunier and Lambert, 1998), 190 MPa for adherent rust (Meunier and Lambert, 1998), and about 200 MPa for inconel (Taylor, 1995). For polymer-particle composite coatings, the threshold pressure linearly increased if PMMA content and hardness, respectively, increased (Briscoe *et al.*, 1997). The progress parameter A_1 depended on coating type and traverse rate. The general trend for the traverse rate was: the lower the traverse rate, the higher the value for A_1. The power parameter B_1 depended on the material. For aluminium the power exponent was about $B_1 = 1$ for low traverse rates, but $B_1 > 1$ for higher traverse rates (Wu and Kim, 1995). For paint systems (epoxy-based see Fig. 2.11(a) and bitumen (Schikorr, 1986)) the exponent tended to $B_1 < 1$. The curves for these coatings at high pressures confirmed a square-root-model for

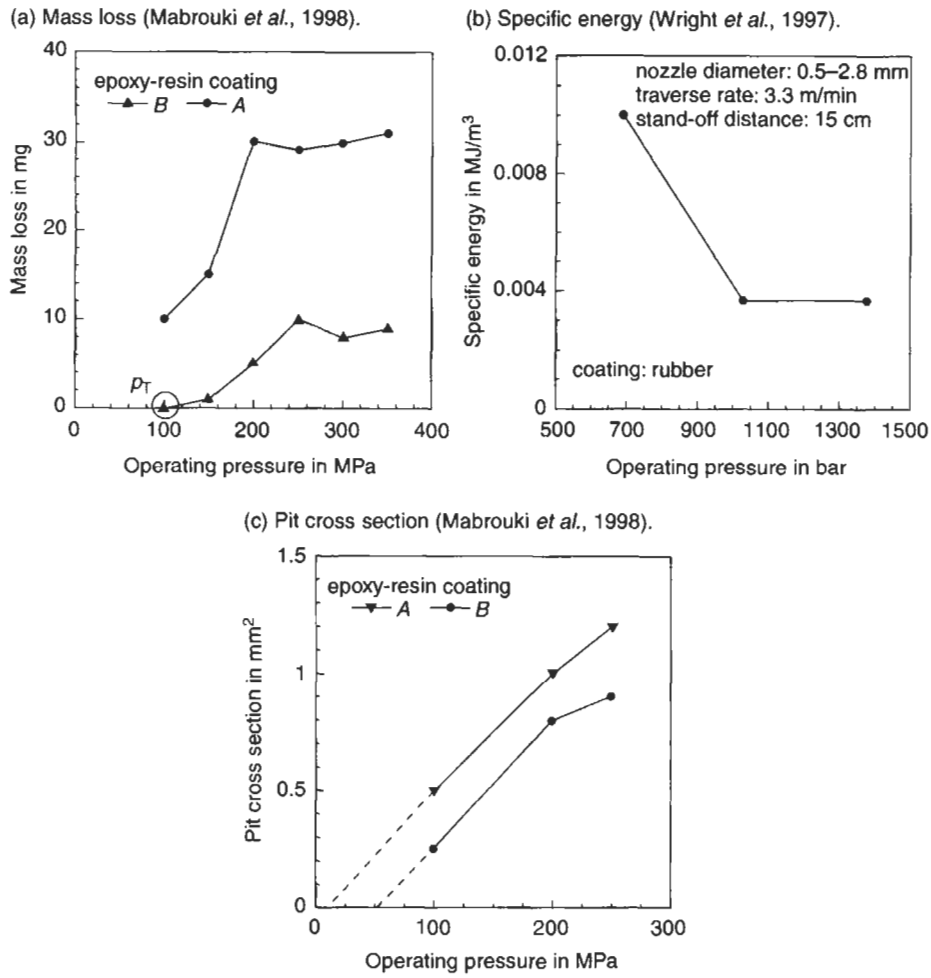

Figure 2.11 Pressure influence on cleaning parameters.

soft-solid coatings developed by Thomas *et al.* (1998). In no case the exponent reached the value of 1.94 as suggested by a cleaning model developed by Leu *et al.* (1998). If $B_1 = 1$ (which may be valid for high traverse rates as usually applied for cleaning processes), the pressure for optimum energy consumption can be estimated from the following relationship:

$$\frac{dE_J}{dm_C} = \frac{d(C \cdot p^{3/2})}{d[A_1 \cdot (p - p_T)]}. \tag{2.30}$$

For $dE_J/dm_C = \text{Min}$, Eq. (2.28) delivers

$$p_o = 3 \cdot p_T. \tag{2.31}$$

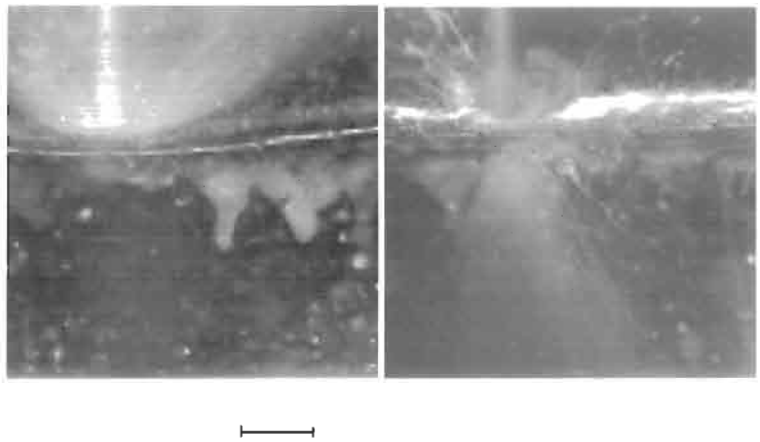

Figure 2.12 Threshold conditions for a latex layer (Weiß and Momber, 1998); left: $p < p_T$; right: $p > p_T$; scale: 5 mm; fibrous substrate.

For the applications shown in Fig. 2.11(a), the energetically optimum pressure ranged between 150 and 360 MPa for epoxy-resin coatings. The higher value exceeds already the limit of commercially available hydroblasting systems. Figure 2.11(b) taken from rubber removal experiments, proved the low specific energy at high pump pressures. Results obtained on epoxy-resin coatings, Fig. 2.11(c), and on aluminium samples (Wu and Kim, 1995) showed that the cleaning width was linearly related to the pump pressure, but the progress was rather low. The progress of the function was also almost independent of the traverse rate. A threshold pressure could not be noted. There is disparity in the threshold pressures if Figs. 2.11(a) and 2.11(c) are compared. From Fig. 2.11(c), threshold pressures would be between 10 and 50 MPa which do not match Fig. 2.11(a). A spot may be seen at $p = 50$ MPa at the surface in case of coating 'B', but still no material is measurably removed.

2.3.3 Nozzle Diameter Influence

The relation between nozzle diameter and mass loss is shown in Fig. 2.13(a). It can be noticed that the function approaches Eq. (2.29) with three characteristic parameters: a threshold nozzle diameter d_T, a progress parameter A_2, and a power exponent B_2. The threshold diameter was, independently of the traverse rate, at about $d_T = 0.05$ mm; this was far from the diameter of commercially applied nozzles. The progress parameter A_2 increased as traverse rate decreased. For low traverse rates, the power parameter was $B_2 > 1$. Figure 2.13(b) illustrates the influence of the nozzle diameter on the cleaning width. The relation was equal to that obtained for the pump pressure. A threshold value could not be noted which was due to the same effect as for the pump pressure.

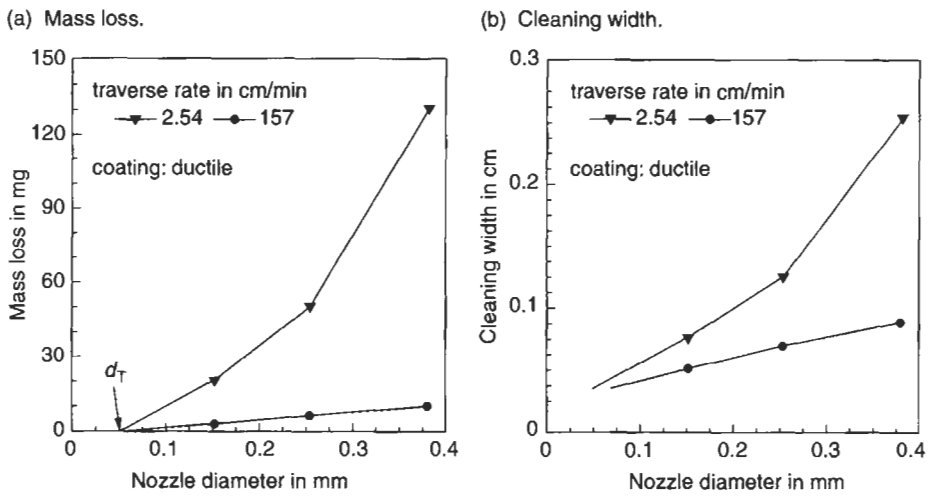

Figure 2.13 Influence of nozzle diameter on cleaning parameters (Wu and Kim, 1995).

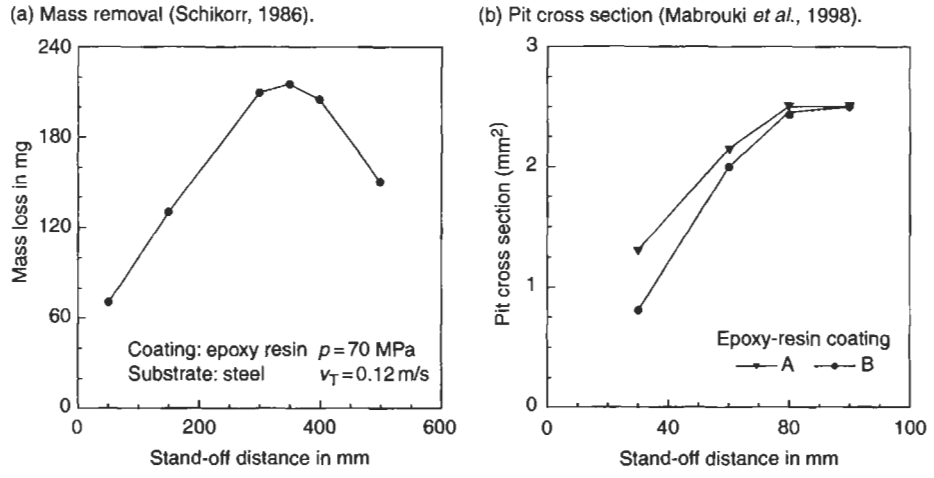

Figure 2.14 Stand-off distance influence on target parameters.

2.3.4 Stand-off Distance Influence

Any coating removal target parameter is very sensitive to variations in stand-off distance. This is illustrated in Figure 2.14. Initially, mass loss increased linearly with the stand-off distance up to a value of $x = 270$ mm (Fig. 2.14(a)). If this value was exceeded, the progress dropped. For a certain optimum stand-off distance, a maximum in the material removal could be observed at about $x_O = 300$ mm ($x_O/d_N = 200$). Similar was the situation with the pit cross section as shown in Fig. 2.14(b). This parameter was also sensitive to variations of the stand-off distance. Similar results were reported by Leu *et al.* (1998) for epoxy-based paints. The optimum stand-off distance was at about $x_O = 80$ mm ($x_O/d_N = 260$) for both paint systems in

Fig. 2.14(b). Both x_O/d_N-values were beyond the jet core (Fig. 2.6) and pointed to an influence of dynamic effects, namely drop impact and structural disturbances.

Leu *et al.* (1998) derived the following relationship between cleaning width and stand-off distance for a stationary water jet:

$$w_C = 2 \cdot C_X \cdot \left[1 - \left(\frac{x}{x^*}\right)^{2/3}\right]^{2/3}. \tag{2.32}$$

The spreading coefficient can be taken as $C_X = 0.033$ from experimental results. The critical stand-off distance was given through (Leu *et al.*, 1998):

$$x^* = 2.82 \cdot \left(\frac{\lambda \cdot c_F \cdot \mu}{\sigma_I}\right)^{1/2} \cdot \left(\frac{d_N}{2 \cdot C_X}\right) \cdot p^{1/4} \cdot \rho_F^{1/4}. \tag{2.33}$$

Here, σ_I is the endurance limit of the coating material (see Fig. 2.19), and λ is a stress coefficient. From Leu *et al.*'s (1998) deviation a ratio $\lambda/\sigma_I = \dot{m}_F \cdot c_F$ could be assumed.

2.3.5 Traverse Rate Influence

Typical relationships between removed mass and traverse rate for different materials are shown in Fig. 2.15(a). Mass loss dropped for all materials as traverse rate increased. It could be seen that the mass loss drop was very dramatic for low traverse rates. The relation is a simple power law

$$m_C = \frac{C_1}{v_T}. \tag{2.34}$$

The constant C_1 depended on the applied coating system and only slightly on operating pressure. The situation was different if mass loss rate was considered as illustrated in Fig 2.15(b). In that case the traverse rate should be rather high to obtain a high mass loss rate. The certain trend depended on the operating pressure. For rather low pressures an optimum traverse rate existed. Such an optimum was observed for the removal of soil films from brass (Kaye *et al.*, 1995). The cleaning rate also increased as the traverse rate increased (Fig. 2.15(c)) suggesting that quickly rotating hydroblasting tools are superior to stationary tools.

A more general relationship for the estimation of the cleaning rate was derived by Sundaram and Liu (1978):

$$\dot{A}_C = v_T \cdot w_{C\max} \cdot \left[1 - \left(\frac{v_T \cdot t_{ET}}{w_{C\max}}\right)^2\right]^{1/2}. \tag{2.35}$$

Here, t_{ET} is a threshold exposure time that will be discussed later. Cleaning is zero both at $v_T = 0$ and at $v_T = w_{C\max}/t_{ET}$. Maximum cleaning rate could be derived by

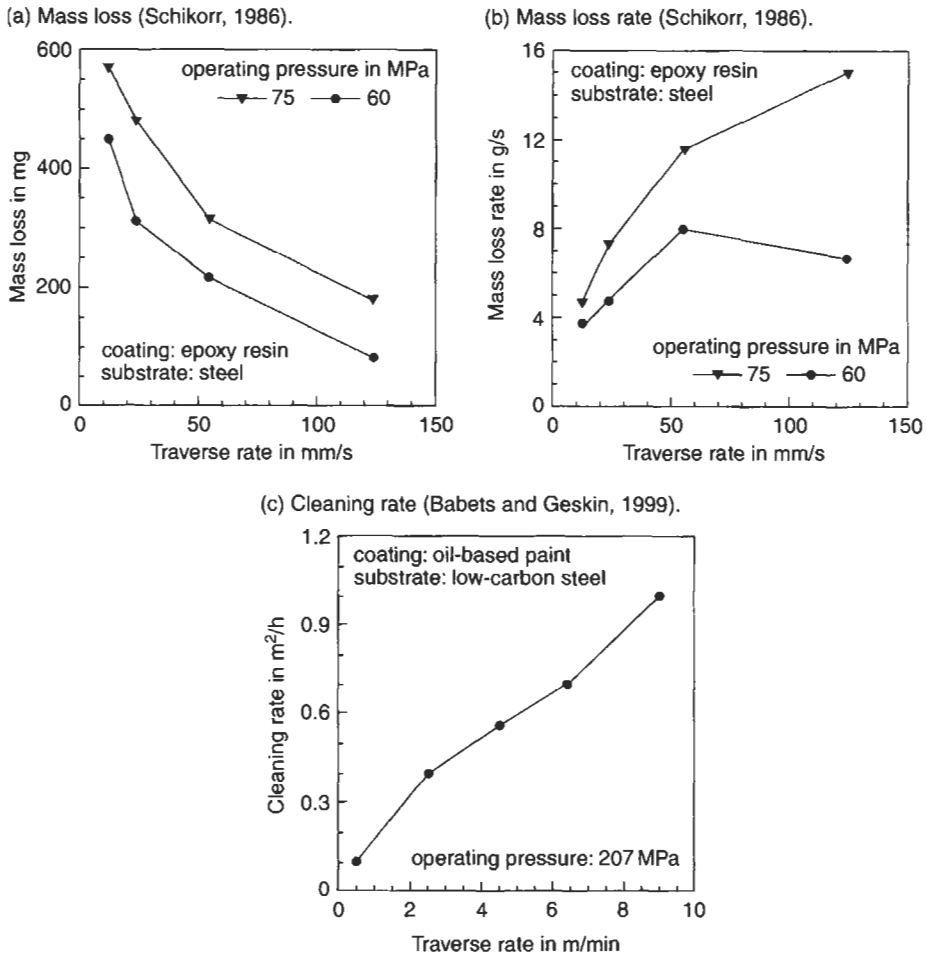

Figure 2.15 Traverse rate influence on cleaning parameters.

solving $d\dot{A}_C/dv_T = 0$. The corresponding traverse rate is given as follows:

$$v_T^* = \frac{0.707 \cdot w_{Cmax}}{t_{ET}}. \tag{2.36}$$

Traverse rate actually expresses the local exposure time:

$$t_E = d_j/v_T. \tag{2.37}$$

The jet diameter can often be replaced by the nozzle diameter ($d_j = d_N$). A plot of local exposure time versus mass loss is shown in Fig. 2.16(a); the results were taken from Fig. 2.15(a) and recalculated with Eq. (2.37). Mass loss increased dramatically at low

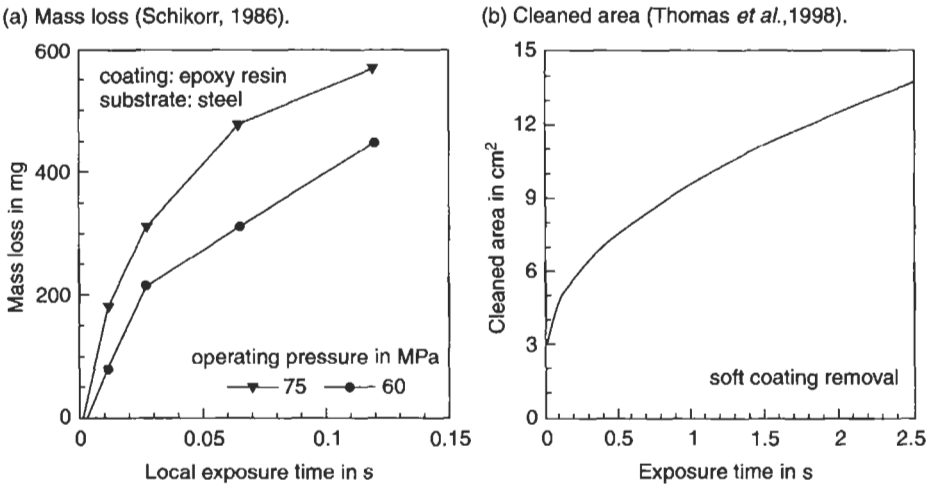

Figure 2.16 Influence of exposure time on target parameters.

exposure time; if the local exposure increased further, efficiency (in terms of the slope of the curve) dropped. From this point of view, short local exposure times (high traverse rates) are recommended. A threshold exposure time could also be noted – it was about 0.005 s for the conditions shown in Fig. 2.16(a). Such a parameter is known from other liquid jet applications, namely concrete hydrodemolition (Momber and Kovacevic, 1994), hydro-abrasive machining (Momber and Kovacevic, 1998) and cavitation erosion (Momber, 2003b). A critical traverse rate exists for most combinations of coating and operating pressure. This critical condition could also be derived from Fig. 2.15(a): it would be the intersection of the curve with the abscissa at very high traverse rates. The most probable explanation is that erosion of the coating starts after a period of damage accumulation by subsequently impinging drops. This aspect is discussed in Section 2.4. No threshold limit exists in Fig. 2.16(b) which was obtained from the removal of rather soft coatings. This relationship could be described by a simple square-root law (Thomas *et al.*, 1998):

$$A_C \propto t_E^{1/2}. \tag{2.38}$$

and this law may apply to any particular coating system (for example to epoxy-based coatings: Mabrouki *et al.*, 1998). However, an exponential regression was also successfully applied to relate exposure time and cleaning width (Louis *et al.*, 1999). The mass loss rate

$$\dot{m}_C = \Delta m_C / \Delta t_E \tag{2.39}$$

must have a maximum at rather short relative exposure times (see Fig. 2.16(a)). After a time of about 0.01 s, a further increase in the exposure time reduced the

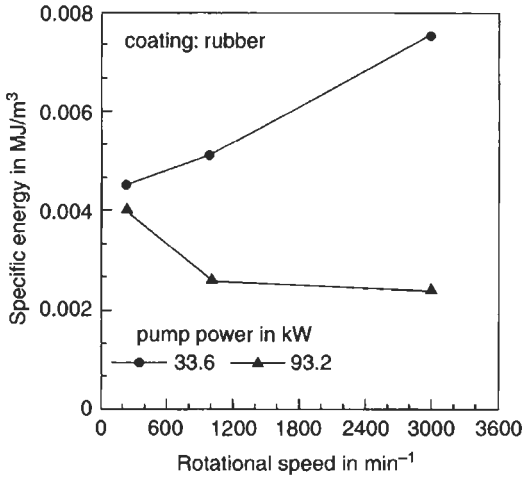

Figure 2.17 Rotational speed influence on specific energy (Wright et al., *1997).*

mass loss rate. If this optimum exposure time is known, a strategy for multi-pass stripping can be developed. Simply introduce the optimum exposure time several times into the duration that corresponds to the desired mass loss rate:

$$n_S = \frac{m_C}{m_{C(t=t_o)}}; \quad n_S = 1, 2, 3, \ldots . \tag{2.40}$$

An example may be calculated based on Fig. 2.16(a). If a mass loss of $m_C = 500$ mg is required to completely penetrate the coating thickness, a local exposure time of $t_E = 0.06$ s is requested. The optimum exposure time for $dm_M/dt_E = \max$ is $t_O = 0.01$ s which gives $m_{C(t=t_O)} = 170$ mg. The theoretical step number calculated from Eq. (2.40) is $n_S = 2.94$, in practice $n_S = 3$. The entire exposure time required to remove the desired coating mass is thus $t_E = 0.03$ s which is about 50% of the time for a one-step removal. The gain in efficiency is also 50%.

The relationship between rotational speed and specific energy is shown in Fig. 2.17. Note that rotational speed and traverse rate were coupled through Eq. (2.8). There was no distinct trend. For a rather high pump power (90 kW could be assumed for hydroblasting applications), specific energy was high for low rotational speeds and approached a lower stable level at higher speeds. The cleaning width had only a weak relationship to the traverse rate. It slightly decreased if the traverse rate increased (Babets and Geskin, 2001).

2.3.6 Impact Angle Influence

Most nozzles in a rotating nozzle carrier are angled (see Chapter 3). Typical angles are between 10° and 15°. The corresponding impact angles are between 75° and 80°. The impact angle influence on the removal of rubber is shown in Fig. 2.18. In the case in question, angled jets improved the cleaning efficiency. However, an

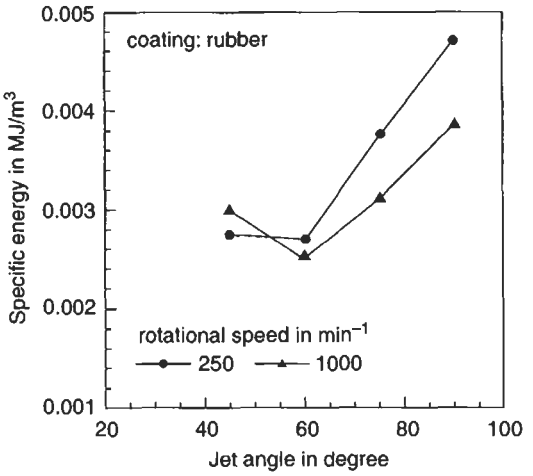

Figure 2.18 Impact angle influence (Wright et al., *1997).*

angle variation between 45° and 60° did not influence the cleaning efficiency much. A perpendicular impact showed worst results from the point of view of energy efficiency. It should be noted that these results were valid only for rubber as a highly deformable material.

2.4 Models of Coating Removal Processes

2.4.1 Drop Impact Model

Springer (1976) developed a coating removal model based on material fatigue due to high-frequency water drop impact. This model was adapted by Meng *et al.* (1998) and applied to water jet erosion. In Springer's model, the paint mass removed per single drop impact is:

$$m_C^* = 73.3 \cdot 10^{-6} \cdot \rho_C \cdot d_D^3 \cdot (\sigma_C / R_C)^4. \tag{2.41}$$

From this equation, the removed mass increases as impact stress, drop diameter and coating material's density increase; and it decreases as coating material's erosion resistance increases. The erosion resistance parameter R_C is given by

$$R_C = \frac{4 \cdot \sigma_U \cdot (b_C - 1)}{(1 - 2 \cdot \nu_C) \cdot (1 + 2 \cdot k \cdot \Psi_{SC})}. \tag{2.42}$$

This equation contains some common engineering properties of the coating, namely ultimate strength and Poisson's ratio. The impedance ratio is defined as

$$\Psi_{SC} = \frac{Z_S - Z_C}{Z_S + Z_C}. \tag{2.43}$$

Table 2.5 Mechanical properties of some coating systems (ACI, 1993; Springer, 1976).

Material	Property				
	Young's modulus E_M in GPa	Tensile strain ε_T	Poisson's ratio ν_C	Ultimate strength σ_U in MPa	Endurance limit σ_I in MPa
Epoxy binder	0.4–0.8	30	–	14	–
Epoxy polymer	0.6–1.0	35	–	–	–
Methacrylate binder	0.7	100–200	–	3–8	–
Polyester binder	0.24–0.62	30	–	14	–
Polyurethane binder	0.3–1.0	150–600	–	6–10	–
Acrylic	2.1	–	0.20	–	45
Epoxy	22.1	–	0.35	221	48
Polyester	19.3	–	0.25	395	386
Polyethylene	2.1	–	0.20	10	4
Polyamide	26.2	–	0.25	386	345
Polyurethane	0.07	–	0.20	–	14

Some values for these properties are listed in Tables 2.4 and 2.5. Values for Ψ_{SC} are for most coating materials between 0.7 and 1. The parameter b_C is a dimensionless value related to the material's fatigue behaviour:

$$b_C = \frac{b_2}{\log(\sigma_U/\sigma_I)}. \tag{2.44}$$

The parameters in that equation are illustrated in Fig. 2.19(a). From that figure,

$$b_2 = \log N_1, \tag{2.45}$$

where N_1 is the life cycle number corresponding to the endurance limit σ_I. Values for the strength parameters of some coating materials are given in Table 2.5. However, the estimation of b_C requires the knowledge of the complete fatigue curve of the material. The dimensionless value k in Eq. (2.42) is the number of stress wave reflections in the coating during the impact time. The parameter σ_C is the average stress on the coating surface:

$$\sigma_C = \sigma_D \cdot \underbrace{\frac{1 + \Psi_{SC}}{1 - \Psi_{SC} \cdot \Psi_{FC}}}_{\Gamma_1} \cdot \left[1 - \underbrace{\Psi_{SC} \cdot \frac{1 + \Psi_{FC}}{1 + \Psi_{SC}}}_{\Gamma_2} \cdot \frac{1 - e^{-\Omega}}{\Omega} \right]$$

$$= \sigma_D \cdot \Gamma_1 \cdot \left[1 - \Gamma_2 \cdot \frac{1 - e^{-\Omega}}{\Omega} \right]. \tag{2.46}$$

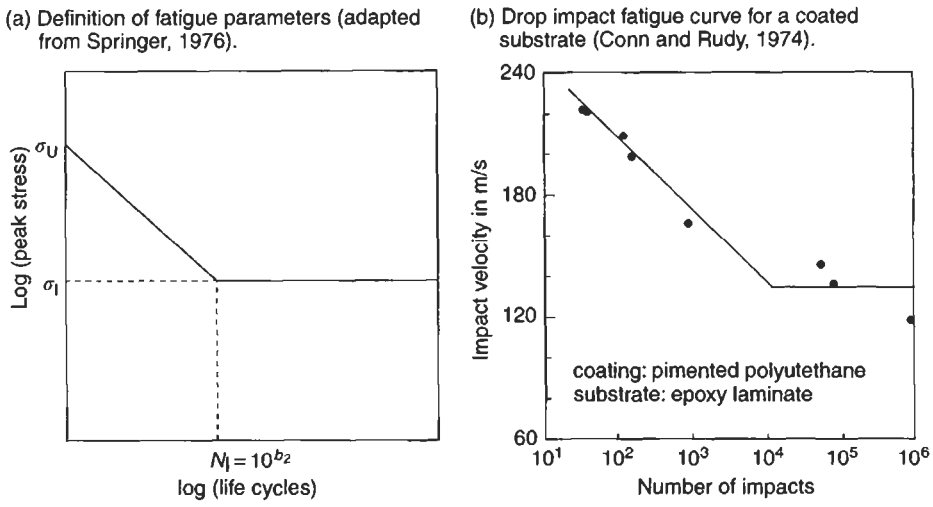

Figure 2.19 Fatigue associated with water drop impact.

Here, σ_D is the impact pressure given by Eq. (2.22). Values for Ψ_{FC}, Γ_1 and Γ_2 are given in Table 2.4. Ω is a parameter related to the coating thickness:

$$\Omega = \frac{d_D}{h_C} \cdot \frac{c_C}{c_F} \cdot \underbrace{\frac{1 + (Z_F/Z_S)}{1 + (Z_C/Z_S)} \cdot \left(\frac{2}{1 + (Z_F/Z_C)}\right)}_{\Gamma_3} = \frac{d_D}{h_C} \cdot \frac{c_C}{c_F} \cdot \Gamma_3. \tag{2.47}$$

The parameter Γ_3 is tabulated in Table 2.4, its value is between 1 and 1.5 for most cases. The number of impacting drops per unit area for a time interval Δt is (Fig. 2.9):

$$\Delta N_D = \frac{6 \cdot \dot{m}_W \cdot \Delta t}{\rho_F \cdot \pi \cdot d_D^3}, \tag{2.48}$$

with

$$\Delta t = \Delta z / v_T \tag{2.49}$$

(z being the direction of traverse jet travel).

2.4.2 Water Jet Cleaning Models

A number of water jet surface cleaning models have been developed over the years. They can be subdivided as follows:

- analytical models (Leu *et al.*, 1998; Meng *et al.*, 1998; Louis *et al.*, 1999);
- erosion based models (Conn *et al.*, 1987);
- fuzzy-logic based models (Babets and Geskin, 2001);

- neural network based models (Babets and Geskin, 1999);
- numerical simulations (De Botton, 1998; Mabrouki *et al.*, 2000; Mabrouki and Raissi, 2002);
- regression models (Kaye *et al.*, 1995; Thomas *et al.*, 1998).

Information about these models may be obtained from the original papers. Most of them assumed accumulated drop impact as the principal material removal mode and, therefore, may relate to the drop impact model introduced in the previous chapter.

Louis *et al.* (1999) defined the following three stages of a water jet cleaning process:

(i) damage accumulation (threshold stage);
(ii) rapid erosion of the upper part of the coating (no interaction with substrate);
(iii) slow erosion of the coating near the substrate.

A criterion for damage accumulation (threshold condition for beginning coating removal) was due to the following (Louis *et al.*, 1999):

$$k^* \cdot \dot{m}_W \cdot \left(\frac{\rho_F \cdot c_F \cdot v_D}{2 \cdot \sigma_U} \right)^{b^*} = 1, \tag{2.50}$$

with $b^* = 13$. The parameter k^* must be estimated by experiments. A further interesting assumption was a decrease in the erosion rate if the impinging drops approach the substrate (stage (iii)). This decrease was modelled due to

$$\dot{h}_E \propto \left(\frac{h_C - h}{h_C} \right)^{C^*} \tag{2.51}$$

(see Fig. 2.10a). The deceleration exponent C^* was between 2.3 and 2.9 (Louis *et al.*, 1999).

An analytical model for the direct calculation of paint removal by a water jet was developed by Meng *et al.* (1996, 1998) and Leu *et al.* (1998). The analysis led to the following equation for estimating the mass of removed paint per unit area (Meng *et al.*, 1998):

$$\frac{m_C}{\text{area}} \propto \left(\frac{p^{0.5n+0.5}}{v_T} \right) \cdot \left(\frac{d_N}{2 \cdot x} \right)^{2n+2}. \tag{2.52}$$

From that equation, mass loss increases as pump pressure and nozzle diameter increases. It drops with an increase in traverse rate and stand-off distance, respectively. For the empirical parameter in that equation, the authors found $n = 2.875$ which delivers $m_C \propto p^{1.94}$. It was, however, shown in Section 2.3.2 that experimentally estimated exponents are notably lower. Therefore, the model seems to be valid for rather low operating pressures. The nozzle exponent ($2 \cdot n + 2 = 7.75$) was also unusually high (compare Fig. 2.13(a)).

Conn *et al.* (1987) defined an 'area cleaning effectiveness' which was actually the ratio between area cleaning rate and jet power:

$$e_A = \frac{\dot{A}_C}{P_J} \tag{2.53}$$

These authors then applied Thiruvengadam's (1967) concept of erosion strength which yielded

$$e_A = \frac{I_J}{P_J \cdot S_C} \propto S_C^{-1}, \tag{2.54}$$

where I_J was an erosion intensity (defined for hydroblasting applications through a given nozzle and a fixed set of operational parameters). The parameter S_C was denoted erosion strength (originally defined for metals) and was in Thiruvengadam's (1967) original work related to the elastic strain energy density. Strain energy density is known to be a characteristic resistance parameter in other erosion situations, namely hydro-abrasive erosion (Momber, 2003d) and cavitation erosion (Momber, 2000d). Equation (2.54) is plotted in a log–log graph in Fig. 2.20. A definite relationship between e_A and S_C can be seen. The values for the erosion strength for cleaning similar materials are closely spaced together, and consequently S_C can be used to characterise an unknown paint–substrate combination as far as operational conditions (I_J in Eq. (2.54) or operating pressure in Fig. 2.20, respectively) are comparable. For a given material group (such as epoxy paint or

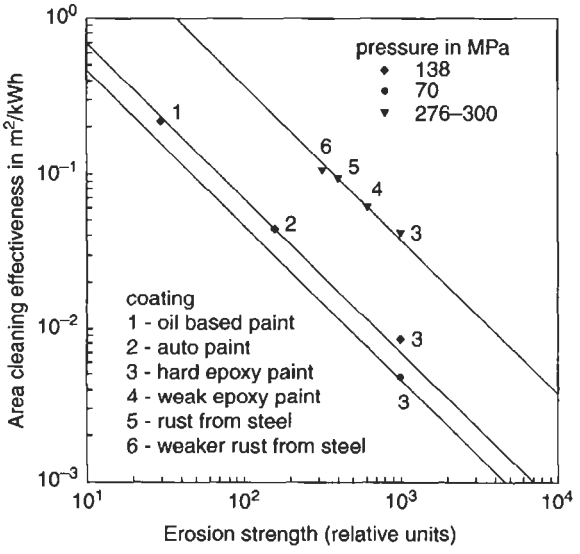

Figure 2.20 Graphical solution of Eq. (2.54) for different materials (values taken from Babets and Geskin, 2001).

rust, respectively, in Fig. 2.20) the weaker material exhibits lower values for S_C. It may, however, be noted that S_C is a relative value only, and some standard for its exact experimental estimation is missing. The estimated values for the erosion strength are listed in Table 2.6.

Zublin (1983) developed a model for the cleaning of oil wells. The model basically related the cleaning speed (equal to the traverse rate of the cleaning tool) to a material parameter 'Cleaning Energy Flux' (CE):

$$v_T \propto CE^{-1}. \tag{2.55}$$

The higher values for CE the higher the resistance of the materials against water jet erosion. Values for several materials typically found in oil wells were estimated by Zublin (1983); they are listed in Table 2.7.

Briscoe *et al.* (1995) defined a parameter α^* in order to describe the response of a deposit (polyethylene glycol) to the erosion by hydrodynamic flows. This parameter characterised the ratio of interfacial fracture energy to deposit bulk fracture energy:

$$\alpha^* \propto T_I \cdot \left(\frac{E_M}{H_M}\right), \tag{2.56}$$

with T_I being the interfacial fracture energy (see Table 5.20); E_M and H_M are Young's modulus and micro-hardness, respectively, of the coating material. The validity of this relationship was studied at a phenomenological level only. However, it was found

Table 2.6 Erosion strengths for various materials and conditions.

Paint /deposit	Erosion strength (relative[1])
Babets and Geskin (2001)	
Hard epoxy paint	1000[1]
Weak epoxy paint	665
Rust from steel	400
Weaker rust from steel	360
Auto paint	180
Oil based paint	30
Conn *et al.* (1987)	
Steel profiling	1000[1]
Paint on steel	6.2
Paint on steel (submerged)	0.65
Antifouling on steel (submerged)	0.09
Heavy fouling (barnacles) on bronze	0.019
Slime, filmy growth on bronze	0.005
Biochemical contaminant on steel	0.00008

[1]Note the different standard conditions.

Table 2.7 CE-values for certain contaminants in oil wells (Zublin, 1983).

Material	CE-value[1]
Barium sulphate	7000
Silicates	6000
Calcium carbonate	5500
Calcium sulphate	4500
Carbonate-sulphate–silica complexes	3800
Water scales and hydrocarbon complexes	3200
Coal tar	3000
Coke with or without complexes	2500
Wax with or without complexes	2000
Paraffins	1200
Sludges	1000
Thixotrophic materials (mud)	800
Non-thixotropic materials	500

[1]Originally given in lb · ft/in^2 (can also be used as relative value).

that the water concentration in the eroding fluid was critical to α^*. If the concentration was rather high, α^* increased and cohesive failure occurred in the bulk of the coating. For a low concentration the erosion mechanism changed, with the coating breaking into several large fragments. This coating detachment was due to interfacial delamination (Briscoe *et al.*, 1995).

CHAPTER 3

Hydroblasting Equipment

3.1 High-Pressure Water Jet Machines

3.1.1 General Structure

3.1.1.1 Definition of high-pressure water jet machines

For on-site applications, high-pressure water jet machines are well established. According to the DIN EN 1829, high-pressure water jet machines are defined correctly as follows: 'Machines with nozzles or other speed-increasing openings which allow water – also with admixtures – to emerge as a free jet.'

3.1.1.2 Basic components and subdivision

High-pressure water jet machines consist of the following major parts:

- drive;
- pressure generator;
- hose lines;
- spraying devices;
- safety mechanisms;
- control and measurement devices.

Mobile high-pressure water jet machines are readily transportable machines which are designed to be used at various sites, and for this purpose are generally fitted with their own undergear or are vehicle mounted, all necessary supply lines being flexible and readily disconnectable. Stationary high-pressure water jet machines are machines designed to be used at one site for a certain period of time but capable of being moved to another site with suitable equipment. They are generally skid or base frame mounted with supply lines capable of being disconnected. Major parts of high-pressure water jet machines are shown in Fig. 3.1. They include base frame, fuel tank, driving engine, couplings, high-pressure plunger pump, filter, header tank, booster pump and valves.

3.1.1.3 Drives

The type of drive depends on the conditions of use. For hydroblasting applications, possible drives include electric motors and combustion engines. Under outdoor conditions, diesel combustion engines are most commonly used: typical power ratings are between 80 and 200 kW. These engines drive the high-pressure pumps as well as any auxiliary energy consumers, such as required centrifugal pumps, compressors or high-pressure tools. Many of the engines connected to plunger pumps will run at a fixed speed (see Table 3.4). However, gear boxes, placed between drive and pump drive shaft, can be used to vary the speed of the crankshaft.

(a) Mobile unit (WOMA GmbH, Duisburg).

(b) Double pump system (Mühlhan Surface Protection Intl. GmbH, Hamburg).

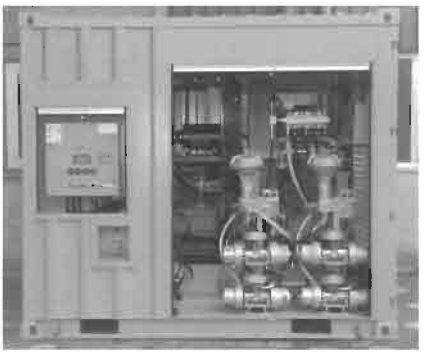

(c) On-board unit (Hammelmann GmbH, Oelde).

(d) Containerised unit (Hammelmann GmbH, Oelde).

Figure 3.1 Structures of hydroblasting machines.

3.2 Pressure Generator

3.2.1 Water Supply

For running high-pressure plunger pumps reliably and for achieving a maximum service life, pump manufacturers recommend drinking water quality. SSPC-SP 12/NACE No. 5 defines standard jetting water as follows: 'Water of sufficient purity and quality that it does not impose additional contaminants on the surface being cleaned and does not contain sediments or other impurities that are destructive to the proper functioning of waterjetting equipment.' But if suitable filter and cleaning arrangements are applied, even river water or seawater can be used. Recommended filter size depends on the sealing system as well as on the operating pressure. Typical sizes are listed in Table 3.1. All water filter arrangements are dependent upon the supply water conditions, and they should be checked at regular intervals, usually not exceeding 8 h.

Usually, especially for high-power pumps, the inlet water must enter the pump under a certain required inlet pressure. Typical values for the inlet pressure are between 0.3 and 0.5 MPa. The inlet pressure is usually generated by

Table 3.1 Recommended water filter sizes (Kauw, 1992).

Operating pressure in MPa	Recommended filter size in μm
<100	100
100–200	10
>200	Manufacturer recommendation

Table 3.2 Recommended water quality for plunger pumps and drinking water quality (WOMA Apparatebau GmbH, Duisburg).

Parameter/element	Permissible value	Drinking water analysis[1]
Temperature	30°C	10–14°C
pH-value	Depends on carbon hardness	7.45–7.7
Hardness	3°–30° D.H.[2]	22.5°–27.5° D.H.[2]
Fe	0.2 mg/l	0.2 mg/l
Mn	0.05 mg/l	0.02 mg/l
Cl	100 mg/l	48–58 mg/l
$KMnO_4$	12 mg/l	–
SO_4	100 mg/l	140–205 mg/l
Cl_2	0.5 mg/l	–
Solved oxygen	min. 5 mg/l	–
Abrasive particles	5 mg/l	–
Conductivity	1000 μS/cm	700–900 μS/cm

[1] Water works Duisburg.
[2] D.H. = German hardness.

centrifugal booster pumps that are part of commercial hydroblasting systems. For some pump types, header tanks located on a higher level than the suction pipe are sufficient.

In order to achieve optimum and reliable pump performance, pump manufacturers recommend drinking water quality. SSPC-SP 12/NACE No. 5 states the following: 'The cleaner the water, the longer the service life of the waterjetting equipment.' More detailed requirements are listed in Table 3.2.

3.2.2 General Structure of High-Pressure Pumps

3.2.2.1 Subdivision and basic components

High-pressure pumps generate the operating pressure and supply water to the spraying device. Generally, they can be divided into positive displacement pumps and hydraulic intensifiers. Positive displacement pumps are standard for hydroblasting applications. In Germany, almost 90% of all on-site devices are driven by positive displacement pumps. The most common form is a triplex (three plunger) pump as shown in Fig. 3.3. Major parts of a positive displacement pump are:

- crank-shaft;
- pump head with low-pressure inlet valves and high-pressure outlet valves;
- high-pressure plunger conversion set;

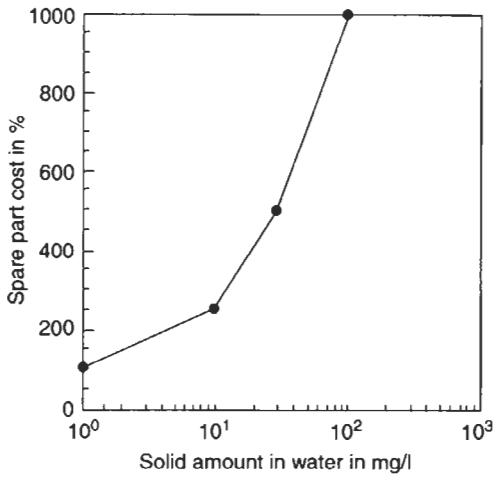

Figure 3.2 Solid content in water and maintenance cost for plunger pumps (Reliance Hydrotec Ltd., UK).

Table 3.3 Typical lifetime values for plunger pump components (Xue *et al.*, 1996).

Pressure in MPa	Component lifetime in h		
	Plunger	Seal	Valve
<30	2500	1500	3000
20–31.5	2000	1000	2500
31.5–50	1500	750	2000
50–70	1000	600	1500
70–100	800	520	1000

- pressure regulator valves;
- switch valves;
- safety devices.

Lifetimes of pump components depend on many parameters, namely water quality (see Table 3.2), maintenance regime and operating pressure (see Table 3.3). Most critical to wear and lifetime is the solid amount in water; this is illustrated in Fig. 3.2. If solid content increases (e.g. due to an insufficient water filter system) cost for replacement parts (valve seats, seals, plungers) increases.

3.2.2.2 Pump head and conversion set

Figure 3.3(b) provides a frontal look at a pump head. The pump head hosts the water inlet and water outlet valve arrangements. It consists normally of corrosive-resistant forged steel, partly also of coated spheroidal graphite cast iron. Typical plunger diameters for on-site high-pressure plunger pumps utilised for hydroblasting applications are between 12 and 22 mm. The plungers are made from coated steel alloys, hard metals or ceramics (the latter material is limited to rather low operating pressures).

(a) General structure (M + T Druckwassertechnik GmbH).

(b) Containerised high-pressure plunger pump (WOMA Apparatebau GmbH, Duisburg).

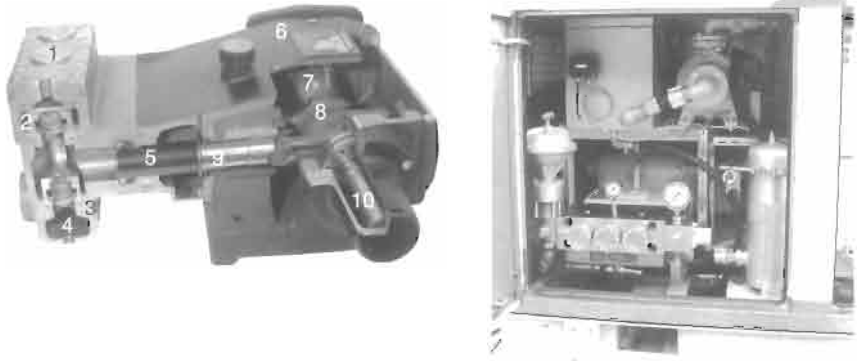

Figure 3.3 High-pressure plunger triplex pump. 1, Pump head; 2, Pressure valve; 3, Suction valve; 4, Inlet champer; 5, Plunger; 6, Gear housing; 7, Crankshaft; 8, Connecting rod; 9, Cross head; 10, Primary shaft.

3.2.2.3 Safety and control devices

Safety and control devices include safety devices and pressure-measuring devices. Safety devices prevent the permissible pressure from being exceeded by more than 2.0 MPa or 15%. These devices include pressure relief valves or burst disks, respectively. Automatic pressure regulating valves limit the pressure at which the pump operates by releasing a proportion of the generated volumetric flow rate back to the pump suction chamber or to waste. It should be used to regulate the water pressure from the pump and is individually set for each operator. Pressure-measuring devices directly measure and display the actual operating pressure. Typical control and safety valve constructions are shown in Fig. 3.4. An air-operated discharge valve (see left section) and a pressure gauge (on top of the pump head) are shown in Fig. 3.3(b).

3.2.3 Pump Performance

3.2.3.1 Performance charts

Plunger pumps can be characterised by performance charts. Pump manufacturers publish performance tables for any commercial pump type. An example is given in Table 3.4. A chart for a typical hydroblasting pump, based on these values, is plotted in Fig. 3.5. In such charts, the most important technical parameters of the pumps, such as power rating, operation pressure, volumetric flow rate, plunger diameter and crank-shaft speed, are related to each other.

3.2.3.2 Hydraulic pump power and hydraulic efficiency

The theoretical hydraulic power consumed by a plunger pump is

$$P_T = 0.0166 \cdot \dot{Q}_N \cdot p. \tag{3.1}$$

Here, p is the operating pressure in MPa, and $\dot{Q}_N$ is the nominal volumetric flow rate in l/min; the power P_T is given in kW. For a given hydraulic power, Eq. (3.1) is a hyperbolic

(a) Safety valve.

(b) Valve for multiple-consumer systems.

(c) Manually operated 2/2-way discharge valve.

(d) Pneumatically operated 3/2-way by-pass valve.

Figure 3.4 Typical control and safety valve constructions (photographs: WOMA GmbH, Duisburg).

function ($y = a/x$), and each hyperbola can be considered as a line of constant power. This is shown in Fig. 3.5 for four different crank-shaft speeds. In practice, however, the consumed power exceeds this theoretical value because of losses due to leakage, pulsations, water compression and other mechanisms. Thus, hydraulic efficiency is calculated to evaluate the efficiency of plunger pumps. This hydraulic efficiency is

$$\eta_H = P_T/P_H. \tag{3.2}$$

Values for η_H depend on pump type and operating pressure: they increase as operating pressure increases; this is illustrated in Fig. 3.6(a). Typically, values

Table 3.4 Performance table of a commercial high-pressure plunger pump.

Plunger diameter in mm	Gear ratio Drive speed in min^{-1} 1500	1800	Crank-shaft speed in min^{-1}	Required drive in kW	Volumetric flow rate in l/min	Permissible pressure in MPa
15		3.57	504	120	22	300
		4.52	398	95	18	
	3.57		420	100	19	
	4.52		331	78	15	
16		3.57	504	117	26	250
		4.52	398	93	20	
	3.57		420	98	21	
	4.52		331	74	17	
18		3.57	504	122	32	200
		4.52	398	96	26	
	3.57		420	100	27	
	4.52		331	78	21	

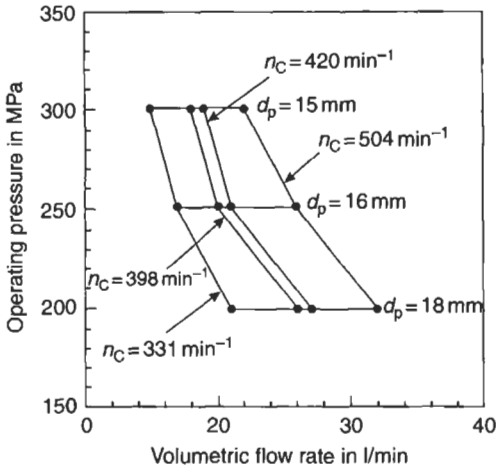

Figure 3.5 Flow chart of a typical high-pressure plunger pump (based on Table 3.4; $H_P = 95$ mm, $N_P = 3$).

between $\eta_H = 0.8$ and $\eta_H = 0.95$ can be considered for the pressure range between 200 and 380 MPa. State-of-the-art high-pressure plunger pumps are capable of generating operating pressures up to $p = 300$ MPa. The maximum permissible operating pressure of a certain pump type depends on the permitted rod force. The corresponding relationship is

$$F_P = (\pi/4) \cdot d_P^2 \cdot p. \tag{3.3}$$

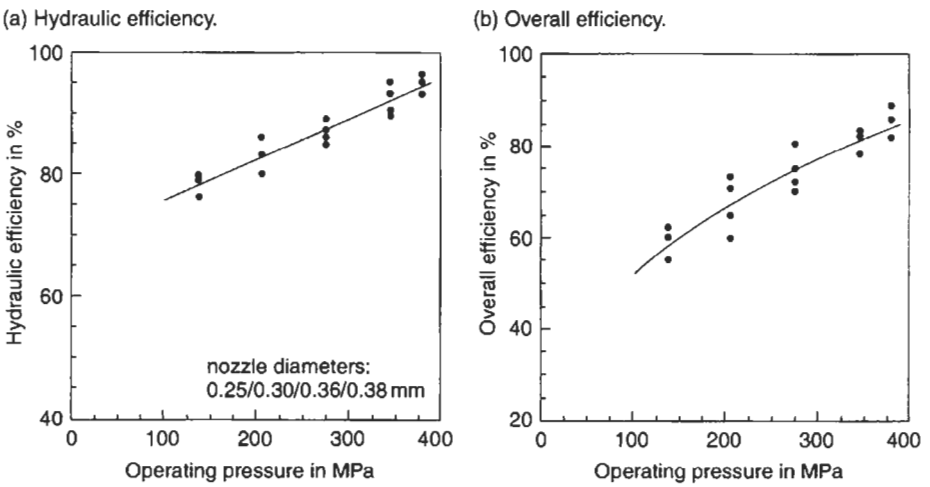

Figure 3.6 Efficiency of high-pressure plunger pumps (Veenhuizen, 2000).

Typical rod force values for high-pressure plunger pumps are between 10 and 120 kN. The overall efficiency of a high-pressure plunger pump can be estimated as follows:

$$\eta_O = \eta_H \cdot \eta_M \cdot \eta_T, \tag{3.4}$$

where η_M is the mechanical efficiency (internal frictional losses) and η_T is the efficiency of energy transmission between drive and pump. Results of measurements are shown in Fig. 3.6(b). The overall efficiency ranges from 60% to about 85% and increases as operating pressure increases. In comparison to overall efficiencies of 60–70% for hydraulically driven intensifier pumps, these values are higher.

3.2.3.3 Nominal volumetric flow rate

The nominal volumetric flow rate delivered by a plunger pump can be approximated as follows:

$$\dot{Q}_N = (1 - \xi_C) \cdot n_C \cdot \frac{d_P^2 \cdot \pi}{4} \cdot H_S \cdot N_P. \tag{3.5}$$

Here, ξ_C is a compressibility parameter, n_C is the crank-shaft speed, d_P is the plunger diameter, H_S is the stroke and N_P is the number of plungers. Typical values for these parameters are listed in Table 3.5. The crank-shaft speed of a pump drive depends on the stroke; the acceleration of the plunger (of the liquid volume, respectively) should not exceed a critical value. For most pumps, the following criterion holds (Vauck and Müller, 1994):

$$n_C^2 \cdot H_S = 1 \ldots 2 \text{ m/s}^2. \tag{3.6}$$

Equation (3.5) is partly graphically illustrated in Fig. 3.5. State-of-the-art plunger pumps are capable of generating nominal volumetric flow rates up to about 1000 l/min. If the operating pressure increases, compressibility of water becomes important. Schlatter (1986) performed a regression analysis for various tabulated

Table 3.5 Performance parameters of plunger pumps for hydroblasting applications.

Parameter	Performance range
Operating pressure in MPa	100–300
Volumetric flow rate in l/min	10–60
Hydraulic power in kW	100–300
Plunger diameter in mm	12–20
Crank-shaft speed in min^{-1}	300–500
Stroke in mm	50–140
Rod force in kN	10–120

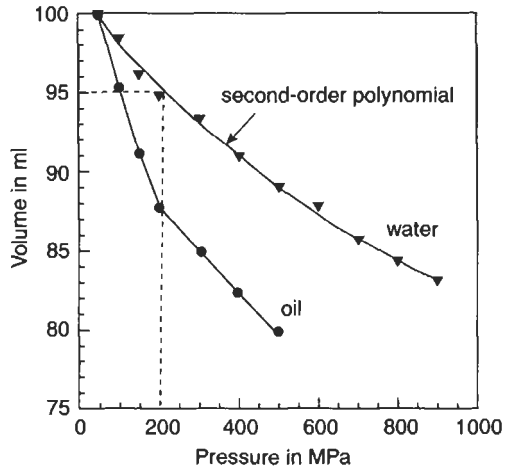

Figure 3.7 Compressibility of water and oil (measurements: Bosch-Rexroth AG, Lohr).

results of measurements. His empirical formula originally applies to the density but is rewritten here for ξ_C:

$$\xi_C = -0.00276 \cdot p^2 + 0.04382 \cdot p. \tag{3.7}$$

The pressure must be inserted in 10^{-2} MPa. For an operating pressure of $p = 200$ MPa, for example, the volume difference due to water compression is about 7.5% ($\xi_C = 0.08$). Note from Fig. 3.7 that a second-order polynomial reasonably fits experimental results. However, the compressibility for a pressure of $p = 200$ MPa is slightly lower (5%) in Fig. 3.7.

Generally, the volumetric flow rate of a plunger pump is not a constant value. It rather oscillates according to a sinus-function:

$$\dot{Q}_N = A_P \cdot v_C \cdot \sin \alpha_C. \tag{3.8}$$

Here, A_P is the plunger cross section, v_C is the circumferential velocity and α_C is the angle of the crank-shaft. This relationship is illustrated in Fig. 3.8. The liquid volume

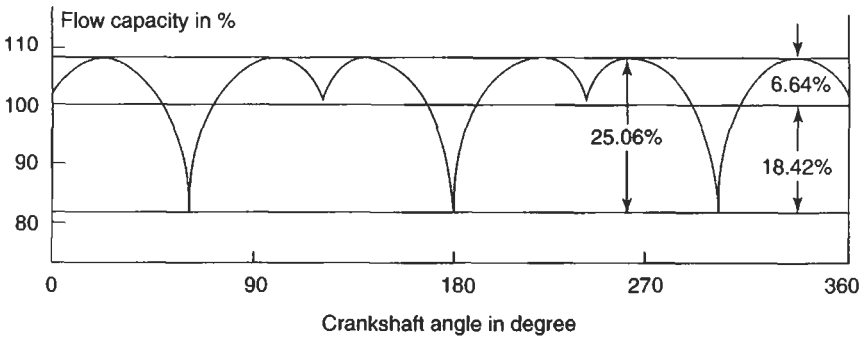

Figure 3.8 Volumetric flow rate oscillation in a triplex plunger pump (Nakaya et al., 1983).

is first accelerated and then decelerated. It can be seen from Eq. (3.8) that the unsteady volumetric flow rate is basically a result of the unsteady circumferential velocity of the crank-shaft. The average plunger speed (which is about the average liquid flow velocity in the pump) is simply given as follows:

$$v_P = 2 \cdot H_S \cdot n_C. \tag{3.9}$$

See De Santis (1995) and Nakaya *et al.* (1983) for further details.

3.3 High-Pressure Hoses and Fittings

3.3.1 General Structure

The transport of the high-pressure water to the spraying devices occurs through high-pressure lines. For on-site applications, these are flexible hose-lines. These lines are actually flexible hoses operationally connected by suitable hose fittings (see Fig. 3.9). Hose fittings are component parts or sub-assemblies of a hose line to functionally connect hoses with a line system or with each other. High-pressure hoses are flexible, tubular semi-finished product designed of one or several layers and inserts. They consist of an outer cover (polyamide, nylon), a pressure support (specially treated high-tensile steel wire), and an inner core (POM, polyamide, nylon). Any hose must be tested for bursting; the permissible operating pressure of hoses should not exceed 40% of the estimated burst pressure. Hoses capable of use for pressures equal to or higher than the maximum operating pressure of the pressure generating unit must be selected. The lifetime of high-pressure hoses depends on the operating pressure; this is shown in Fig. 3.10. Typical nominal lengths of high-pressure hoses are between $l_H = 3$ m and $l_H = 120$ m. Table 3.6 contains typical technical parameters for hoses used in hydroblasting applications.

Figure 3.9 High-pressure hose with fitting (photograph: WOMA GmbH, Duisburg).

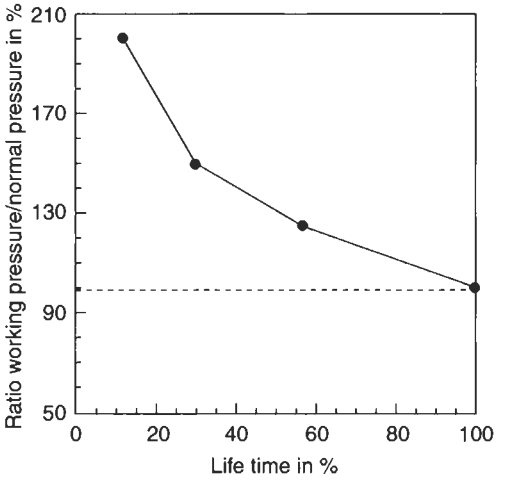

Figure 3.10 Operating pressure and hose lifetime (JISHA, 1992).

Table 3.6 Technical data of high-pressure hoses for hydroblasting operations.

Nominal width in mm	Maximum operating pressure in MPa	Maximum delivery length in m	Specific weight in kg/m	Minimum bend radius in mm
4	280	200	0.54	200
5	325	200	0.41	150
8	210	200	0.60	200
8	300	200	1.10	250
10	200	200	1.01	250
20	140	200	1.82	350

3.3.2 Pressure Losses in Hose Lines

3.3.2.1 General relationships

A permanent problem with high-pressure hoses is the pressure loss in the hose-lines. An approach for estimating the pressure loss is

$$\Delta p = \xi_F \cdot \frac{\rho_F}{2} \cdot v_F^2 \cdot \frac{l_H}{d_H}. \tag{3.10}$$

Here, ξ_F is a friction number, ρ_F is the water density, v_F is the flow velocity, l_H is the hose length and d_H is the hose diameter. The flow velocity of the water inside a hose can be estimated by applying the law of continuity:

$$v_F = \frac{4 \cdot \dot{Q}_N}{\pi \cdot d_H^2}. \tag{3.11}$$

The friction number depends on the Reynolds-Number, Re, and on the ratio between hose diameter and relative internal wall roughness, k:

$$\xi_F = f\left(\mathrm{Re}, \frac{d_H}{k}\right). \tag{3.12a}$$

This number can be estimated from the so-called Nikuradse-Chart which can be found in standard books on fluid mechanics (e.g. Oertel, 2001). An empirical relationship is

$$\frac{1}{\xi_F^{1/2}} = 1.74 - 2 \cdot \log\left(\frac{18.7}{\mathrm{Re} \cdot \xi_F^{1/2}} + \frac{2 \cdot k}{d_H}\right), \tag{3.12b}$$

with $\mathrm{Re} = v_F \cdot d_H / \nu_F$. Eqs. (3.10)–(3.12) deliver:

$$\Delta p \propto d_H^{-5}. \tag{3.13}$$

This equation illuminates the overwhelming influence of the hose diameter on the pressure loss. To substitute these pressure losses, a certain amount of additional power

$$\Delta P = \Delta p \cdot \dot{Q}_N \tag{3.14}$$

must be generated by the high-pressure pump.

3.3.2.2 Pressure loss charts and hose selection

Manufacturers of hydroblasting equipment publish pressure-loss charts or pressure-loss tables which can be used for estimating real pressure losses in hoses (see Fig. 3.11 for an example). An empirical rule for selecting the proper hose diameter is: the flow

velocity in the hose should not exceed the value of $v_F = 8$ m/s. Based on Eq. (3.11), the corresponding minimum hose diameter is

$$d_H = 1.63 \cdot \dot{Q}^{1/2}. \tag{3.15}$$

In that equation, the volumetric flow rate is in l/min, and the hose diameter is in mm. If no standard diameter is available for the calculated value, the next larger diameter should be selected. As an example: for a volumetric flow rate of 40 l/min, Eq. (3.15) delivers 10.3 mm; the recommended internal hose diameter is $d_H = 11$ mm. Equation (3.15) is graphically illustrated in Fig. 3.12.

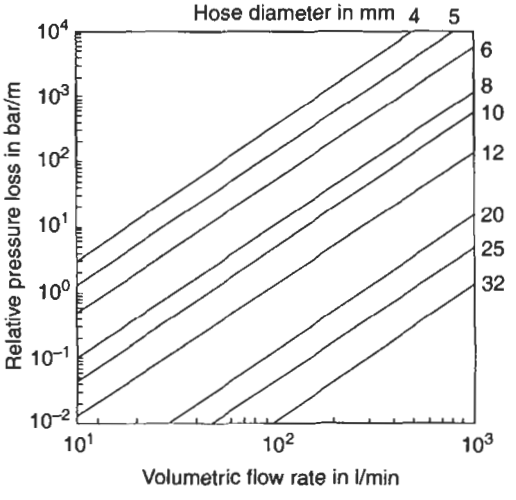

Figure 3.11 Pressure losses in high-pressure hoses.

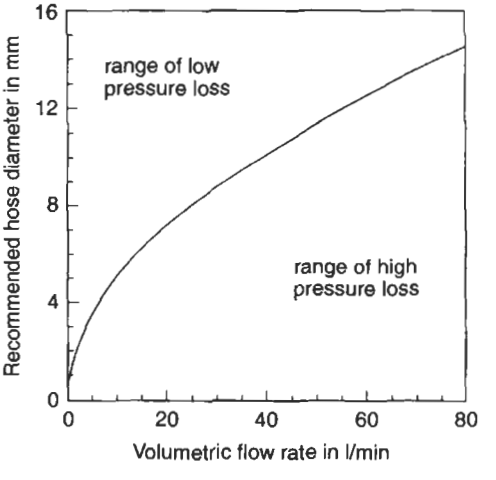

Figure 3.12 Selection of suitable hose diameters.

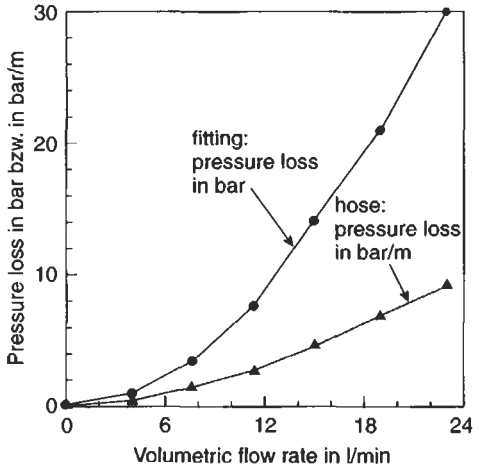

Figure 3.13 Approximated pressure losses in high-pressure fittings (based on measurements of Raghavan and Olsen, 1989).

3.3.2.3 Pressure loss in fittings

The correct pressure losses in hose fittings should be measured for any individual fitting. However, such values are not available in most cases. The following empirical approximation can be performed according to the curves plotted in Fig. 3.13: the pressure loss in a single fitting is equal to the pressure loss in a hose of equal diameter with a length of 3 m. If, for example, a volumetric flow rate of 40 l/min and a hose diameter of 11 mm are used, the pressure loss estimated from Fig. 3.11 is $p_V = 0.75$ bar/m. Thus, the pressure loss in the fitting is 0.225 MPa. This corresponds to a power loss of $\Delta P = 0.15$ kW. For hydroblasting tools and valves, special pressure loss-diagrams are available.

3.4 Hydroblasting Tools

3.4.1 General Structure and Subdivision

3.4.1.1 Hand-held tools

A hand-held hydroblasting tool can be used as long as the jet reaction force does not increase beyond a value of $F_R = 250$ N. For reaction force levels $150\text{ N} < F_R < 250$ N, hand-held guns can only be used with additional body support. The classical tool for manual hydroblasting applications is the high-pressure gun as illustrated in Fig. 3.14. It consists of hand grip, pressure housing, trigger, control units and nozzle pipe. The guns can be equipped with different nozzle carriers as discussed in Section 3.5. Any tool can be run with mechanical (valve), electric or pneumatic control, respectively. According to the valve type, hand-held tools can further be subdivided into dry shut-off safety valve and dump safety control valve. Dry shut-off valves, normally hand-controlled, automatically shut off flow to the gun when released by the operator,

but retain the operating pressure within the supply line when so shut off. Dump safety control valves automatically terminate significant flow to the gun when released by the operator, thus relieving the operating pressure within the whole system by diverting the flow rate produced by the pump to atmosphere through an orifice and dump line, which must be of sufficient size. The flow of the high-pressure water through the gun causes pressure losses. These losses can be estimated from pressure loss graphs provided by manufacturers; an example is shown in Fig. 3.15.

Figure 3.14 Hydroblasting gun with nozzle carriers (photograph: WOMA Apparatebau GmbH, Duisburg).

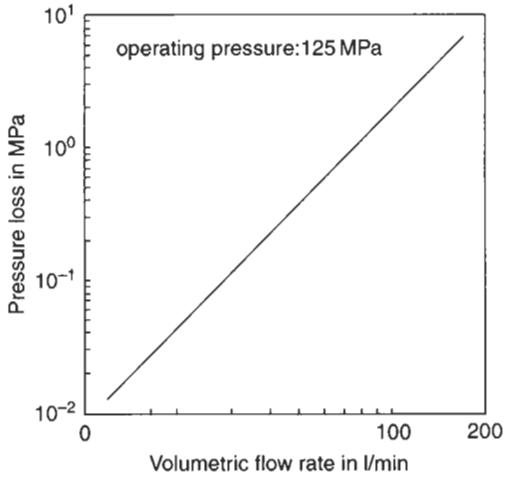

Figure 3.15 Pressure loss graph of a hydroblasting gun (WOMA Apparatebau GmbH, Duisburg).

(a) Hand-held wall cleaning tool (Hammelmann GmbH, Oelde).

(c) Mechanically guided tool (Hammelmann GmbH, Oelde).

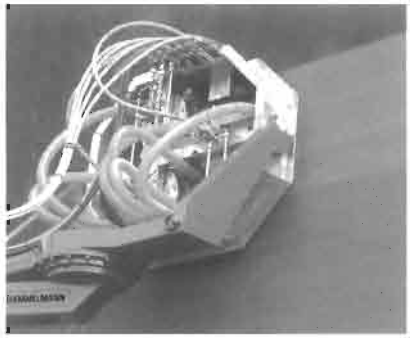

(b) Floor cleaning tool (WOMA GmbH, Duisburg).

(d) Self-adhering, mechanised tool (WOMA GmbH, Duisburg).

Figure 3.16 Emission-free performing hydroblasting tools.

A special hand-held hydroblasting tool for emission-free surface preparation applications is shown in Fig. 3.16(a). These tools are equipped with sealing systems consisting of brushes or, in case of very high sealing demands, of sealing lips. Typical technical parameters for two tool types – for floor cleaning and for wall cleaning – are listed in Table 3.7.

3.4.1.2 Mechanised tools

Mechanised hydroblasting tools are usually applied for large-scale applications, such as ship hulls or large storage tanks. Most of these tools are also equipped with sealing systems and perform emission-free. Mechanised tools often comprise more than one nozzle carrier and are, therefore, more efficient than hand-held tools. The simplest way to use this type of tools is to mount it at conventional guiding/lifting systems, such as cherry pickers or mechanical platforms. Such an application is illustrated in Fig. 3.16(c). More advanced tools are self-adhering and self-climbing. A typical hydroblasting tool designed for automatic applications is shown in Fig. 3.16(d):

it comprises a pneumatically driven rotating nozzle carrier. Typical technical parameters of this tool are listed in Table 3.8. As for hand-held tools, this unit can fully be sealed to prevent any emission of water vapour or dust. This tool can be connected to vacuuming systems. Recent reviews about mobile blasting tools are provided by Goldie (1999, 2002).

3.4.2 Jet Reaction Force

The border between hand-held and mechanised tools is set by the permissible reaction force generated by a water jet. In Europe regulations exist which forbid the application of hand-held devices if the axial component of the reaction force exceeds the critical value of $F_R = 250$ N (25 kg). In the F_R range of 150 and 250 N, hand-held guns are allowed, but they need to be reinforced by body support or by a second hand grip. These relationships are illustrated in Fig. 3.17 which also shows critical

Table 3.7 Technical parameters of emission-free performing hydroblasting tools.

Parameter	Water jetting tool		
	ETRC[1]	Vacujet[1, 2]	Lizard[1, 3]
Maximum operating pressure in MPa	210	250	200
Maximum volumetric flow rate in l/min	20	20	40
Maximum rotational speed min^{-1}	2500	2500	2500
Weight in kg	9.2	ca. 36	ca. 55
Working width in mm	180	ca. 225	ca. 380
Number of nozzles	up to 4	up to 8	up to 10

[1] Trade names WOMA Apparatebau GmbH, Duisburg.
[2] See Fig. 3.16(b).
[3] See Fig. 3.16(d).

Table 3.8 Mechanised hydroblasting tools (Goldie, 1999).

Model[1]	Hydrocat	Dockmaster[2]	Hydro-Crawler	Spin-Jet
Head size in mm	830 × 625 × 370	1400 × 1100 × 290	965 × 940 × 635	686 × 762 × 480
Head weight in kg	80		247	79
Maximum pressure in MPa	275	250	276	280
Maximum flow rate in l/min	24	85	53	42
Traverse rate in m/min	6	–	<3.65	6
Cleaning width in mm	300	750	475	250
Cleaning rate in m^2/h	<100	150–300	<50	<90

[1] Models are trade names of manufacturers.
[2] See Fig. 3.16(c).

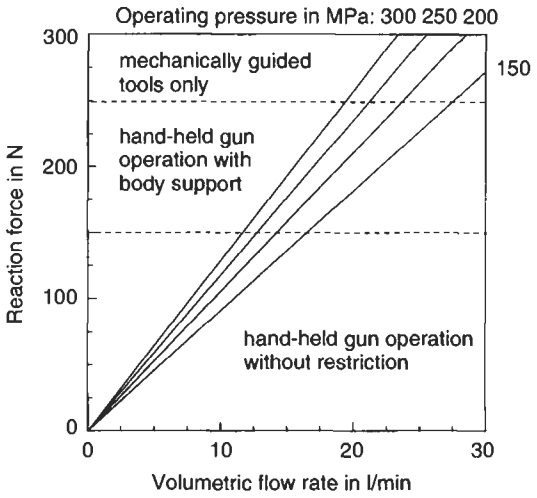

Figure 3.17 Critical conditions for hand-held gun operation (see Eq. (3.16)).

combinations of operating pressure and volumetric flow rate. An average rule says that an operator may be capable of holding about one-third of his body weight (Summers, 1991). For example: an operator with a body weight of 75 kg could resist a reaction force of $F_R = 250$ N.

The reaction force of a water jet can be estimated through impulse flow conservation:

$$\dot{I}_J = \dot{m}_W \cdot v_J = 0.743 \cdot \dot{Q}_N \cdot p^{1/2} = F_R. \tag{3.16}$$

Here, $\dot{I}_J$ is the jet impulse flow, $\dot{m}_W$ is the water mass flow rate, and v_J is the jet velocity. In the right term of Eq. (3.16), p is in MPa, $\dot{Q}_N$ is in l/min, and F_R is in N. It can be seen that the reaction force is critically related to the volumetric flow rate (and thus to the nozzle orifice cross section). Selected results are plotted in Fig. 3.17.

3.5 Nozzle Carriers

3.5.1 Rotating Lead-Throughs

A basic part of any rotating nozzle carrier is a lead-through. This construction enables the flow of high-pressure water through rotating parts. The permissible rotational speed can be as high as several thousands revolutions per minute. An operational problem with rotating nozzle carriers is the water volume loss as the high-pressure water passes the lead-through. This loss depends on the operating pressure and can be approximated with the following equation:

$$\dot{Q}_L = \xi_L \cdot p^{1/2}. \tag{3.17}$$

Here, the volumetric flow rate is in l/min, and the operating pressure is in MPa. The constant has an approximate value of $\xi_{l,} = 0.47$ for operating pressures up to 120 MPa. The rate the water jet traverses at over the surface is a function of the rotational speed of the nozzle carriers:

$$v_T = \omega_T \cdot r_T. \tag{3.18}$$

Here, ω_N is the rotational speed and R_N is the radial distance between rotational centre and nozzle location. Typical values for rotational speeds are listed in Table 3.7.

3.5.2 Self-Propelling Nozzle Carriers

Self-propelling rotating nozzle carrier heads (Fig. 3.18(a)) are usually applied for hand-held jetting guns. The driving force is supplied by a radial component of the jet

(a) Self-propelling (Hammelmann GmbH, Oelde).

(b) Externally (pneumatically) driven (WOMA GmbH, Duisburg).

Figure 3.18 Rotating nozzle carriers for hydroblasting applications.

reaction force:

$$F_R^* = \sin \theta_R \cdot F_R. \tag{3.19}$$

According to Eq. (3.16) the driving force – and thus the rotational speed – is related linearly to the volumetric flow rate, and has a square-root relationship with the operational pressure. Equation (3.19) shows also that rotational speed – and thus the exposure time of the exiting water jet – cannot be varied independently of volumetric flow rate (nozzle diameter, respectively) and operational pressure. Therefore, the performance of self-propelling rotating nozzle carrier heads can hardly be optimised. On the other hand, no additional energy and no additional lines or hoses are required for driving them. A typical performance chart of a self-propelling rotating nozzle carrier is shown in Fig. 3.19(a).

3.5.3 Externally Driven Nozzle Carriers

Externally driven rotating nozzle carrier heads are driven by separate mechanisms. Hydraulic and mechanical drives can be found usually in mechanised tools or in stationary systems fed by plunger pumps with comparatively high values of hydraulic power. They are very efficient for driving large hydroblasting tools. Pneumatic drives are used for hand-held cleaning tools as well as for on-site abrasive water jet cutting systems. A typical pneumatic drive device is shown in Fig. 3.18(b).

For externally driven nozzle carrier heads, rotational speed, operational pressure and volumetric flow rate can be varied independently from each other: this is illustrated in Fig. 3.19(b). Additional energy is required to drive external nozzle carriers; a typical value for a pneumatically driven carrier is 0.09 kW which is a negligible part of the overall hydraulic energy.

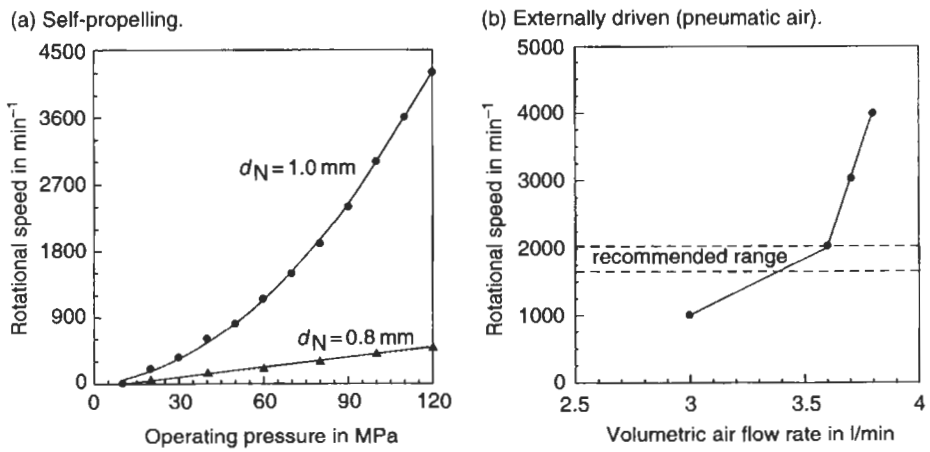

Figure 3.19 Performance charts of rotating nozzle carriers.

3.6 Hydroblasting Nozzles

3.6.1 Nozzle Types and Wear

3.6.1.1 Nozzle types

The water jet nozzle (sometimes called orifice) is an extremely important component of any hydroblasting machine. In the nozzle, the potential energy of the incoming pressurised water is transformed into the kinetic energy of the exiting high-speed water jet. Various nozzle types are known, usually designed for certain applications; this includes the following types:

- pipe cleaning nozzles for operating pressures up to 250 MPa with several orifices, directed sidewards or backwards, for tube bundle cleaning;
- pipe cleaning nozzles for operating pressures up to 140 MPa for cleaning large-diameter pipes;
- whirl jet nozzles for operating pressures up to 75 MPa for cleaning partially or fully blocked tube bundles;
- round jet nozzles with continuous flow channel for operating pressures up to 200 MPa;
- round jet nozzles with sapphire inserts for operating pressures up to 350 MPa;
- fan jet nozzles for operating pressures up to 200 MPa;
- injection nozzles for operating pressures up to 400 bar for the formation of hydro-abrasive water jets.

Depending on the nozzle design, one can distinguish between continuous nozzles and discontinuous nozzles. In the operational pressure range up to $p = 100$ MPa, continuous nozzles are most commonly used. They are conically designed and made from hardened steel. For ultra-high pressure applications, because of the comparatively low volumetric flow rates, the discontinuous nozzles are becoming increasingly used. They are characterised by a sapphire-made insert (see Figs. 3.20 and 3.22(a)). Nozzle performance strongly depends on upstream conditions. This is illustrated in Fig. 3.21.

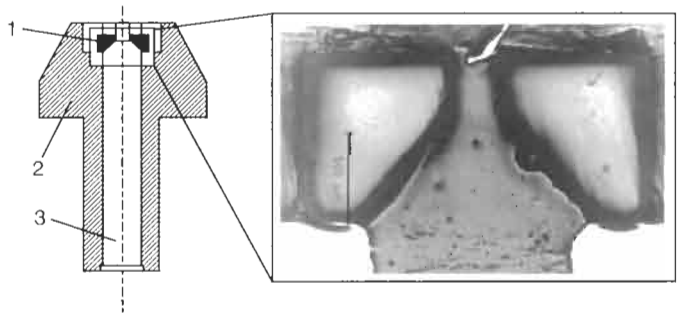

Figure 3.20 Typical hydroblasting nozzle (photograph: Wasserstrahllabor Hannover). 1, Sapphire inlet; 2, Nozzle holder; 3, Flow stabilizer.

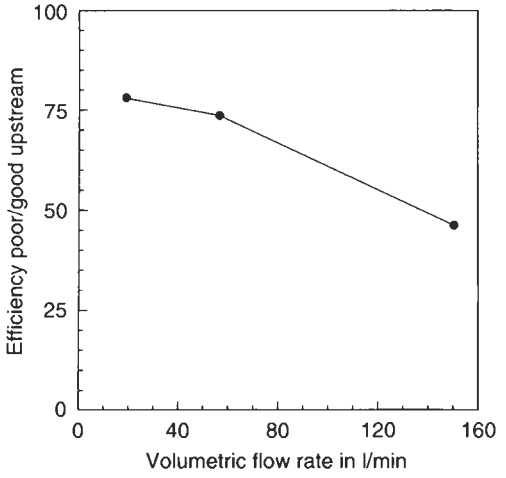

Figure 3.21 Influence of upstream conditions on nozzle performance (measurements: Wright et al., *1999).*

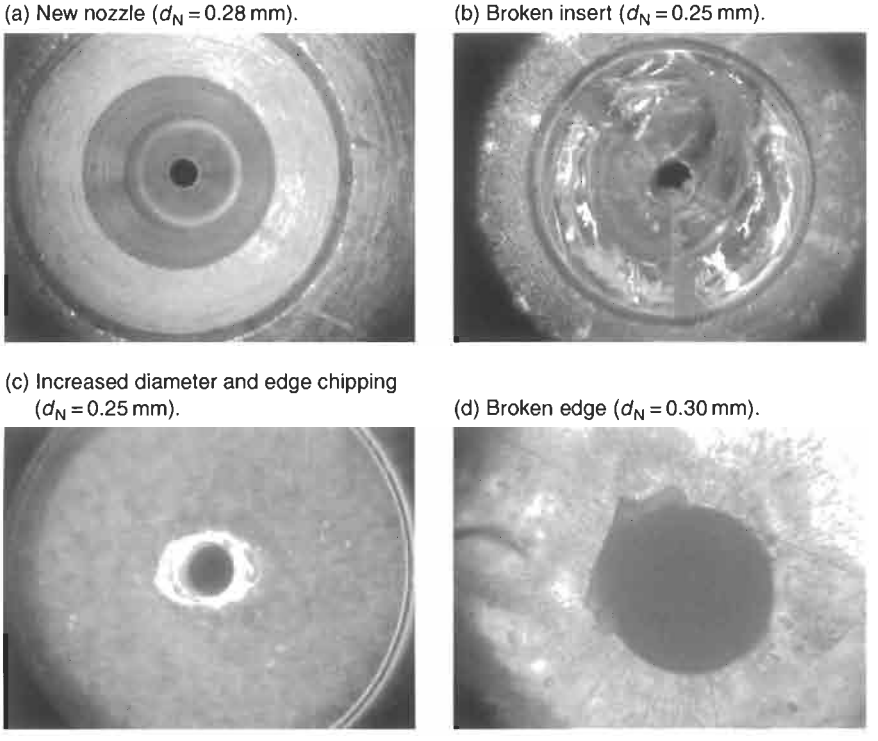

Figure 3.22 Characteristic wear types in hydroblasting sapphire nozzles.

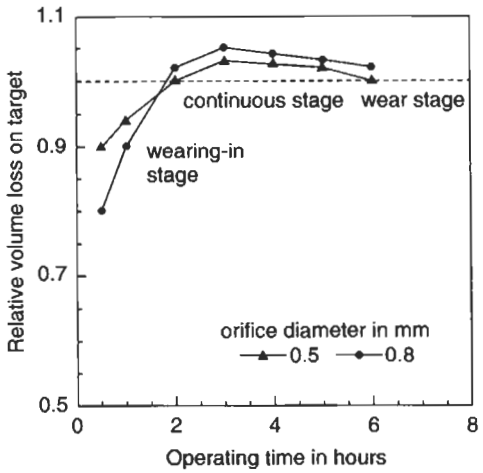

Figure 3.23 Wear stages in a typical sapphire nozzle (measurements: Werner, 1991).

Depending on the volumetric flow rate supplied by the pump, efficiency decreases down to 50% if poor upstream conditions apply.

3.6.1.2 Nozzle wear

Nozzle wear may be divided into the following two cases:

- breakage of nozzle body (see Fig. 3.22(c)–(d));
- steady decrease in nozzle exit diameter (see Figs. 3.23 and 3.24).

The wear of the nozzles depends on several parameters, among them operating pressure, water quality, nozzle design and material. As Fig. 3.23 shows, three stages can be distinguished during the performance of a discontinuous nozzle: (i) an introduction stage, (ii) a continuous stage and (iii) a wear stage. It is interesting to note that the flow conditions improve in the introduction state. The reason is that sharp corners inside the nozzle are worn away by the high-speed water flow. The improved flow conditions lead to the increasing material removal capability of the jet as illustrated in Fig. 3.23. General statements about nozzle lifetime cannot be made as the wear characteristics of a nozzle depends too much on the operational conditions. Certain wear types are illustrated in Fig. 3.22.

3.6.2 Optimisation of Nozzle Arrangements

3.6.2.1 Velocity and volumetric flow rate transfer

The velocity of the water jet as it leaves the nozzle can be approximated with Eq. (2.4). The nozzle diameter (strictly speaking, the cross section of the nozzle

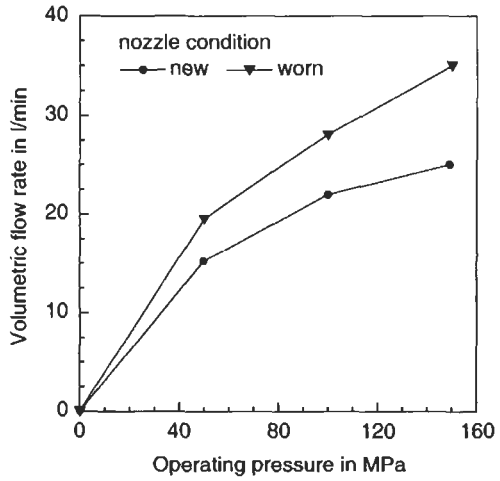

Figure 3.24 Increase in volumetric flow rate due to nozzle wear (measurements: Staskiewicz, 1995).

arrangement) determines the actual volumetric flow rate as well as the actual reaction force of a jet. The actual volumetric flow rate is approximately:

$$\dot{Q}_A = N_N \cdot \alpha \cdot \frac{\pi}{4} \cdot d_N^2 \cdot \mu \cdot \left(\frac{2 \cdot p}{\rho_F}\right)^{1/2} = \varepsilon \cdot \dot{Q}_N. \tag{3.20}$$

Here, N_N is the number of nozzles. The parameter α is often called the discharge coefficient considering losses due to nozzle flow. A very typical value is $\alpha = 0.7$ for discontinuous sapphire nozzles. Figure 3.25 contains a graph for typically applied nozzle diameters in hydroblasting. The parameter ε is the ratio between real volumetric flow rate and nominal volumetric flow rate:

$$\varepsilon = \underbrace{\frac{\dot{Q}_A}{\dot{Q}_N}}_{\text{flow rate-ratio}} = \underbrace{\alpha \cdot \frac{N_N}{N_P} \cdot \left(\frac{d_N}{d_P}\right)^2}_{\text{cross section-ratio}} \cdot \underbrace{\frac{\mu \cdot (2 \cdot p)^{1/2} \cdot \rho_F^{-1/2}}{n_C \cdot H_S}}_{\text{velocity-ratio}}. \tag{3.21}$$

The product $n_C \cdot H_S$ is half the plunger velocity given by Eq. (3.9). Compressibility effects are neglected. For a given pump configuration, this equation links operating pressure and nominal volumetric flow rate to the nozzle arrangement. The use of ε for system optimisation was in detail discussed by Momber (2000a). The following relationship can be derived from Eq. (3.21):

$$d_N \propto p^{-1/4}. \tag{3.22}$$

This relationship can be used to control nozzle wear. If nozzle diameter increases due to wear, operating pressure in the pump drops. Because operating pressure can be measured easily on-line, it is a suitable control parameter.

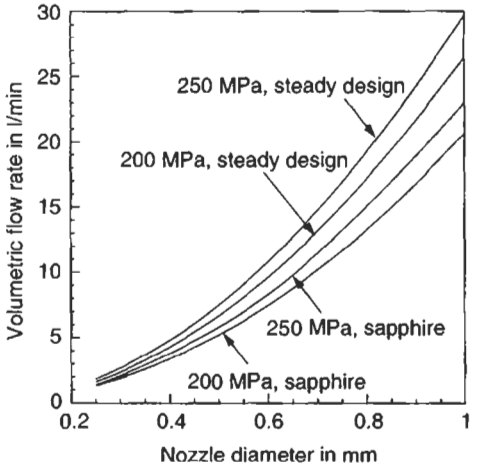

Figure 3.25 Relationship between nozzle diameter, pump pressure, nozzle type and volumetric flow rate.

3.6.2.2 Optimum nozzle arrangement

If losses in pump, hose line and tool are neglected and the entire cross section is optimally distributed over several orifices or nozzles, the ideal case $\varepsilon = 1$ occurs. The optimum cross section is then

$$A_N = N_N \cdot \frac{\pi \cdot d_N^2}{4} = 0.265 \cdot \frac{\dot{Q}_N}{p^{1/2}}. \tag{3.23a}$$

In that equation, $\dot{Q}_N$ is in l/min, p is in MPa, and A_N is in mm^2. See Fig. 3.26 for a graphical solution. The optimum nozzle diameter is

$$d_N^* = \left(\frac{4 \cdot A_N}{\pi \cdot N_N}\right)^{1/2}. \tag{3.23b}$$

Here, d_N^* is in mm. However, the case $\varepsilon = 1$ (which is characterised by any solid line in Fig. 3.26) is rather unusual in practice. The following, more realistic cases can be distinguished:

(i) $\varepsilon > 1$; $d_N > d_N^*$; this case could happen for a worn (Fig. 3.24) or broken nozzle (Fig. 3.22c–d). In a system without response, operating pressure drops according to

$$\Delta p = p \cdot \left(\frac{1}{\varepsilon^2} - 1\right). \tag{3.24}$$

(ii) $\varepsilon < 1$, $d_N < d_N^*$; this case could happen due to nozzle clogging. In a system without response, a safety valve opens and bypasses a certain amount of

the volumetric flow rate given by

$$\Delta\dot{Q}_N = (1 - \varepsilon) \cdot \dot{Q}_N. \tag{3.25}$$

(iii) $\varepsilon \neq 1$; this is due to the restriction of commercially available nozzle diameters.

These cases are illustrated in Fig. 3.27. Many operators are practising the case (ii) because they assume that the initial wear of the nozzle, that increases the nozzle

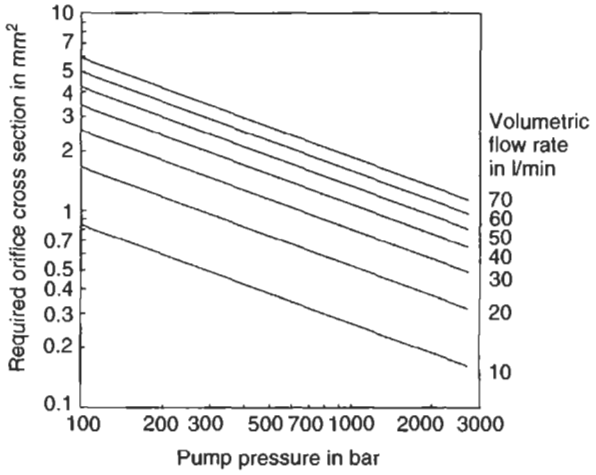

Figure 3.26 Typical nozzle cross sections for hydroblasting tools.

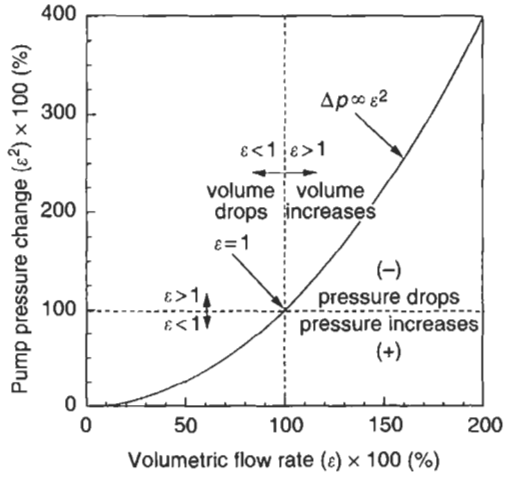

Figure 3.27 Optimisation scheme for hydroblasting systems (Momber, 2000a).

diameter step-by-step, will later guarantee optimum performance conditions ($\varepsilon = 1$). Table 3.9 lists results of comparative calculations for a typical hydroblasting system. Note the increase in hydraulic efficiency if a hydroblasting equipment with response is used. The situation improves further if systems with direct on-line control of the crank-shaft speed are used. These systems vary the crank-shaft speed according to the following equation:

$$n_C^* = \varepsilon \cdot n_C. \tag{3.26}$$

The control parameter is usually the operating pressure measured with pressure gauges directly at the pump (see Eq. (3.22)). If Eq. (3.21) is set to $\varepsilon = 1$, any change in the operating pressure can be compensated through Eq. (3.26).

3.6.2.3 Performance ranges

Equation (3.20) shows a hyperbolic relationship between orifice diameter and orifice number. In Fig. 3.28 for a hand-held gun used for hydroblasting, each hyperbola is a

Table 3.9 Optimisation of a hydroblasting system (see Momber, 2000a) $n_C = 398\ \text{min}^{-1}$, $H_S = 95$ **mm**, $N_P = 3$, $d_P = 16$ **mm**, $p = 200$ **MPa.**

Parameter	$\varepsilon < 1$		$\varepsilon > 1$	
	Without response	With response	Without response	With response
ε	0.785	0.943	1.129	1.055
Δp in MPa	+124.5	+25	−43.1	−20
$\Delta\dot{Q}$ in l/min	4.3	1.2	–	–
ΔP_H in %	21.5	6.0	21.5	10

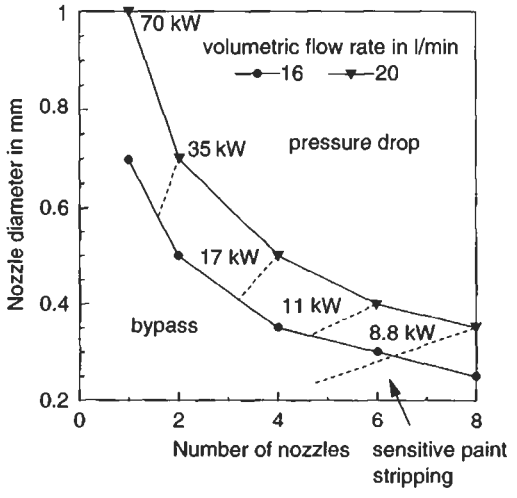

Figure 3.28 Application chart of a typical hydroblasting nozzle carrier; $p = 200$ MPa; drive: pneumatically driven, $\omega_T = 2500\ \text{min}^{-1}$.

line of constant orifice cross section (or constant volumetric flow rate, or constant hydraulic power, respectively). The resulting performance ranges are of great practical importance.

In the case $N_N = 1$, the entire hydraulic energy delivered by the pump is focused in one jet that possesses a high kinetic energy (in the considered case: $E_J \cong 16$ Ws). This is very favourable for performing heavy material removal work, such as removing thick protective coating systems. However, this variant is not suitable for selective paint stripping as there is a risk that the underlying material layer will be damaged. Therefore, the hydraulic energy can be divided into several portions by using several nozzles or orifices (in Fig. 3.28: up to 8 nozzles). In the case of 6 nozzles, 6 jets having a notably lower kinetic energy ($E_J \cong 2.4$ Ws each) are formed that work very gently and do not damage any underlying material. Note that this figure also contains two regions 'pressure drop' and 'bypass'. These regions correspond to the cases (i) and (ii), respectively, as defined in Section 3.6.2.2.

3.7 Vacuuming and Water Treatment Systems

3.7.1 Vacuuming and Suction Devices

Vacuuming and water treatment systems will soon become a standard requirement for an environmentally successful application of hydroblasting systems. However, commercial systems are already developed. Figure 3.29 shows vacuuming units designed for hydroblasting tools that perform at an operating pressure up to 200 MPa and volumetric flow rates between 10 and 40 l/min. The unit shown in Fig. 3.29(b)

(a) Low volumetric flow rate (Hammelmann GmbH, Oelde).

(b) High volumetric flow rate (WOMA GmbH, Duisburg).

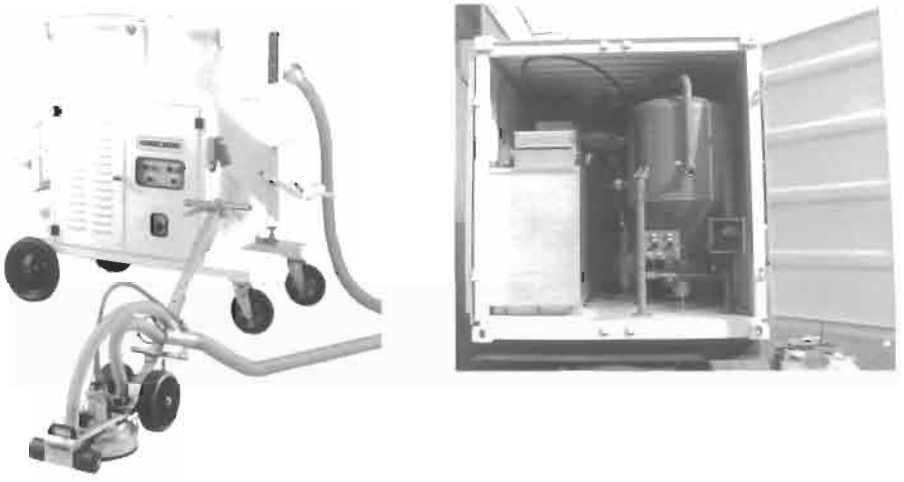

Figure 3.29 Vacuuming devices for hydroblasting applications.

consists of a drive (usually) electric, a vacuum pump (liquid-ring-pump) and a 2 m^3-vessel with level control for contaminated water. At a pressure of 5 bar, the maximum vacuum is about 50%. The unit requires a drive of 29 kW. It is containerised and can be connected directly to water treatment systems.

3.7.2 Water Treatment Systems

A modular system for the treatment of waste water from cleaning and surface preparation operations is illustrated in Fig. 3.30. It can be installed in a mobile version as well as containerised. The basic accessories of the system are:

- bypass-channel compressor;
- vacuum vessel for temporary storage of the suspension;
- buffer vessel as a catcher;
- double-diaphragm pump for the transport between buffer vessel and reaction vessel;
- sand filter;
- activated carbon filter;
- double-diaphragm pump for pumping the water through the filter;
- compressor;
- precipitation/flocculation agent;
- containers for the disposal of the final products.

Figure 3.30 Modular water treatment system for hydroblasting applications (WOMA Apparatebau GmbH, Duisburg).

Table 3.10 Technical parameters of the water treatment system shown in Fig. 3.30.

Parameter	Data range
Suspension throughput	800–2500 l/h
Filter cake moisture	25–30%
Required space	ca. 9 m^2
Empty weight	ca. 1000 kg
Feeding device	plug 380 V/50 Hz

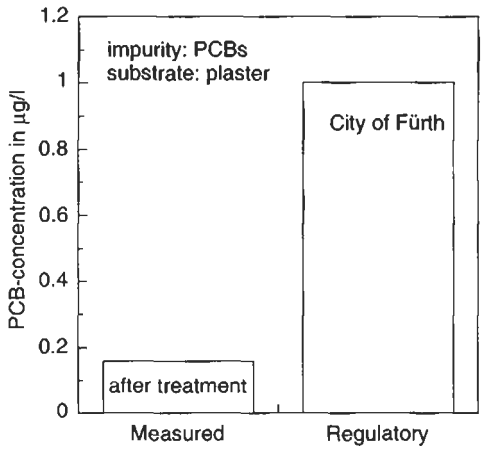

Figure 3.31 Efficiency of water treatment system shown in Fig. 3.30.

The technical characteristics of the water treatment system are listed in Table 3.10. The efficiency of the system is illustrated in Fig. 3.31. The suspension consisting of jetting water and removed paint or rust particles is sucked off by a bypass-channel compressor directly at the water tool, and is collected in the vacuum vessel. The suspension is then pumped into a reaction vessel by a diaphragm pump. In order to avoid the sedimentation of the solid particles, the pulp is permanently moved by an agitating machine. During the agitating period, a precipitation/flocculation agent is metered. After the agitation, the sedimentation of the slurry in the reaction vessel starts. Via a clear-water outlet and a slurry outlet, the suspension enters the band-pass filter. During the filtration, a vacuum is generated at the filter fabric by two air-driven diaphragm pumps. The water that is cleaned due to the filtration, is pumped into the sewage by the diaphragm pump via a filter based on sand or on activated carbon, respectively. The solids separated during the filtration generate a filter cake on the fibrous web. This cake is removed by a peel-knife and falls into a catcher.

CHAPTER 4

Steel Surface Preparation by Hydroblasting

4.1 Efficiency of Hydroblasting

4.1.1 General Aspects

Numerous factors affect the efficiency of hydroblasting processes. Experience shows that the most important factors are the following:

(i) existing coating type, adhesion and condition;
(ii) experience and organisation of the working crew;
(iii) geometry and accessibility of the objects.

The first aspect is illustrated in Fig. 4.1: the influence of the coating system on the efficiency can be seen clearly. These results, however, apply to repair work only. In case of new construction, efficiency depends in particular on type and thickness of mill scale.

The second aspect is illustrated in SSPC-SP 12/NACE No. 5 (2002) as follows: 'Regardless of the surface conditions, production rates usually improve when: (a) The operator gains additional experience with high- and ultrahigh-pressure water jetting, or (b) Mechanized, automated water jetting is used.' Similarly, ISO 12944-4 states the following: 'Personnel carrying out surface preparation work shall have ... sufficient technical knowledge of the processes involved.' The problem is discussed by Kuljian and Melhuish (1999) who found that experienced crews can be twice as productive as inexperienced crews. Experience from on-board hydroblasting has shown that skilled operators can outperform inexperienced operators even by a factor of 3 to 4 in terms of cleaning rate (Kierkegaard, 2000). Observations made with other cleaning

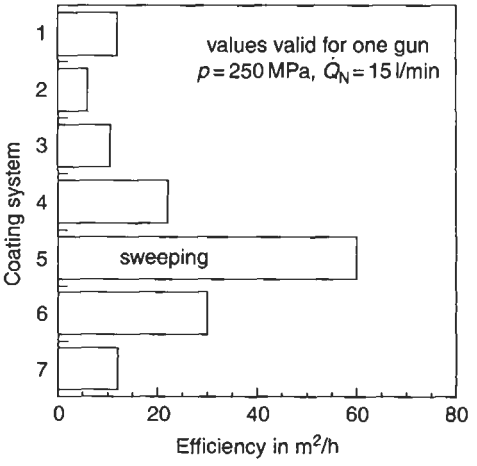

Figure 4.1 Coating system influence on hydroblasting efficiency (Calder Ltd., Worcester, UK). 1, Interguard epoxy + Intervinux acrylic; 2, Intershield epoxy + Intervinux acrylic; 3, Interswift antifouling + Intershield epoxy; 4, Interswift fouling, only leaving Interturf tie coat and anti-corrosive intact; 5, Heavy flash rust; 6, Interprime + Interlac alkyd on topside area of bow; 7, Multiple coats of alkyd or chlorinated rubber on deck areas. (Paint trade names according to International Paint).

operations, such as casting cleaning or tube bundle cleaning, show that not only experience of an operator, but also special training and education, counts for higher efficiency. In the case of pipework cleaning, the cleaning rate nearly doubles if an untrained operator is replaced by a graduate operator (Swan, 1983). An interesting superposition of efficiency parameters (i) and (ii) is outlined in SSPC-SP 12/ NACE No. 5 (2002): 'New metal with tightly adhering mill scale requires the highest level of operator skill and concentration to produce a clean surface by water jetting. Older, more corroded, or previously coated surfaces require an average level of skills and concentration to achieve desired results.'

For the treatment of complex geometries, such as communication towers, the following main factors were found to affect hydroblasting efficiency (Holle, 2000):

- location and access within the containment;
- size and shape of existing members.

The complex geometry of such structures is the reason for rather low efficiency values; for the hydroblasting of typical complex structure with a surface of ca. 24,000 m^2 they range between 2.2 and 7.6 m^2/h (Holle, 2000). Other examples on the influence of working configuration are reported in NSRP (1998): hydroblasting the cramped flat underbottom of a ship is at least twice as slow as removing the same coating system on the flat vertical side of an underwater hull. Similarly, manoeuvring inside a heavily stiffed internal tank can certainly slow down an operation. These restrictions, however, apply to dry grit-blasting as well. A detailed investigation showed that only 25–30% of the interior limited access surface could be cleaned by grit-blasting; also profile depth was only 85% of the values generated during normal grit-blasting procedures (Bullard *et al.*, 2002).

4.1.2 Aspects of Site Management and Operators' Fatigue

Job management has a notable effect on efficiency especially if the job environment is not a stable factor in hydroblasting. Here, experience is again an issue. However, other problems are of importance as well, namely the following (ASE, 2001):

- Work delay occurs while operators are waiting for broken equipment to be repaired.
- Preventive maintenance is being performed during the blast shift and subsequently displaces operators who would be blasting regularly.
- Relocating a high-pressure unit is often a timely process. The qualified technician must evaluate the desired location of the pump, search for a suitable power source and obtain the connecting cables before work can continue.
- Electrical outages and power supply problems disrupt entire teams during operation. When electrical services on the dock are interrupted, qualified technicians must be utilised to restart the units.
- Lack of hose management causes significant delay time.

- Dressing in and inspecting personal protective equipment is a time consuming function of the manual operator.
- Cranes are often unable to make lifts at night due to poor lighting. Therefore, high-pressure units and other equipment cannot be moved at appropriate speed.

A further aspect that affects efficiency is operator fatigue, especially if the hydroblasting equipment is run manually. Typical problems associated with fatigue were investigated in an extensive site study (ASE, 2001). They can be summarised as follows:

- Various lengths of the water-filled high-pressure hose are supported fully by the operator as he works. Both the weight of the hose itself and the pull from horizontal friction increase the fatigue.
- The weight of the hydroblasting gun is fatiguing to the operator; this weight is completely supported by the arms of the operator.
- Two triggers of equal size, aligned in a linear plane place additional strain on the operator.
- In order to reach surfaces behind obstructions, an operator is forced to position his gun in awkward angles.
- Operators often lock their bodies into a static position to stabilise against the jet reaction force. This puts intense strain on the lower extremities. This strain is magnified if the operator stands in a basket on a high-reach.
- While blasting overhead in areas with low clearance, the operator is often forced to a squatting position to blast; this directs forces to the knees.
- Working in overhead areas with tall clearances, the operators are often forced to reach overhead with the water tool to make contact with the surface. This compounds forces in the elbows and shoulders.
- Operators are often uncomfortable due to high humidity (which exists, e.g., under ships or in tanks).
- Operators are often uncomfortable due to cumbersome personal protective equipment which can become saturated (pads and linings collect the blast water in the air and add weight to the equipment).
- Operators often have their vision obstructed by fogged safety glasses. Hydroblasting on days with elevated temperatures and humidity can lead to condensation on most glass and plastic surfaces.
- Operators often have their vision impaired by poor lighting at night.
- Operators often do not practice sound ergonomic principles as they perform their duties.
- Operators experience decreases in productivity as their shift progresses. Even after standard breaks, production at the end of the shift is significantly less than at the beginning.

Major conclusions drawn from these observations are that the use of ergonomic training (which may be done by contractors) and the development of ergonomic support devices (which may be done by manufacturers) will lead to increased productivity.

4.1.3 Efficiency Studies

An extensive investigation about the productivity and efficiency of hydroblasting processes was performed by the US Navy (NSRP, 1998). This report subdivides the paint removal processes into the following tasks:

- selective stripping;
- sweeping and spot blasting to bare metal;
- coating removal to bare metal.

Efficiency is defined as

$$E_C = A_C/t_B. \tag{4.1}$$

Here, t_B is the actual blasting time, where the blaster crew is working with open nozzles. The real working time was also estimated during the job observations as follows:

$$t_W = t_B + t_D. \tag{4.2}$$

The parameter t_D characterises nozzle down time (operator's rest, maintenance, etc.). Figure 4.2(a) displays results from selective paint stripping. Notable differences can be seen between the individual preparation jobs. If freeboard and underwater hull are compared, efficiency is higher for underwater hull stripping. Comparative test showed an extremely high efficiency (up to 72 m^2/h) at outer hulls where semi-automatic methods were used. A very interesting result appears, however, if efficiency and working time are compared. Whereas blasting time is at a more or less constant level (see Fig. 4.2(b)), efficiency varies in a wide range. Average blasting time is about 82%, which means a nozzle-off time of about 18%.

Figure 4.3 displays results for removal involving a sweep and spot blast to bare metal. Corroded areas were spot blasted to bare metal. The efficiency of these preparation jobs

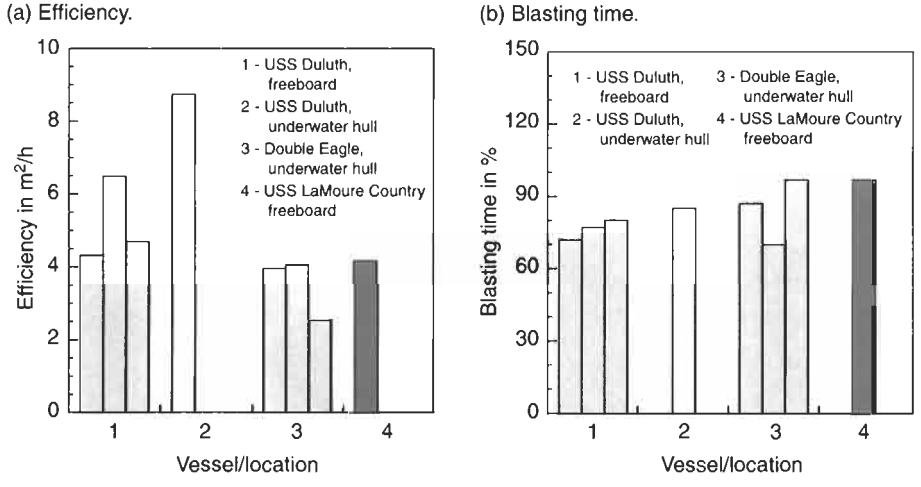

Figure 4.2 Efficiency of selective paint stripping (NSRP, 1998).

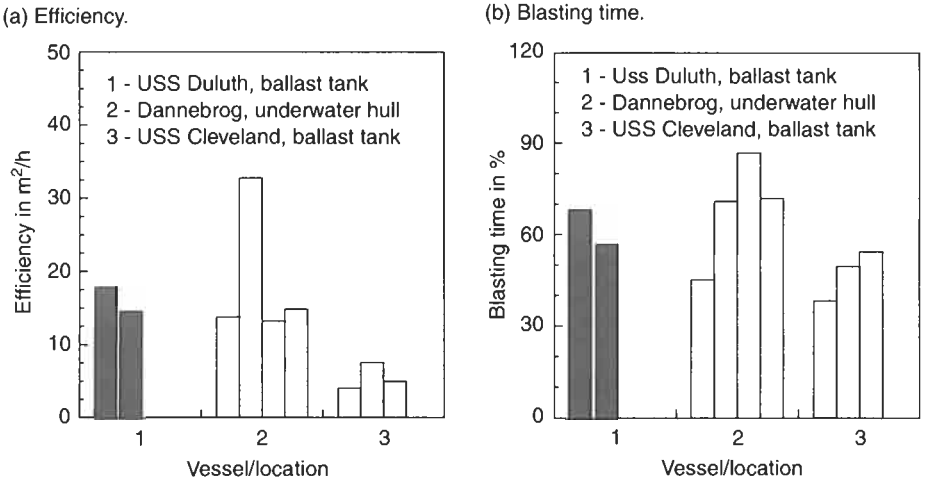

Figure 4.3 Efficiency of sweeping and spot blasting (NSRP, 1998).

is rather high (Fig. 4.3(a)) which agrees with the results in Fig. 4.1. However, the efficiency for the ballast tank sweeping (1) is surprisingly high considering the very special geometrical conditions in such tanks. Group (2) exhibits results from the removal of damaged shop primer during new construction. The differences in the efficiency are due to the variations in primer thickness (ranging from 13 to 51 μm). Again, no relationship between efficiency and blasting time can be seen. However, blasting time is rather low for the ballast tanks jobs; the average value is 53% (Fig. 4.3(b)). Fatigue of the worker is quite high for ballast tank stripping which is characterised by complex geometries, poor visibility, high moisture content and heat. This may be the reason for the high nozzle-off time of about 47%.

Figure 4.4(a) illustrates the efficiency for complete coating removal to bare metal. All jobs were performed with mechanical blasting units. The first data group (1) contains production runs of flight deck non-skid removal with a closed-loop hydroblasting unit. The group (2) shows results obtained with a fully automated blasting system. The graph verifies very high efficiency values for such a system. Odwazny *et al.* (2002) reported that robotic machinery can increase production rates up to 300% compared to gun-operation. It must, however, be noted that machines of this type comprise rather high volumetric flow rates, several times higher than usually applied for a hand-held gun. Although the nozzle-off times (an average value is 27% from Fig. 4.3(b)) are notably lower than those for ballast tank stripping, they are higher than the nozzle-off times of the gun-jobs displayed in Fig. 4.2(b).

The following production rates can be assumed based on the results of NSRP (1998):

- Average production rates for selective stripping of outer hull coatings with open-circle, hand-held guns range from 3.5 to 8.0 m^2/h per gun.
- Average production rates for sweeping and spot blasting inside of tanks with hand-held guns range from 14.4 to 15.4 m^2/h per gun.
- Average production rates for sweeping and spot blasting of outer hull coatings with hand-held guns is 17.8 m^2/h per gun.

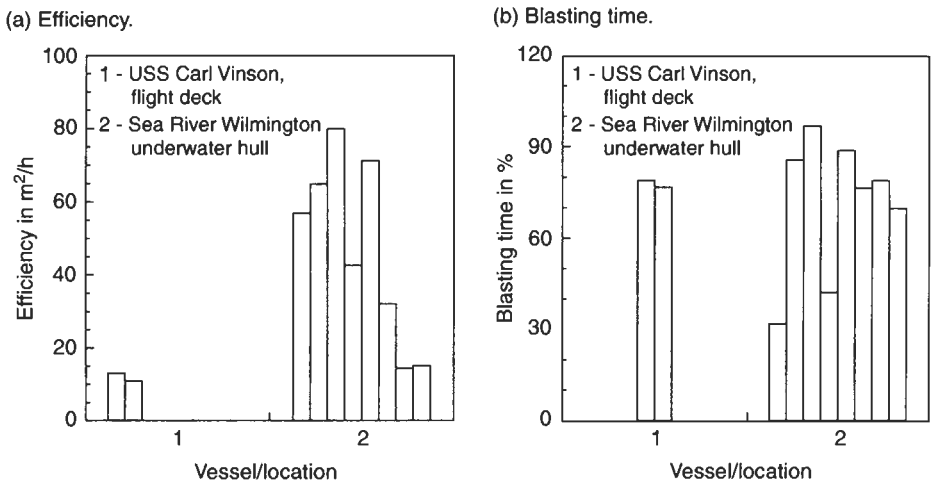

Figure 4.4 Efficiency of coating removal to bare metal (NSRP, 1998).

Table 4.1 Efficiency of coat stripping with hand-held tools (Da Maia, 2000); $p = 210$ MPa, $\dot{Q}_N = 2 \times 21$ l/min.

Day	Areas in m^2	Working time in h[1]	Productivity in m^2/h
Poop deck			
1st day	70	7.4	9.46
2nd day	224	23.7	9.45
3rd day	166	18.2	9.12
Total	460	49.3	9.33
Hatch covers (quality: Dw3[2]; layer thickness: 300 to 600 µm, damaged)			
1st day	90	9.2	9.78
2nd day	385	39.9	9.65
3rd day	405	50.1	8.08
4th day	530	49.9	10.62
5th day	385	43.3	8.90
6th day	444	38.4	11.56
Total	2239	230.8	9.79

[1]Gun-hours.
[2]See Table 6.2.

- Average production rate for the complete removal of severely damaged outer hull coatings using open-cycle hand-held guns is 13.7 m^2/h per gun.
- Average production rate for the complete removal of non-skid flight deck down to bare metal using a closed-loop machine is 12.1 m^2/h per gun.
- Average production rate for the complete removal of outer hull coatings down to bare metal using an open-cycle self-contained machine is 42.4 m^2/h per gun.

Another aspect is illustrated by the results listed in Table 4.1. It seems that the total area to be treated and the working day do not influence efficiency. Table 4.2 lists

Table 4.2 Production rates from robotic non-skid removal from aircraft carrier decks (Anonymous, 2002b).

Robot type	Total removal in m^2	Average production in m^2/day
48-in cut robot	3844	268
24-in cut robot	2304	148
Articulating No. 1	2579	163
Articulating No. 2	227	17
Total	8954	596

productivity rates obtained from non-skid coatings from aircraft carrier decks. This job was accomplished using articulating head robots, similar to the device shown in Fig. 3.16(c), as well as semi-automated vacuum attached robots (see Fig. 3.16(d)). The production numbers listed in Table 4.2 are from a 15-day period.

4.2 Cost Aspects

4.2.1 General Investments

Hydroblasting consumes a notable part of refurbishment budgets. A typical value for a 28,400 m^2 project is 42% (Trotter, 2001). For comparison: paint supply cost = 22.1%; painting cost = 20.7%; scaffolding cost = 15.1%. Some investment features for a typical hydroblasting system are shown in Table 4.3.

4.2.2 General Cost Structure

A general cost structure may include the following positions:

- investment high-pressure unit;
- investment high-pressure tools;
- investment nozzle carrier heads;
- investment water treatment system;
- nozzle wear;
- fuel (or electricity, respectively);
- fresh water and sewage;
- operators' wages.

Figure 4.5 illustrates general relationships based on the assumptions made in Table 4.3. The major amount of the cost is covered by operator's wages. This situation will, however, change if mechanical or robotic machinery is applied, which will in turn increase investment cost. Fuel also consumes a notable cost; this is, however, an energy optimisation problem. It may be noted that this cost can be lowered if pressure

Table 4.3 Typical hydroblasting investments.

Equipment	Investments		Hourly costs	
	in €	in %	in €/h	in %
High-pressure unit	100,000	59.5	37	57.8
Four high-pressure guns	10,000	5.9	4	6.2
Four nozzle carrier heads	8000	4.8	3	4.7
Water treatment system	50,000	29.8	20	31.3
Total	168,000	100	64	100

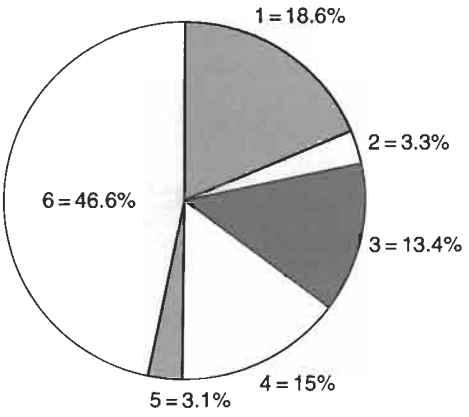

Figure 4.5 Cost structure of a typical hydroblasting system (gun operation). 1, Investment high-pressure unit; 2, investment gun, nozzle carrier, nozzles; 3, nozzle wear; 4, fuel (diesel); 5, water and sewage; 6, wages.

controlled units with direct response are used (see Section 3.6.2). Costs due to nozzle wear must be considered. The number of nozzles in a typical rotating nozzle carrier is 8, which gives a total number of 32 for the four guns considered for the calculation. The assumed average nozzle lifetime is 30 h. This value depends mainly on water quality.

A comparative cost structure for various surface preparation methods, namely grit-blasting and robotic hydroblasting, is listed in Table 4.4. It may be noted that the cost for fresh water and sewer water are not considered in that study.

A special case is hydroblasting application on ships at sea. This application is usually done with equipment hired during the period of journey. When calculating the cost of on-board maintenance in relation to similar costs in a shipyard, the simple price per square metre is not a sufficient indicator. The following comparison of the cost of doing the work in a shipyard and at sea is based on a bulk carrier with 32,500 m^2 of interior tank area to be cleaned (Kierkegaard, 2000). In the yard, the total cost is calculated at US$ 1,561,000. This includes the

Table 4.4 Cost structures of various preparation methods (Anonymous, 2002b).

Direct operating costs[1]	Preparation method	
	Grit-blasting	Robotic hydroblasting
Labour		
Crew required	20	6
Labour cost per man/h	20	40
Total labour cost/h	400	240
Total in m^2/h	200	200
Hours spent per 10,000 m^2	50	50
Total labour cost	20,000	12,000
Consumables		
Grit cost and disposal coat/h	1050	32
Fuel cost/h (machine)	117.5	48.80
Fuel cost/h (vacuum)	–	20
Fuel cost/h (filtration)	–	10
Jets cost/h	–	20
Wear cost (seals, nozzles, etc.)	–	10
Misc. filtration expenses cost/h	–	10
Hours spent per 10,000 m^2	50	50
Total consumables cost	58,360	7444
Equipment use/maintenance		
Diesel engine cost/h	25	10
Smaller engine cost/h	–	7.50
Compressor cost/h	187.50	–
Hours spent per 10,000 m^2	50	50
Total engine maintenance cost	10,625	875
Total cost to clean 10,000 m^2	88,985	20,319
Cost per m^2	8.90	2.03

[1]All cost in US$; surface quality: Sa2/HB2 (see Table 6.2.); grit consumption: 50 kg/m^2.

following cost:

- The cost of surface preparation and coating application (US$ 910,000), which is the cost per square metre (US$ 28/m^2) times the surface area to be coated.
- The cost of paint (US$ 156,000) applied at a dry film thickness of 300 μm.
- The off-hire cost (US$ 495,000) of having the ship in dock and not earning revenue, which is calculated by the ship's daily revenue rate (US$ 16,500) times the number of working days required (30 days in that case).

At sea, the total cost is calculated at US$ 1,170,000. This is calculated on the basis of a cost per square metre of US$ 36/m^2 times the surface area to be coated. This figure includes the cost of having the riding crew on board, the cost of surface preparation and coating application, as well as the paint cost. Therefore, the savings from on-board maintenance would be a maximum of US$ 391,000. The savings in off-hire cost is the primary economic benefit of performing coating maintenance at sea.

4.3 Problems of Disposal

4.3.1 Disposal of Solid Materials

4.3.1.1 General problems with waste disposal

Waste can result from a variety of activities related to surface preparation and coating work. Surface preparation, in particular, can produce a considerable amount of waste, mainly spent blasting media and old removed paint or rust products. Older paint systems especially contain hazardous materials, such as heavy metals, dioxine, PCBs, etc. A recent report stated that in the USA about 581,000 steel structures contain lead-based coatings, mainly highway bridges, rail bridges and oil tanks (Randall *et al.*, 1998). Typical examples for hazardous substances contained in paint systems are listed in Table 4.5. Most of these substances are not degradable; knowledge of their health (and disposal) risk is essential:

- lead is extremely poisonous;
- PCB has chronic toxic effects;
- tar derivatives are carcinogenic;
- chromium-containing dust causes cancer and alters DNA.

These substances can also irritate the skin and cause eczema. A major problem with the removal of these paint types is the contamination of air and soil. Chromium, for example, may affect micro-organisms and prevent the air exchange of the soil. Any blasting medium (solid or liquid) is contaminated with these substances. For spent abrasive materials, for example, the lead contamination level can be as high as

Table 4.5 Hazardous substance analysis of paint systems.

Substance	Content in paint (%)	Reference
Cadmium	0.014[1]	Dupuy *et al.* (2001)
Cadmium	0.003–0.01	Marshall (2001)
Chromium	0.86[1]	Dupuy *et al.* (2001)
Chromium	1.65	Holle (2000)
Chromium	2.99	Holle (2000)
Chromium	0.093–0.21	Marshall (2001)
Lead	0.31–13.5	Dupuy *et al.* (2001)
Lead	0.132–0.710	Marshall (2001)
Lead	6.14	Holle (2000)
Lead	11.11	Holle (2000)
Lead	14–20	Mickelsen and Johnston (1995)
PCB	0.12	Holle (2000)
PCB	0.16	Holle (2000)
Zinc[2]	80–85	Tinklenberg and Doezema (1998)

[1]Maximum values.
[2]Zinc rich paint.

840 mg/kg (Carlson and Townsend, 1998), the zinc contamination level can be as high as 37,000 mg/kg, and the cadmium contamination level can be as high as 13 mg/kg (Tinklenberg and Doezema, 1998). See Table 4.6 for potential concerns with abrasive waste from ship maintenance facility. Concentrations of leachable metals in spent abrasives that are of particular danger to groundwater are listed in Table 4.7. For these reasons, methods that prevent or reduce the uncontrolled formation of dry dust and do not generate solid waste are superior from the point of view of health and the environment.

A duty of care that addresses waste generation, control and disposal, which is a statutory duty that applies to producers, holders, carriers of waste, and those who treat waste, has four major aims (Abrams, 1999):

- to prevent any other person from depositing, disposing of, or recovering controlled waste (residential, commercial, industrial) without a waste management license or in a manner likely to cause environmental pollution or harm to health;
- to ensure that waste is safely and securely contained, both in storage and in transport, in such a way that it cannot escape;
- to ensure that if waste is transferred that it only goes to an authorised person;

Table 4.6 Concerns with abrasive waste from ship maintenance (Carlson and Townsend, 1999).

Metal	Direct exposure		Groundwater-leaching
	Residential	Industrial	
Arsenic	yes	possibly	no
Cadmium	no	no	no
Chromium	no	no	no
Copper	yes	no	possibly
Iron	yes	no	possibly
Lead	no	no	possibly
Nickel	no	no	no
Selenium	no	no	no
Zinc	no	no	yes[1]

[1]Compare Table 4.7.

Table 4.7 Leachable metals in spent abrasive (Tinklenberg and Doezema, 1998).

Condition	Leachable metals in mg/l					
	Arsenic	Zinc	Lead	Cadmium	Chromium	Copper
Virgin abrasive	<0.2	<0.3	<0.2	<0.05	<0.05	<0.1
Spent abrasive[1]	–[2]	770	0.23	0.01	–[2]	–[2]

[1]After zinc-rich paint removal.
[2]Results below detection limits.

- to ensure that when waste is transferred, there is a clear, written description of it so the person receiving the waste can handle it properly and safely without committing any offence.

The following steps are helpful to meet the obligations mentioned above:

- Identification of all types of activity involved in the project (e.g. paint removal; storage of chemicals, fuels and paints; application of paint).
- Identification of all sources of waste in terms of 'waste streams' (e.g. dry removed paint, blasting water, abrasive and its packaging, dust, chemicals and their packaging, wet paints, fuel), and the estimation of the quantities of waste from each process step prior to the job start.
- Determination of a means of handling and storing waste in order to control and minimise pollution risks. This could include the following:
  - Minimising the amount of abrasives or contaminated water which can be done by some type of containment with extraction if necessary;
  - Storage of contaminated waste in a properly bounded area;
  - Examination of transfer methods from the storage area to the waste contractor to minimise risk of spillage.

4.3.1.2 Comparative disposal studies

The absolute annual abrasive consumption in North America is listed in Table 4.8. The total consumption which is about 3.3 millions tons per year must be disposed or recycled, respectively. Figure 4.6 shows typical values for solid disposal measured during the treatment of a ship hull. The specific disposal rate is defined as the ratio between efficiency and solid particles collected during the treatment:

$$R_S = \dot{m}_S / E_C. \tag{4.3}$$

Therefore, the physical unit is kg/m^2. Grit-blasting generates a high amount of solids which is basically due to the abrasive materials spent for the surface preparation. The specific disposal rate increases if the desired surface preparation level increases. It is lowest for simple sweeping jobs and highest for a high-quality surface (Sa2.5). The low values measured during hydroblasting basically include the paint removed during the job. Note that the specific disposal rate doubles for the higher pressure level. This is

Table 4.8 Annual abrasive consumption in North America (Hansink, 1998).

Abrasive type	Consumption in tons per year
Silica sand	2,000,000
Coal slag	750,000
Copper slag	100,000
Steel grit	300,000
Staurelite	70,000
Garnet	30,000
All others	50,000

probably due to the higher requirements on surface quality (which was probably the reason to increase pump pressure up to 165%). Using average values for hydroblasting and grit-blasting, the specific amount of abrasives spent to remove a given mass of paint is about 60 kg/m^2. The values plotted in Fig. 4.6 are taken from a ship hull cleaning project. A typical value for steel bridge surface preparation by grit-blasting is 42 kg/m^2; in that case a surface of 120,000 m^2 was blasted with 5 tons grit (Ochs and Maurmann, 1996). Another example is reported by Kaufmann (1998): for a 10,000 m^2 highway steel bridge a total of 50 tons of grit was required; this corresponds to an abrasive consumption of 50 kg/m^2. More examples are listed in Table 4.9.

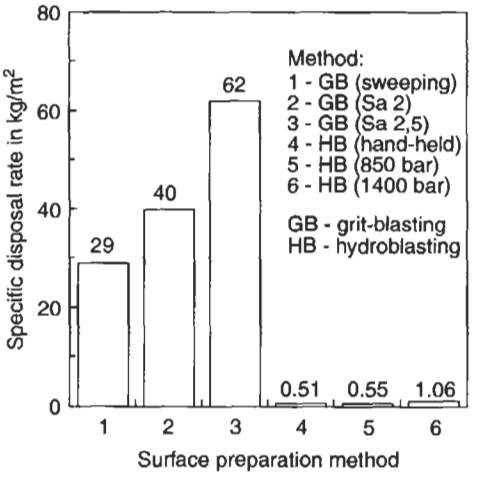

Figure 4.6 Disposal rates for ship hull treatment (Palm and Platz, 2000).

Table 4.9 Abrasive consumption during grit-blasting.

Abrasive type	Abrasive consumption in kg/m^2	Efficiency in m^2/h	Method	Reference
Copper slag	26.2	10.7	slurry blasting	Da Maia (2000)
Copper slag[1]	25.0	12.2	slurry blasting	Da Maia (2000)
Sand	22.3	9.2	slurry blasting	Da Maia (2000)
Bauxite	31.9	–	dry blasting	Uhlendorf (2000)
Coal slag	50	4	dry blasting	Cluchague (2001)
Copper slag	40	–	dry blasting	Beltov and Assersen (2002)
Dolomite	129.6	5.7	dry blasting	Andronikos and Eleftherakos (2000)
Garnet	108.6	10.5	dry blasting	Andronikos and Eleftherakos (2000)
Nickel slag	91.4	12.0	dry blasting	Andronikos and Eleftherakos (2000)
Olivine	105.6	8.7	dry blasting	Andronikos and Eleftherakos (2000)
Steel grit	40	–	dry blasting	Beltov and Assersen (2002)
Coal slag	12	8	thermo blasting	Cluchague (2001)

[1]Recycled.

A comparative cost calculation for the treatment of railway bridges by grit-blasting and hydroblasting was performed by Meunier and Lambert (1998). Using an average abrasive consumption of 40 kg/m^2, the following statements could be made:

- supplying abrasives before the blasting starts: 350 FrF/t (equivalent to 14 FrF/m^2) = 19%;
- recovery, transport of waste and discharge of abrasives (average distance 100 km): 24 FrF/m^2 = 32%;
- right to discharge abrasives according to Frech Class 1 (tax): 900 FrF/t (equivalent to 36 FrF/m^2) = 49%.

This corresponds to total cost of 74 FrF/m^2 (= 100%). It is interesting to note that about 50% of the costs are due to the disposal of the spent abrasive material only. In the case of hydroblasting, the spent water and the solid waste resulting from the removed paint (0.1–0.3 kg/m^2) only represented a cost of 2 FrF/m^2.

4.3.1.3 Paint chips

Typical specific chip disposal rates are between 0.3 and 1 kg/m^2 (see Fig. 4.6 and previous section). For the treatment of 3320 m^2 of a maritime construction, 2.7 tons of paint was disposed of; this is a disposal rate of 0.8 kg/m^2 (Uhlendorf, 2000). Kaufmann (1998) reported 14 tons of (zinc containing) paint slurry after the hydroblasting of a 10,000 m^2 highway steel bridge; this delivers a chip disposal rate of 1.4 kg/m^2. The precise value depends on the paint system, rust content and applied blasting equipment. The paint chips can easily be removed from the jetting suspension by solid–liquid-separators. The easiest, but also slowest method is to install suspension tanks. Table 4.10 lists results of a chemical analysis of solid waste from a ship hydroblasting project.

4.3.2 Disposal and Treatment of Water

4.3.2.1 Water consumption

The water consumption during hydroblasting basically equals the volumetric flow rate generated by the pump. This is a conservative approach because it is the actual

Table 4.10 Analysis of solid waste from hydroblasting (Rice, 1997) (paint system: several primer layers, two coats of anti-corrosive paint, four coats of antifouling paint).

Material	Concentration in mg/kg
Arsenic	<20
Barium	1950
Cadmium	<20
Chromium	234
Copper	296.000
Lead	217
Nickel	329
Selenium	<20
Silver	<20
Zinc	6700

volumetric flow rate of the nozzle system that must be considered. These relationships are discussed in more detail in Section 3.6.2. It is important to know that operating pressure and volumetric flow rate cannot be varied independently if a certain pump power is given (see Fig. 3.5). A rule of thumb is: the higher the pressure for a given pump power, the lower the volumetric flow rate.

A very appropriate parameter is the relative water consumption which relates the volumetric flow rate to the efficiency of the hydroblasting job:

$$W = \dot{Q}_A / E_H. \tag{4.4}$$

This parameter is given in l/m^2. Table 4.11 lists typical values for steel surface preparation (on ships) with single hand-held guns. Specific water consumption depends on the type and condition of coating, on-site conditions, on performance parameters of the hydroblasting system and on the tools used. Basically, automated equipment will consume less water per square meter than hand-held equipment. It must, however, be taken into account that about 30% of the water evaporates (Anonymous, 1997), mainly due to heat generation during the blasting process.

4.3.2.2 General regulations for sewage/river water

There are regulatory limits for waste water pollutants: these limits may differ from country to country. Table 4.12 shows the limits of various types of waste water

Table 4.11 Specific water consumption during ship hydroblasting (parameters: $p = 200$ MPa; $\dot{Q}_N = 20$ l/min; tool: hand-held gun).

Coating system[1] /blasting job	Water consumption in l/m^2
Interguard epoxy + Intervinux acrylic	85
Intershield epoxy + Intervinux acrylic	170
Interswift antifouling + Intershield epoxy	100
Interswift antifouling, only leaving Interturf tie coat and anti-corrosive intact	50
Heavy flash rust (removed by water jet sweeping)	17
Interprime + Interlac alkyd on top side area of bow	34
Multiple coats of alkyd or chlorinated rubber on deck areas	85

[1]Paint trade names according to International Paint.

Table 4.12 Limits of waste water pollutants[1] in rivers (Meunier, 2001).

Nature of the pollutant	Limit in kg/day	
	System A	System D
Material in suspension	20	5–20
Constant oxygen demand	120	30–120
Dissolved metals	1	0.1–1
Hydrocarbons	5	0.5–5

[1]Conditions: waterway flowing at >0.5 m^3/s and at least a kilometre away from a bathing zone or a potable water intake.

pollutants allowed by two systems in France for a waterway flowing at a volumetric flow rate of larger than 0.5 m^3/s. Table 4.13, in contrast, lists regulatory limits for the acceptance by a municipal sewer system. Therefore, any waste water from hydroblasting jobs must be treated appropriately in order to meet these and other regulatory limits. Tables 4.12 and 4.13 comprise different units for the pollutants. In flowing systems, such as rivers, the permissible limit is given in kg/day; the precise values depend on the volumetric flow rate of the river and the location of the blasting site. For municipal waste water devices, such as sewers, the limit is usually given in mg/l.

Filtration is the minimum treatment of water from hydroblasting sites. An example is shown in Table 4.14 for hydroblasting jobs at rivers (usually bridge

Table 4.13 Regulatory limits for water inlet in municipal sewers (City Frankfurt am Main).

Parameter	Limit
Temperature in °C	35
pH-value	6.0–9.5
Element limit in mg/l	
Cyanide (CN)	5.0
Solvents, organic	10.0
Solvents, halogenated hydrocarbons	5.0
Mineral oil and grease	20.0
Organic oil and grease	50.0
Phenols	20.0
Sulphates (SO_4)	400
Arsenic (Ar)	0.1
Lead (Pb)	2.0
Cadmium (Cd)	0.5
Chromium (Cr)	2.0
Iron (Fe)	20.0
Copper (Cu)	2.0
Nickel (Ni)	3.0
Mercury (Hg)	0.05
Selenium (Se)	1.0
Silver (Ag)	2.0
Zinc (Zn)	5.0
Tin (Sn)	3.0

Table 4.14 Daily levels of dissolved lead in wastewater at various sites (Meunier, 2001).

Date	Location	Levels in the mixture mg/l		Content in g/day[1]
		Before filtration	After filtration	
June 1997	Buzancais	–	3.5	58
July 1997	Buzancais	–	2.8	47
September 1998	Clion	4.32	1.75	38
September 1998	St Andre Cubzac	11.5	4.18	32

[1]Conversation from mg/l to g/d depends on volumetric pump flow rate, number of jetting tools and number of hours worked per day.

Table 4.15 Analysis of effluent after hydroblasting (Rice, 1997); see Table 4.10 for the analysis of the corresponding solid.

Material	Effluent in mg/l	Recycled water in mg/l
Arsenic	0.10	<0.10
Barium	17.3	0.14
Cadmium	<0.10	<0.10
Chromium	0.39	<0.10
Copper	19.7	0.11
Lead	<0.10	<0.10
Nickel	0.39	<0.10
Selenium	0.20	<0.10
Silver	<0.10	<0.10
Zinc	13.2	<0.10

Table 4.16 Lead level reduction due to waste treatment (Frenzel, 1977).

Treatment step	State	Lead level in mg/l
After jetting	Sludge	4.40
	Containment material	<5
After separation and resin filtration	Water	0.26
	Paint chips	0.41

surface preparation). After suitable filtration, the lead-containing water meets the requirements for dissolved metals as listed in Table 4.12. A further example for sewer systems is shown in Table 4.13 where the effluent qualities before filtration and after filtration are compared. The original effluent contains very high contents of copper and zinc which exceeds the limits given in Table 4.13. After treatment, the waste water meets the requirements (see Table 4.15). Similar problems often occur with lead containing paint systems. In a case where lead was involved (Frenzel, 1997), the jetting water and the sludge were vacuumed daily with filters and pumped into a three-stage water separator to remove the lead paint chips. Before discharge at the local waste treatment facility, the water was pumped through a resin filter, neutralised and transferred to a covered holding tank. Table 4.16 lists the treatment steps along with the corresponding lead levels. A table showing an equal trend is published by Dupuy (2001).

4.4 Safety Features of Hydroblasting

4.4.1 General Safety Aspects

ISO 12944-4 states the following for surface preparation in general: 'All relevant health and safety regulations shall be observed.' Hydroblasting has a high injury potential: high-speed water jets can damage skin, tissue, and – if abrasives are

involved – even bones (see Axmann *et al.*, 1998). General sources of danger to hydroblasting operators include the following (BGV, 1999):

- reactive forces generated by the exiting water jets (see Section 3.4.2);
- cutting capability of the high-speed jets;
- hose movements (especially during switch-on of the pump);
- working in areas of electric devices;
- uncontrolled escape of pressurised water;
- damaged parts being under pressure;
- dust and aerosol formation;
- sound emitted from equipment and water jet;
- impact from rebounding debris from the jet impact point.

To protect operators and those not directly in the blasting operation, the area around a work site that will be required for the hydroblasting operation must be defined. The boundary of this area must be clearly marked by the hydroblasting team, providing both a visible and a physical barrier to entry by unauthorised personnel. A typical example is shown in Fig. 4.7.

A pre-service and operational checklist for hydroblasting operations is recommended. This list should answer the following questions (WJTA, 1994):

Date: ...
Location: ...
Unit being cleaned ...

- Is the area, including the other end of the unit being cleaned, adequately barricaded, with proper warning signs posted (see Fig. 4.7)?
- Have precautions been taken to protect all electrical equipment?
- Is there any hazard to personnel from possible damage to equipment, such as release of corrosive chemicals, flammable liquids, or gases?
- Are all fittings of the correct pressure rating in accordance with regulations?
- Are all hoses of the correct pressure rating in accordance with regulations?
- Are all hoses in good operating condition?
- Are all fittings in good operating condition?
- Are all nozzles free from plugging and in good operating condition?
- Is the filter on the pump suction clean and in good operating condition?
- Is there an adequate water supply?
- Have precautions been taken against freezing?
- Do all personnel have the proper equipment for this job?
- Do all the personnel have the proper training for this job?
- Are all personnel qualified to perform this work?
- Has the complete hook-up been flushed and air removed from the system before installing the nozzle?
- Has hook-up, including pipes, hoses and connections, been pressure tested with water at the maximum operating pressure?
- Is the dump system operating properly (will it dump when released)?
- Are all control systems operational?

Figure 4.7 Warning (no entry) sign for hydroblasting site (Association of High Pressure Water Jetting Contractors, London).

- Is the location of first aid equipment and an emergency medical centre known?
- Has the job site been examined to determine if confined space entry requirements apply?
- Has the job been examined for environmental considerations, with action as appropriate?

It is also recommended to carry out a risk assessment of the actual environment where a hydroblasting job will be done before starting the job. This risk assessment may include (French, 1998):

- How access is to be gained?
- Is there a need for scaffolding?
- Is there confined space?
- What is the surface like where the operators will have to stand?
- The availability of daylight or artificial light.
- The presence of electrical supplies/equipment.
- Water source and its drainage.
- Nature of contaminant: Is it toxic? Is it a pathogen? Is it asbestos based? Is it harmful or corrosive?
- General layout that will allow visual contact between of the hydroblasting team.
- Permit requirements.

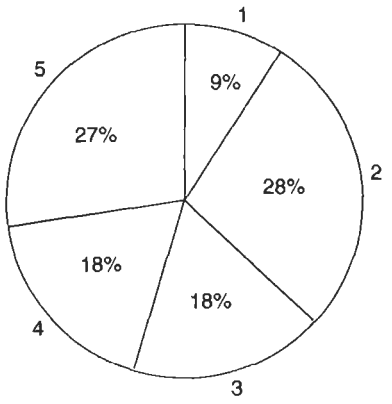

Figure 4.8 Percentage of operators involved in incidents (reference: AUSJET News, August 2000). Operator's experience: 1, 60 months; 2, 3 months; 3, 24 to 60 months; 4, 12 to 24 months; 5, 12 months.

- Safety of access (e.g. working on motorways or hazardous areas such as refinery where flameproof equipment and earthing to avoid static electricity may be required).
- Who or what will be affected by flying debris?
- Is noise a problem?
- Will containment be necessary?
- Where will the effluent go?

Statistics of incidents have shown that the average experience of operators affected their involvement in incidents. These relationships are presented in Fig. 4.8. It can be seen that the risk of incidents reduces if average experience increases. Operators, who have worked with hydroblasting equipment less than 12 months, were involved in 55% of all incidents. In that context, ISO 12944-4 states the following: 'Personnel carrying out surface preparation work shall have suitable equipment and sufficient technical knowledge of the processes involved.'

4.4.2 Emissions

4.4.2.1 Air sound emission

There are four major sources of air sound generated during hydroblasting operations:

- sound emitted from the pressure generating unit (pump, engine, power transmission);
- sound emitted from the high-speed water jet travelling through the air;
- sound emitted from the erosion site;
- sound emitted from accompanying trades.

State-of-the-art high-pressure plunger systems are regularly equipped with sound insulating hoods or even placed in containers. Thus, the air sound emission is limited

up to 70–75 dB(A). More critical is the air sound emitted by the water jet. This noise is generated due to friction between the high-speed jet and the surrounding air as well as due to turbulences. Thus, the sound level depends on the relative velocity between jet and air, and on the surface exposed to friction. Consequently, air sound level increases as pump pressure, nozzle diameter and stand-off distance increase. Some results of direct measurements shown in Figs. 4.9 and 4.10 verify these general trends. However, as shown in Fig. 4.9, the frequency of the sound generated plays an additional role. For rotating nozzle carriers, the very quick radial movement generates turbulences and flow interruptions further contributing to the noise. If a nozzle

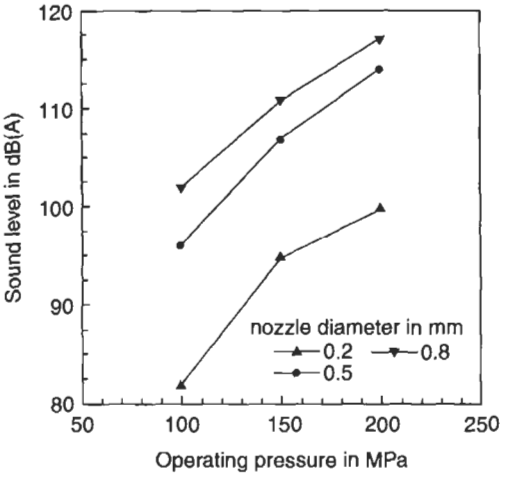

Figure 4.9 Pressure and nozzle diameter influence on sound level (Measurements: Werner, 1991a).

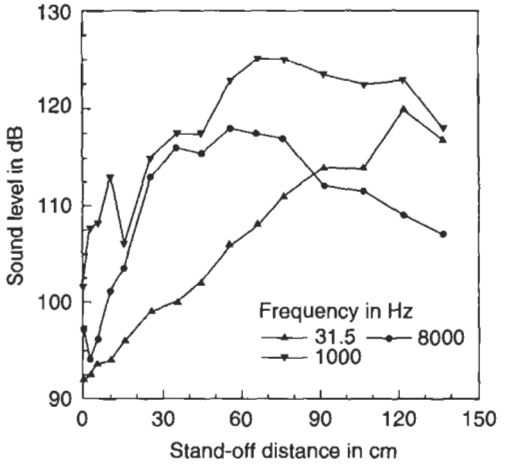

Figure 4.10 Influence of stand-off distance and frequency on sound level (Measurements: Barker et al., *1982).*

carrier comprises several small-diameter nozzles instead of one large-diameter nozzle, the total jet area increases and so does the noise level. That is why rotating devices usually generate rather high noise levels. It is reported (Barker *et al.*, 1982) that high amplitudes occur in the frequency range between $f_L = 1–8$ kHz, and at rather low impact angles (<30°). However, this seems to be true for small stand-off distances only (Fig. 4.10).

Figure 4.11 contains results of measurements performed at different blasting sites. One example from a hydroblasting site (Fig. 4.11(b)) is also shown. Note that the actual blasting jobs (dry grit-blasting, hydroblasting, shot blasting, wet blasting) generate the highest noise levels among all trades. Shot blasting (which works with shrouded blasting tools) and wet blasting are comparatively silent. Noise generated during hydroblasting can notably be reduced if shrouded or sealed tools are used (see

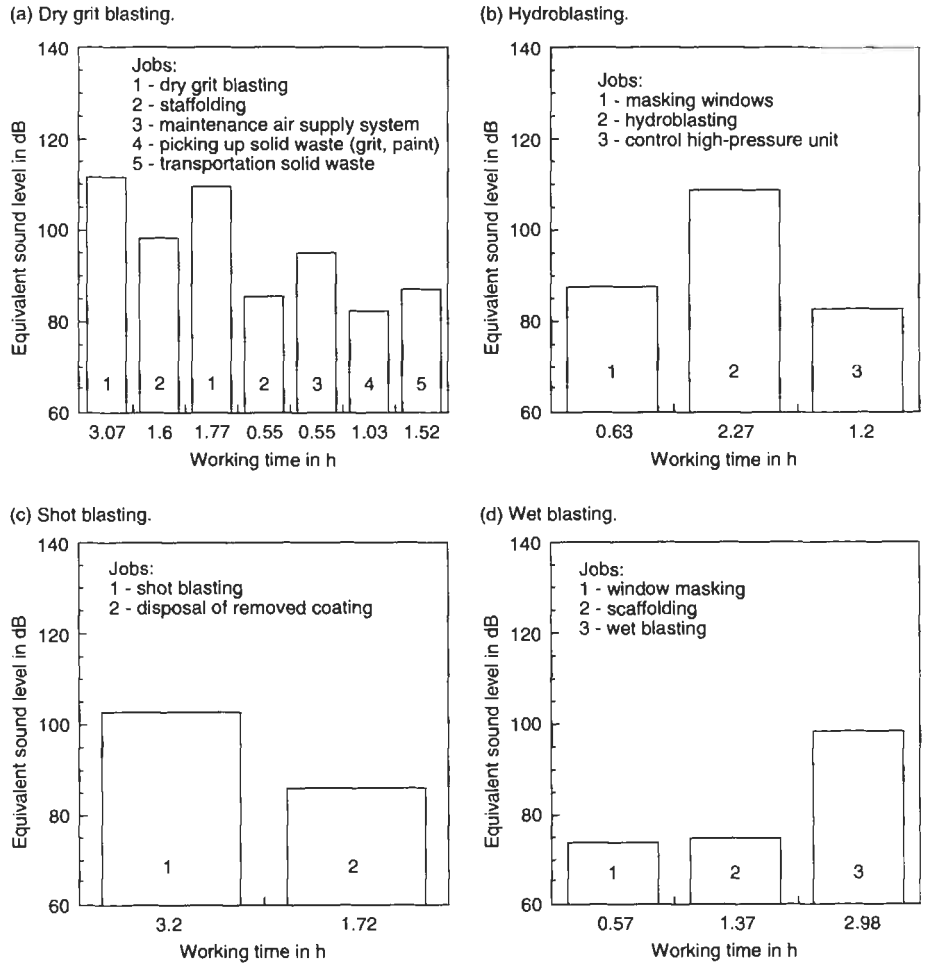

Figure 4.11 Results from noise-level measurements during steel surface preparation jobs (BIA-Report, 1997).

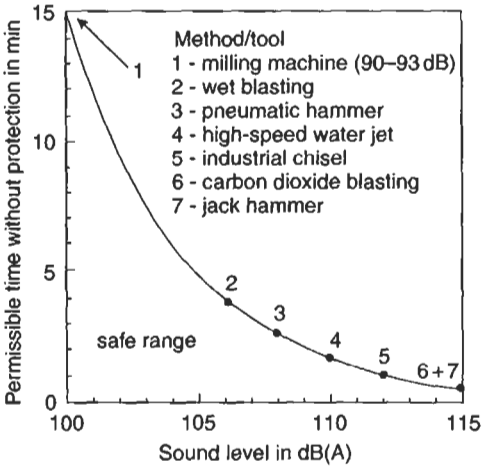

Figure 4.12 Critical exposure times for different preparation tools (solid line according to BGV (2001); points from different sources).

Fig. 3.16). The permissible air noise level depends on the exposure time. This is illustrated in Fig. 4.12 based on regularity limits stated in BGV (2001). It can be concluded from that graph that ear protection equipment must be worn by any personnel involved as hydroblasting operators (see Section 4.4.3).

4.4.2.2 Body sound

Body sound is a result of waves carrying noise and travelling through solid materials. Therefore, even if windows, doors, etc. are properly closed to lock out airborne noise, persons may anyway experience certain noise levels. This noise is generated due to vibrations; they occur during the tool impact and depend on the acoustic properties, especially on the sound velocity and the acoustic impedance, of both the material to be subjected and the preparation tool. The evaluation parameters of the vibration are its amplitude and its velocity (frequency).

There are some measurements available from concrete facades treated with different preparation tools. Amplitudes and vibration velocities generated by the tools are plotted in Fig. 4.13(a). It clearly illustrates the extremely low body sound generated during hydroblasting. Figure 4.13(b) shows that frequency and velocity of the vibrations are at a more or less constant level for hydroblasting, even if the distance from the vibration source varies significantly.

4.4.2.3 Aerosols and airborne dust

A mist of water, vapour and solid particles is generated during hydroblasting in the immediate environment of the operator. Unfortunately, this mist is difficult to control. The only way to prevent it is the use of shrouded tools (see Table 3.7 and Fig. 3.16). Another way to protect the operator is the application of mechanically guided

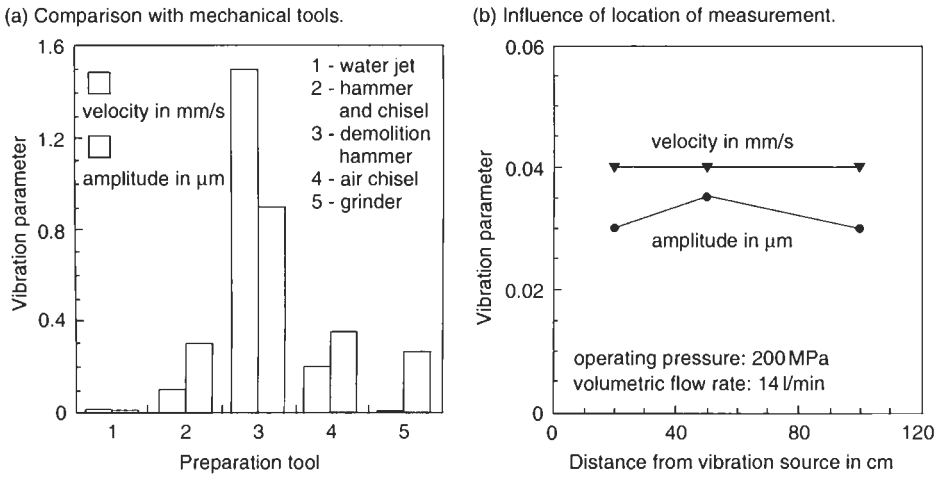

Figure 4.13 Results of body sounds measurements on facades (Werner and Kauw, 1991).

tools or robotic machinery. Anyway, both methods fail when it comes, for example, to a ballast tank or ship superstructure cleaning. A major problem is with aerosols that contain microscopically small particles from the removed coating. Because many old coatings contain lead, there is a critical situation as the lead may contaminate the operator's blood due to breathing the aerosol. There are the following two critical levels:

- Action Level (AL = 30 $\mu g/m^3$); if an operator works in an area that at or above that level, the employer must give medical surveillance and training in the hazards of working with lead.
- Permissible Exposure Limit (PEL = 50 $\mu g/m^3$); This limit is for the average amount of lead in the air over an 8-hour day.

Extensive studies have shown that airborne lead concentration does not depend on the main lead concentration in coating systems to be removed (DHHS, 1997); the correlation between these parameters is very weak (correlation = 0.22). It is, therefore, the surface preparation method that determines airborne lead. Blasters and painters are particularly endangered by lead exposure; this is verified by a comprehensive medical surveillance program designed to prevent lead toxicity in bridge workers, including blasters. Some results of these studies are shown in Fig. 4.14, and it can be seen that painters and blasters experience the highest blood lead levels among all job categories.

Air monitoring tests carried out by the Houston Harbour Authorities (Marshall, 1996) and the US Navy (Anonymous, 1997) have shown that the lead concentrations in aerosols generated during hydroblasting are below the regulatory levels. Some results are displayed in Fig. 4.15 and in Table 4.17. Note the low levels for the hydroblasting applications. The blood of hydroblasting operators was analysed during several lead paint stripping jobs; some results of pre-job and post-job blood lead

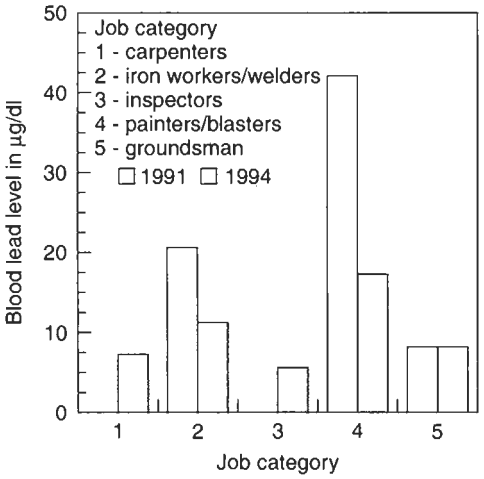

Figure 4.14 Blood lead levels for bridge workers (Maurer et al., *1995).*

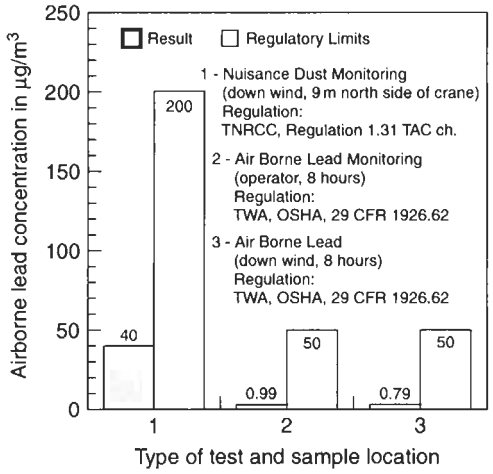

Figure 4.15 Air monitoring results from hydroblasting of steel cranes in a shipyard (Houston Port Authority).

level testings are shown in Fig. 4.16. Further results are reported in Anonymous (1997). Although the lead level increases during the blasting job, the regulatory limit is significantly undercut. Systematic lead concentration measurements were performed during the refurbishment of an old power plant for the first ten days (Dupuy, 2001). Fifteen samples were taken with only one above the 'no detection' level. The detected sample was 40 $\mu g/m^3$. Interestingly, the project management decided to remove any respirator requirements initially enforced during the job and to implement a random sampling as necessary to ensure personnel safety.

Table 4.17 Measured airborne lead levels for different preparation methods.

Object /condition	Lead level in $\mu g/m^3$	Reference
Hydroblasting		
Galvanised communication towers	1.5–29	Holle (2000)
Structural steel construction	2–12	Dupuy (2001)
Dock side container crane	2.2[1]	Marshall (2001)
Dock side container crane	0.79[1,2]	Marshall (1996)
Dock side container crane	<0.99[1,3]	Marshall (1996)
Slurry blasting		
Highway overpass structure	10.4–34.4	Anonymous (1998)
Steel bridge	45.7–305[3]	Frenzel (1997)
Steel bridge	40.1–52.7[4]	Frenzel (1997)
Vacuum blasting		
Steel bridge	27–76[3]	Mickelsen and Johnston (1995)
Grit-blasting		
Blast room	1–100,000	Adley and Trimber (1999)
Steel bridge (blaster)	36–4401	Conroy *et al.* (1996)
Steel bridge (sweeper)	12–3548	Conroy *et al.* (1996)
Steel bridge (foreman)	12–3423	Conroy *et al.* (1996)
Steel bridge (equipment operator)	39–1900	Conroy *et al.* (1996)
Steel bridge (helper)	22–501	Conroy *et al.* (1996)
Steel bridge (operator)	50–450[1]	Randall *et al.* (1998)
Petrochemical tank	3.31[1,3]	Frenzel (1997)
Ice blasting		
Steel bridge	175	Snyder (1999)

[1]TWA 8 hours.
[2]Downwind.
[3]Gun operator.
[4]Outside containment.

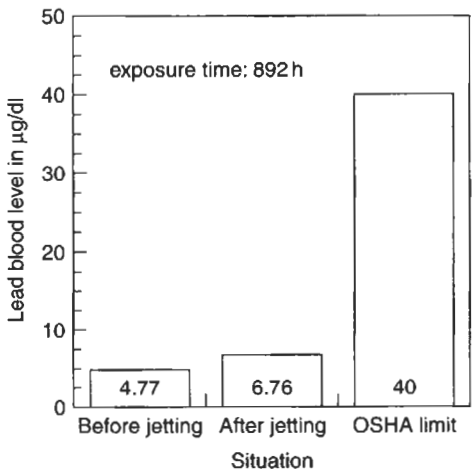

Figure 4.16 Results of lead blood level measurements (Frenzel, 1997).

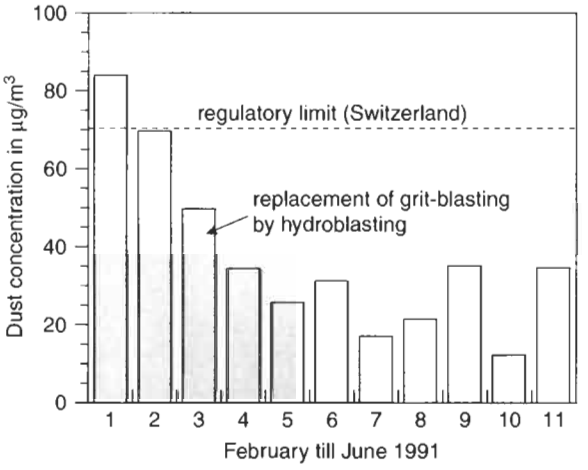

Figure 4.17 Long-term air monitoring during steel blasting (Kaufmann and Zielasch, 1998).

The mechanisms of how hazardous dust in aerosols are suppressed during hydroblasting are not completely understood. A 1995 report from the US National Institute for Occupational Safety and Health (NIOSH) on lead abatement hazards stated the following about hydroblasting: 'The water suppresses the dust by agglomerating the dust into the water droplets' (cited by Dupuy, 2001).

Kaufmann and Zielasch (1998) reported on long-term air monitoring during the refurbishment of a steel bridge in Switzerland. The job was started with grit-blasting. However, this method was soon replaced by hydroblasting, mainly because of the high dust emission that exceeded regulatory limits. This situation is illustrated in Fig. 4.17. Note that during the introductory phase of the project, where grit-blasting was applied, the legal limit of 70 $\mu g/m^3$ was exceeded. After grit-blasting was replaced by a hydroblasting method that featured a robotic tool as well as limited gun operations, the regulatory limit could be met during the entire project which lasted over three years (1991 till 1994). A similar situation is shown in Fig. 4.18 showing personnel air monitoring results from lead abatement on structural steel performed over a duration of one month.

Other problems associated with dust formation are illustrated in Fig. 4.19. A very high amount of working time is required to wrap and unwrap the object to be stripped (in the certain case a marine vessel) before and after grit-blasting, and to clean up the yard site after the blasting job. Several hundreds of additional working hours are required in the example shown in Fig. 4.19. For a ship hull of about 8000 m^2 five to seven day wrapping up the vessel using an eight-man crew would be required. Unwrapping would require another four to five days (Nelson, 1996).

4.4.2.4 Vibration effects on the operator

Vibrations generated over a longer period of time in the arms of operators may cause so-called 'white fingers'. The vibration generated by the tool is transmitted through

the operator's hand where it does damage to the blood vessels in the fingers (VDI, 1987). Therefore, regulations state minimum working hours depending on the intensity of the vibrations. The intensity is usually given by an acceleration value a_V. Results of measurements obtained from different surface preparation tools (including hydroblasting tools) are shown in Fig. 4.20. Note from this figure that any point above the solid line is critical to health. Exposure time is the total time for which vibrations enter the hand per day, whether continuously or intermittently.

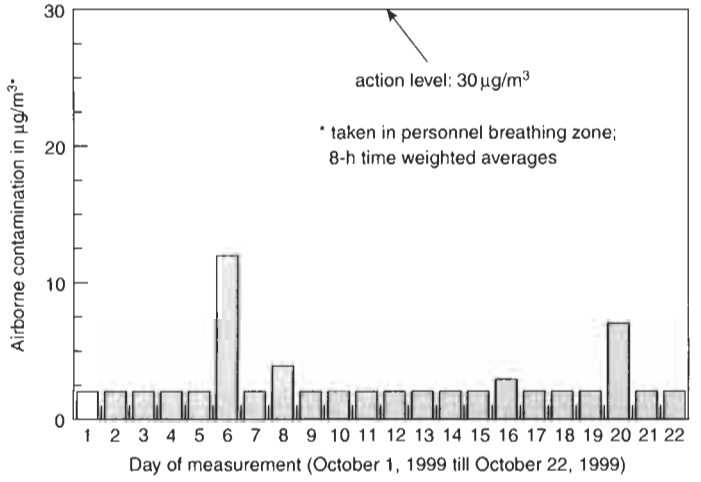

Figure 4.18 Air monitoring results obtained from lead abatement of steel by hydroblasting (measurements: Dupuy, 2001).

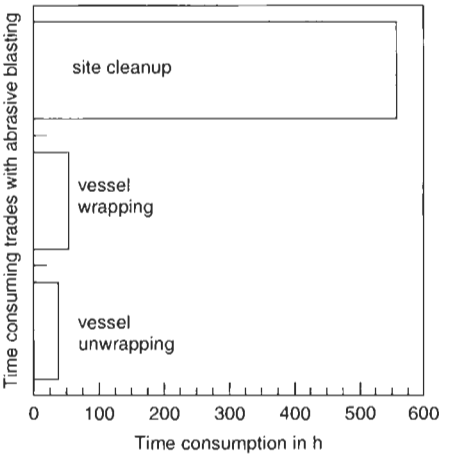

Figure 4.19 Additional working time in a shipyard due to dust formation (Navy cargo ship in a drydock).

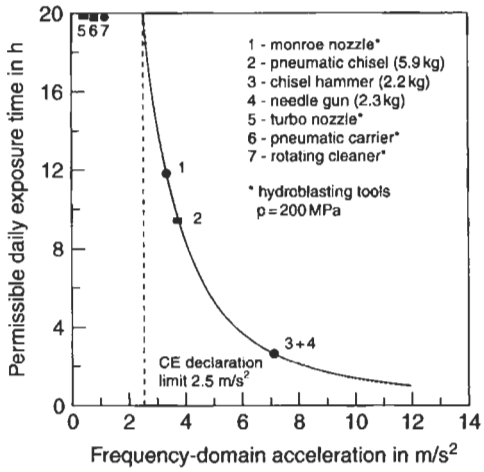

Figure 4.20 Limits for exposure of the hand per day to vibrations (solid line according to Siebel and Mosher (1984); points from different sources).

Acceleration values for hydroblasting tools are lower than those measured for mechanical tools. However, for hand–arm-vibrations the EC-machine guide requires the following:

- any value in excess of $a_V > 2.5$ m/s^2: the measured acceleration value must be stated in the tool manual (e.g. $a_V = 3.17$ m/s^2 for monroe nozzle);
- any value equal to or lower than $a_V = 2.5$ m/s^2: it must be stated in the tool manual that $a_V \leq 2.5$ m/s^2 (e.g. for the turbo nozzle, pneumatic carrier and rotating cleaner).

4.4.3 Risk of Explosion

Electric discharge sparks can be a source of explosion during hydroblasting. Safety hazard analyses identified that static electric charges occur in the following four circumstances (Miller, 1999):

- liquids flowing through piping at rates (velocity) greater than 1 m/s;
- liquids passing through fine filters or orifices;
- liquids being sprayed;
- liquids impacting fixed parts.

These conditions essentially describe the formation and use of high-speed water jets for hydroblasting. Charge generation is proportional to the square of the jet velocity and inversely proportional to the square of the liquid's conductivity. If electric conductivity of a liquid exceeds the value of 10^{-8} S/m, the risk of dangerous electric charges is very low (ZH 1/200, 1980). From this point of view, water can be considered a low-risk liquid (Table 4.18). However, this criterion cannot be applied to water

Table 4.18 Physical properties of liquids (ZH 1/200, 1980).

Liquid	Electric conductivity in S/m	Dielectric constant (20°C)
Diesel oil	10^{-13}	2
Gasoline	10^{-13}	2
Water (dist. in air)	10^{-3}	2.45
Water (clean)	$5 \cdot 10^{-3}$	2.45

sprays that are usually formed during hydroblasting applications. Even if water itself has a rather high electric conductivity, carrier concentrations of droplet clouds can reach critical values. Serious investigations about the explosion risk of water jets included tests with rather low operating pressures up to 50 MPa. It could be shown that density of volume charge of a water droplet cloud increased steeply with rising pressures up to a pressure level of 10 MPa. If this value was exceeded, density of volume charge remained on a saturation level of about 240 nC/m^3 for pressures up to 50 MPa (Post *et al.*, 1983).

If the following requirements are met for tank cleaning applications, hydroblasting is not critical from the point of view of electrostatics (Post *et al.*, 1983):

- metallic tanks; tank volume not larger than 30 m^3 (or tank diameter not higher than 3 m for conventional heights);
- maximum operating pressure of 50 MPa;
- maximum volumetric flow rate of 300 l/min;
- number of tanks;
- all parts must be connected to ground.

However, these criteria basically apply to low-pressure cleaning jobs and not to the paint stripping applications covered by this book.

4.4.4 Personnel Protective Equipment

Required personnel protective equipment for hydroblasting operators includes the following items (JISHA, 1992; WJTA, 1994; AHPWJC, 1995):

- Head protection (helmet): All operators shall be supplied with a safety helmet which shall be worn at all times while at the worksite. Where necessary the helmet should incorporate face protection (see Fig. 4.21(b)).
- Eye protection (goggles, face shield): Suitable eye protection (adequate for the purpose and, of adequate fit on the person) shall be provided to, and worn by, all operators (see Fig. 4.21(b)).
- Hearing protection (foam earplugs, earmuffs, strap with plastic earplugs): Suitable hearing protection shall be worn while in the working area; see 4.4.2.1 and Fig. 4.21(b)).
- Body protection (wet suit, reinforced safety suits): All operators shall be supplied with suitable waterproof protective clothing, having regard to the type of

(a) Wet suit, gloves, boots.

(b) Helmet with face and hearing protection.

Figure 4.21 Protective clothing for hydroblasting operators (photographs: WOMA GmbH, Duisburg).

hazards in relation to the work being undertaken (see Fig. 4.21(a)). This must be used where there is a risk to health or a risk of injury.

- Hand protection (rubber gloves, reinforced gloves): Hand protection shall be supplied to all team members and shall be worn where there is a risk of injury or contamination to the hands (see Fig. 4.21(a)).
- Foot protection (steel-toed boots): All operators shall be supplied with suitable boots or Wellingtons with steel toe caps, and where necessary additional strap-on protective shields (see Figs. 4.21(a) and 4.22).

These shall be worn when there is a risk of injury.

- Respiratory protection (sometimes with supplied air); see Section 4.4.2.3): Where necessary, suitable respiratory protection which is either type approved or conforms to an approved standard must be worn.

Typical personnel protective clothing and equipment for hydroblasting operators are shown in Figs. 4.21 and 4.22. Table 4.19 lists results of direct water jet impact tests on the body protection worn by the operator in Fig. 4.22. Further recommendations are given by French (1998), Momber (1993a), Smith (2001), and Vijay (1998b).

The use of hydroblasting equipment for the surface preparation on ships on sea, which often includes ballast tank cleaning, requires special safety and health considerations to establish the following parameters (Henderson, 1998):

- where best to place the units on deck?
- the best method of securing the units?

Figure 4.22 Special body protection for hydroblasting operators (photograph: Warwick Mills, New Ipswich).

Table 4.19 Results of resistance tests with body protection (Anonymous, 2002a).

Operating pressure in MPa	Volumetric flow rate in l/min	Nozzle diameter in mm	Distance in m	Traverse speed in m/s	Exposure time[1] in s	Result
18	13.0	1.2	7.5	0.5	0.0024	no penetration
50	19.7	1.2	7.5	0.5	0.0024	no penetration
100	19.3	1.0	7.5	0.5	0.0020	no penetration
150	15.0	0.8	7.5	0.5	0.0016	no penetration
200	17.0	0.8	7.5	0.5	0.0016	no penetration

[1]Calculated with d_N/v_T.

- optimum hose runs;
- the capacity, number, and type of ventilation fans required;
- ventilation trunking requirements;
- the ship's power supplies, their location, voltage, amperage, and cycles;

- fresh water requirements, the capability of the vessel to supply sufficient fresh water for the work and the location of the supply points;
- entry and exit points in each tank for personnel and equipment;
- requirements for access equipments in the tanks;
- lightning requirements and how to best illuminate substrates;
- accommodations arrangements for hydroblasters.

4.4.5 Confined Spaces

Surface preparation jobs as well as painting jobs are often performed in confined spaces, for example, manholes, pipelines, storage vessels, bridge box beams, interior tower cells and ballast tanks. A typical example is shown in Fig. 4.21. Not all confined spaces are considered hazardous. However, they must be considered hazardous if they contain or have the potential to contain the following (OSHA, 1993):

- Hazardous atmospheres.
  This includes (i) lack of oxygen, (ii) presence of explosive gases and vapours, and (iii) presence of toxic dusts, mist and vapours.
- Engulfment hazards.
  This includes spaces containing materials like salt, coal, grain and dirt that can easily shift and trap an operator.
- An internal configuration (slopes or inward configurations) that could trap or asphyxiate.
  This includes spaces where the bottoms are sloped or curved (e.g. narrow openings at the bottom of a silo) may trap or asphyxiate operators.
- Any other recognised serious hazards.
  This includes moving parts, power connections, liquid and anything else that can cause bodily harm.

This special situation requires special training because it is reported that operators are still getting hurt in confined spaces. The most important things to understand about hazards in confined spaces are as follows (Platek, 2002):

- What hazard will be encountered?
- What equipment or means will offer protection from those hazards?
- How the equipment is used?
- Who can perform the work?
- What happens if something goes wrong?

When a confined space is evaluated, three questions regarding that space should be answered:

- Is the space large enough that the operator can place part or all of his body into it?
- Does it have limited entry and exits?
- Is it designed to work in continuously?

Training and education are the major methods to reduce risks if work is performed in confined spaces. OSHRA 29 CFR 1910.146 states: 'The employer shall provide training so that all employees whose work is regulated by this section acquire the understanding, knowledge, and skills necessary for the safe performance of the duties assigned under this section.' Adequate training must be delivered when permit-required confined spaces are encountered and for all of the duties performed in and around a confined space.

CHAPTER 5

Surface Quality Aspects

5.1 Surface Quality Features

ISO 8502 (1995) states the following: 'The performance of protective coatings of paint and related products applied to steel is significantly affected by the state of the steel surface immediately prior to painting. The principal factors to influence this performance are:

(i) the presence of rust and mill scale;
(ii) the presence of surface contaminants, including salts, dust, oil and greases;
(iii) the surface profile.'

Numerous standards have been issued to define these factors (see also Chapter 6), and testing methods are available to quantify them. Hydroblasted surfaces show some distinct features, and extensive experimental studies have been performed to address this special point, often in direct comparison to other surface preparation methods.

5.2 Adhesion Strength

5.2.1 Definitions and Measurement

According to Bullett and Prosser (1972) 'the ability to adhere to the substrate throughout the desired life of the coatings is one of the basic requirements of a surface coating, second only to the initial need to wet the substrate.' Adhesion is based upon adhesive forces that operate across the interface between substrate and applied coating to hold the paint film to the substrate. These forces are set up as the paint is applied to the substrate, wets it, and dries. The magnitude of these forces (thus, the adhesion strength) depends on the nature of the surface and the binder of the coating. Five potential mechanisms cause adhesion between the surfaces of two materials:

- physical adsorption;
- chemical bonding;
- electrostatic forces;
- diffusion;
- mechanical interlocking.

In the mechanical interlocking mechanism, the macroscopic substrate roughness provides mechanical locking and a large surface area for bonding; the paint is mechanically linked with the substrate. Adhesive bonding forces could be categorised as primary valency forces and secondary valency forces as listed in Table 5.1.

Adhesion depends on numerous circumstances, among them substrate profile (see Section 5.7), substrate cleanliness (see Section 5.3), and type and application of the subsequent coating system. Adhesion between substrate and coating can be

Table 5.1 Bonding forces and binding energies (Hare, 1995).

Force	Type	Description	Example	Binding energy in kcal/mole
Ionic	Primary valency	Bonding formed by transfer of valency electrons from the outer shell of an electron-donating atom into outer shell of an electron-accepting atom to produce a stable valency configuration in both.	Metal salts	150–250
Covalent	Primary valency	Bonding formed when one or more pairs of valency electrons are shared between two atoms.	Most organic molecules	15–170
Coordinate	Primary valency	Covalent type bond where both the shared pair of electrons are derived from one of the two atoms.	Quaternary ammonium compounds	100–200
Metallic	Primary valency	Bonding in bulk phase of metals between positively charged metallic ions and the electron cloud in the lattice points of the structure.	Bulk metals	27–83
Hydrogen bonding	Secondary valency	Forces set up between the unshared electrons on a highly electronegative atom on one molecule and the weak positive charge from the 'exposed' proton of a hydrogen atom.	Water	<12
Dispersion	Secondary valency	Weak forces in all molecules that are associated with temporary fluctuations in electron density caused by the rotation of electrons around atomic nuclei.	Most molecules	<10
Dipole	Secondary valency	Intermolecular forces set up between weak and electronegative charge on one polar molecule and electropositive charge on a second polar molecule.	Polar organics	<5
Induction	Secondary valency	Very weak dipole-like forces between non-polar molecules set up by weak dipoles induced by the proximity of other strongly polar molecules.	Non-polar organics	<0.5

Table 5.2 Cohesion strength of substrates.

Substrates	Cohesion strength in MPa
Aluminium[1]	>107
Steel[1]	>386
Zinc[1]	>228
Coatings	
Epoxy polyamide[2]	12
Epoxy polyamide[3]	7.4

[1] Gaughen (2000).
[2] Relius Coatings, Oldenburg.
[3] Carbonline, St Louis.

evaluated by different methods, including the following:

- pull-off testing (ISO 4624; ASTM D4541);
- penknife disbondment;
- cross-cut testing (ASTM 3359; DIN EN ISO 2409);
- falling ball impact.

The pull-off test delivers quantitative information about the adhesion (usually given in N/mm^2 or MPa), while the picture of the rupture provides information about the weakest part of the system. Typical failure types observed are either adhesion failure (substrate-coating) or cohesion failure (internal coating failure). Table 5.2 lists cohesive strength values of some metallic substrate materials. More detailed designation is mentioned in Table 5.3. Rigidly seen, a plain adhesion failure will not occur. This restriction is reinforced by XPS (X-ray photoelectron spectroscopy) measurements by de Vries *et al.* (1983) who found traces of polymeric material on the substrate surface of a metal–polymer interfacial fracture which appeared to be a purely adhesive failure from an optical examination.

Desired adhesion depends on the certain case of application. The US Navy, however, has defined a general minimum pull-off strength of 3.4 MPa measured per ASTM D4541 (Kuljan and Holmes, 1998).

5.2.2 Adhesion to Bare Steel Substrates

Several systematic studies have been performed to estimate the adherence of coating systems to steel panels prepared by different methods. Long-term tests in salt water were performed by Allen (1997) and Morris (2000). These studies included hand wire brushing, needle gunning, hydroblasting and grit-blasting. The results, listed in Tables 5.3 and 5.4, illustrate the complex relationships between preparation methods and applied coating systems. Cross-cut, measured after 36 months, was almost independent on the preparation method for many epoxy coatings; exceptions were coal tar epoxy and pure epoxy tank lining, where wire brushing and needle gunning showed worse results compared to hydroblasting and grit-blasting. Penknife disbondment and impact resistance, both measured after 24 months, showed worst

Table 5.3 Results of comparative long-term adhesion tests after 12, 24 and 36 months (Morris, 2000).

Method ↓	Cross-cut in mm			Impact resistance[1]			Pull-off adhesion in MPa[2]		
Time in months →	12	24	36	12	24	36	12	24	36
Solventless epoxy (2 × 125 µm DFT)									
Wire brushing	0	0	0	2	2	3	2.8/S	3.5/S	2.8/S
Needle gunning	0	0	0	1	1	2	2.8/S	5.5/S	5.2/S
Hydroblasting Dw2	0	0	0	0	0	1	6.9/S	7.6/I	8.3/G
Hydroblasting Dw2 FR	0	0	0	2	3	3	3.5/I	11.0/I	8.6/I
Hydroblasting Dw3	0	0	0	0	0	1	3.5/I	11.0/I	10.7/G
Hydroblasting Dw3 FR	0	0	0	0	1	1	4.1/I	8.3/I	11.0/I
Grit-blasting Sa 2 1/2	0	0	0	1	2	2	5.5/I	12.4/I	10.3/G
Glass flake epoxy (2 × 125 µm DFT)									
Wire brushing	0	0	10	1	1	3	4.1/S	4.1/S	2.1/S
Needle gunning	0	0	2	2	2	3	2.4/S	5.5/S	8.9/S
Hydroblasting Dw2	0	0	0	1	1	1	6.9/G	11.0/I	>17.9/G
Hydroblasting Dw2 FR	0	0	0	1	2	2	3.4/G	15.2/G	>17.2/G
Hydroblasting Dw3	0	0	0	0	0	1	7.6/G	10.3/I	9.7/I
Hydroblasting Dw3 FR	0	0	0	1	1	1	6.9/G	16.9/I	>17.2/I
Grit-blasting Sa 2 1/2	0	0	0	0	0	1	6.9/G	13.8/G	13.1/G
Low temperature cure glass flake epoxy (2 × 125 µm DFT)									
Wire brushing	0	0	10	1	1	1	2.8/S	4.6/S	7.6/S
Needle gunning	0	0	12	1	1	2	4.1/S	3.4/S	12.1/S
Hydroblasting Dw2	0	0	0	2	2	2	6.9/G	17.2/G	16.6/G
Hydroblasting Dw2 FR	0	0	0	2	2	2	5.2/G	14.5/I	11.7/G
Hydroblasting Dw3	0	0	0	0	0	1	3.4/G	15.2/G	10.3/G
Hydroblasting Dw3 FR	0	0	0	0	1	1	5.5/G	16.9/I	13.8/G
Grit-blasting Sa 2 1/2	0	0	0	1	1	2	6.9/G	13.8/G	12.4/G
Modified epoxy (2 × 125 µm DFT)									
Wire brushing	0	0	0	1	1	3	4.8/S	5.5/S	2.8/S
Needle gunning	0	0	0	2	3	3	2.1/S	2.8/S	4.1/S
Hydroblasting Dw2	0	0	0	0	0	0	6.9/I	12.8/I	10.3/I
Hydroblasting Dw2 FR	0	0	0	1	2	2	3.8/I	11.0/I	8.6/I
Hydroblasting Dw3	0	0	0	0	0	1	6.9/I	10.8/I	9.7/I
Hydroblasting Dw3 FR	0	0	0	0	0	0	4.1/I	15.2/I	7.9/I
Grit-blasting Sa 2 1/2	0	0	0	0	0	1	6.9/I	13.1/I	9.7/G

[1]0 = no cracking; 1 = very slight cracking, no detachment; 2 = slight cracking, no detachment; 3 = moderate cracking, no detachment.

[2]Failure mode: S = substrate; I = intercoat; G = glue.

results for mechanical methods (especially for wire brushing). Impact resistance was more a function of the coating system than the preparation method, thus grit-blasted substrate was, on the whole, only slightly superior to manual preparation under the conditions of impact testing. Regarding the pull-off strength, measured with a commercial adhesion tester, blasting methods were superior to mechanical methods. Some results are shown in Fig. 5.1. There was a certain trend for blasting

Table 5.4 Results of comparative adhesion tests on ballast tank coatings (Allen, 1997).

Method	Adhesion parameter		
	Falling ball impact[1]	Pull-off adhesion in MPa[2]	Penknife disbondment in mm
	Epoxy coating (solvent-less)		
Wire brushing	2	2.8/S	6
Needle gunning	1	2.8/S	5
Hydroblasting Dw2	0	6.9/G	0
Hydroblasting Dw2 FR	4	3.4/G	0
Hydroblasting Dw3	0	3.4/G	0
Hydroblasting Dw3 FR	0	4.1/G	0
Grit-blasting Sa 2 1/2	1	5.5/G	0
	Coal tar epoxy		
Wire brushing	4	2.1/S	10
Needle gunning	3	2.4/S	7
Hydroblasting Dw2	0	5.2/I	0
Hydroblasting Dw2 FR	2	6.9/I	0
Hydroblasting Dw3	0	6.9/I	0
Hydroblasting Dw3 FR	2	6.9/I	0
Grit-blasting Sa 2 1/2	1	6.6/I	0
	Epoxy system		
Wire brushing	2	2.1/S	5
Needle gunning	2	2.8/S	3
Hydroblasting Dw2	2	6.9/G	0
Hydroblasting Dw2 FR	0	5.5/G	0
Hydroblasting Dw3	0	5.2/G	0
Hydroblasting Dw3 FR	0	6.9/G	0
Grit-blasting Sa 2 1/2	0	5.5/G	0
	Glass flake epoxy		
Wire brushing	2	2.8/S	5
Needle gunning	1	4.1/S	3
Hydroblasting Dw2	1	6.9/G	0
Hydroblasting Dw2 FR	4	5.2/G	0
Hydroblasting Dw3	0	3.4/G	0
Hydroblasting Dw3 FR	0	5.5/G	0
Grit-blasting Sa 2 1/2	0	6.9/G	0

[1]0 = no cracking, no detachment; 1 = slight cracking, no detachment; 2 = slight cracking and detachment; 3 = moderate cracking, no detachment; 4 = moderate cracking, slight detachment.

[2]Failure mode: G = glue; I = intercoat; S = substrate.

methods in that pull-off adhesion increased with time. Under simulated ballast tank conditions, coatings applied to hydroblasted surfaces performed far better than coatings applied to mechanically prepared substrates, and equal to those on grit-blasted surfaces. The influence of flash rust on coating performance was also investigated by Allen (1997) and Morris (2000). Selected results are shown in Fig. 5.2. In more than half the cases, allowing the hydroblasted surfaces to flash rust reduced the

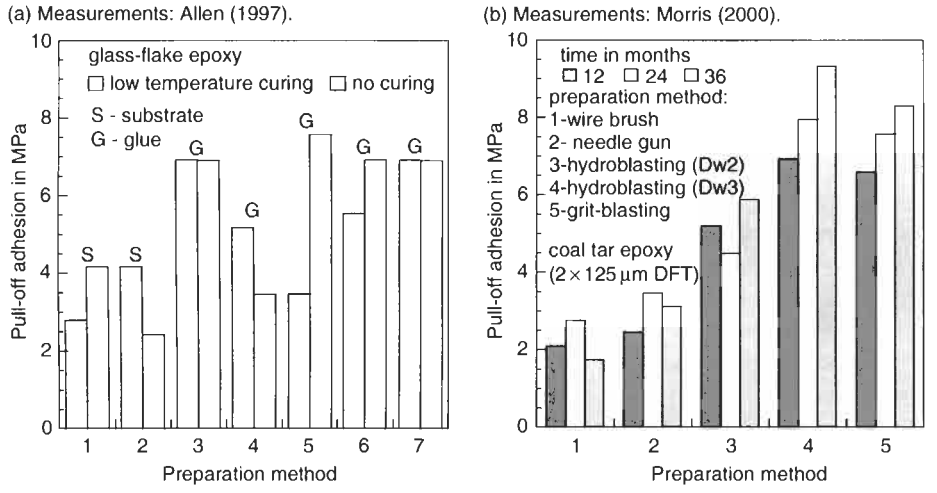

Figure 5.1 Pull-off adhesion after surface preparation – simulated ballast tank conditions.

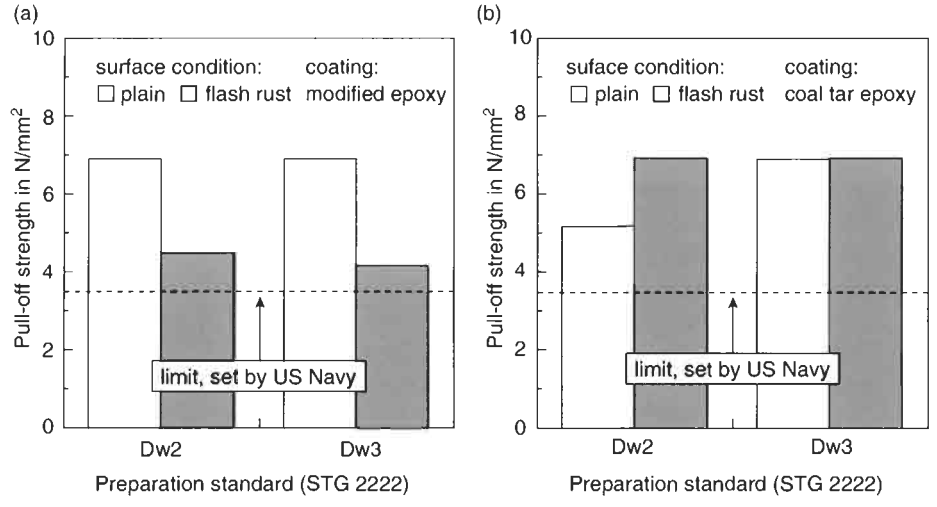

Figure 5.2 Influence of flash rust on pull-off strength (Allen, 1997).

pull-off adhesion values by an average of approximately 30%, but they were still very reasonable values. However, it was obvious that the effects of flash rust depended on the applied coating system and surface preparation standard. Whereas flash rust deteriorated pull-off adhesion for modified epoxy, it did not influence the performance of a coal tar epoxy coating system. However, the often heard general statement 'adhesion on hydroblasted surfaces deteriorates because of flash rust' is definitively wrong in the light of systematic long-term investigations.

The failure mode may be an additional parameter for adhesion evaluation. Basically, adhesive failure (denoted 'S' in Fig. 5.1(a)) and cohesive failure (denoted 'G'

in Fig. 5.1.(a)) can be distinguished. Cohesive failure in a coating layer points to a high degree of bonding between coating and substrate. It was often observed that paint failure was a mixture of both failure modes, and the appearance of a certain mode was denoted in percentage terms (see Table 5.4). However, as shown in Tables 5.3 and 5.4 substrate failure (denoted 'S') and coat detachment occurred usually from mechanically prepared surfaces, whereas glue failure (denoted 'G') and intercoat failure (denoted 'I') were the principal failure mode on most of the hydroblasted and grit-blasted surfaces.

Tests on contaminated substrates showed that the level of dissolved salts affects the value and type of adhesion of coatings to substrates. With cero contaminants, the mode of failure was cohesive within the primer coat. As the salt level increased, progressively less primer remained adhered to the steel surface. At a higher contamination level, there was a change from mixed to total adhesive failure of the primer (Allan *et al.*, 1995).

Information about the pull-off strength of coating systems applied to plain, uncoated steel substrates profiled with high-speed water jets is provided in Section 5.7.4.

5.2.3 Integrity of Remaining Coatings

For coating removal specifications such as selective stripping, spot and sweep blasting where tightly adhering coatings are remaining (see Fig. 5.3), it is important to know if the integrity of these coatings may be affected due to the jet impact. Table 5.4 lists some results of measurements on ballast tank coatings. All final adhesion values were high: in all but one case (outboard web) the adhesion actually increased. Comparing the initial and final failure modes for the locations in the ballast tank where adhesion increased, the failure mode with respect to the top coat decreased. From the data presented in Table 5.5, it can be concluded that hydroblasting did not negatively affect the adhesion of the remaining 'tight' coating

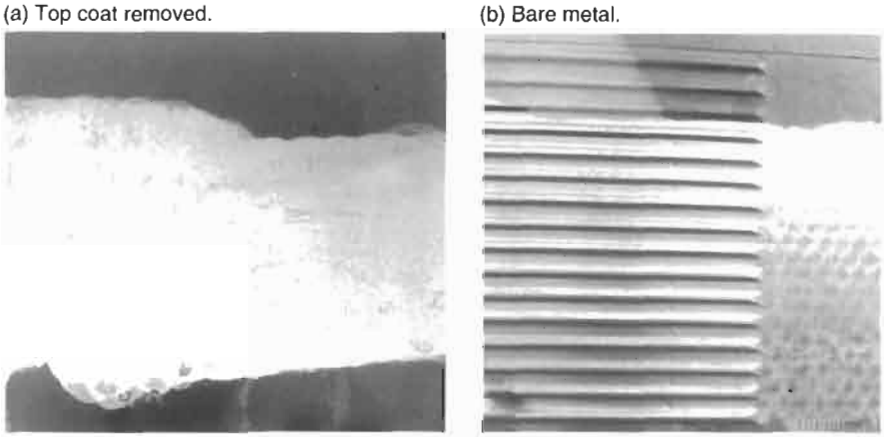

Figure 5.3 Selective paint stripping through hydroblasting.

Table 5.5 Adhesion of remaining coatings after hydroblasting (NSRP, 1998) (object: ballast tank USS Duluth; measurements: according to ASTM D 4541; coating: white epoxy primer (100 μm), blue epoxy top coat (100 μm)).

Location	Adhesion in MPa	Failure mode
	Initial values (prior to hydroblasting)	
Outboard atmospheric	5.7	10% cohesive, 90% adhesive to top coat
Inboard atmospheric	5.7	10% cohesive, 90% adhesive to top coat
Outboard web	4.8	50% adhesive to top coat, 50% primer to steel
Inboard immersion	5.5	70% adhesive to button, 30% adhesive to top coat
Inboard immersion	4.8	50% primer to steel, 25% adhesive to top coat, 25% adhesive to button
	Final values (after hydroblasting)	
Outboard atmospheric	>6.9	50% cohesive in top coat, 50% adhesive to button
Inboard atmospheric	5.9	10% primer to steel, 50% adhesive to top coat, 40% cohesive in adhesive
Outboard web	3.4	100% primer to steel
Inboard immersion	>6.9	50% primer to steel, 50% adhesive to top coat
Inboard immersion	6.6	60% primer to steel, 40% cohesive in adhesive

to the substrate. It seemed that hydroblasting rather removed weak, deteriorated portions of the exposed coating layers.

5.3 Flash Rust

5.3.1 Definitions and Measurement

Flash rust is a light oxidation that occurs as a steel surface, which is originally wet, dries. ISO 12944-4 provides the following definition: 'Slight rust formation on a prepared steel surface soon after preparation.' The formation of flash rust is commonplace in liquid-based blasting applications, but can also appear with grit-blasting if abrasives are contaminated. Steel surfaces usually show flash rust within one half to two hours after hydroblasting, or longer depending on environmental conditions. It was shown in the work of Le Calve *et al.* (2002) that the temporal formation of flash rust on hydroblasted steel surfaces occurred in two stages. First, the progression of rusting occurred over a relatively stable transition stage (Fe^{2+}-concentration between 15 and 35 g/m^2). In the second stage, the progression followed an exponential function (Fe^{2+}-concentration of upto 10 g/m^2). The beginning of this second stage depended on the level of cleanliness. Typical values were between 2 and 10 days. Re-coating of the hydroblasted surface should be performed during the first stage (Le Calve *et al.*, 2002).

Flash rust is pure iron oxide and, therefore, is not critical to applied coatings from the point of view of chemical compatibility. The problem with flash rust is rather an adhesion problem. If the rust does not adhere to the steel substrate it acts

like a separation agent that prevents contact between substrate and coating. Flash rust adherence is defined in several standards. Usually, the definitions according to SSPC-12/NACE 4 can be found in paint specifications. These definitions are listed in Table 6.6. As an example, a requirement of a certain paint specification (Hempadur 4514) reads: 'A flush rust of FR-2 for atmospheric conditions, and FR-2 (preferably FR-1) for water conditions, respectively, is acceptable prior to coating.' Another, more rigid specification (Interline 104, zinc tank coating) claims: 'The system must be applied before oxidation of the steel occurs.' In that case, no flash rust is allowed and must be removed by an additional cleaning method prior to coating. An alternative flash rust definition is given in the French Standard NFT 35-520; this standard is the only one that states flash rust concentrations in a quantitative term: Fe g/m^2. The degree of flash rusting can affect the long-term performance of paint system since excessive rust can prevent proper adhesion. However, experience from practical trials and work carried out in shipyards showed that lightly flash rusted surfaces provided a good substrate for painting. Some results are summarised in Tables 5.4–5.6. See also Fig. 5.2 for the influence of flash rust on coating adherence. In some cases, the adhesion between coating and flash rusted substrates even exceeded those of the corresponding non-rusted substrates. A systematic investigation about the influence of flash rust on the performance of coating systems, including the effect of initial surface conditions, was performed by Le Calve *et al.* (2003): some results are listed in Table 5.7. It can be noted that the relationships are rather complex: although most coating systems perform less well than a reference sample if severe flash rust (0F2) is present, this result is not valid for all systems. The coating system P4, for example, still performs well on a heavily flash rusted surface.

Methods to evaluate flash rust adherence are listed in Table 6.5. These methods are only qualitative and can only give a feeling about the adhesion to the steel surface. A more appropriate and quantitative method is outlined in Hempel's

Table 5.6 Flash rust effects on long-term adhesion after 12, 24 and 36 months (Morris, 2000).

Preparation method ↓	Time in months →	Pull-off adhesion 12	24	36
	Coal tar epoxy (2 × 125 μm DFT)			
Hydroblasting Dw 2		5.2	4.5	5.9
Hydroblasting Dw 2 FR		6.9	9.7	11.0
Hydroblasting Dw 3		6.9	7.9	9.3
Hydroblasting Dw 3 FR		6.9	6.9	9.7
	Pure epoxy tank lining (2 × 125 μm DFT)			
Hydroblasting Dw 2		6.9	8.3	7.6
Hydroblasting Dw 2 FR		5.5	10.3	9.3
Hydroblasting Dw 3		5.2	9.7	10.3
Hydroblasting Dw 3 FR		6.9	11.4	12.4

Table 5.7 Effects of flash rust concentrations on coating performance (Le Calve *et al.*, 2003).

Initial condition	Flash rusting	Coating system P1[1]			Coating system P2[2]			Coating system P3[3]			Coating system P4[4]		
		Corrosion	Adhesion	Overall	Corrosion	Adhesion	Overall	Corrosion	Adhesion	Overall	Corrosion	Adhesion	Overall
Sa 2 1/2	OF0[5]	1	1	1	1	0	0	1	0	0	0	1	0
	OF1[5]	1	1	1	1	1	1	1	1	1	0	0	0
	OF2[5]	1	0	0	1	0	0	0	0	0	1	1	1
Rust grade C	OF0	0	1	0	0	1	0	0	0	0	0	0	0
	OF1	0	0	0	0	0	0	0	0	0	0	0	0
	OF2	0	0	0	0	0	0	0	0	0	0	0	0
Degraded shop primer	OF0	1	0	0	1	0	0	–	–	–	0	0	0
	OF1	1	0	0	1	1	1	–	–	–	0	0	0
	OF2	1	0	0	1	0	0	–	–	–	0	0	0

[1]P1 = epoxy vinyl (100 μm and 80 μm) + silicone alkyd 2 × 30 μm.
[2]P2 = epoxy (140 μm) + polyurethane (100 μm).
[3]P3 = 2 × acrylic solvent-borne (120 μm).
[4]P4 = water-borne epoxy (140 μm) + water-borne acrylic (100 μm).
[5]French Standard NFT 35-520: OF0 = 0–1.5 Fe g/m^2; OF1 = 3–5 Fe g/m^2; OF2 = 7–8 Fe g/m^2.

Table 5.8 Flash rust definitions according to Hempel's tape test.

Definition[1]	Tape test result
FR-1 (L)	No rust on the tape. No or only a slight change of the test spot.
FR-2 (M)	Slight localised red-brown rust on the tape. A significant change of the test spot, possibly showing localised areas of black rust.
FR-3 (H)	Significant, uniform red-brown rust on the tape; also showing grains of black rust. A significant change of the test spot, also showing localised areas of black rust.

[1] See Section 6.5 for definitions.

water jetting standard: the so-called tape test. The test procedure includes the following steps:

1. Select a spot on which to perform the test.
2. Attach a piece of tape (as specified in ASTM D 3359) in a length of at least 5 cm and rub thoroughly with a fingertip – not a fingernail – to make the tape adhere firmly.
3. Peel off the tape and place it on a piece of white paper for reference.
4. Repeat steps 2. and 3. for a total of nine times on exactly the same spot using a new piece of tape each time.

The flash rust degree is assessed on the basis of the amount and type of rust present on the tenth piece of tape and on the appearance of the test spot relative to that of the adjacent areas. This is summarised in Table 5.8. Visual examples are provided in Fig. 6.3.

5.3.2 Effects on Coating Performance

The use of water jets in combination with rust tolerant coating systems is a promising strategy for the maintenance of deteriorated steel surfaces. It is known that the capability of a primer to penetrate existing rust layers depends on the decontamination level of the rust. The penetration capability is weak if the rust contains salts. This was verified through comparative metallographic studies by Kaiser and Schütz (2001) on clean and contaminated, respectively, steel samples (see Fig. 5.4). The authors defined three levels of salt contaminations:

(i) NaCl: <5 mg/m^2 (0.5 μg/cm^2); Na_2SO_4: <50 mg/m^2 (5 μg/cm^2);
(ii) NaCl: 8.1 mg/m^2 (0.81 μg/cm^2); Na_2SO_4: 1125.7 mg/m^2 (112.6 μg/cm^2);
(iii) NaCl: 876.5 mg/m^2 (87.6 μg/cm^2); Na_2SO_4: 188.5 mg/m^2 (18.8 μg/cm^2).

If samples were almost clean (i), the coatings enclosed and integrated the rust completely. The coatings penetrated up to the substrate surface. This case is shown in Fig. 5.4(a). Penetration capability decreased if the rust contained sulphate (ii); rust particles were not enclosed completely in that case, and flaws occurred between substrate and coating. These flaws are clearly visible in Fig. 5.4(b). The worst results, as illustrated in Fig. 5.4(c), were obtained with highly chloride contaminated rust (iii).

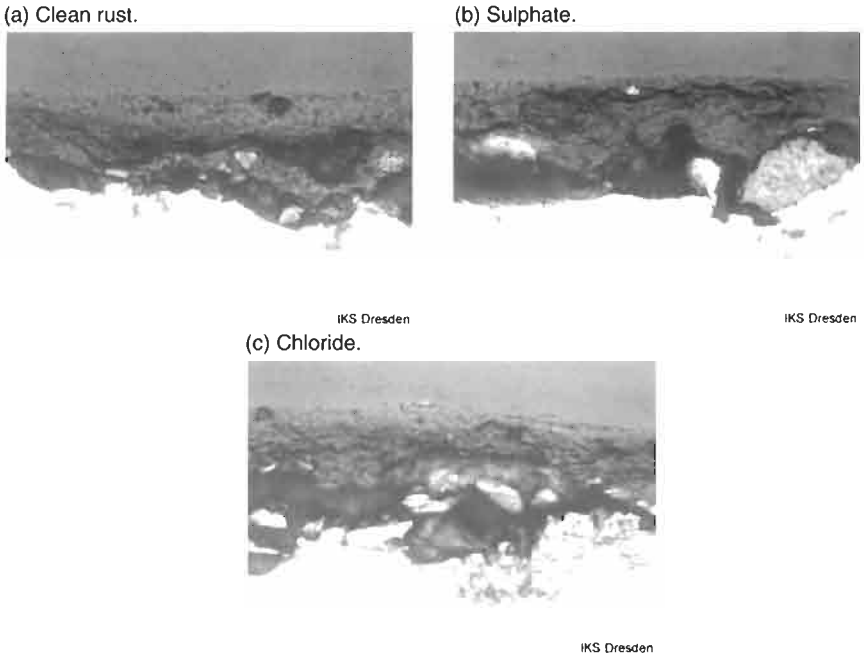

Figure 5.4 The effect of rust contamination on paint penetration capability; magnification: 200× (photographs: Institut für Korrosionsschutz GmbH, Dresden).

Large gaps with widths of 30–40 μm appeared between coating and substrate. These gaps contained rust particles that were not incorporated into the paint and this caused deteriorated adhesion between the steel and the paint system. Table 5.9 lists further quantitative results. They confirm that chloride contaminated steel substrates exhibited the lowest values for adhesion strength, and the highest values for degree of blistering and degree of rusting for all coating systems. These results were due to the reduced rust penetration capability of the applied paint systems. Thus, rust, in itself, is not a problem; rather it is the contaminants that the rust contains.

Delucchi *et al.* (1999) performed capacitance measurements on surface tolerant coatings applied to pre-rusted steel substrates. The criteria for evaluation were capacitance or changes in capacitance with time, respectively. A low capacitance or a stable capacitance value with time, respectively, characterised good coating performance. The results, listed in Table 5.10, illustrated the good performance of the surface tolerant coatings. The change in coating capacitance after 840 h was about 30% in most cases. These values were much lower than values obtained from measurements on substrates covered with old coatings. Thus, the types of surface tolerant coatings investigated performed especially well on pre-rusted surfaces. The table also shows a strong relationship between capacitance and adhesion strength; the higher the capacitance, the lower is the adhesion strength.

Table 5.9 Evaluation of coatings for rusted substrates after one year environmental weathering (Kaiser and Schütz, 2001).

Coating	DFT in μm	Rust contamination	Blistering[1]	Rust[2] degree	Adhesion[3] strength MPa	Failure type
Noverox +	204 ± 22	none	0	Ri 0	1.3 ± 0.6	A/B 10, B/C90
HS epoxy	213 ± 17	NaCl	5/2	Ri 0	1.1 ± 0.6	A/B100
	199 ± 20	Na_2SO_4	3/2	Ri 0	1.4 ± 0.2	A/B40, B/C60
Noverox +	213 ± 24	none	0	Ri 0	3.7 ± 1.4	A/B50, C50
DS-mica	221 ± 16	NaCl	5/2	Ri 1	3.2 ± 1.0	A/B70, C30
	208 ± 21	Na_2SO_4	0	Ri 1	4.0 ± 0.8	A/B20, C80
Antitrust +	173 ± 15	none	0	Ri 0	1.0 ± 0.6	B/C100
HS epoxy	192 ± 18	NaCl	5/2	Ri 0	1.9 ± 0.6	A/B100
	182 ± 21	Na_2SO_4	4/2	Ri 0	1.9 ± 0.6	A/B40, B/C60
Antitrust +	181 ± 17	none	0	Ri 0	4.2 ± 1.0	A/B20, C80
DS-mica	178 ± 9	NaCl	5/2	Ri 1	3.6 ± 1.2	A/B80, C20
	169 ± 11	Na_2SO_4	0	Ri 0	4.3 ± 1.5	A/B20, C80
Noxyde	148 ± 15	none	2/2	Ri 0	2.1 ± 0.4	A/B80, B20
	136 ± 11	NaCl	5/2	Ri 2-3	2.0 ± 0.9	A/B80, B20
	151 ± 10	Na_2SO_4	3/2	Ri 0	2.9 ± 0.4	A/B90, B10

[1]ISO 4628-2.
[2]ISO 4628-3.
[3]DIN EN 24624.

Table 5.10 Evaluation of surface tolerant coatings for pre-rusted substrates (Delucchi *et al.*, 1999).

Coating	Capacitance in pF/cm^2		Adhesion in MPa
	Initial	After 840 hours	
Primer + intermediate coat + topcoat	21.0	26.4	4.4
Primer + intermediate coat + topcoat	22.1	32.7	2.4
Primer + intermediate coat + topcoat	19.9	27.7	3.8
Primer + intermediate coat + topcoat	23.2	30.9	2.9
High-built one-coat system	103.3	129.3	2.0
High-built one-coat system	210.7	228.5	1.0

5.4 Non-Visible Contaminants – Salt Content

5.4.1 Definitions and Measurement

Soluble salts are very widespread on steel substrates. A major source is sea salt which affects especially ships, offshore structures and waterfront constructions. However, soluble salts can also arise from chemical processes, cooling towers, agricultural processes and burning of sulphur-containing coal. The detrimental effect of water-soluble contaminants at the steel/paint interface is well known. The amount of salts, especially chlorides, on blasted surfaces is essential for the performance of the applied coating systems. However, paint manufacturers usually do not specify permissible salt concentrations in their data sheets. One of the rare examples, where salts are mentioned at all, states the following: 'Check for soluble salts levels.' (Alocit 28.14; epoxy coating – zinc primer).

Surface contamination by soluble salts has always been an issue for the corrosion protection industry. It was, however, the replacement of lead-based paints (Pb_3O_4) by other paint types due to environmental concerns that caused a different look at salts with respect to coating performance. A unique property of lead compounds is their capability of binding up soluble salts. Other coating compounds do not have this capability and it is for that reason that salt contamination became an issue in surface preparation and coating. Salt occupancy applies to non-visible surface contaminants according to SSPC-TU 4. Table 5.11 provides a description of non-visible surface cleanliness definitions. The level of non-visible contaminants that may remain on the surface is usually expressed as mass per unit area, much often in $\mu g/cm^2$. The prime salts most commonly encountered are chlorides, sulphates and nitrates. Chlorides, however, tend to be more soluble than other salts and of lower formula weight. It, therefore, usually produces rather high osmotic pressures.

There are several methods used to estimate the salt level on blasted steel substrates, namely

- direct salt measurement (swab method, adhesive cell method) – salt concentration (e.g. ppm, mg/l), cross section (e.g. cm^2) and volume (e.g. ml) must be known to estimate salt contamination (e.g. $\mu g/cm^2$);

Table 5.11 Description of non-visible surface cleanliness definitions (SSPC-SP 12/NACE No. 5).

Term	Description of surface
NV-1	Free of detectable levels of soluble contaminants, as verified by field or laboratory analysis using reliable, reproducible methods.
NV-2	Less than 7 $\mu g/cm^2$ of chloride contaminants, less than 10 $\mu g/cm^2$ of soluble ferrous ion levels, or less than 17 $\mu g/cm^2$ of sulphate contaminants as verified by field or laboratory analysis using reliable, reproducible test methods.
NV-3	Less than 50 $\mu g/cm^2$ of chloride or sulphate contaminants as verified by field or laboratory analysis using reliable, reproducible test methods.

- measurement of electric conductivity (total soluble salts) – usually expressed in $\mu S/cm$ for liquid solutions;
- spectrometry (cannot deliver results in terms of salt content per cross section, e.g. $\mu g/cm^2$).

The last method can not only detect a certain salt type, but also its components: in the case of chlorides, not only the chloride can be detected, but also components, such as sodium hypochloride, chlorine oxide, chlorine dioxide, or hydrochloric acid (Trotter, 2001). Exhaustive information about testing of steel substrates for soluble salts and soluble iron corrosion products as well as analysis methods is provided in ISO 8502, Parts 1 to 13.

5.4.2 Effects on Coating Performance

Chloride content on the substrate significantly influences the performance of coating systems. Rust development under the paint film and osmotic blistering are commonly observed at an early stage in paint coatings applied over contaminated steel substrates. This is verified by Soltz (1991) and more recently by Mitschke (2001) and Kaiser and Schütz (2001). These authors have shown the following:

- chlorides significantly reduced the capability of paint to penetrate and enclose rust (see Paragraph 5.3.2);
- time to osmotic blistering is decreased if the chloride concentration is increased (see Table 5.12);
- maximum service temperature of linings is decreased if the chloride concentration is increased (1.0 $\mu g/cm^2$ lowers the maximum service temperature by about 6°C);
- number of blisters are increased if the chloride concentration is increased (see Fig. 5.5).
- much higher levels of sulphate contamination (>250 $\mu g/cm^2$) were required to cause coating blistering compared to chloride. Therefore, blistering from seawater sulphate contamination does not appear to be a primary problem.

Table 5.12 Time to failure by blistering for linings (Mitschke, 2001).

Chloride level in µg/cm²	Time to blistering in weeks at various temperatures				
	88°C	77°C	66°C	54°C	43°C
		Epoxy novolac, DFT 320 µm			
0.6	>56	>56	>56	>56	>56
1.4	>56	>56	>56	>56	>56
3.9	>56	>56	>56	>56	>56
5.3	>56	>56	>56	>56	>56
7.6	>56	36	>56	>56	>56
		Epoxy, DFT 193 µm			
0.6	3	26–36	>56	>56	>56
1.4	6	26–36	>56	>56	>56
3.9	6	26–36	>56	>56	>56
5.3	5	26	>56	>56	>56
7.6	2	2	4	10	>56
		Epoxy, DFT 239 µm			
0.6	36	11	12	>56	>56
1.4	3	7	12	>56	>56
3.9	1.5	3	7	>56	>56
5.3	1.5	3	7	>56	>56
7.6	1.5	1.5	3	5	3
		Epoxy novolac, DFT 262 µm			
0.6	>56	>56	>56	>56	>56
1.4	>56	>56	>56	>56	>56
3.9	>56	>56	>56	>56	>56
5.3	>56	>56	>56	>56	>56
7.6	>56	>56	>56	>56	>56
		Epoxy, DFT 252 µm			
0.6	1.5	>56	>56	>56	>56
1.4	1.5	1.5	4	>56	>56
3.9	1.5	1.5	3	>56	>56
5.3	1.5	1.5	10	>56	>56
7.6	1.5	1.5	3	>56	>56
		Epoxy, DFT 252 µm			
0.6	36–43	>56	>56	>56	>56
1.4	36–43	43–56	>56	>56	>56
3.9	3	3	>56	>56	>56
5.3	23	23	>56	>56	>56
7.6	3	3	43–56	>56	>56

The very extensive study performed by Soltz (1991) also contains an investigation about the effect of chloride-contaminated abrasives on the coating performance.

However, the major criterion for salt content is the safe or permissible, respectively, salt level that prevents under-rusting or blistering of the applied paint system. There

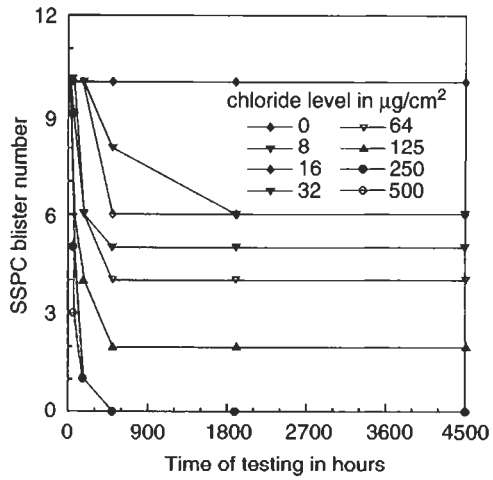

Figure 5.5 The effect of chloride level on blistering in coal tar epoxy coatings (Soltz, 1991).

Table 5.13 Permissible chloride levels on steel substrates.

Institution	Permissible chloride content in µg/cm²
NASA	5
US Navy (non-immersion service)[1]	5
US Navy (immersion service)[1]	3
NORSOK (immersion service)[3]	2
Hempel (non-immersion service)[2]	19.5
Hempel (immersion service)[2]	6.9

[1] Cited in Appleman (2002).
[2] Hempel Paints.
[3] NORSOK Standard M-501, 1999.

are different values available in the literature; some are summarised in Tables 5.13 and 5.14, and in Fig. 5.6. It must be considered that these global values may be modified for certain applications and coating systems; in those cases paint manufacturers should be consulted. Zinc-based systems are far less vulnerable to salt concentration than are barrier systems, for example. Thresholds for chlorides and sulphates also depend on dry film thickness (DFT) of the applied paints (Table 5.14). Further information is provided by Alblas and van London (1997). It is important to realise that each different coating/substrate system is likely to have various parameters, including the chloride levels it can tolerate, that are unique to itself.

5.4.3 Substrate Cleanliness after Surface Preparation

A number of investigations were performed in order to evaluate the chloride content of steel substrates prepared by different surface preparation methods; this includes the studies of Allen (1997), Brevoort (1988), Dupuy (2001), Forsgren and Applegren

Table 5.14 Critical salt thresholds that result in early paint deterioration (Appleman, 2002; Morcillo and Simancas, 1997).

Coating system	DFT in μm	Salt thresholds in μg/cm²	
		Chloride (Cl)	Sulphate (SO_4)
Unknown	125–225	7–30	70–300
Unknown	25–35	>1	–
Unknown	7–11	6–25	9–35
Unknown	thin films	7	16
Unknown	100–150	–	58.8
Unknown	60–190	6–30	100–250
Unknown	130–180	5–10	50–100
Epoxy phenolic	one coat	1	–
Epoxy polyamide	three coats	5	–
Coal tar epoxy	254	50	–
Fusion-bonded epoxy	–	<3	–
Tank lining epoxy	–	10–20	–
Epoxy mastic	two coats	7	–

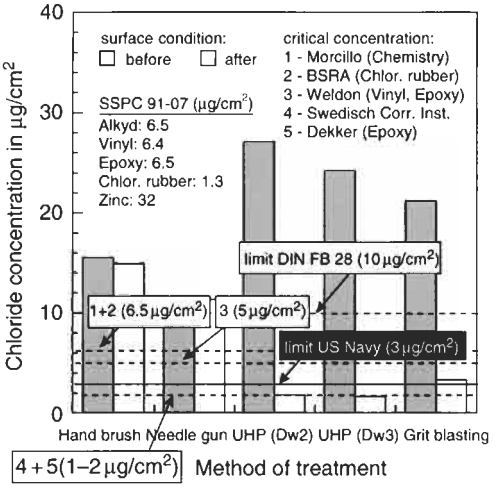

Figure 5.6 Permissible and realised chloride levels in ballast tanks (measurements: Allen, 1997).

(2000), Kuljian and Melhuish (1999), Morris (2000), Trotter (2001), NSRP (1998) and van der Kaaden (1994). Some results are summarised in Tables 5.15 and 5.16. A notable reduction in chloride level could be noted if wet blasting and hydroblasting were applied. In both cases the water flow involved in the preparation process entered pores, pits, pockets, etc. and swept the salt away. This mechanism was verified by results of SEM-inspections of hydroblasted surfaces (Trotter, 2001). Mechanical methods, such as needle gunning or wire brushing, did not remove soluble salts with the same reliability. Striking features were the high values for soluble iron, potassium

Table 5.15 Chloride levels measured after different pre-treatment methods (Forsgren and Applegren, 2000).

Method	Chloride level in $\mu g/cm^2$		
	Bresle (10 min)	SSM (10 s)	SSM (10 min)
No pre-treatment			
	44.8	47.5	61.3
	54.8	72.8	96.3
	15.2	–[1]	–[1]
	24.8	–[1]	–[1]
Wet blasting			
	1.6	1.4	2.7
	1.6	0.7	2.0
	0	1.7	3.1
	3.2	1.5	4.1
Hydroblasting			
	1.6	15.2	–
	0.8	1.8	4.2
	0	2.4	4.6
	1.2	0.1	2.1
	2.4	4.8	10.3
	1.2	0	1.0
	0	0	0.8
Wire brush			
	28.8	63.5	–
	16.0	32.6	58.9
	23.2	15.2	25.0
	17.6	18.1	30.3
Needle gun			
	27.6	19.9	42.6
	21.2	20.9	35.0
	26.8	41.3	96.1
	29.6	20.6	31.5
Dry grit blasting			
	4.4	8.3	14.8
	6.8	10.8	16.5

[1]No measurements.

and chloride after grit blasting in Table 5.17. Obviously, rust and sea salt could not be removed efficiently by this method. A study that included other salts (sulphates, phosphates, nitrates) was performed by Howlett and Dupuy (1993). This study showed the same trends as for the chlorides (see Table 5.16). It was further found that grit blasting did not remove chlorides to safe levels 50% of the time.

Conductivity readings (which characterise not only chloride content, but all dissolved salts) from hydroblasted surfaces were reported by Kuljian and Melhuish (1999). In most cases, conductivity levels dropped significantly after hydroblasting; 75% of all readings were under 20 $\mu S/cm$, and 95% are under 40 $\mu S/cm$. Results of this study are shown in Fig. 5.7. Interesting results were

Table 5.16 Surface contaminant results from different preparation methods (Howlett and Dupuy, 1993).

Substrate	Contaminant	Salt level in surface preparation method given in $\mu g/cm^2$			
		Uncleaned	Grit-blasted	Hydroblasted	Hydro-abrasive blasted
A-36 steel with mill scale	Sulphates	40	3	0	4
	Phosphates	0	0	0	3
	Chlorides	2	2	1	0
	Nitrates	0	6	0	6
A-285 Grade 3 steel with mill scale	Sulphates	5	5	0	1
	Phosphates	0	1	0	6
	Chlorides	4	3	1	1
	Nitrates	0	11	1	3
Rusted water service pipe	Sulphates	5	2	1	2
	Phosphates	1	2	0	6
	Chlorides	28	32	1	0
	Nitrates	6	1	1	8
Intact coating on water service pipe	Sulphates	8	4	0	0
	Phosphates	0	2	0	3
	Chlorides	6	1	1	0
	Nitrates	4	2	1	5
H_2S scrubber plate	Sulphates	39	7	0	3
	Phosphates	0	0	0	2
	Chlorides	12	8	0	1
	Nitrates	0	1	0	3
Heat exchanger shell	Sulphates	7	4	0	0
	Phosphates	0	0	0	7
	Chlorides	17	31	0	0
	Nitrates	0	3	0	6

Table 5.17 Soluble substances on prepared surfaces (Navy Sea System Comm., 1997).

Element	Soluble substance in $\mu g/cm^2$	
	Hydroblasting	Grit-blasting
Nickel	0.006	0.057
Zinc	0.063	1.512
Manganese	0.003	0.031
Magnesium	0.021	0.672
Calcium	0.121	1.989
Copper	0.033	0.250
Aluminium	0.003	0.352
Lead	0.015	0.045
Iron	0.018	9.450
Potassium	0.414	0.513
Sodium	0.855	42.03
Chloride	0.846	62.55
Sulphate	0.211	1.260
Total	2.611 (100%)	120.71 (4623%)

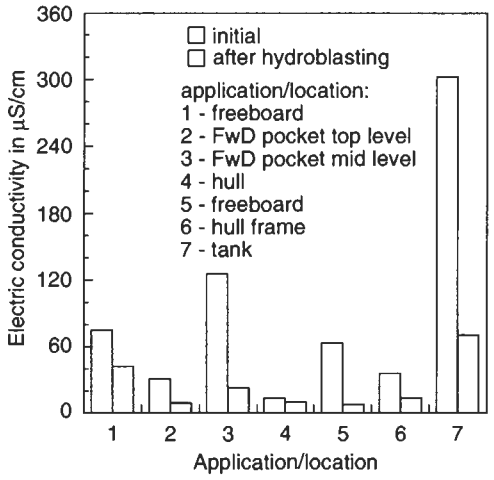

Figure 5.7 Conductivity readings on hydroblasted surfaces (NSRP, 1998).

obtained with seawater as the blasting medium. It was confirmed that a secondary fresh water blast was required in that case in order to guarantee a sufficiently clean surface.

5.5 Embedded Abrasive Particles

5.5.1 General Problem and Particle Estimation

Embedded grit is commonplace on grit-blasted surfaces and the prevention of this phenomenon during hydroblasting is becoming one of the most critical arguments. Embedded particles may act as separators between substrate and coating system, similar to dust. It was shown in a study by Soltz (1991) that this applied to larger size grit particles if they were left on surfaces and then painted over. If abrasive particles are notably contaminated with salts they may even cause rusting and blistering. This can happen even with small amounts of fine dust (Soltz, 1991). Certain studies were performed to investigate particle embedment during grit blasting, mainly by applying the following methods:

- low-power stereo zoom microscope (Fairfull and Weldon, 2001);
- the secondary electron-mode of SEM (Fairfull and Weldon, 2001; Momber *et al.*, 2002a); see Fig. 5.8(a);
- the back-scattered mode of SEM (Amada *et al.*, 1999; Momber *et al.*, 2002a,b); see Fig. 5.8(b);
- EDXA-plots from SEM-imaging (Momber, 2002b); see Fig. 5.9.

It was noted that the first method delivers generally much lower values than the SEM back-scatter images showed.

(a) Secondary electron mode.

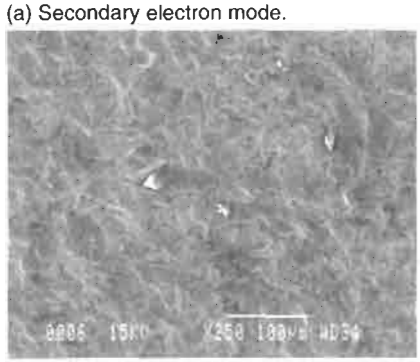

(b) Back-scattered mode, same image as (a).

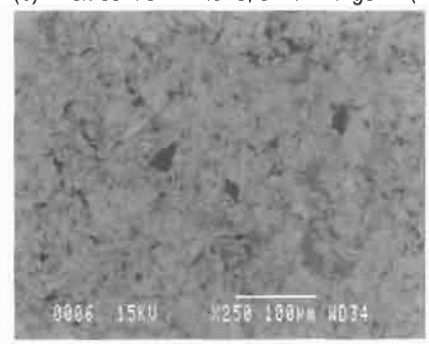

(c) Back-scattered mode.

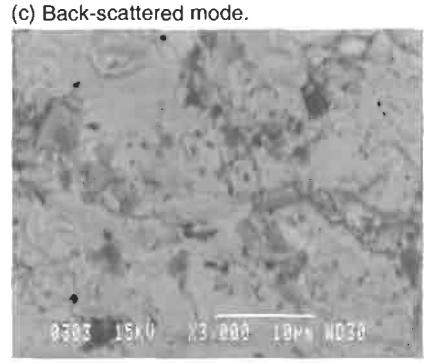

Figure 5.8 SEM-images of embedded grit (Momber et al.*, 2002a).*

5.5.2 Quantification and Influence on Coating Performance

Experimental results showed that grit embedment depended mainly on impact angle and abrasive type. The impact angle influence is shown in Fig. 5.10; an increase in the embedment could be noted as increased impact angle. Maximum embedment occurred at a 90° impact angle (Amada *et al.*, 1999). The dependence of embedment on the abrasive type is illustrated in Table 5.18; the dramatically different results for the investigated abrasives illustrate the effect of grit type and morphology. It seemed that slag material (except nickel slag) was very sensitive to grit embedment. Experiments with copper slag showed that the comminution (breakdown) behaviour of individual particles during the impact of the steel surface seemed to play an important role. It was apparent that the embedment was not simply due to discrete particles embedded in the substrate, but rather to extreme breakdown of the slag abrasive into minute particles, or a physical smearing of the grit over the surface (Fairfull and Weldon, 2001). A special effect was grit 'overblasting' due to multiple grit-blasting steps. This phenomenon applied to the grit blasting of already blasted surfaces (as usually occurring in grit blasting of deteriorated coatings or rusted steel surfaces). As shown in Table 5.24, 'overblasting' increased the contamination level due to additional grit embedment.

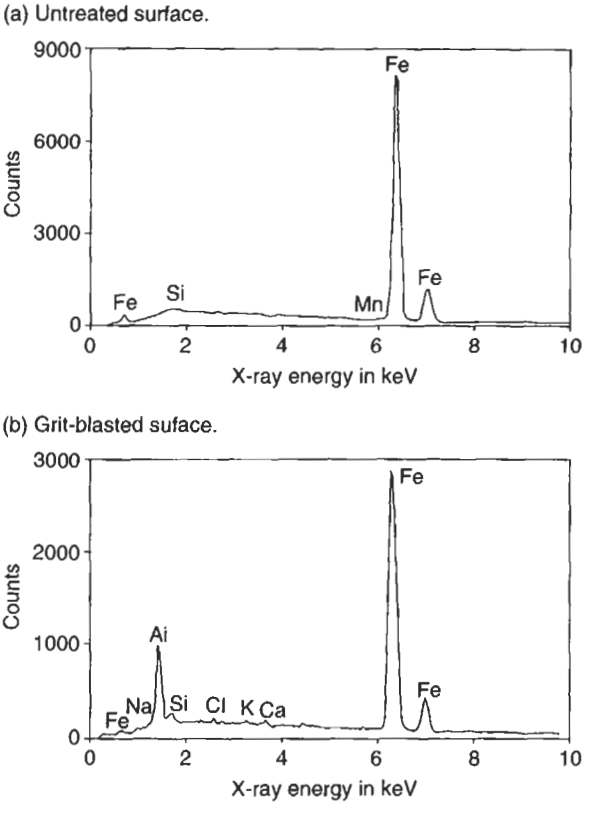

Figure 5.9 EDXA plots illustrating embedded grit residue (Momber, 2002).

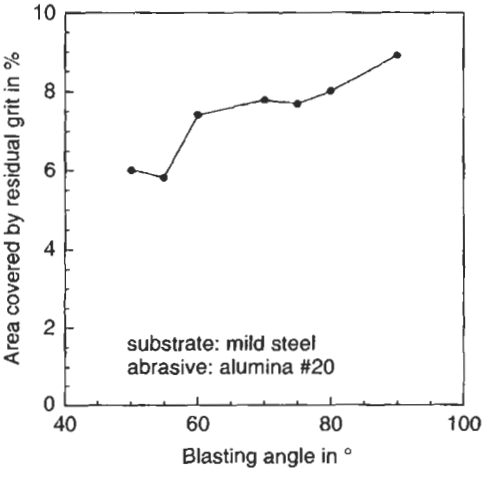

Figure 5.10 Blasting angle influence on grit embedment (measurements: Amada et al., *1999).*

Table 5.18 Embedment of grit particles in a carbon steel (measurements: Fairfull and Weldon, 2001).

Abrasive type	Embedment in %
Staurolite	0.1
Iron oxide	0.7
Silica sand	2.9
Nickel slag	1.2
Steel grit	4.1
Olivine	15.1
Copper slag	41.5
Garnet A	2.1
Garnet B	4.7
Coal slag A	11.1
Coal slag B	25.3

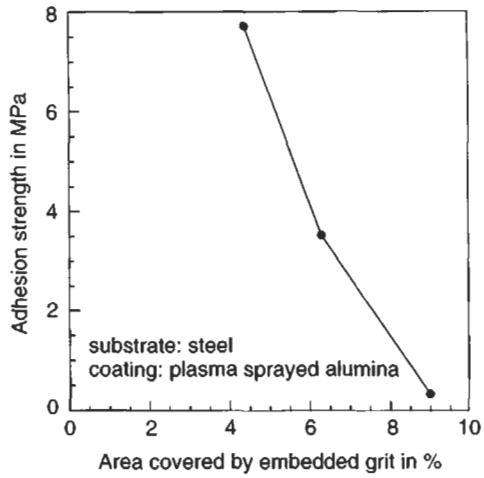

Figure 5.11 Influence of particle embedment on adhesion strength (measurements: Griffith et al., *1999).*

Embedded grit reduced the adhesion of the subsequent coating to the substrate. Figure 5.11 shows measurements of the adhesion strength as a function of the amount of embedded grits. The adhesion strength significantly reduced as the substrate surface contained embedded grit particles.

5.6 Wettability of Steel Substrates

Wettability of a substrate influences the performance of coating formation (Griffith *et al.*, 1997). Wettability is usually given in terms of contact angle of a liquid drop to the substrate (compare Fig. 5.19). A liquid drop spread measurement technique as introduced by Momber *et al.* (2002a) can also be applied to estimate the wettability of eroded surfaces. The Captive Drop Technique (CDT) as shown in Fig. 5.12 can be

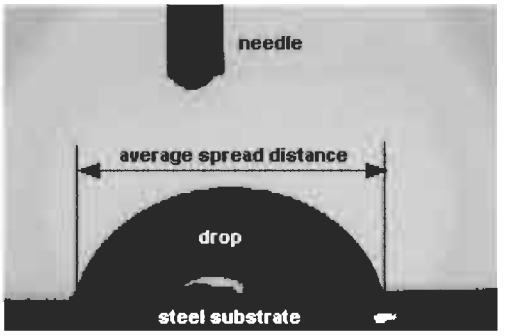

Figure 5.12 Drop spread distance measurement testing (Momber et al., *2002a) (scale: needle outside diameter is 1.5 mm).*

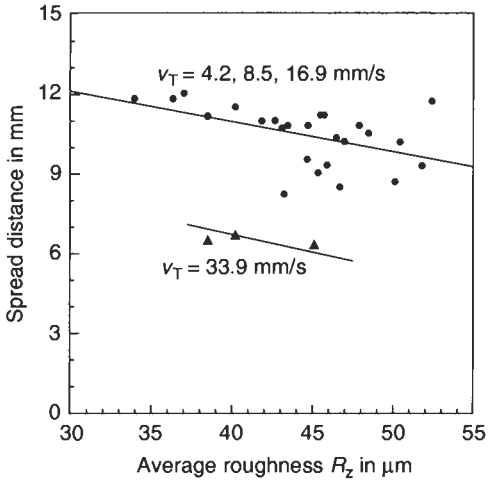

Figure 5.13 Roughness and wettability of hydroblasted carbon steel surfaces (measurements: Momber et al., *2002a).*

used for the generation and placement of the corresponding drops. The drop liquid is usually Cyclohexane which performs better than water. After the drop has been placed, a contact measuring machine consisting of video camera and computer is used for measuring the spread distance under equilibrium conditions. The larger the spread distance, the better the wettability of the surface. Results of the measurements are displayed in Fig. 5.13. These results are from hydroblasting tests on plain substrate material (no coating was removed). Note that wettability decreased as average roughness increased. This trend was also valid for other roughness parameters. However, wettability was unexpectedly low for high hydroblasting traverse rates, and the general relationship failed in these cases. This discrepancy was explained by Momber *et al.* (2002a) through microcrack formation in the substrate.

For high traverse rates, the local exposure time was not sufficient to form a net of intersecting fatigue cracks, and no material removal occurred. These aspects were discussed in more detail by Momber *et al.* (2002b).

5.7 Roughness and Profile of Substrates

5.7.1 Influence of Roughness on Coating Adhesion

ISO 8502 states the profile of a surface as one of the three major properties that influence coating performance. Substrate roughness is frequently specified by paint manufacturers, but not by all. An example specification reads as follows: 'For stainless steel: homogeneous and dense angular profile according to ISO Comparator "Medium" (G) or $R_Z = 50$ μm, respectively.' (Hempadur 45141). Many paint data sheets specify the average maximum roughness R_{Y5} rather than the global average roughness (R_a). Methods of how to evaluate substrate roughness are outlined in ISO 8503:

- profile comparator (ISO 8503-1, ISO 8503-2);
- microscope (ISO 8503-3);
- stylus instrument (ISO 8503-4).

Table 5.19 provides a comparison between comparator values and corresponding roughness values. According to those definitions, the specification mentioned above would require a fine comparator profile. However, comparator profiles are basically developed for steel abrasives, in detail for steel shot (comparator profile 'S'), and steel grit (comparator profile 'G'). Despite this limitation, comparators are used throughout the corrosion protection industry to evaluate profiles formed by other, non-metallic abrasive materials. Many commercial portable stylus instruments read the following profile parameters: R_a, R_Z and R_{max} (R_Y). These parameters are illustrated in Fig. 5.14. However, the arithmetical mean roughness (R_a) is not specified in coating sheets; the two other parameters are.

Roughness and profile notably affect adhesion between substrate and coating to be applied. Respective investigations were performed by Griffith *et al.* (1997) and Hofinger *et al.* (2002): two examples are presented in Table 5.20 and Fig. 5.15, respectively. Griffith *et al.* (1997) found that adherence of plasma sprayed alumina coatings to steel substrates improved if substrate average roughness (Fig. 5.15),

Table 5.19 Steel substrate profile parameters.

Comparator level	Profile (R_{Y5})[1] in μm
Fine	25–60
Medium	61–100
Coarse	101–125

[1] R_{Y5} denotes the average of five in-line measurements.

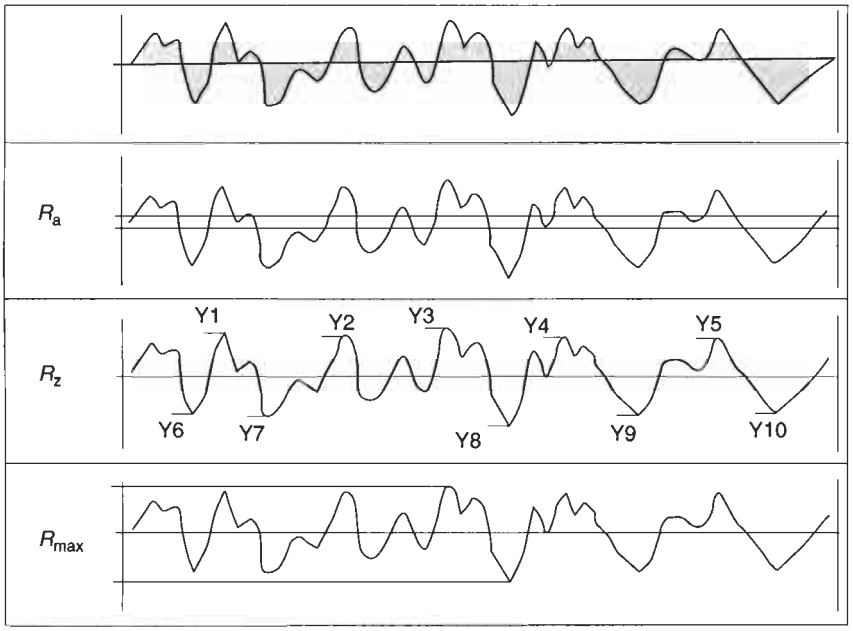

Figure 5.14 Surface roughness (profile) parameters (Hempel Book of Paints).

Table 5.20 Roughness effect on interface fracture energy (Hofinger *et al.*, 2002).

Roughness R_a in μm	Roughness R_Z in μm	Interface fracture energy in N/m
1.3	9.6	500 ± 30
2.2	15.4	530 ± 50
4.8	29.7	580 ± 40

average peak slope and peak spacing of the profile increased. However, the relationship for the peak spacing failed if a certain value for the peak spacing (ca. 250 μm) was exceeded. If this case occurred, adhesion between substrate and coating reduced. Therefore, profile parameters must be optimised in order to obtain a maximum adhesion. Hofinger *et al.* (2002) performed fracture experiments on interfaces between steel substrates and plasma sprayed coatings. As their results showed, a higher amount of energy was required to separate coating and substrate as substrate roughness increased (Table 5.20). Morcillo *et al.* (1989) investigated the effect of numerous parameters on roughness influence and found that there is a critical surface profile, the value of which is determined by the environment along with the type and thickness of the coating system. As the coating system increased in thickness, the effect of the surface profile on coating performance diminished. The critical surface profile was found to be a function of the aggressiveness of the environment – a more aggressive environment resulted in a lower critical profile.

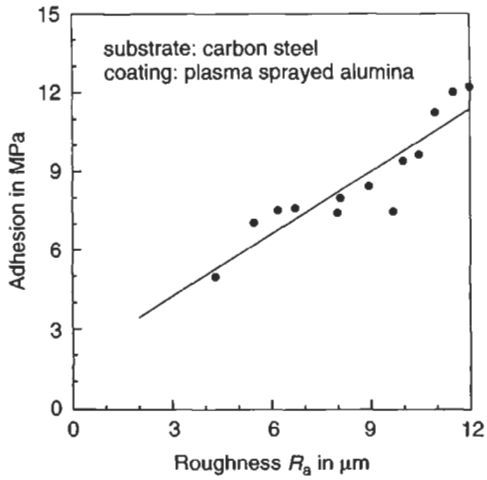

Figure 5.15 Roughness effect on adhesion (Griffith et al., *1997).*

5.7.2 Influence of Roughness on Paint Consumption

Paint consumption can be approximated as follows (Richardt, 1998):

$$C_P = \frac{DFT}{10 \cdot S_V} \cdot \frac{1}{\chi_C}. \tag{5.1}$$

Here, DFT denotes dry film thickness. S_V is the solid by volume that indicates what is left on the surface as a dry film after the solvents of the applied coating material have evaporated; this parameter is specified in most paint data sheets. The parameter χ_C is finally a loss correction factor, depending on specified DFT, applied method, substrate surface geometry and profile, wind conditions, etc. The dependence of χ_C on application method and substrate profile is listed in Table 5.21. It can be seen that paint consumption increases if profiled surfaces are painted instead of surfaces without profiles. It is mainly for that reason that paint manufacturers sometimes specify a maximum substrate roughness for certain types of coatings.

5.7.3 Surface Profiles on Remaining Coatings

If hydroblasting is used to remove deteriorated parts of a coating system and to expose tightly adhering coating layers it imparts a profile on the intact paint. This is shown in Fig. 5.3(a). These profiles can be measured using profile tapes; results of such measurements are listed in Table 5.22. As seen, the profiles of the coating surfaces ranged form 33 to 107 µm. This was an excellent profile (on paint) to accept overcoats of anti-corrosive coatings (NSRP, 1998).

Table 5.21 Paint loss correction factor χ_C (Richardt, 1998).

DFT in µm (one coat)	Roller / brush method		Airless spray method	
	Surface without profiles	Surface with profiles	Surface without profiles	Surface with profiles
1–25	0.57	0.54	0.44	0.42
26–50	0.62	0.59	0.48	0.46
51–100	–	–	0.57	0.54
>100	–	–	0.62	0.59

Table 5.22 Results of profile readings on exposed intact coatings (NSRP, 1998) (testing standard: ASTM D 4417, Method C).

Location	Profile in µm
USS Double Eagle	
Over anti-corrosive	43
Over anti-corrosive	33
Over anti-corrosive	43
Trinmar offshore pumping station	
Tank 16, over bare metal	102
Tank 16, over bare metal	112
Tank 16, over primer	102
Tank 16, over primer	96
Tank 16, over top coat	66
Tank 16, over top coat	91
Tank 16, over top coat	48
Tank 16, over top coat	46
Tank 19, over bare metal	86
Tank 19, over bare metal	107
Tank 19, over primer	96
Tank 19, over top coat	104
Tank 19, over top coat	43

5.7.4 Profiles on Hydroblasted Steel Substrates

It is often believed that hydroblasting cannot 'appreciably impart a profile on steel.' (NSRP, 1998). However, this statement is not generally true, and certain investigations were performed dealing with the use of high-speed water jets as a profiling method (Taylor, 1995; Knapp and Taylor, 1996; Miller and Swenson, 1999; Momber *et al.*, 2002a). Miller and Swenson (1999) found that material removal of the substrate might occur during hydroblasting under certain process conditions. Examples are shown in Fig. 5.16; notable surface modifications can be seen as results of the hydroblasting process.

(a) Right: untreated; left: hydroblasted. (b) Right: hydroblasted; left: grit-blasted.

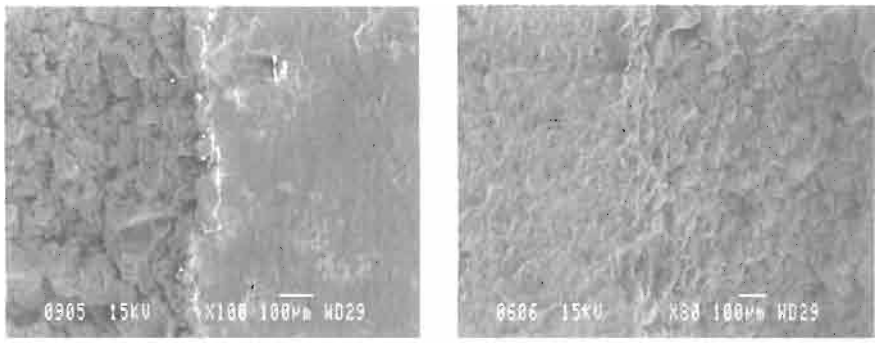

Figure 5.16 Hydroblasted steel surfaces (low-carbon steel).

Results of profile readings on hydroblasted virgin steel samples are summarised in Table 5.23. Similar values were reported by Taylor (1995). As can be seen, hydroblasting formed a notable profile on the substrate. However, performance rates were very slow in these cases. It was shown that roughness parameters of a substrate profiled by hydroblasting depended on specific material removal (in g/cm^2): the higher the material removal, the higher are the roughness values (Momber *et al.*, 2002a). Hydroblasted surfaces showed narrower spacing between profile peaks as compared to the grit-blasted samples. This is a very important issue because it is known that narrow peak spacing increases the adhesion to applied coatings (Griffith *et al.*, 1999). The adhesion properties of hydroblasted steel substrates were investigated in some detail by Knapp and Taylor (1996). The adhesion strength measured after hydroblasting was equal or even superior to values measured after grit-blasting. Typical adhesion strength readings are displayed in Fig. 5.17(a). It was also found that the standard deviation of strength readings was rather low for hydroblasting (Fig. 5.17(b)); it is conclusive that hydroblasting delivers a desired adhesion over a given cross section with a higher probability than grit-blasting. It may, however, be noted that these tests were performed at very high operating pressures of $p = 345$ MPa which is beyond the capacity of on-site plunger pumps. Nevertheless, the results were very promising and hydroblasting has a certain future capability to profile virgin steel surfaces.

5.7.5 Profiles on 'Overblasted' Steel Substrates

Further interesting aspects associated with grit-blasting are illustrated in Figs. 5.18 and 5.19. Figure 5.18 shows the influence of multiple grit-blasting ('overblasting') on the roughness values of steel substrates. The virgin steel is denoted '0', grit-blasted steel is denoted 'I', and twice grit-blasted steel is denoted 'II'. Note that – as expected – a single grit-blasting step (as performed during the new building of a ship) increased any roughness parameter, whereas the second grit-blasting step

Table 5.23 Results of hydroblasting profiling tests (Momber *et al.*, 2002a) (operating pressure: 200–275 MPa).

Specimen (preparation method)	Roughness parameter in µm					
	R_a	R_{max}	R_Z	R_S	R_t	R_P
Untreated	0.80	9.50	7.83	1.17	16.35	5.27
Grit-blasting 1	2.27	18.40	15.90	2.73	19.23	8.80
Grit-blasting 2	1.87	15.00	12.77	2.27	15.43	6.67
Grit-blasting + hydroblasting 1	8.00	52.20	44.30	33.10	52.67	22.00
Grit-blasting + hydroblasting 2	8.13	55.60	44.00	32.41	57.83	23.73
Grit-blasting + hydroblasting 3	8.87	60.27	50.17	36.73	62.13	26.13
Hydroblasting 1	9.77	63.23	51.00	38.20	64.30	29.33
Hydroblasting 2	8.50	51.40	45.73	34.57	52.03	22.27
Hydroblasting 3	9.20	55.07	49.40	36.87	62.17	28.13
Hydroblasting 4	6.77	52.50	41.27	29.33	52.77	23.37
Hydroblasting 5	7.77	52.60	43.87	31.97	53.33	22.60
Hydroblasting 6	7.43	52.17	43.57	31.87	54.43	23.27
Hydroblasting 7	6.10	50.03	35.83	26.27	51.17	19.87
Hydroblasting 8	8.60	54.87	46.17	34.70	57.63	25.93
Hydroblasting 9	8.47	56.30	46.27	34.33	59.33	25.53
Hydroblasting 10	7.83	55.30	46.20	33.87	56.77	26.43

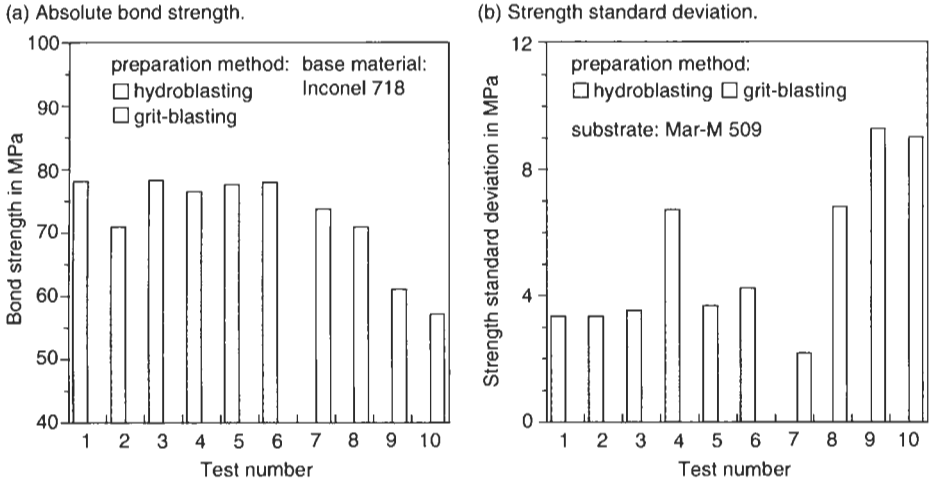

Figure 5.17 Adhesion testing on substrates profiled by hydroblasting (Knapp and Taylor, 1996).

(as performed during the stripping of worn coatings or rust) again decreased the roughness. Although these are preliminary results it may be possible that grit-blasting affects the original profile in a negative way. Similar relationships are shown in Fig. 5.19 which displays results of comparative contact angle measurements.

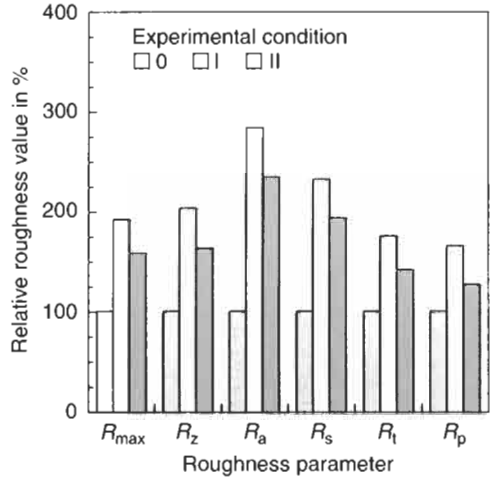

Figure 5.18 Multipass grit-blasting effect on profile roughness (Momber, 2002).

Considering a non-porous material, an increase in the contact angle may be the result of an increase in surface roughness according to Wenzel's (1939) formulation:

$$r_R = \frac{\cos \theta_R}{\cos \theta_0} \propto \frac{A_R}{A_0}. \tag{5.2}$$

Here, r_R is a so-called roughness factor considering the profile of a rough surface, θ_R is the contact angle of the rough surface, A_R is the true (rough) surface, and A_0 is a perfectly smooth surface (in the case discussed here this is the surface of the untreated surface). For a completely smooth (untreated) surface, $r_R = 1$ and $\theta_R = \theta_0$. It can be seen from Eq. (5.2) that the contact angle increased as the roughness factor increased. From Fig. 5.19, it can be seen that contact angle at the twice grit-blasted steel surface was lower than the contact angle at the initially eroded surface. Therefore, roughness decreased. The exact values are given in Table 5.24. This 'overblasting' caused the surface to have a high number of flat regions, a lower peak to valley height and a significant number of laps and tears due to the folding and plastic deformation. This was verified by comparative SEM-studies (Momber, 2002b). Other authors (Griffith, 2001) described similar phenomena.

5.8 Aspects of Substrate Surface Integrity

Substrate surface integrity may include surface properties, namely hardness, residual stresses and fatigue limit. The liquid drop technique has been used in the laboratory for surface integrity enhancement for several years. Corresponding studies were

(a) Plain, untreated surface ($\theta_A = 145°$).

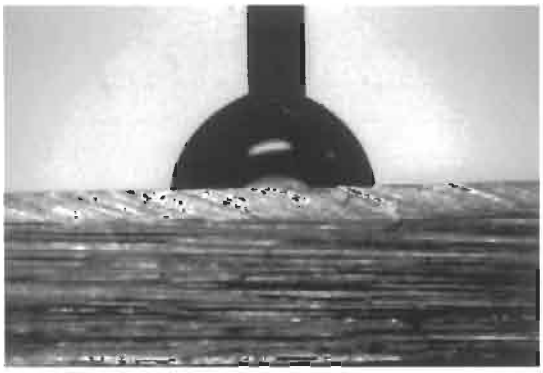

(b) Grit-blasted surface ($\theta_A = 169°$).

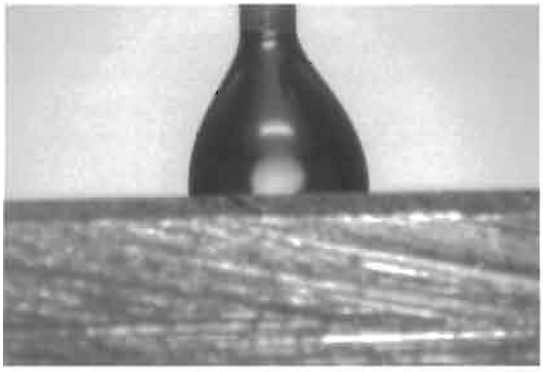

(c) Twice grit-blasted surface ($\theta_A = 141°$).

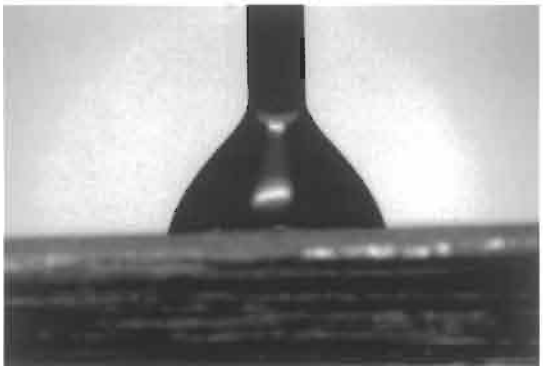

Figure 5.19 Advancing contact angles on steel surfaces (Momber, 2002).

Table 5.24 Results of grit 'overblasting' (Momber, 2002).

Parameter	Test condition		
	Untreated (0)	One grit-blasting step (I)	Two grit-blasting step (II)[1]
Contact angle (advancing) θ_A in °	145.4	168.9	140.6
Contact angle (receding) θ_R in °	131.9	157.8	117.4
Contact angle (equilibrium) θ_E in °	130.7	137.3	135.3
Roughness factor r_R	1.0	1.13	1.09
Grit contamination in %	0	6.6	7.4
R_{max} in μm	9.50 ± 3.50	18.40 ± 0.90	15.00 ± 1.20
R_Z in μm	7.83 ± 2.87	15.90 ± 0.10	12.77 ± 0.47
R_a in μm	0.80 ± 0.30	2.27 ± 0.43	1.87 ± 0.07
R_S in μm	1.17 ± 0.03	2.73 ± 0.27	2.27 ± 0.07
R_t in μm	16.35 ± 5.80	19.23 ± 1.47	15.43 ± 1.03
R_P in μm	5.27 ± 2.63	8.80 ± 1.60	6.67 ± 0.37

[1] Overblasting.

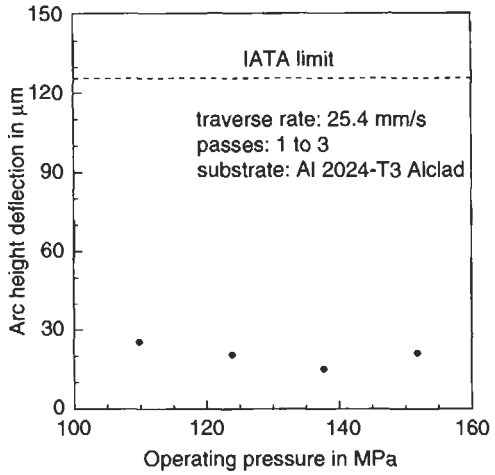

Figure 5.20 Arc height deflection on hydroblasted composites (Harbaugh and Stone, 1993).

performed, among others, by Colosimo *et al.* (2000), Haferkamp *et al.* (1989) and Tönshoff *et al.* (1995). Water jets can induce residual compressive stresses due to plastic flow on the surface of metals. Test series that addressed this issue was run by Harbaugh and Stone (1993) on aircraft coatings and substrates with operating pressures up to 152 MPa. Arc height deflections from Almen stripes hit by the water jets were determined for plain and coated aluminium alloys and related to residual stresses created in the material during hydroblasting. Some examples are shown in Fig. 5.20. Deflections were less than 38 μm for coated specimens, and less than 76 μm for plain metals. However, a critical threshold of 127 μm was in no case

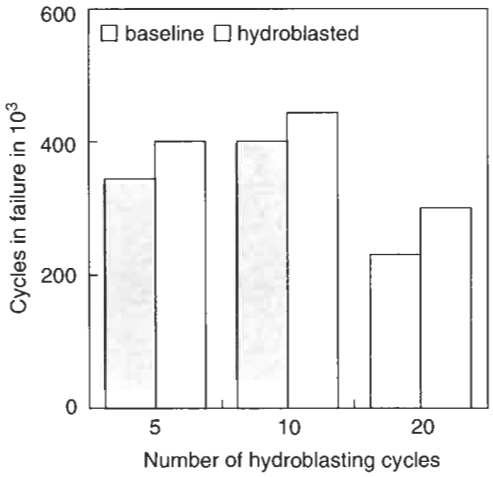

Figure 5.21 Results of fatigue tests on hydroblasted fuselage sections (Volkmar, 1992).

exceeded. This agreed with results obtained by Volkmar (1992). The higher values for the uncoated material can be explained through additional energy dissipation during coating deformation and removal.

Fatigue life becomes a problem if water jets are applied to sensitive structures, such as airplane fuselage or wings. Holographic and strain gauge measurements performed during fatigue and vibration tests on airplane fuselages have shown that induced fatigue life reduction is below critical levels for 100 mm stand-off distance between nozzle exit and surface (Volkmar, 1992). Cycle tests on a hydraulic testing machine evidenced that fatigue is not a concern. Representative results are plotted in Fig. 5.21. (These tests have been performed with rather low operating pressures of 50 MPa.)

CHAPTER 6

Hydroblasting Standards

6.1 Introduction

A number of standards have been developed during recent years in order to define and to characterise steel surfaces prepared by hydroblasting. These standards are more or less based on the standard preparation grades given in ISO 8501-1 (uncoated parts of the surface), and ISO 8501-2 (partial surface preparation). Two types of standards can be distinguished, namely written standards and visual standards.

- Written standards:
  - SSPC-SP 12/NACE No. 5: 'Surface Preparation and Cleaning of Metals by Waterjetting Prior to Recoating' (1995).
- Visual standards issued by independent organisations:
  - STG Guide No. 222: 'Definition of preparation grades for high-pressure water-jetting' (1992).
  - SSPC-VIS 4/NACE 7: 'Guide and Reference Photographs for Steel Surfaces Prepared by Waterjetting' (2001).
  - US Navy: 'Process Guide for Waterjetting Operations in Navy Shipyards'.
- Visual standards issued by paint manufacturers:
  - Hempel: 'Photo Reference Water Jetting' (1997).
  - International Paint: 'Hydroblasting Standards' (1995).
  - Jotun: 'Degrees of Flash Rusting – Guidelines for Visual Assessment of Flash Rusting' (1995).

Hydroblasting surface standards cover the following surface issues (see Fig. 6.1):

- initial condition (rusty steel or primers);
- visual surface preparation definition (visible contaminants, cleaning degrees);
- non-visible surface cleanliness definition (basically salt levels);
- flash-rusted surface definition.

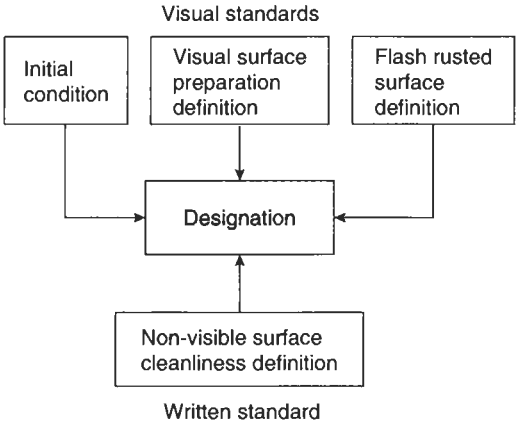

Figure 6.1 Issues of hydroblasting/water jetting standards.

Table 6.1 Contents of hydroblasting/water jetting standards.

Standard	Surface reference for				
	Rusty steel	Coating/ primer	Flash rust	Salt level	Cleaning degree
SSPC-SP 12/NACE No. 5[1]			x	x	x
SPC-VIS 5/NACE 7	x	x	x		x
Hempel's Photo Reference	x	x	x		x
International Hydroblasting Standards	x		x		x
STG Guide No. 2222	x	x			x
Jotun Guidelines on Flash Rusting			x		

[1]Written standard.

Table 6.1 provides a general review of the content of the standards.

There are three very important points to be addressed if hydroblasting/water jetting standards are applied:

(i) The first point is that hydroblasted surfaces do not look the same as those produced by dry abrasive blasting, or by slurry or wet blasting.

(ii) The second point is that visual standards should always be used in conjunction with the written text, and should not be used as a substitute for a written standard.

(iii) The third point is that some of the standards are limited to certain substrate materials. Hempel's Water Jetting Standard states: 'The steel is normal shipbuilding steel'. The SSPC-VIS 4/NACE VIS 7 limits its range to 'unpainted rusted carbon steel and painted carbon steel.' Therefore, care must be taken in applying these standards to other substrate materials.

6.2 Initial Conditions

Initial conditions are designated in several standards (see Table 6.1). These conditions can be subdivided into two groups:

(i) rusty steel (C, D);
(ii) primers or coatings.

The initial steel grades C and D often characterise 'new construction' conditions; they are adapted from ISO 8501-1 (1988). They apply to uncoated steel surfaces that are deteriorated due to severe corrosion. These rust grades are defined as follows:

- steel grade C:
  'Steel surface on which the mill scale has rusted away from which it can be scraped, but with slight pitting visible under normal vision.' (see Fig. 6.4(a)).
- steel grade D:
  'Steel surface on which the mill scale has rusted away and on which general pitting is visible under normal vision.' (see Fig. 6.2(a)).

(a) Rusty steel (rust grade D; below the rusty layer a thin, almost black oxide layer is adhering to the steel).

(b) Old coating, consisting of several layers, damaged on top sides, DFT 300–370 µm.

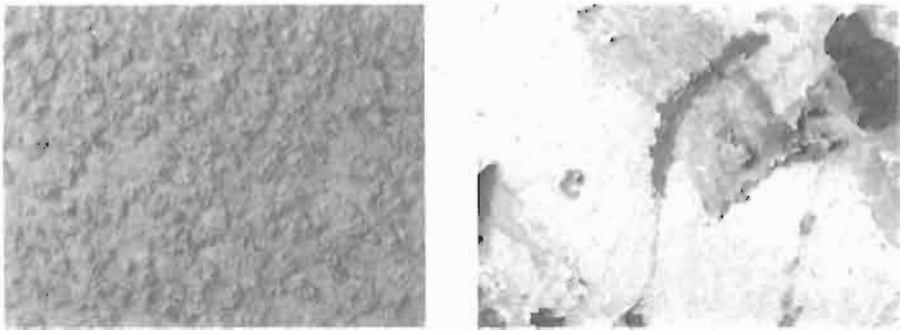

Figure 6.2 Examples for initial conditions of a plain steel and a previously coated surface (STG 2222).

Previously coated steel surfaces are characterised as 'maintenance' conditions. There is a large number of possible systems and coating conditions. Cleaning results do not depend on the intensity of cleaning only in these cases, but also essentially on the type, thickness and adhesion of the coating systems, and on earlier surface preparation steps. For these reasons, only analogous applications to real cases can usually be derived. The coated steel surfaces considered in the hydroblasting standards include the following coating/primer systems and conditions:

- paints applied over blast-cleaned surface; paints mostly intact (see Fig. 6.3(a));
- painting systems applied over mill-scale bearing steel; systems thoroughly weathered, thoroughly blistered or thoroughly stained;
- degraded painting systems applied over steels (see Fig. 6.2(b));
- multilayer systems with intercoat flaking and underrust;
- shop primers with mechanical damage and white rust.

The most detailed descriptions of previously applied coatings can be found in STG 2222 (1992). This standard provides degree of rusting (Ri2 to Ri4) in accordance with ISO 4628-3 and DIN 53210, and total film thickness of the paint systems.

6.3 Visual Surface Preparation Definitions and Cleaning Degrees

Visible contaminants and cleaning degrees are defined in all standards except Jotun's Flash Rust Standard (see Table 6.1). Visible contaminants include the following:

- rust;
- previously existing coatings;
- mill scale;
- foreign matter.

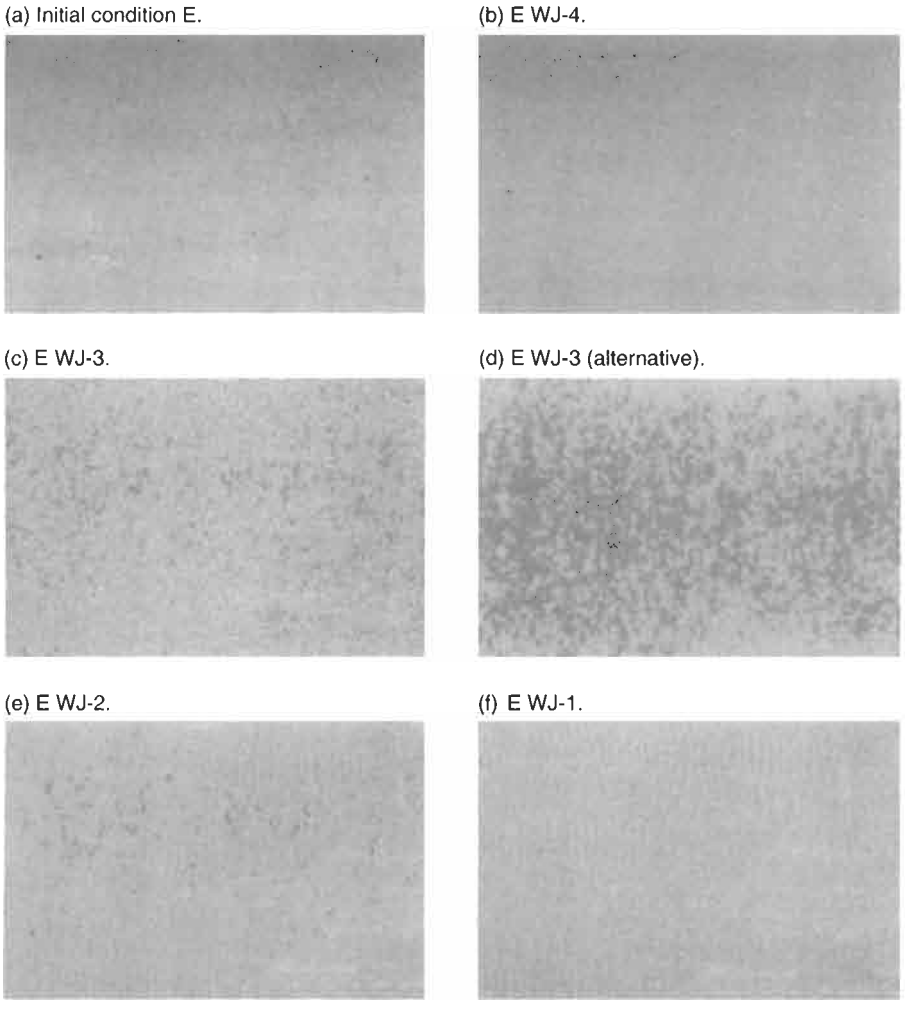

Figure 6.3 Examples for cleaning degrees (compare Table 6.3). Previously painted steel surface; light-coloured paint applied over blast-cleaned surface; paint mostly intact (SSPC-VIS 4/NACE VIS 7).

Cleaning degrees are defined according to the presence of these matters. The highest cleaning degree always requires that the surface shall be free of all these matters, and have a metal finish. The cleaning degrees designated in all standards are based on the definitions given in ISO 8501-1 for blast cleaned surfaces. Comparative cleaning degrees are listed in Table 6.2.

Of particular interest are the definitions given in SSPC-12/NACE No. 4 because they are adapted by numerous other standards, and because the definitions provide a quantitative measure of surface cleanliness (in terms of limited percentage of adherent foreign matter). These definitions are listed in Table 6.3. A typical surface preparation specification for a coating system (Amercoat® 357, Ameron International) reads as

Table 6.2 Comparative cleaning degrees (visible contaminants).

Standard	Cleaning degree			
ISO 8501-1	Sa 1	Sa 2	Sa 2 1/2	Sa 3
SSPC	SP 7	SP 6	SP 10	SP 5
NACE	4	3	2	1
SSPC-SP 12/NACE No. 5	WJ-4	WJ-3	WJ-2	WJ-1
Hempel's Photo Reference	WJ-4	WJ-3	WJ-2	WJ-1
International Hydroblasting Standard	–	HB 2	HB 2 1/2	–
STG Guide No. 2222	Dw 1	Dw 2	Dw 3	–

Table 6.3 Visible surface preparation standards (SSPC-12/NACE No. 4).

Term	Description of surface (when viewed without magnification)
WJ-1	Clean to bare substrate: the surface shall be cleaned to a finish which is free of all visible rust, dirt, previous coatings, mill scale and foreign matter. Discoloration of the surface may be present.
WJ-2	Very thorough or substantial cleaning: the surface shall be cleaned to a matte (dull, mottled) finish which is free of all visible oil, grease, dirt and rust except for randomly dispersed stains of rust, tightly adherent thin coatings and other tightly adherent foreign matter. The staining or tightly adherent matter is limited to a maximum of 5% of the surface.
WJ-3	Thorough cleaning: the surface shall be cleaned to a matte (dull, mottled) finish which is free of all visible oil, grease, dirt and rust except for randomly dispersed stains of rust, tightly adherent thin coatings and other tightly adherent foreign matter. The staining or tightly adherent matter is limited to a maximum of 33% of the surface.
WJ-4	Light cleaning: the surface shall be cleaned to a finish which is free of all visible oil, grease, dirt, dust, lose mill scale, loose rust and loose coating. Any residual material shall be tightly adherent.

follows: 'UHP waterjeting per SSPC-SP12/NACE No.5, WJ-2L or better is acceptable for coated steel previously prepared to SP-10 or better.' (See Table 6.3 for definition of WJ-2.) Examples of visual designations of the cleaning degrees listed in Table 6.3 are provided in Fig. 6.3, based on the removal of light-coloured paint applied over blast-cleaned surface, and in Fig. 6.4, based on the preparation of a rusted surface. Paint manufacturers recommend that, to ensure good adhesion, surfaces should be cleaned to one of the grades higher than WJ-4 (Kronborg, 1999).

6.4 Non-Visible Surface Cleanliness Definitions

Problems associated with non-visible contaminants, in particular with soluble salts, are discussed in detail in Section 5.4. Non-visible contaminants are considered

Table 6.4 Definitions for non-visible surface cleanliness (SSPC-SP 12/NACE No. 5).

Term	Description of surface
NV-1	Free of detectable levels of soluble contaminants, as verified by field or laboratory analysis using reliable, reproducible methods.
NV-2	Less than 7 $\mu g/cm^2$ of chloride contaminants, less than 10 $\mu g/cm^2$ of soluble ferrous ion levels, or less than 17 $\mu g/cm^2$ of sulfate contaminants as verified by field or laboratory analysis using reliable, reproducible test methods.
NV-3	Less than 50 $\mu g/cm^2$ of chloride or sulphate contaminants as verified by field or laboratory analysis using reliable, reproducible test methods.

only in the written standard SSPC-SP 12/NACE No. 5, but are limited to water-soluble chlorides, iron-soluble salts and sulphates. This standard distinguishes between the three levels of non-visible contaminants listed in Table 6.4. Other non-visible contaminants, namely thin oil or grease films are not specified. None of the visual standards defines non-visible contaminants simply because they cannot be detected by the naked eye. However, some standards mention the ability of hydroblasting to remove salt, particularly from badly pitted and corroded steels. Paint manufacturers usually do not specify non-visible contaminants because of the problems outlined in Section 5.4.2. A rather typical demand reads as follows: 'Prior to coating, primed surface must be... free of all contaminants including salts.' (Amercoat® 357, Ameron International). Such vague specifications are difficult to meet, and care must be taken to consult the paint manufacturer for a more detailed information. Information about permissible salt levels is provided in Tables 5.13 and 5.14.

6.5 Flash Rusted Surface Definitions

Problems associated with flash rust are discussed in detail in Section 5.3. Degrees of flash rusting are defined in several standards (see Table 6.1). Basically, the temporal development of rusting is considered, and flash rusting degrees are defined and distinguished according to the following criteria:

(i) colour of the rust layer (e.g., 'yellow-brown rust layer');
(ii) visibility of the original steel surface (e.g., 'hides the original surface');
(iii) adherence of the rust layer (e.g., 'loosely adherent').

In the early stage of flash rusting (FR-1, L, JG-2), the rust layer is usually of a brown colour; the original steel surface is partially discoloured; the rust is tightly adhering. In the latest stage of flash rusting (FR-3, H, JG-4), the colour turns to red; the original steel surface is hidden; the rust is loosely adhering. The tape method according to Hempel's Water Jetting Standard, that can be used to quantify flash rust degrees, is already described in Section 5.4 (see also Fig. 6.4). Other simple, and only

qualitative methods are listed in Table 6.5. It can be seen that a rough estimate of heavy flash rust is its capability to significantly mark 'objects' (cloth, dry hand) brushed against or wiped over it. A typical specification statement for a coating system (Hempadur 4514, Hempel Paints) applied to flash rusted surfaces reads as follows: 'A flush rust of FR-2 for atmospheric conditions, and FR-2 (preferably FR-1) for water conditions, respectively, is acceptable prior to coating.' Examples of visual designations of the flash rust definitions listed in Table 6.6 are provided in Fig. 6.4, based on the surface preparation of rusted steel surfaces.

Methods for the removal of flash rust that is too heavy for coating applications are recommended in several standards. These methods include brushing (for small areas) and washing down with pressurised (pressure above 7 MPa) fresh water. Although pressure washing causes the surface to re-rust, it is possible to reduce the degree of flash rust from heavy to light.

Table 6.5 Approximate methods for estimating heavy flash rust adhesion.

Standard	Method for estimating heavy flash rust adhesion
International Hydroblasting Standard (H)	This layer of rust will be loosely adherent and will easily mark *objects* brushed against it.
SSPC-VIS 4/NACE VIS 7 (H)	The rust is loosely adherent, and leaves significant marks on a *cloth* that is lightly wiped over the surface.
Hempel Photo Reference Water Jetting (FR-3)	The rust is loosely adhering and will leave significant marks on a *dry hand*, which is swept over the surface with a gentle pressure.

Table 6.6 Flash rust surface definitions (SSPC-SP 12/NACE No. 5).

Term	Description of surface (when viewed without magnification)
No flash rust	A steel surface which exhibits no visible flash rust.
Light (L)[1] others: Slight (JG-2)[2] (FR-1)[3]	A surface which exhibits small quantities of a yellow-brown rust layer through which the steel substrate may be observed. The rust or discoloration may be evenly distributed or present in patches, but it is tightly adherent and not easily removed by lightly wiping with a cloth.
Moderate (M)[1] others: Moderate (JG-3)[2] (FR-2)[3]	A surface which exhibits a layer of yellow-brown rust that obscures the original steel surface. The rust layer may be evenly distributed or present in patches, but it is reasonably well adherent and leaves light marks on a cloth that is lightly wiped over the surface.
Heavy (H)[1] others: Considerable (JG-4)[2] (FR-3)[3]	A surface which exhibits a layer of heavy red-brown rust that hides the initial surface condition completely. The rust may be evenly distributed or present in patches, but the rust is loosely adherent, easily comes of and leaves significant marks on a cloth that is lightly wiped over the surface.

[1]Equivalent definition in International Hydroblasting Standards.
[2]Designation according to Jotun.
[3]Designation according to Hempel.

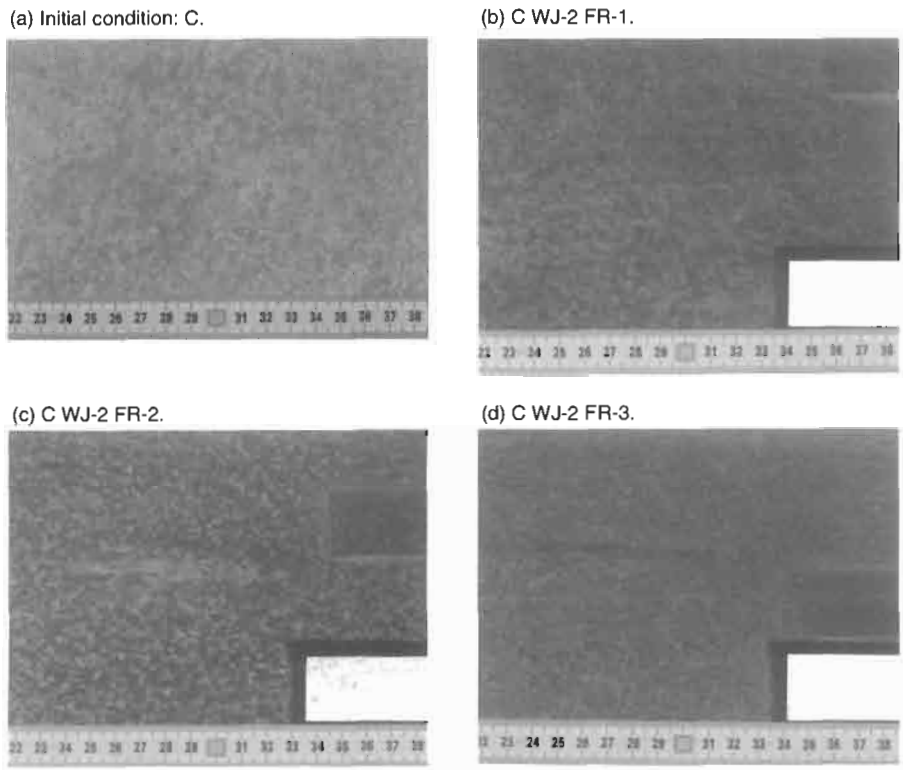

Figure 6.4 Visual flash rust designations (compare Tables 6.5 and 6.6); rusty steel: rust grade C (Hempel Photo Reference Water Jetting).

6.6 Special Advices

Hydroblasting/water jetting standards all contain sections with special advice which should be read with care. These include the following:

- Procedures for using standards (especially photographs);
- Inspecting areas of difficult access (e.g. backs of stiffening bars);
- Inspecting blasted surfaces prior to flash rusting;
- Limitations to hydroblasting (e.g. the removal of oil and grease, or milscale);
- Time of surface assessment.

CHAPTER 7

Alternative Developments in Hydroblasting

7.1 Pulsed Liquid Jets for Surface Preparation

7.1.1 Types and Formation of Pulsed Jets

It has been shown in the previous Chapters that any impacting water jet exhibits two pressure levels: an impact pressure in the very early stage of jet impact (p_D), and a stagnation pressure (p_{ST}) that is established after the impact period. The impact pressure is given through Eq. (2.23), the stagnation pressure can be estimated based on Bernoulli's law:

$$p_S = (\rho_W/2) \cdot v_J^2. \tag{7.1}$$

The ratio between these pressure levels depends on the jet velocity and can be estimated from $p_S = p_D$ as follows:

$$R_P = \frac{p_D}{p_S} = \frac{2 \cdot c_F}{v_J}. \tag{7.2}$$

This relationship is illustrated in Fig. 7.1 in terms of operating pressures. The pressure ratio equals the value $R_P = 1$ for $v_J = 2 \cdot c_F$. The corresponding operation pressure would be $p \cong 4 \cdot 10^3$ MPa. This high value cannot be realised by commercial plunger pumps or pressure intensifiers. For a rather low pressure, say 30 MPa, the pressure ratio is about $R_P = 11$ (see Fig. 7.1). It was shown in Section 2.4.2 that erosion efficiency increases as operating pressure increases. This relationship challenges the use of mechanisms able to produce high-speed fluid slugs. Basically, the following two types of pulsed water jets can be distinguished (see Fig. 7.2):

- low-frequency water jets ($f_P = 1$ kHz);
- high-frequency water jets ($f_P > 5$ kHz).

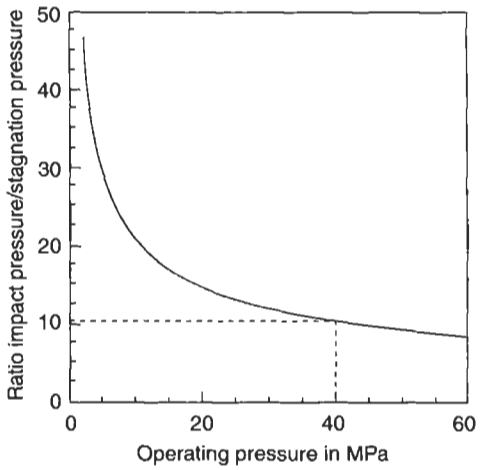

Figure 7.1 Pressure ratio during jet impact.

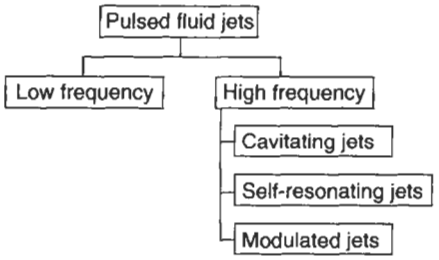

Figure 7.2 Subdivision of pulsating jets.

Both techniques involve the modulation of continuous high-speed water jets. The difference to 'naturally pulsed jets' (formed due to aero-dynamic drag, see Fig. 2.6) is that the jets are artificially interrupted. Pulsed jets can be produced in several ways using different driving energy sources. When considering the use of pulsed jet devices, the following criteria should be kept in mind:

- size and weight;
- ease of manufacture;
- cost effectiveness;
- mobility;
- reproducibility of cleaning results;
- reliability under site conditions;
- safety.

Therefore, only a few technical solutions, although more were successfully applied under laboratory conditions, can currently be used under site conditions; they include the following:

- cavitating jets;
- ultrasonically modulated jets;
- self-resonating jets.

Technical fundamentals as well as applications of these types of pulsating jets to surface cleaning will be discussed in the subsequent sections. Low-frequency pulsating water jets, such as water cannons, are frequently applied to break and fracture massive solids, but they are not suitable for decoating and paint stripping; see Momber (1998a) for more details about this technique.

The two most important parameters of pulsed liquid jets are loading intensity and loading frequency. For some pulsed liquid jet concepts water jet velocity and pulse frequency cannot be varied independently from each other. Both parameters must be selected according to the material to be eroded. Materials usually called ductile may require high-frequency loading, whereas materials usually considered brittle may be more sensitive to a longer loading period. Loading intensity is basically a function of jet velocity. Frequency, however, depends on the mechanism used to form the pulsating jet.

7.1.2 Surface Preparation with Cavitating Water Jets

It was proved that cavitation erosion is a very promising method for efficient coating removal (Kaye *et al.*, 1995). Cavitation is defined as the formation, growth and collapse of vapour filled cavities in liquid flow. The cavity bubbles begin as tiny undissolved gas nuclei in the liquid. Subsequent to their formation and growth in the localised regions of higher local pressure, the cavities are carried by the flow into the regions of higher local pressure where they collapse. Detailed descriptions of cavitation phenomena are provided in the standard literature (Knapp *et al.*, 1970; Lecoffre, 1999). Cavitation can damage and erode materials by the following mechanisms:

- generation of shock waves due to symmetric bubble implosion;
- formation of micro-jets due to non-symmetric bubble implosion (Lauterborn and Bolle, 1975), see Fig. 7.3);
- collapse of bubble clusters (Dear and Field, 1988).

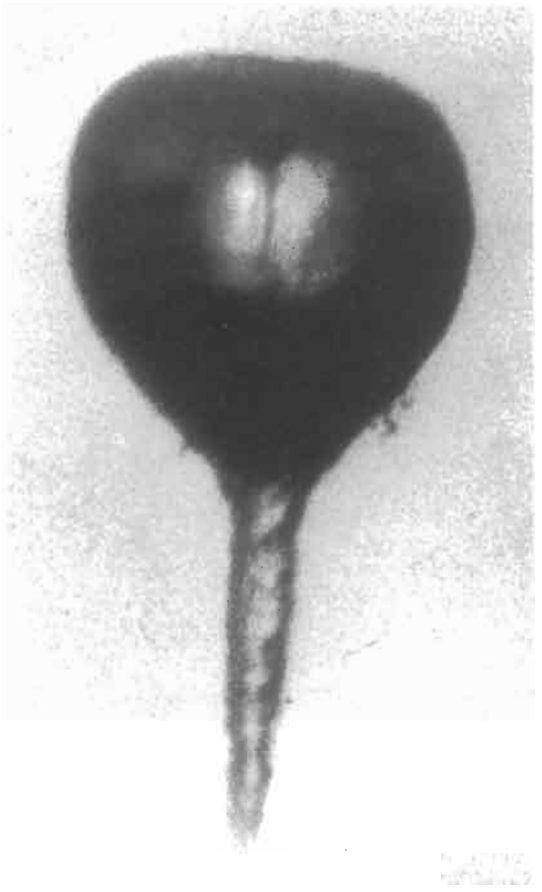

Figure 7.3 Micro-jet formation during non-symmetric bubble implosion (photograph: Lauterborn, Univ. Göttingen).

However, a superposition of several individual mechanisms is very likely. The pressure generated during the implosion and collapse of cavitation bubbles is typically in the range of several 10^2 MPa. Conn (1972) provides an analysis of the collapse pressure of vapour bubbles cavitating in the region where a fluid jet impacts a material surface. This pressure is given by

$$p_J = \frac{p_S}{6.35} \cdot \exp(2/3 \cdot \alpha_G). \tag{7.3}$$

The equation illustrates the influence of the gas content in the jet on the collapse pressure. A graphical solution of Eq. (7.3) for different gas content is provided in Fig. 7.4 (the stagnation pressure is replaced by the jet velocity). This graph also shows that collapse pressures exceed even the impact pressure developed during the impact of a fluid slug by an order of magnitude. A pressure ratio, R_P^*, can again be defined to evaluate the effectiveness of cavitating water jets:

$$R_P^* = \frac{p_J}{p_D} = \frac{v_J}{12.7 \cdot c_F} \cdot \exp(1/\alpha_G). \tag{7.4}$$

Values for the pressure ratio can be as high as $R_P^* = 32$ as shown in Fig. 7.4. However, concrete values depend on gas content and bubble size (Houlston and Vickers, 1978).

Fouling removal tests with cavitating water jets and self-resonating water jets were performed by Conn and Rudy (1978); the results are listed in Table 7.1. The cleaning rates are rather high compared to values known from standard hydroblasting applications.

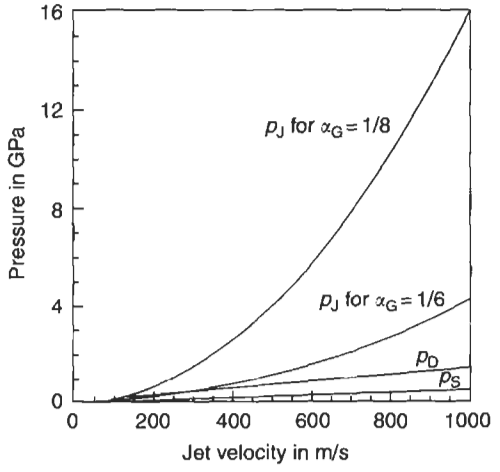

Figure 7.4 Collapse pressures in cavitating water jets.

Table 7.1 Cleaning efficiency of cavitating water jets (Conn and Rudy, 1978).

Nozzle configuration	Cleaning rate in m^2/h[1]	Specific energy in m^2/kWh[1]
1×6.4 mm	44.5	0.90
1×3.2 mm	16.7	1.52
6×3.0 mm	167	–

[1] Epoxy coated steel panels.

Figure 7.5 Structure of an ultrasonically modulated water jet (photograph: VLN Advanced Technologies Inc.).

Figure 7.6 On-site device for the formation of ultrasonically modulated jets (photograph: VLN Advanced Technologies Inc.).

7.1.3 Surface Preparation with Ultrasonically Modulated Water Jets

Ultrasonic waves generated within a nozzle can be employed to modulate a continuous stream of water to produce either pulsed or cavitating jets (see Vijay *et al.*, 1993). The structure of a water jet modulated by this technique is illustrated in Fig. 7.5.

An on-site device for the generation of ultrasonically modulated water jets is shown in Fig. 7.6. The entire system consists of a pump, an ultrasonic power generator with

a converter, a high-pressure dump gun, a high-pressure hose and numerous accessories. The pump delivers a volumetric flow rate of 22.7 l/min at a maximum operating pressure of 41.4 MPa. The ultrasonic power generator has a capacity of 1.5 kW of output at a resonant frequency of $f_P = 20$ kHz. Coating removal tests performed on ships with this equipment showed the following (Vijay *et al.*, 1999):

- the machine's overall size (0.787 m × 0.838 m × 1.4 m) made it ideal for use on ships;
- as the weight was well balanced, it could be manoeuvred about the ship with relative ease;
- rubber casters, with swivels and locking features, were found to be durable to withstand the weight and vibrations of the machine;
- control panel buttons were robust to withstand rough handling in industrial setting;
- moisture in the electrical plug was a problem for the faulty operation of the ultrasonic unit;
- wide variations in the temperature did not affect the performance of the ultrasonic unit.

The certain material removal mode depends mainly on coating structure. On brittle coatings, at operating pressures of 7 MPa, the corresponding impact pressure (160 MPa) forms a hemispherical crack on the layer. With further impacts, the crack propagates radially through the layers to the layer/primer interface. This stream of water then enters these cracks and peels off the coating layer by layer. For higher operating pressures, the adhesive forces between substrate and primer may be exceeded by the impacting fluid slug. These mechanisms are described in detail by Vijay *et al.* (1997).

Results from coating removal tests performed with this technique are displayed in Fig. 7.7. It is shown that modulated jets can remove coating systems with pressures

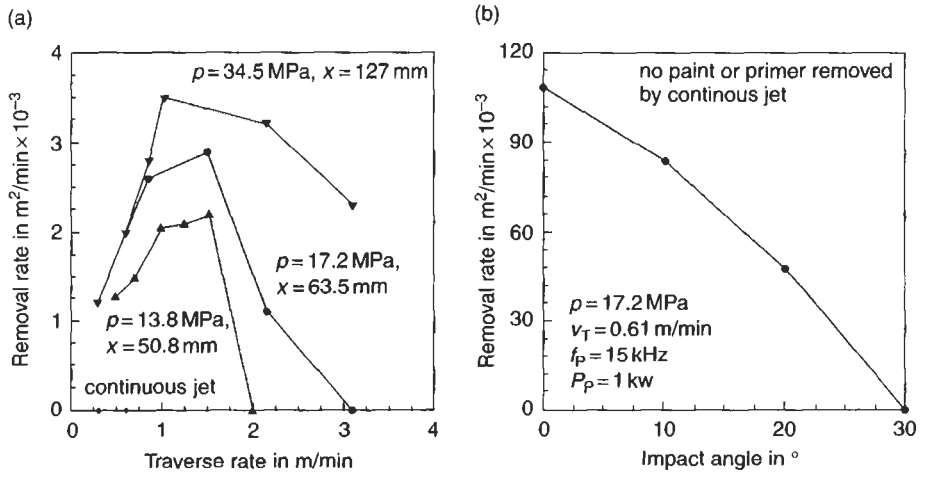

Figure 7.7 Parameter influence (traverse rate (a) and impact angle (b)) on coating removal with modulated water jets (Vijay et al., *1997).*

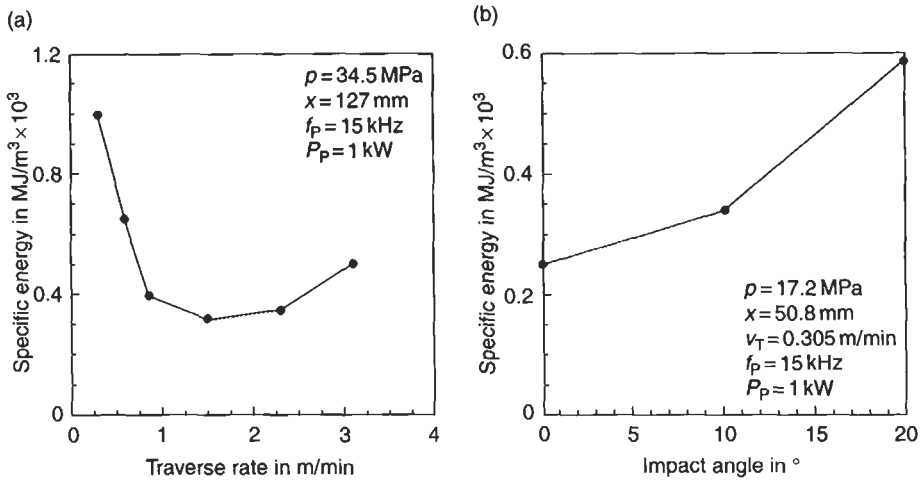

Figure 7.8 Specific energy for coating removal with modulated water jets (Vijay et al., *1997).*

much lower than the corresponding pressures of continuous water jets. Certain coating systems can be stripped with modulated jets only in the given pressure range. Figure 7.7(a) shows that a definite traverse rate of the nozzle carrier exists for maximum coating removal efficiency. This optimum traverse rate decreases if operating pressure increases. Note from Fig. 7.8(a) the minimum in the specific energy is in the range of medium traverse rates. Modulated jet should be applied at perpendicular angles; this is illustrated in Figs. 7.7(b) and 7.8(b). Maximum erosion occurs at an angle of $\phi = 90°$, whereas no erosion takes place with a jet inclined at an angle of $\phi = 30°$. As expected, specific energy increases if impact angle deviates from 90°. Typical removal rates for a non-skid coating are up to 4.5 m^2/h; the certain value depends on traverse rate and stand-off distance. An optimum stand-off distance is $x_O = 25$ mm in many cases (Vijay *et al.*, 1999).

7.1.4 Surface Preparation with Self-Resonating Water Jets

Self-resonating pulsating jets are formed by running a jet flow through a specially designed nozzle; acoustic resonance effects force the vibration and disintegration of the jet. This principle was first noted with air jets (Crow and Champagne, 1971; Morel, 1979). Several self-resonating nozzle system concepts can be distinguished. They are described in detail in the original literature (Johnson *et al.*, 1984; Chahine *et al.*, 1985). A non-dimensional parameter which defines the periodic characteristic of self-resonating jets is the Strouhal number, given through:

$$S_d = \frac{f_P \cdot d_J}{v_J}. \tag{7.5}$$

This number combines acoustic and aerodynamic parameters. It is known that optimum performance of pulsating water jets occurs for Strouhal numbers between

Figure 7.9 Appearance of a self-resonating water jet, $v_j = 83.8$ m/s, $f_P = 4.6$ kHz (photograph: Dynaflow® Inc., Jessup).

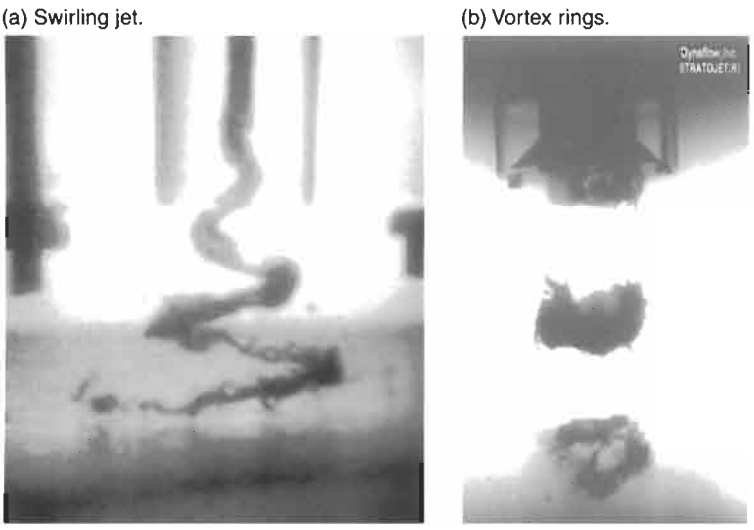

Figure 7.10 Structural elements of self-resonating water jets (photographs: Dynaflow® Inc., Jessup).

0.3 and 1.2. However, mechanically interrupted jets usually operate at frequencies which produce Strouhal numbers well below the optimum range. Acoustically resonated jets, however, meet the requirements of optimum Strouhal numbers. The discontinuous appearance of a resonating water jet is illustrated in Fig. 7.9. Structural elements of self-resonating water jets, formed in different nozzles, are shown in Fig. 7.10.

Self-resonating jets can reliably remove contaminants from metal substrates. Some comparative results are listed in Tables 7.2 and 7.3. Note that cleaning rate increases if self-resonating jets are used. However, specific cleaning energy increases as well. The improved cleaning capability of self-resonating jets is in the first place a result of the wider width of the cleaned paths. Promising experience was collected with this cleaning technique during the removal of asbestos with operating pressures up to 69 MPa; the efficiency reported is between 23 and 28 m^2/h (Conn, 1989). Problems of handling, safety and training in relation with the on-site use of self-resonating water jets are discussed by Conn (1991).

It seems from Fig. 7.11 that self-resonating jets do not perform very efficiently at rather large stand-off distances. It may be noted that a conventional water jet has a

Table 7.2 Cleaning capability of self-resonating jets (Chahine *et al.*, 1983).

Parameter	Conventional jet	Self-resonating jet
Operating pressure in MPa	3.1	3.1
Cleaning width in mm	25	51
Cleaning rate in m^2/h	56	111
Specific energy in m^2/kWh	19.8	27.5

Table 7.3 Ship hull cleaning with a self-resonating water jet (SERVOJET®) (results: Conn and Chahine (1983)).

Nozzle type	Surface quality	Operating pressure in MPa	Typical cleaning rate in m^2/h	Typical specific cleaning energy in m^2/kWh
Circular orifice, diameter 1.1 mm	Sa 1	48.2	16.7–29.7	0.12–0.19
	Sa 1	55.1	20.8–21.9	0.15–0.16
	Sa 1	62.0	14.8	0.11
	Sa 2	48.2	8.5–18.6	0.06–0.12
	Sa 2	55.1	6.6–13.3	0.05–0.10
	Sa 2	62.0	5.3	0.04
Fan (15°) nozzle, equivalent diameter 0.9 mm	Sa 1	48.2	10.3–21.5	0.09–0.17
	Sa 1	62.0	21.5	0.20
	Sa 2	48.2	4.2–7.5	0.04–0.06
	Sa 2	62.9	1.0	0.01

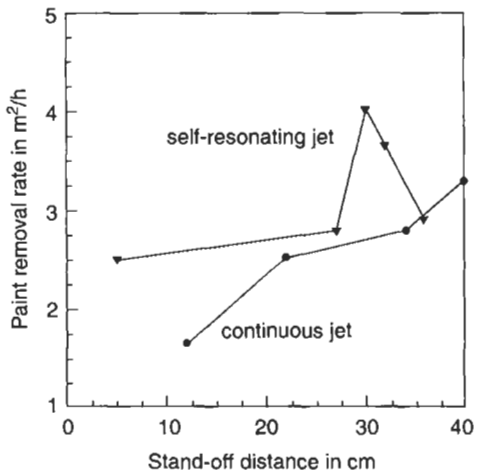

Figure 7.11 Comparative paint removal results (Chahine et al., *1983).*

dynamic component ('natural pulsation') due to drop formation if a certain jet length is reached (see Fig. 2.3). The corresponding loading regime is comparable to that generated by the self-resonating jet. Therefore, the removal efficiency of the conventional jet approaches that of the discontinuous jet. However, at small stand-off distances self-resonating jets perform much more effectively.

7.2 Hydro-Abrasive Jets for Surface Preparation

7.2.1 Types and Formation of Hydro-Abrasive Jets

A comprehensive review of hydro-abrasive jets is given by Momber and Kovacevic (1998). From the point of view of jet generation, the following two types hydro-abrasive jets can be distinguished:

- injection jets;
- suspension jets.

A hydro-abrasive injection jet is formed by accelerating small solid particles (garnet, aluminium oxide, silica carbide) through contact with one or more high-speed water jets. The high-speed water jets are formed in orifices placed on top of the mixing-and-acceleration head. The solid particles are dragged into the mixing-and-acceleration head through a separate inlet due to the vacuum created by the water jet in the mixing chamber. The mixing between the solid particles, water jet and air takes place in the mixing chamber, and the acceleration process occurs in a focusing tube. Typical designs for mixing-and-acceleration devices are illustrated in Fig. 7.12. Technical parameters of hydro-abrasive cleaning heads are listed in Table 7.4. After the mixing-and-acceleration process, a high-speed three-phase suspension leaves this tube at velocities of several hundred meters per second. This suspension is the actual tool for hydro-abrasive applications. The entire mixing-and-acceleration process is described in detail by Momber and Kovacevic (1998).

The velocity of the abrasive particles can be approximated by the following equation, based on momentum balance:

$$v_A = \alpha_A \cdot \frac{v_J}{1 + (\dot{m}_A/\dot{m}_W)}. \tag{7.6}$$

Here, α_A is a momentum transfer parameter; a typical value is $\alpha_A = 0.7$ (Momber and Kovacevic, 1998). The mass flow rate ratio is frequently called the mixing ratio:

$$\dot{m}_A/\dot{m}_W = R_M. \tag{7.7}$$

Equation (7.6) is solved for different mixing ratios; the results are shown in Fig. 7.13. For simplicity it is assumed that abrasive particles and water phase in the hydro-abrasive jet have equal velocities (in reality a slip exists of about 10%). The kinetic energy of a hydro-abrasive water jet is

$$E_A = \underbrace{\sum_{i=1}^{N_P} E_{Pi}}_{\text{abrasive particle}} + \underbrace{\frac{m_w}{2} \cdot v_A^2}_{\text{water phase}} \tag{7.8}$$

The number of particles, N_P, depends on abrasive particle size and mass flow rate. The left term is the energy provided by the abrasive particles to the erosion site. This portion, denoted 'abrasive particle' is about 10% of the total kinetic energy of a hydro-abrasive

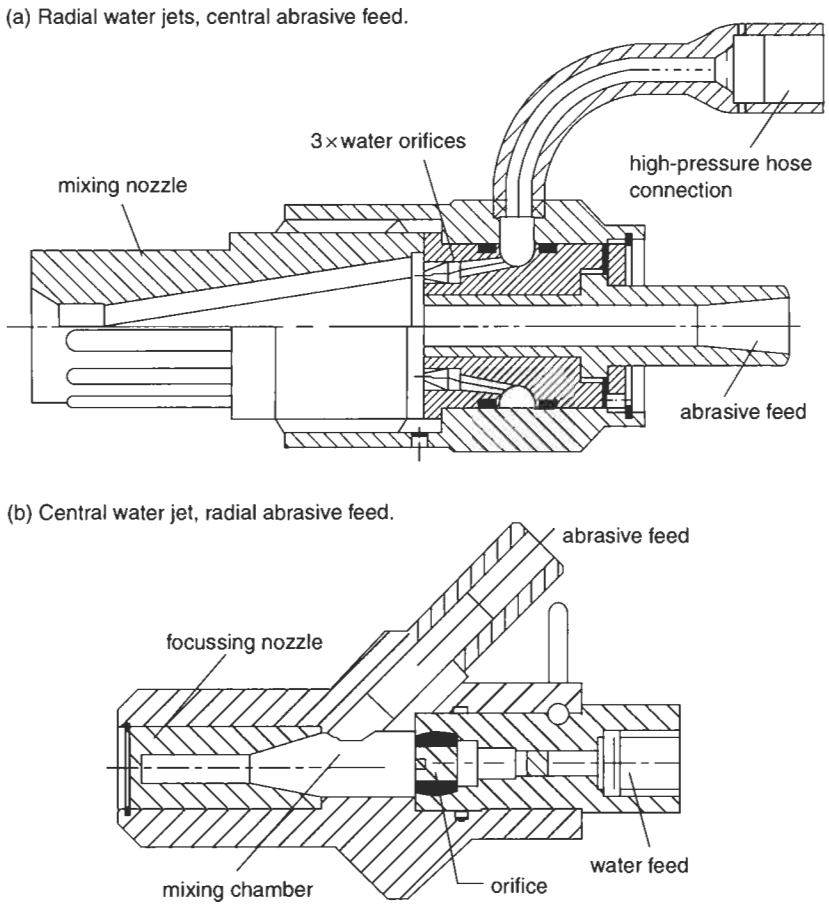

Figure 7.12 Abrasive mixing devices for injection jet formation (WOMA GmbH, Duisburg).

Table 7.4 Technical data of on-site abrasive mixing devices (see Fig. 7.12).

Parameter	Mixing head (a)[1]	Mixing head (b)[1]
Operating pressure in MPa	100	75
Volumetric water flow rate in l/min	21–33	min. 30
Abrasive size in mm	0.5–1.4	max. 2.0
Number and diameters of water orifices	3 × 0.9 mm	1 × 1.5 mm
Weight in kg	–	0.5

[1] Letters refer to the mixing devices in Fig. 7.12.

jet (Momber, 2001); the remaining 90% are carried by the water phase of the jet (denoted 'water phase'). These relationships are illustrated in Fig. 7.14.

7.2.2 Alternative Abrasive Mixing Principles

Several alternative developments for abrasive injection systems have been developed. Figure 7.15(a) shows a nozzle that is designed with an annular slit connected to a

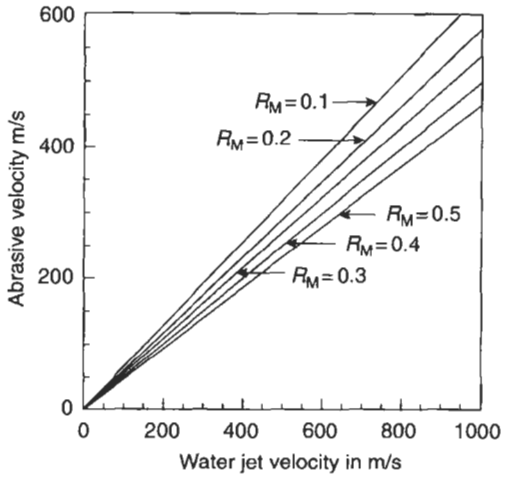

Figure 7.13 Velocity of abrasives in a hydro-abrasive injection jet (calculated with Eq. (7.6)).

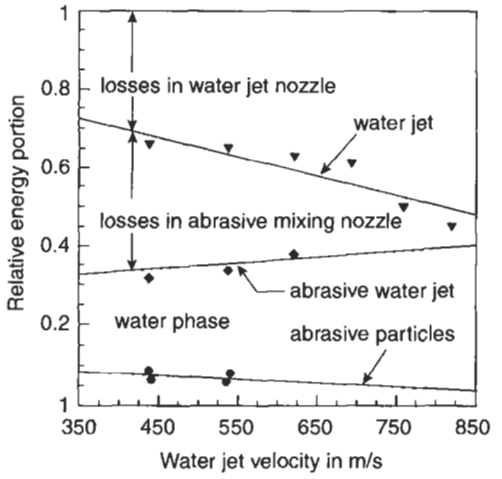

Figure 7.14 Energy content in a hydro-abrasive injection jet (measurements: Momber, 2001).

conical cylinder. The slit supplies the high-speed water that passes through the conical cylinder and deforms into a spiral flow. An inlet on top of the nozzle feeds the abrasives. The water jet focuses well and the abrasive particles concentrate in the central axis of the water jet. Also, turbulence and focus wear are reduced (Hori *et al.*, 1991). However, operating pressures used are very low and range between 4 and 6 MPa. The highest reported water jet velocity is about $v_0 = 35$ m/s. Despite these rather low values the system is very efficient in rust removal from steel substrates as shown in Table 7.5.

(a) Central annular water jet (Hori et al., 1991).

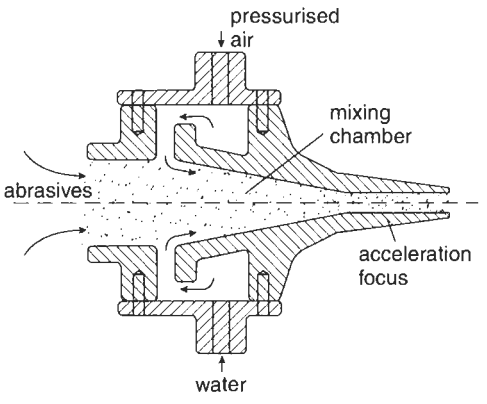

(b) Central annular air jet (Hamada et al., 1991).

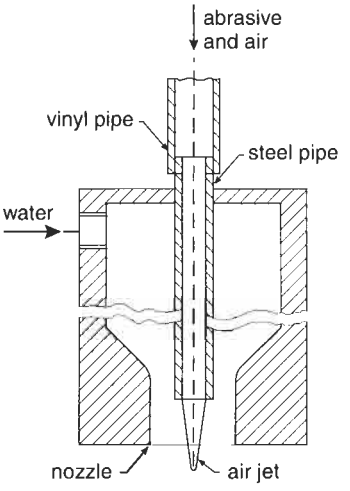

(c) Rotated water jet (Liu, 1991).

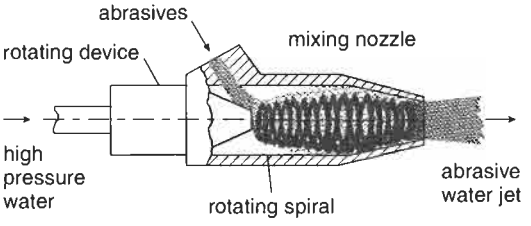

Figure 7.15 Alternative abrasive mixing principles.

Table 7.5 Efficiency of a rotating abrasive jet derusting system (Liu, 1991).

Operating pressure in MPa	Efficiency in m^2/h
4	8.1
5	13.1
6	13.8

Figure 7.15(b) illustrates a similar principle. In this case, the abrasives are mixed into an annular air jet through an inner steel pipe. The high-speed water jet enters the mixing chamber through a side entry and accelerates the mixture. Visualization experiments showed that the abrasives mix very homogeneously. However, this system can be run at low pump pressures of about $p = 14$ MPa only (Hamada *et al.*, 1991). Although this principle is very promising, no on-site applications are reported so far.

Figure 7.15(c) illustrates a further alternative mixing principle. The water flow that enters the mixing chamber centrally is directly turned into a vortex flow that

flows through the nozzle and forms a vortex water-jet. The rotated movement of the water jet improves abrasive suction capability and mixing efficiency (Liu, 1991). This system is limited to operating pressures of about $p = 10$ MPa, and requires large orifice ($d_0 = 3$ mm) and focus ($d_F = 7$ mm) diameters.

7.2.3 Surface Preparation with Hydro-Abrasive Jets

The removal of coatings or rust from steel substrates is not a completely new application of hydro-abrasive jets: the first trials were reported in the 1970s and some results are listed in Table 7.6. At that time, plunger pumps were capable of generating maximum operating pressures of about 75 MPa which are not sufficient for surface preparation with plain water jets. However, this technology is still under consideration, especially in certain countries such as China (Xue *et al.*, 1993). Some recent results of ship hull derusting with hydro-abrasive injection jets are displayed in Fig. 7.16.

A more recent and innovative development is the use of hydro-abrasive suspension jets for rust stripping. Such a system is shown in Fig. 7.17. It consists basically of water tank, abrasive supply device, high-pressure pump, blasting gun and abrasive collecting device. Experience with this technology is reported by Liu *et al.* (1993). The

Table 7.6 Ship hull cleaning with hydro-abrasive injection jets (WOMA Apparatebau GmbH).

Job/quality	Efficiency in m^2/h	Abrasive size in mm	Operating pressure in MPa	Abrasive consumption in kg/m^2
Flash rust removal	12–16	0.2–1.2	30	5–8
Bare metal	8–12	0.2–1.2	30	8–12
Bare metal	10–12	0.2–0.3	30	10–12
Heavily corroded steel	6–8	0.5–2.0	25	50

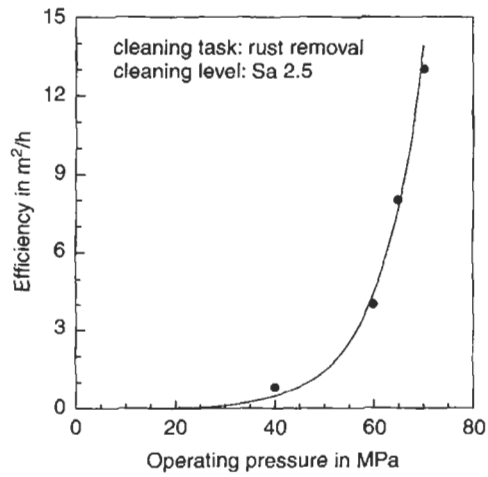

Figure 7.16 Rust removal with hydro-abrasive water jets (Xue et al., *1993).*

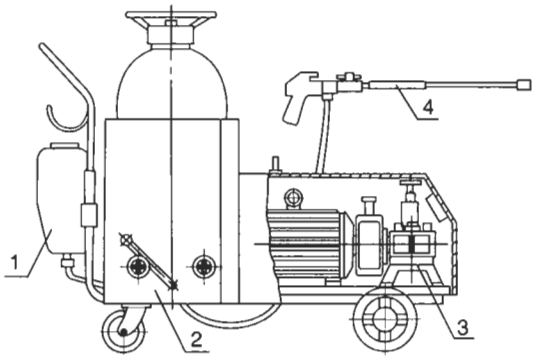

1. Water tank;
2. Abrasive supply device;
3. High-pressure pump;
4. Blasting gun.

Figure 7.17 Structure of a hydro-abrasive suspension jet system for rust removal (Lui et al., *1992, 1993).*

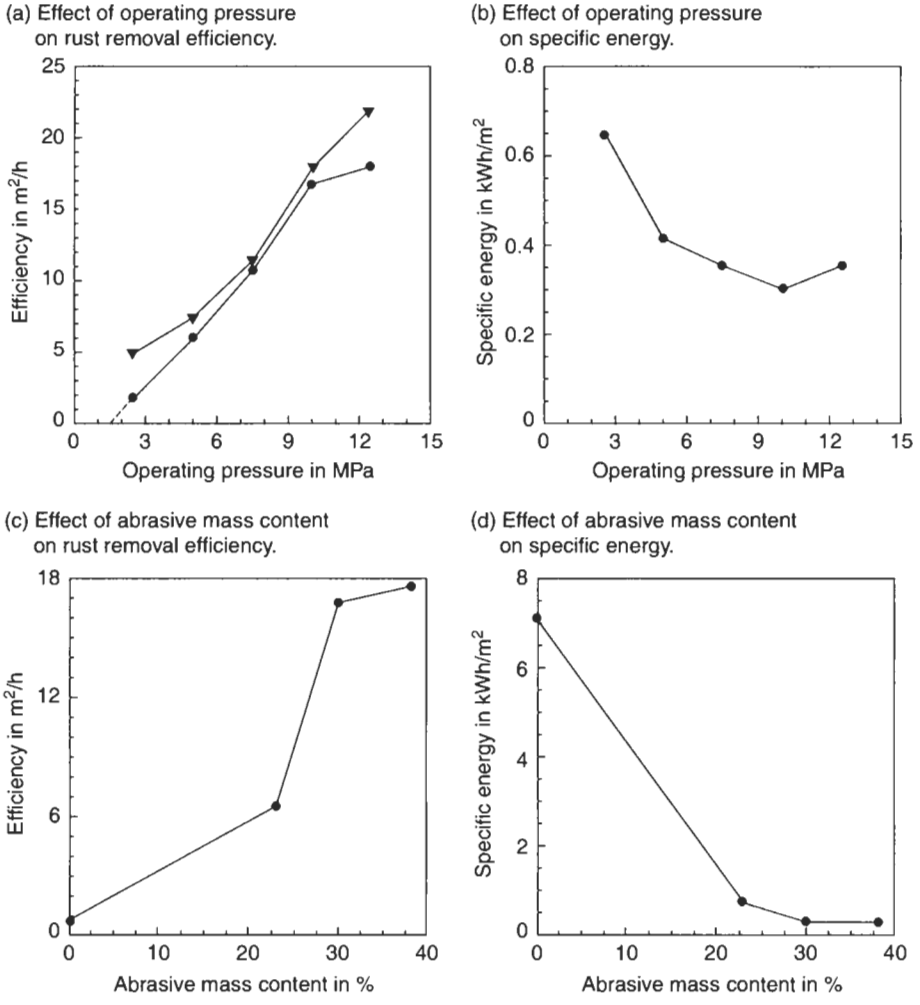

Figure 7.18 Parameter effect on rust removal with 'Premajet'-system (Liu et al., *1993).*

abrasive materials can be reused; an abrasive used five times retained about 90% of its erosion capability. The recovery capacity is 3000 kg/h. Major influencing parameters are operating pressure and abrasive mass content. Examples of how these parameters affect efficiency and specific energy are shown in Fig. 7.18. Note that a certain pressure range exists with minimum energy consumption (Fig. 7.18(b)); this result agrees with results obtained during coating removal with plain water jets (see Fig. 2.11(b)). There also seems to exist a threshold pressure (about 1.5 MPa in Fig. 7.18(a)) which also confirms experience from hydroblasting operations.

7.2.4 Surface Preparation by Ultra-High Pressure Abrasive Blasting

Numerical simulations of the mixing-and-acceleration process during the formation of hydro-abrasive injection jets show that the entry velocity of the abrasive particles notably affects the exit velocity of the accelerated abrasive particles. The higher the entry velocity the higher the exit abrasive velocity. An increase in the entry velocity from 6.2 to 10 m/s results in an increase in the exit velocity of the abrasives by about 25% (Himmelreich, 1992) which in turn increases kinetic energy up to 60%.

It may, therefore, be beneficial to accelerate the abrasive particles before they enter the mixing nozzle. Such a device is shown in Fig. 7.19. In this device the abrasive particles are accelerated by an air jet prior to their contact with the high-speed water jet. Thus, it combines air-driven abrasive blasting and high-pressure hydroblasting. Consequently, the system is frequently called as UHPAB-system (ultra-high pressure abrasive blasting). Figure 7.20 shows UHPAB-systems in operation.

Results from site applications of this technology are listed in Table 7.7. The efficiency is high and exceeds that of hydroblasting processes in some cases, such as for the removal of epoxy or non-skid coatings. The UHPAB-method combines advantages from abrasive blasting (formation of a profile; removal of hard and resistant coatings) with advantages from hydroblasting (minimum dust formation, high capability of removing surface contaminants). The technique is very flexible: the basic equipment can be used for dry blasting, hydroblasting or mixed blasting.

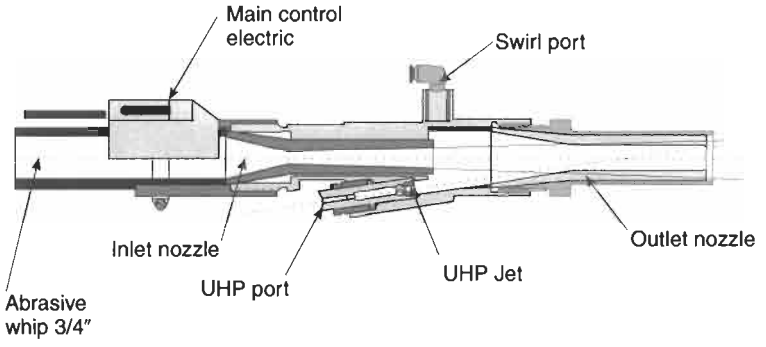

Figure 7.19 Two-stage acceleration process of abrasive particles in an injection system (Mühlhan Surface Protection Intl. GmbH, Hamburg, 2001).

(a) Ship deck decoating.

(b) Ship hull decoating.

Figure 7.20 Ultra-high pressure abrasive blasting (UHPAB) systems in operation (photographs: Mühlhan Surface Protection Intl. GmbH, Hamburg).

7.3 High-Speed Ice Jets for Surface Preparation

7.3.1 Types and Formation of High-Speed Ice Jets

The generation of secondary waste and the disposal of solids are major problems of any abrasive blasting application. One solution to avoid this problem is the use of soluble abrasive materials. The first approach of using (water) ice particles for surface cleaning was probably that of Galecki and Vickers (1982). These authors inserted crushed ice particles into an air jet and performed cleaning tests on different paint systems. Later, Truchot *et al.* (1991) were the first to mix ice particles into a high-speed water jet. Figure. 7.21 shows the structure of an air-driven ice jet.

Table 7.7 Efficiency of ultra-high pressure abrasive blasting (Mühlhan, 2001).

Parameter	Coating type	
	Epoxy or non-skid (1500–2500 μm)[1]	Chlorinated rubber (1500 μm)[1]
Instantaneous efficiency in m^2/h	16.0	8.0
Average efficiency in m^2/h	10.2	6.0
Average clean-up rate in m^2/h	4.1	2.5
Productivity in m^2/h	2.95	1.76
Consumables		
Fuel in l/m^2	1.52	2.58
Water in l/m^2	58	99
Abrasives in kg/m^2	33	66
Labour in h/m^2	0.33	0.57

m^2/h: h is in man hours.

[1] Coating thickness.

Figure 7.21 Exiting ice-air-jet; air pressure: 0.544 MPa, ice mass flow rate: 20 g/min (photograph: New Jersey Inst. Technology, Newark).

A general technical problem with ice blasting is the production and maintenance of a stable and controlled ice particle flow. Different methods have been developed to solve these problems, including the following:

- cooling of water and sub-cooling of the ground ice particles in liquid nitrogen (Galecki and Vickers, 1982, Truchot *et al.*, 1991);
- growth of individual ice particles in a still or flowing cryogenic gas (Kiyohashi and Handa, 1998);
- mixing of (water) ice and dry ice (Geskin *et al.*, 1999), see Fig. 7.21;
- direct cooling of water spray (Kiyohashi and Handa, 1999; Siores *et al.*, 2000), see Fig. 7.22.

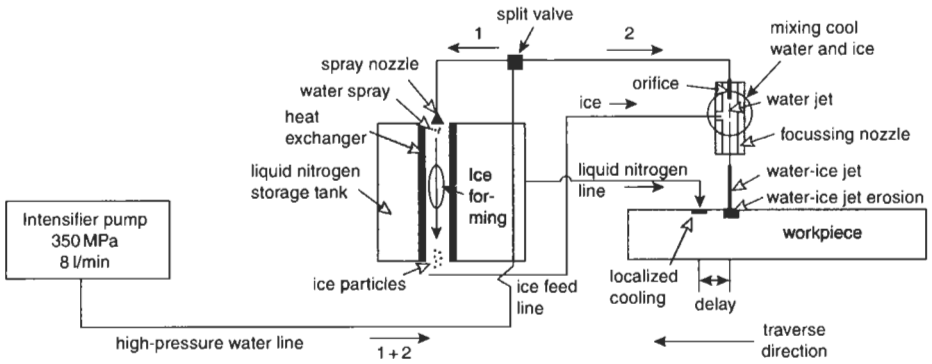

Figure 7.22 Schematic diagram of an ice formation system, based on spray cooling (Siores et al., *2000).*

Table 7.8 Properties of water ice (Hobbs, 1974; Wang *et al.*, 1995; Shishkin, 2002).

Parameter	Value	Temperature in °C
Bulk modulus in GPa	10	−5
Crushing strength in MPa	3	−10
Density in kg/m^3	917	0
Indentation hardness in MPa	25	−2.7
Longitudinal wave velocity in m/s	3520	0
Poisson's ratio	0.5	0
Tensile strength in MPa	1.5	−10
Thermal conductivity in W/(m·°C)	2	0
Wave impedance in 10^6 kg/(m^2·s)	3.22	0
Young's modulus in GPa	10	−5

Several investigations on the influence of technical and physical parameters on the size of generated ice particles were performed by Shishkin *et al.* (2001). It was found, amongst other factors, that the final ice particle diameter increases if water flow rate and surrounding temperature increase. Most properties of ice depend on its temperature; a comprehensive review about these relationships is given by Hobbs (1974). Table 7.8 lists typical physical and mechanical properties of ice.

7.3.2 Surface Preparation with High-Speed Ice Jets

The damage mechanisms during ice particle impact are comparable to those described for water drop impact in Section 2.2, including the existence of a threshold velocity. The reason is that ice particles deform and flow during the impact on solid surfaces. This is evidenced by high-speed camera sequences (Wang *et al.*, 1995); see Fig. 7.23. However, a detailed description of the paint removal process during ice particle impact is still not available. A parameter study on rust removal by air jet driven ice particles was performed by Liu *et al.* (1998). Some results are shown in Fig. 7.24. The general efficiency is rather low. However, optimum parameter combinations exist for ice mass flow rate and ice particle size for maximum removal efficiency. Efficiency also increases if ice temperature increases.

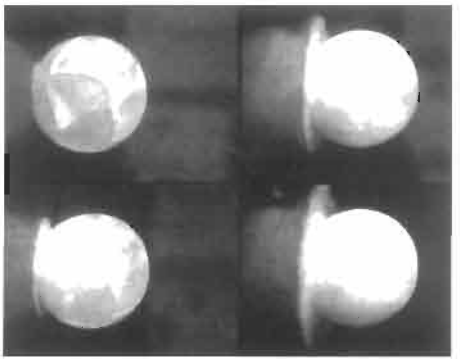

Figure 7.23 Deformation of an impacting ice particle (photograph: Cavendish Laboratory, Cambridge).

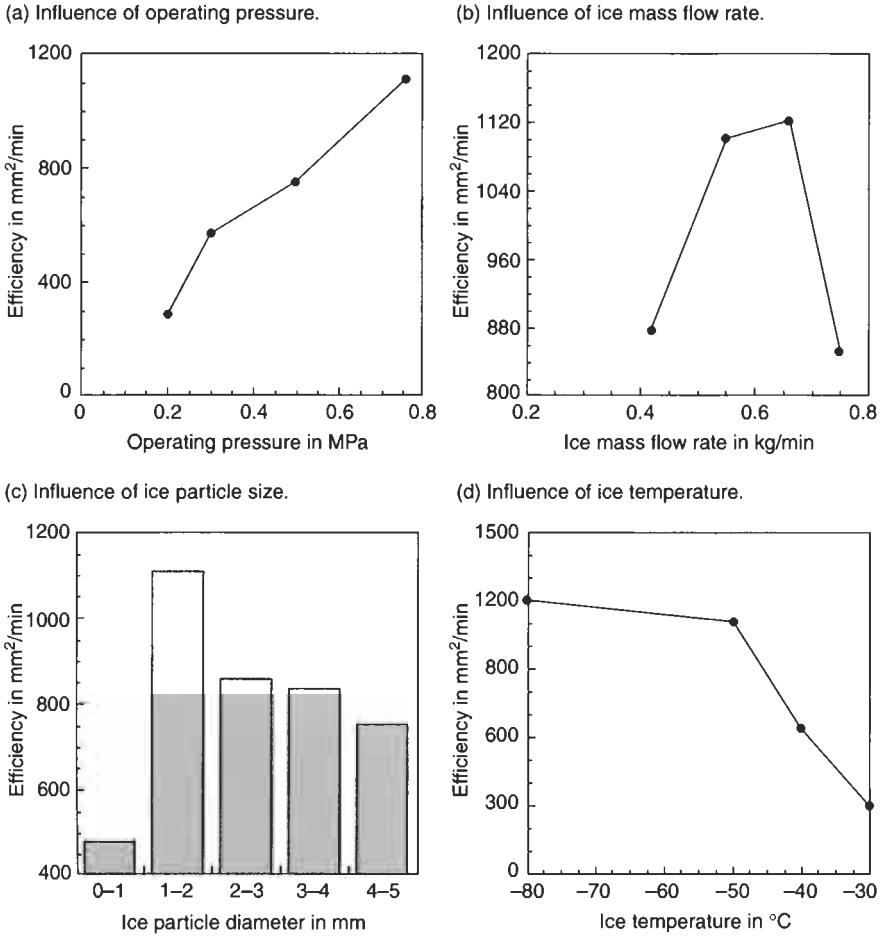

Figure 7.24 Parameter influence during the derusting of steel with ice particles (Liu et al., *1998).*

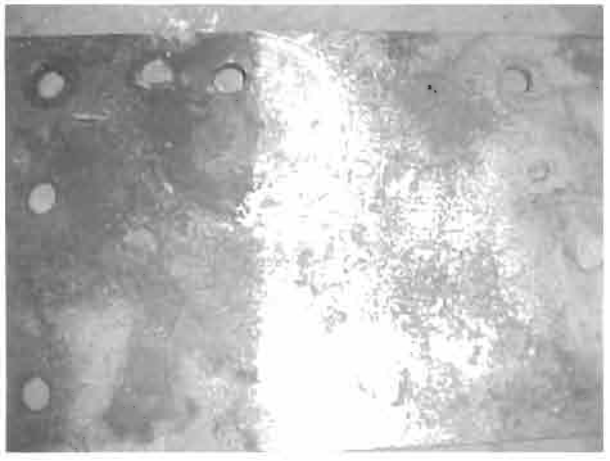

Figure 7.25 Removal of highly adhesive rust from carbon steel substrate with an ice-abrasive jet (photograph: New Jersey Inst. Technology, Newark).

Numerous cleaning applications of ice-water jets are reported by Geskin *et al.* (1999), Shishkin (2002) and Shishkin *et al.* (2001). Graffiti could be selectively removed from painted steel panels. Whereas the graffiti was removed with the ice jet, no damage to the underlying highly adhesive oil paint occurred . Promising experience was also collected during the removal of heavy rust from corroded carbon steel plates (see Fig. 7.25), and during the stripping of thick tar layers from aluminium substrate. Other base materials cleaned include organic glass, polished steel, soft plastic, photo films and cotton fabric.

7.3.3 Caustic Stripping and Ice Jetting

A very recent approach is the development of a hybrid technique to remove lead-based coatings. This approach includes three subsequently performed steps of application:

- application of a caustic stripper (NaOH) to the coating;
- removal of the reacted coating by mechanical means (scraping);
- removal of paint and residual caustic by ice jetting.

Caustic stripping is, however, possible only if the coating contains drying oil. The process does not work on polyurethane or epoxy coatings. Ice jetting is basically a plain cleaning application and only supports the entire removal process. The mechanisms acting during the cleaning include mechanical displacement through ice particle impact, scrubbing as a result of frictional forces, and flushing due to flowing water after the ice is molten.

An application of this method is reported by Snyder *et al.* (1998). Two steel bridges of a total surface of about 3,500 m^2 were treated. Two transportable ice jetting machines, driven by a 40 kW generator, were used. They consumed a volumetric

Table 7.9 Parameters of caustic stripping/ice jetting of steel bridges (Snyder *et al.*, 1998).

Application/parameter	Value
Stripper used	208 l
Stripper film thickness	150–200 μm
Stripper spray time (2 pumps)	1 h
Stripper reaction time	4 h
Residue scraping time (2 men)	2 h
Ice jetting time	2 h
Liquid waste from ice jetting	< 7.611

Figure 7.26 Use of ice jetting during a steel bridge rehabilitation project (photographs: Universal Ice Blast, Bellevue, WA).

water flow rate of 90 l/h which corresponded to an ice consumption of 100 kg/h. The air pressure of the compressors used for ice jetting was 0.86 MPa. More information is provided in Table 7.9. Air monitoring for lead dust outside the containment area was carried out for the initial 2-week period with negative results. For inside the containment area, the highest personal monitor reading registered by the ice jetting operators was 175 $\mu g/m^3$. The significance of these low readings is that the caustic/ice jetting process can provide total lead paint removal without the requirement of 'class A' containment and large vacuum trucks. There is, however, a restriction to that method as the stripper works best in the temperature range of 20–35 °C at a high relative humidity (Snyder *et al.*, 1998). Figure 7.26 illustrates the use of ice jetting during on-site applications.

7.4 Water Jet/Ultrasonic Device for Surface Preparation

A combined water jet/ultrasound device for the removal of coating systems from ships or other large metallic structures is proposed by Bar-Cohen *et al.* (2002).

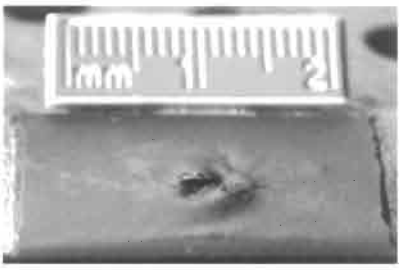

Figure 7.27 Coating pre-damage due to ultrasound loading (NASA Jet Propulsion Laboratory, Pasadena, CA).

In addition to utilising a high-speed water jet to remove paint and a robotic crawler to scan the jet along the coated structure, the system utilises high-intensity ultrasound to loosen the paint just ahead of the water jet in order to ensure more nearly complete removal. The improved system also includes a quantitative gauging subsystem that measures the thickness of the paint as well as a qualitative gauging subsystem that generates an approximate map of paint residues; these subsystems provide real-time feedback for control of the crawler, water jet and ultrasonic subsystems. The ultrasonic subsystem exploits a combination of heating and mechanical stresses to loosen the coatings. In the focal zone, the intense ultrasound can raise the temperature up to several hundred degrees Celsius, causing the paint to blister. In the presence of the mismatch of acoustic impedances between the paint and the metallic substrate, the ultrasound gives rise to tensile and shear stresses that contribute to blistering (see Fig. 7.27). The paint is further damaged if ultrasonic cavitation is present. The ultrasonic paint-loosening subsystem includes a piezoelectric transducer that generates focused ultrasonic waves; the transducer is mounted on the crawler and positioned to concentrate the ultrasound into the surface layer of water on the workpiece near the advancing water jet. The transducer is activated with a combination of two ultrasonic signals – one at a frequency of several hundred kHz and one at a frequency of tens of kHz. The latter signal is effective in producing cavitation in water. The more highly focused higher-frequency ultrasound propagates into the lower-frequency ultrasonic field, raising the intensity of the total ultrasonic field in the focal region above the threshold for cavitation. The qualitative thickness-gauging subsystem is supposed to include a comb array of springy wire electrodes that would be scanned along the substrate behind the water jet. By simple electrical contact (or lack thereof) with the metal substrate, the electrodes would give indications of the removal or non-removal, respectively, of paint from their respective locations. In real-time, contact/non-contact signals from the wires could be multiplexed and sent as feedback to a control subsystem. For non-real-time inspection, contact/non-contact signal data acquired by scanning along the substrate could be used to generate a map of paint residues.

References

Abrams, S., 1999, Handling and disposal of waste. *Protect. Coat. Europe*, Vol. 4, No. 5, 24–29.

ACI Committee 548, 1993, Guide for polymer concrete overlays. *ACI Mat. J.*, Vol. 90, 499–522.

Adamson, N., 1998, Performance of coating systems using numerical life prediction. *J. Protect. Coat. & Linings*, Vol. 15, No. 7, 50–62.

Adley, D. and Trimber, K., 1999, Evaluation of substitute materials for silica sand in abrasive blasting. *J. Protect. Coat. Linings*, Vol. 16, No. 8, 49–71.

AHPWJC, 1995, *Code of Practice for the Use of High Pressure Water Jetting Equipment*. Association of High Pressure Water Jetting Contractors, London.

Alba, H., Brandt, C., Bremer, H., Eickelpasch, N., Kalwa, H., Louis, H., Reiter, W., 1999, The application of abrasive water suspension jets (AWSJ) for the dismantling of nuclear power plants. *Proc. Int Symp. on New Appl. of Water Jet Technol.* (ed. R. Kobayashi), Ishinomaki, 443–450.

Alblas, B.P., van Londen, A.M., 1997, The effect of chloride contamination on the corrosion of steel surfaces: a literature review. *Protect. Coat. Europe*, Vol. 2, No. 2, 16-25.

Allan, S.J., May, R., Taylor, M.F., Walters, J., 1995, The effect of salts on steels and protective coatings. *GEC J. of Research*, Vol. 12, 86–92.

Allen, B., 1997, Evaluating UHP waterjetting for ballast tank coating systems. *Protect. Coat. Europe*, Vol. 2, No. 10, 38–64.

Amada, S., Hirose, T. and Senda, T., 1999, Quantitative evaluation of residual grits under angled blasting. *Surface and Coatings Technol.*, Vol. 111, 1–9.

Andronikos, G. and Eleftherakos, A., 2000, Alternative surface preparation methods for ship-repairing. *Proc. PCE Conf. and Exhibition*, Technol. Publ., Pittsburgh, 253–262.

Anonymous, 1997, Waterjetting removes lead paint on communication facility. *J. Protect. Coat. Linings*, Vol. 14, No. 5, 33–36.

Anonymous, 1998, On monitoring airborne lead dust during water jetting. *PMC*, Vol. 2, 8–9.

Anonymous, 2002a, New HSE legislation could save lives in UHP water jetting operations. *Int. Ship Repair News*, July/August, 45–47.

Anonymous, 2002b, Advances in high-production robotic UHP water blasting. *Shiprepair and Conversion Technol.*, 2nd Quarter, 35–40.

Appleman, B.R., 2002, Advances in technology and standards for mitigating the effect of soluble salts. *J. Protect. Coat. & Linings*, Vol. 19, No. 5, 42–47

ASE, 2001, Report on recommendation of industrial engineering solutions to decrease the fatigue factor associated with the uhp water blasting process. Maritec-ASE, Agreement No: 2000932, January.

Axmann, H.-D., Laurinat, A., Flügel, M., Louis, H., 1998, Schädigungsmuster von Hochdruck-Wasserstrahlen und Hochdruck-Wasser-Abrasivstrahlen an der Hand. *Handchir. Mikrochir. Plast. Chir.*, Vol. 30, 263–268.

Babets, K. and Geskin, E.S., 1999, Fuzzy logic model of waterjet depainting: grapho-analytical approach. *Proc. 10th Amer. Water Jet Conf.* (ed. M. Hashish), WJTA, St Louis, Paper 6.

Babets, K. and Geskin, E.S., 2001, Development of a generic procedure for modelling of the water jet cleaning. *Proc. 11th Amer. Water Jet Conf.* (ed. M. Hashish), WJTA, St Louis, 765–777.

Baker, D.W., Jolliffe, K.H. and Pearson, D., 1966, The resistance of materials to impact erosion damage. *Phil. Trans. Roy. Soc. London*, Vol. A260, 193–203.

Bar-Cohen, Y., Bao, X., Marzwell, N., 2002, Water-jet/ultrasonic removal and real-time gauging of paint. *NPO-21063, NASA's Jet Propulsion Laboratory*, Pasadena, California.

Barker, C.R., Cummings, A. and Andersson, M., 1982, Jet noise measurements on hand-held cleaning equipment. *Proc. 6th Int. Symp. Jet Cutting Technol.* (ed. H.S. Stephens), BHRA, Cranfield, 161–178.

Beltov, S. and Assersen, N., 2002, Shipyard blasting and painting facilities. *J. Protect. Coat. Linings*, Vol. 19, No. 7, 47–48.

BGV, 1999, Unfallverhütungsvorschrift "Arbeiten mit Flüssigkeitsstrahlern", BGV D15, Steinbruchs-Berufsgenossenschaft.

BGV, 2001, Unfallverhütungsvorschrift "Lärm", BGV B3, Steinbruchs-Berufsgenossenschaft.

BIA, 2000, Ermittlung von Grundlagen zur Gefährdungsanalyse und Entwicklung von Präventionsmaßnahmen. Bericht 638.23/077-HAV/AVA, Berufsgenossenschaftliches Institut für Arbeitssicherheit, Sankt Augustin.

BIA-Report, 1997, Lärmbelastung an Baustellenarbeitsplätzen Teil V. BIA-Report 2/97, Hauptverband der gewerblichen Berufsgenossenschaften, Sankt Augustin.

Blades, B., 1994, Energy distribution and computer modelled nozzle design in high pressure water jet coating removal. *Proc. 7th Nat. Thermal Spray Conf.*, Boston, 421–424.

Bond, R.D. and Makai, J., 1996, Removal of compensator coating at Paks Nuclear Power Plant, Hungary. *Jetting Technol.* (ed. C. Gee), Mechan. Engng. Publ. Ltd., London, 663–675.

Bourne, N.K., Obara, T. and Field, J.E., 1997, High-speed photography and stress gauge studies of jet impact upon surfaces. *Phil. Trans. Roy. Soc. London*, Ser. A, Vol. 355, 607–623.

Brevoort, G.H., 1988, Abrasive blasting and salt contamination: a case history. *J. Protect. Coat. Linings*, Vol. 5, No. 5, 24–71.

Briscoe, B.J., Pickles, M.J., Julian, K.S. and Adams, M.J., 1995, Erosion by surface coatings in hydrodynamic flows. *Wear*, Vol. 181–183, 759–765.

Briscoe, B.J., Pickles, M.J., Julian, K.S. and Adams, M.J., 1997, Erosion of polymer-particle composite coatings by liquid jets. *Wear*, Vol. 203, 88–97.

Bullard, J., Corbett, W.D., Mozelewski, F.A., 2002, Corrosion protection of limited access areas common to bridge structural steel design. *J. Protect. Coat. & Linings*, Vol. 19, No. 9, 46–50.

Bullett, T.R., Prosser, J.L., 1972, Measurement of adhesion. *Prog. Organ. Coat.*, Vol. 1, 45–71.

Camus, J.J., 1971, High-speed flow in impact and its effect on solid surfaces. *PhD Thesis*, University of Cambridge, Cambridge.

Carlson, J.R. and Townsend, T.G., 1998, Management of solid waste from abrasive blasting. *Practice Periodical of Hazardous, Toxic, and Radioactive Waste Management*, Apr., 72–77.

Carlson, J.R. and Townsend, T.G., 1999, Assessment of waste abrasive blasting media from ship maintenance facilities and sandblasting contractor sites. *Proc. CCSE/ASCE Environ. Engng Conf.*, 651–660.

Carter, E.E., 1998, Containing the cold war's hot waste. *Civil Engng Magazine*, Nov., 1–7.

Chahine, G.L., Conn, A.F., Johnson, V.E. and Frederick, G.S., 1983, Cleaning and cutting with self-resonating pulsed water jets. *Proc. 2nd US Water Jet Conf.* (ed. D.A. Summers *et al.*), Univ. of Rolla Press, Rolla, 195–205.

Chahine, G.L., Johnson, V.E., Conn, A.F. and Frederick, G.S., 1985, Passively interrupted impulsive water jets. *Proc. 3rd US Water Jet Symp.* (ed. N. Styler), US Bureau of Mines, WJTA, Paper 34, 1–9.

Chen, W.L. and Geskin, E.S., 1991, Measurement of the velocity of abrasive waterjet by the use of laser transit anemometer. *Jet Cutting Technol.* (ed. S. Stephens), Elsevier Sci. Publ. Ltd., Amsterdam, 23–36.

Choo, S. and Teck, P.C., 1990, Removal of rubber deposits from runways using hydrojetting techniques. *Proc. 2nd Rim Int. Conf. Water Jet Cutting*, Singapore, 217–227.

Ciccu, R. and Bortolussi, A., 1998, Water jet in dimensional quarrying. *Water Jet Applications in Construction Engineering* (ed. A.W. Momber), A.A. Balkema, Rotterdam, 289–305.

Cluchague, P., 2001, New innovations in surface preparation. *Protect. Coat. Europe*, Vol. 6, No. 11, 13–18.

Colosimo, B.M., Monno, M., Semeraro, Q., 2000, Process control in waterjet peening. *Int. J. Mater. Product Technol.*, Vol. 15, 10–19.

Conn, A.F., 1972, Recent developments of the cavitating water jet ('cavijet') method - additional material on paper A3. *Proc. 1st Int. Symp. Jet Cutting Technol.* (eds. T.E. Brock & C.R. Richardson), BHRA, Cranfield, A/106-A/110.

Conn, A.F., 1989, Asbestos removal with self-resonating water jets. *Proc. 5th Amer. Water Jet Conf.* (ed. M.M. Vijay and G.A. Savanick), WJTA, St Louis, 133–139.

Conn, A.F., 1991, A technology transfer case history: introducing water jetting to the asbestos abatement industry. *Jet Cutting Technol.* (ed. E. Saunders), Elsevier, London, 441–447.

Conn, A.F. and Chahine, G., 1985, Ship hull cleaning with self-resonating pulsed water jets. *Proc. 3rd US Water Jet Conf.* (ed. N. Styler), US Bureau of Mines, WJTA, 1–19.

Conn, A.F., Rudy, S.L., 1974, Effects of fatigue and dynamic recovery on rain erosion. *ASTM STP 567*, 239–269.

Conn, A.F. and Rudy, S.L., 1978, Conservation and extraction of energy with the Cavijet™. *Proc. 4th Int. Symp. Jet Cutting Technol.* (eds. J. Clarke and H.S. Stephens), BHRA, Cranfield, H2/19-H2/38.

Conn, A.F., Gracey, M.T. and Rosenberg, W., 1987, A relative cleanability factor. *Proc. 4th US Water Jet Conf.* (eds. M. Hood and D. Dornfield), ASME, New York, 133–136.

Conroy, L.M., Menezes-Lindsay, R.M., Sullivan, P.M., Cali, S. and Forst, L., 1996, Lead, chromium, and cadmium exposure during abrasive blasting. *Arch. Environ. Health*, Vol. 51, 95–99.

Crine, J.P., 1988 (ed.) *Hazards, Decontamination, and Replacement of PCB*. Plenum Press, New York and London.

Crow, S.C. and Champagne, F.H., 1971, Orderly structure in jet turbulence. *J. Fluid Mech.*, Vol. 48, 547–591.

Da Maia, M.L., 2000, Alternatives to conventional methods and equipment for surface preparation. *Proc. PCE 2000 Conf. Exhibition*, Technol. Publ., Pittsburgh, 349–359.

Dear, J.P. and Field, J.E., 1988, A study of the collapse of arrays of cavities. *J. Fluid Mech.*, Vol. 190, 409–425.

De Botton, G., 1998, The interaction of a coated target and an impinging water drop. *Wear*, Vol. 219, 60–72.

Delucchi, M., Miglio, E., Cerisola, G., 1999, Laboratory testing of surface-tolerant coatings for protective maintenance of steel structures. *Protect. Coat. Europe*, Vol. 4, No. 9, 40–44.

De Santis, G.J., 1985, Operational and maintenance misconceptions of high pressure power pumps. *Proc. 3rd U.S. Water Jet Conf.* (ed. N. Styler), US Bureau of Mines, WJTA, 12–19.

De Vries, J.E., Holubka, K., Dickie, R.A., 1983, X-ray photoelectron spectroscopy study of corrosion-induced paint adhesion loss on conversion-coated steel. *Ind. Eng. Chem. Prod. Res. Div.*, Vol. 22, 256–261.

DHHS, 1997, Protecting workers exposed to lead-based paint hazards – A report to congress. *DHHS (NIOSH) Publ. No. 98-112*, Jan. 1997.

DIN/EN, 1995. *Hochdruckreiniger, Hochdruckwasserstrahlmaschinen – Sicherheitstechnische Anforderungen*. DIN/EN 1829, Entwurf Juni 1995, Europäisches Komitee für Normung, Brüssel, Belgium.

Dupuy, R., 2001, Ultra-high-pressure waterjetting for maintenance coatings applications. *J. Protect. Coat. Linings*, Vol. 18, No. 8, 68–75.

Dupuy, R., Ashworth, R. and Frenzel, L., 2001, Turning a liability into an asset – the story of an old power plant. *Proc. 11th Amer. Water Jet Conf.* (ed. M. Hashish), WJTA, St Louis, Paper 56.

Engel, O.G., 1973, Damage produced by high-speed liquid-drop impacts. *J. Appl. Phys.*, Vol. 44, 692–704.

Engel, P.A., 1978, *Impact Wear of Materials*. Elsevier Sci. Publ. Comp., Amsterdam.

Erdmann-Jesnitzer, F., Laschimke, R., 1966, Untersuchungen zur hydrodynamischen Beanspruchung bei Tropfenschlag. *Archiv f.d. Eisenhüttenwesen*, Jg. 37, 997–1012.

Fairfull, C.L. and Weldon, D.G., 2001, Salt contaminated abrasives and their effect on coating performance. *Proc. SSPC Conf.*, Atlanta.

Field, J.E., 1999, Liquid impact: theory, experiment, applications. *Wear*, Vol. 233–235, 1–12.

Foldyna, J., Hauner, M., Sedlarik, A., 1998, Utilization of waterjets in SS-23 missiles dismantling. Jetting Technol. (ed. H. Louis), Prof. Engng. Publ., Bury St. Edmunds, 485–489.

Fosgren, A. and Applegren, C., 2000, Comparison of chloride levels remaining on the steel surface after various pretreatments. *Proc. PCE Conf. Exhibition*, Technol. Publ., Pittsburgh, 271–283.

Fossey, R.D., Blaine, J.G., Tyler, L.J., Sabin, M. and Summers, D.A., 1997, Practical problems in the demilitarization of munitions. *Proc. 9th Amer. Water Jet Conf.* (ed. M. Hashish), WJTA, St Louis, 673–682.

French, M.A., 1998, Safety in high-pressure water jetting. *Water Jet Applications in Construction Engineering* (ed. A.W. Momber), A.A. Balkema, Rotterdam, 387–397.

Frenzel, L.M., 1997, Continuing improvement initiatives of surface preparation with water jetting. *Proc. 9th Amer. Water Jet Conf.* (ed. M. Hashish), WJTA, St Louis, 697–716.

Galecki, G. and Vickers, G.W., 1982, The developments of ice-blasting for surface preparation. *Proc. 6th Int. Symp. Jet Cutting Technol.*, BHRA, Cranfield, 59–79.

Gaughen, C.D., 2000, Quantifying sound coating adhesion. *SP-2067-SHR*, Naval Facilities Engng. Center, Port Hueneme, Special Publication.

Geskin, E.G., 1998, In-situ reactor cleaning by ultra-high pressure water jets. *Water Jet Applications in Construction Engineering* (ed. A.W. Momber), A.A. Balkema, Rotterdam, 339–350.

Geskin, E.S., Shishkin, D. and Babets, K., 1999, Application of ice particles for precision cleaning of sensitive surfaces. *Proc. 10th Amer. Water Jet Conf.* (ed. M. Hashish), WJTA, St Louis, Paper 22.

Goldie, B., 1999, Comparing robotic units made to clean vertical surfaces with UHP waterjetting. *Protect. Coat. Europe*, Vol. 4, No. 9, 9–18.

Goldie, B., 2002, A look at mobile blasting and UHP units for horizontal surfaces. *J. Protect. Coat. Linings*, Vol. 19, No. 3, 58–62.

Griffith, B., 2001, *Manufacturing Surface Technology*. Penton Press, London.

Griffith, B.J., Gawne, D.T. and Dong, G., 1997, The role of grit blasting in the production of high-adhesion plasma sprayed alumina coatings. *Proc. Inst. Mech. Engrs., Part B*, Vol. 211, 1–9.

Griffith, B.J., Gawne, D.T. and Dong, G., 1999, A definition of the topography of grit-blasted surfaces for plasma sprayed alumina coatings. *Trans. ASME, J. Manuf. Sci. Engng.* Vol. 121, 49–53.

Gross, H.W. and Weisinger, F., 1998, High pressure injection technique for soil conditioning. *Water Jet Applications in Construction Engineering* (ed. A.W. Momber), A.A. Balkema, Rotterdam, 231–243.

Haferkamp, H., Louis, H., Tönshoff, H.K., Brinksmeier, E., Laurinat, A., Roth, P., 1989, Gezielte Randzonenverbesserung durch Hochdruckwasserstrahlen. *Mechanische Oberflächenbehandlung* (eds. E. Broszeit & H. Steindorf), DGM Informationsgesellschaft, 155–163.

Halbartschlager, J., 1985, Untersuchung verschiedener Entlackungsverfahren der Automobilindustrie unter besonderer Berücksichtigung umwelttechnischer Belange. *VDI-Fortschritt-Berichte*, Reihe 3, Nr. 109, VDI-Verlag, Düsseldorf.

Hamada, S., Kamiyama, S., Tsubota, M. *et al.*, 1991, The structure of an annular jet and its characteristics (ed. D. Saunders), *Jet Cutting Technol.*, Elsevier Appl. Sci., London, 69–72.

Hansink, J., 1998, On the issue of health and silica sand as a blasting abrasive. *J. Protect. Coat. & Linings*, Vol. 15, No. 11, 90–95.

Harbaugh, D.J., Stone, M.A., 1993, The effect of high pressure water on material integrity of selected aircraft coatings and substrates. *SAE-Paper* 931062, 22–30.

Hare, C.H., 1995, Adhesive and cohesive failure: definitions and fundamental macro-effects. *J. Protect. Coat. & Lining*, Vol. 12, No. 10, 177-187.

Hartland, P., 2000, Vocational training in Norway. *Protect. Coat. Europe*, Vol. 5, No. 7, 47.

Heimhardt, H.J., 1998, Application of the water jet technology for the 'high pressure soil washing process'. *Water Jet Applications in Construction Engineering* (ed. A.W. Momber), A.A. Balkema, Rotterdam, 217–229.

Henderson, M., 1998, UHP waterjetting on vessels while at sea. *Protect. Coat. Europe*, Vol. 15, No. 11, 16–19.

Hilmersson, S., 1998, Hydrodemolition of concrete structures – basics and field experience. *Water Jet Applications in Construction Engineering* (ed. A.W. Momber), A.A. Balkema, Rotterdam, 163–175.

Himmelreich, U., 1992, Fluiddynamische Modelluntersuchungen an Wasserabrasivstrahlen. *VDI Fortschritt-Berichte*, Reihe 7, Nr. 219.

Himmelreich, U. and Rieß, W., 1991, Laser-velocimetry investigations of the flow in abrasive water jets with varying cutting head geometry. *Proc. 6th Amer. Water Jet Conf.* (ed. T.J. Labus), WJTA, St Louis, 355–369.

Hobbs, P.V., 1974, *Ice Physics*. Clarendon Press, Oxford.

Hofacker, S.A., 1993, The large aircraft robotic paint stripping system. *Proc. 7th Amer. Water Jet Conf.* (ed. M. Hashish), WJTA, St Louis, 613–628.

Hofinger, I., Raab, K., Möller, J., Bobeth, M., 2002, Effect of substrate surface roughness on the adherence of NiCrAlY thermal spray coatings. *ASM J. Thermal Spray Technol.*, Vol. 11, 387-392.

Holle, D., 2000, Ultra-high-pressure waterjetting of hazardous coatings on galvanized communication towers, *J. Protect. Coat. Linings*, Vol. 17, No. 11, 71–85.

Hori, K., Matsumae, Y., Cheng, X. *et al.*, 1991, Development of a new mixing nozzle assembly for high pressure abrasive water jet applications (ed. D. Saunders), *Jet Cutting Technol.*, Elsevier Appl. Sci., London, 193–206.

Horigushi, T. and Kajihara, K., 1988, Development of piling system of precast piles by applying rotary jets. *Proc. 9th Int. Symp. Jet Cutting Technol.* (ed. P.A. Woods), BHRA, Cranfield, 591–610.

Houlston, R. and Vickers, G.W., 1978, Surface cleaning using water-jet cavitation and droplet erosion. *Proc. 4th Int. Symp. Water Jet Technol.* (eds. J. Clarke and H.S. Stephens), BHRA, Cranfield, H1/1-H1/18.

Howells, W.G., 1998, Enhancing waterjetting by use of water soluble additives. *Water Jet Applications in Construction Engineering* (ed. A.W. Momber), A.A. Balkema, Rotterdam, 41–50.

Howlett, J.J. and Dupuy, R., 1993, Ultrahigh-pressure water jetting for deposit removal and surface preparation. *Mater. Performance*, Jan., 38–43.

JISHA, 1992, Safety Guidelines for Water Jet Machining. Japan Industrial Safety and Health Association, Tokyo, Japan.

Johnson, V.E., Conn, A.F., Lindenmuth, W.T., Chahine, G.L. and Frederick, G.S., 1984, Self resonating cavitating jets. *Proc. 6th Int. Symp. Water Jet Technol.* (eds. H.S. Stephens and E.B. Davies), BHRA, Cranfield, Paper A1, 1–25.

Jung, R.G. and Drucks, M., 1996, Optimierung der Reinigung von Filtertüchern bei betrieblich eingesetzten Filtrationsanlagen. *Aufbereitungs-Technik*, 37. Jg., 142–148.

Kaiser, W.-D., Schütz, A., 2001, Hochdruckwasserstrahlen und restrostverträglicher Beschichtungsstoff – Eine mögliche Instandsetzungsstrategie. WEKA, *Korrosionsschutz durch Beschichtungen und Überzüge auf Metallen*, Band 2, Teil 9, Kapitel 8.5, September, 1–26.

Kaufmann, B., 1998, Traggrund Stahl: Gibt es Alternativen zum Sandstrahlen? Seminarunterlagen, Der Traggrund – ein ständiger Konfliktherd? Schweizerischer Fachverband für Hydrodynamik am Bau, Würenlingen.

Kaufmann, B. and Zielasch, A.H., 1998, Renovation of steel constructions by a combined waterjetting – waste recycling method. *Water Jet Applications in Construction Engineering* (ed. A.W. Momber), A.A. Balkema, Rotterdam, 313–323.

Kauw, V., 1992, Hochdruckwasserstrahlen in der Baupraxis. Lehrgangsunterlagen, Lehrgang 15178/83.153, TA Esslingen.

Kaye, P.L., Pickles, C.S., Field, J.E. and Julian, K.S., 1995, Investigating of erosion processes as cleaning mechanisms in the removal of thin deposited soils. *Wear*, Vol. 186–187, 413–410.

Kierkegaard, H., 2000, Using UHP waterjetting for coating maintenance on ship at sea. *J. Protect. Coat. Linings*, Vol. 17, No. 1, 38–47.

Kiyohashi, H. and Handa, K., 1998, Numerical simulation of growth of ice particles in cryogenic liquefied gas for ice abrasive jet. *Proc. 5th Pacific Rim Int. Conf. Water Jet Technol.* (eds. M.M. Vijay *et al.*), New Delhi, 510–520.

Knapp, J.K. and Taylor, T.A., 1996, Waterjet roughened surface analysis and bond strength. *Surface Coat. Technol.*, Vol. 86–87, 22–27.

Knapp, R.T., Daily, J.T. and Hammitt, F.G., 1970, *Cavitation*. McGraw Hill, New York.

Knipfer, C. and Funke, H.-W., 1997, Lärmbelastung an Baustellenarbeitsplätzen. Teil V. *BIA Report*, Hauptverband der gewerblichen Berufsgenossenschaften, St. Augustin.

Kogler, P.A., Ault, J.P., Farshon, C.L., 1995, Environmental acceptable materials for the corrosion protection of steel bridges. *Final Report*, Ocean City Research Corp., February, 1995.

Kronborg, P., 1999, Fundamentals of waterjetting and priming steel surfaces on ships. *Protect. Coat. Europe*, Vol. 4, No. 3, 42–45.

Kuljan, G., Holmes, B.S., 1998, U.S. Navy experience with waterjetting. *Protect. Coat. Europe*, Vol. 3, 16–21.

Küfer, K.-H., 1999, Zur Energieverteilung von rotierenden Wasserstrahlwerkzeugen. Inst. f. Techno- und Wirtschaftsmathematik, Kaiserslautern.

Kuljian, G.G. and Melhuish, D.C., 1999, Water-jetting productivity study for the marine industry. *Proc. 10th Amer. Waterjet Conf.* (ed. M. Hashish), WJTA, St Louis, Paper 42.

Labus, T.J., 1991, Pulsed fluid jet technology. *Proc. 1st Asian Conf. Recent Adv. Jetting Technol.* (ed. J.S. Tan), CI Prem. Ltd, Singapore, 136–143.

Lauterborn, W. and Bolle, H., 1975, Experimental investigations of cavitation bubble collapse in the neighborhood of a solid boundary. *J. Fluid Mech.*, Vol. 72, 391–399.

Le Calve, P., Lacam, J.M. and Meunier, P., 2002, Quantification of the products of corrosion after UHP waterjetting. *Protect. Coat. Europe*, Vol. 19, No. 9, 22–29.

Le Calve, P., Meunier, P., Lacam, J.M., 2003, Evaluation of the behavior of reference paint systems after UHP waterjetting. *J. Protective Coatings & Linings*, Vol. 20, No. 1, 48–54.

Lecoffre, Y., 1999, *Cavitation - Bubble Trackers*. A.A. Balkema, Rotterdam.

Lee, C.I., Kim, W.M., Kim, H.M. and Kim, D.I., 1999, Testing of waterjets for rock surface treatment. *Proc. Int. Symp. New Appl. Water Jet Technol.* (ed. R. Kobayashi), Ishinomaki, 171–178.

Lelaidier, M. and Spitz, J.A., 1978, Part played by high-pressure water in the nuclear decontamination process. *Proc. 5th Int. Technol. Meeting Nuclear Industries*, Basel, 1–11.

Lenz, J. and Wielenberg, M., 1998, Cleaning of sewage systems by high-pressure water jetting. *Water Jet Applications in Construction Engineering* (ed. A.W. Momber), A.A. Balkema, Rotterdam, 351–363.

Lesser, M.B., 1995, Thirty years of liquid impact research: a tutorial review. *Wear*, Vol. 186, 28–34.

Lesser, M.B. and Field, J.E., 1983, The impact of compressible liquids. *Ann. Rev. Fluid Mech.*, Vol. 15, 97–122.

Leu, M.C., Meng, P., Geskin, E.S. and Tismeneskiy, L., 1998, Mathematical modeling and experimental verification of stationary waterjet cleaning process. *Trans. ASME, J. Manuf. Sci. Engng.*, Vol. 120, 571–579.

Liu, B., 1991, The rotated injection abrasive jet rust cleaning system. *Jet Cutting Technol.* (ed. D. Saunders), Elsevier Appl. Sci., London, 221–233.

Liu, B., Shang, Y., Yao, H. and Zhang, G., 1992, The recent Premajet cutting and derusting technology. *Jet Cutting Technol.* (ed. A. Lichtarowicz), Kluwer Acad. Publ., Dordrecht, 451–460.

Liu, B.L., Jia, B., Zhang, D., Wang, C., Li, N. and Yao, H., 1993, The Premajet derusting and abrasive recovery system. *Proc. 7th Amer. Water Jet Conf.* (ed. M. Hashish), WJTA, St Louis, 629–641.

Liu, B.L., Liu, L.H. and Wu, L., 1998, Research on the preparation of the ice jet and its cleaning parameters. *Jetting Technol.* (ed. H. Louis), Profes. Engng. Publ., Bury St. Edmunds, 203–209.

Louis, H., Milchers, W. and Pude, F., 1999, Experimental and theoretical investigation of the decoating process by pure waterjet. *Proc. 10th Amer. Water Jet Conf.* (ed. M. Hashish), WJTA, St Louis, Paper 54.

Lohse, U., 1929, Versuche an einer Naβputzanlage. *Gießerei*, Jg. 16, 1137–1144.

Mabrouki, T., Raissi, K., 2002, Striping process modelling: interaction between a moving waterjet and coated target. *Int. J. Mach. Tools & Manuf.*, Vol. 42, 1247–1258.

Mabrouki, T., Cornier, A. and Raissi, K., 1998, The study of HP pure waterjet impacts as the primary mechanism of paint decoating process. *Jetting Technol.* (ed. H. Louis), Mechan. Engng. Publ. Ltd., London, 563–577.

Mabrouki, T., Raissi, K. and Cornier, A., 2000, Numerical simulation of high-velocity pure water-jet impingement on coated materials. *Jetting Technol.* (ed. H. Louis), BHR Group, Cranfield, 199–217.

Marshall, A.K., 1996, Lead removal with waterjetting. *J. Protect. Coat. Linings*, Vol. 13, No. 2, 47–51.

Marshall, A.K., 2001, Waterjetting and recoating dockside at the port of Houston authority. *J. Protect. Coat. Linings*, Vol. 18, No. 5, 63–69.

Meng, P., Geskin, E.S., Leu, C. and Tismenetskiy, L., 1996, Waterjet in-situ reactor cleaning. In: *Jetting Technol.* (ed. C. Gee), Mechan. Engng. Publ. Ltd., London, 347–358.

Meng, P., Geskin, E.S., Leu, M.C. and Tismeneskiy, L., 1998, An analytical and experimental study of cleaning with moving waterjets. *Trans. ASME, J. Manuf. Sci. Engng.*, Vol. 120, 580–589.

Meunier, P., 2001, Safely discharging waste water from UHP waterjetting work on rail bridges in France. *Protect. Coat. Europe*, Vol. 18, No. 1, 49–53.

Meunier, P. and Lambert, P., 1998, The experience of SNCF in preparing previously painted metal surfaces by UHP waterjetting. *Protect. Coat. Europe*, Vol. 15, No. 9, 34–37.

Mickelsen, R.L., Johnston, O.E., 1995, Lead exposure during removal of lead-based paint using vacuum blasting. *J. Protect. Coat. & Linings*, Vol. 12, No. 2, 78–84.

Miller, P.I., 1999, Fluid jet ignition hazards safety analysis. *Proc. 10th Amer. Water Jet Conf.* (ed. M. Hashish), WJTA, St. Louis, Paper 70.

Miller, R.K. and Swenson, G.J., 1999, Erosion of steel substrates when exposed to ultra-pressure waterjet cleaning systems. *Proc. 10th Amer. Water Jet Conf.* (ed. M. Hashish), WJTA, St. Louis, Paper 52.

Mitschke, H., 2001, Effects of chloride contamination on the performance of tank and vessel linings. *J. Protect. Coat. & Linings*, Vol. 18, No. 3, 49-56.

Momber, A.W., 1993a, *Handbuch Druckwasserstrahl-Technik*. Beton Verlag GmbH, Düsseldorf.

Momber, A.W., 1993b, Recent developments in water jet use in ground and traffic area rebuilding. *Proc. 7th Amer. Water Jet Conf.* (ed. M. Hashish), WJTA, St Louis, 561–571.

Momber, A.W., 1995, Environmental applications of high speed water jet technology – preliminary results. *J. Jet Flow Engng.*, Vol. 12, 46–53.

Momber, A.W., 1997, Investigations into decoating and recycling of pipeline elements using the high-pressure water jet technique. *Inst. Mechan. Engnrs., J. Mechan. Process Engng*, Vol. 211, 129–135.

Momber, A.W., (ed.) 1998a, *Water Jet Applications in Construction Engineering*. A.A. Balkema, Rotterdam.

Momber, A.W., 1998b, Hydrodemolition – the case for waterjetting. *Concrete Engng Int.*, April, 34–38.

Momber, A.W., 2000a, A dimensionless number for the control of ultra-high pressure systems. *Inst. Mechan. Engrs., J. Power Energy*, Vol. 213, 645–655.

Momber, A.W., 2000b (ed.) *Materialrecycling mit Hochdruckwasserstrahlen*. Expert-Verlag, Renningen.

Momber, A.W., 2000c, Hydrodynamic cleaning of heat exchangers. *Heat Exchanger Fouling* (ed. H. Müller-Steinhagen), Publico Publ., Essen, 98–107.

Momber, A.W., 2000d, Short-time cavitation erosion of concrete. *Wear*, Vol. 241, 47–52.

Momber, A.W., 2001, Energy transfer during the mixing of air and solid particles into a high-speed waterjet: an impact force study. *Experimental Thermal Fluid Sci.*, Vol. 25, 31–41.

Momber, A.W., 2002, Multiple grit-blasting of low-carbon steel surfaces. Unpublished results.

Momber, A.W., 2003a, An SEM-study of high-speed hydrodynamic erosion of cementitious composites. *Composites Part B: Engng*, Vol. 34, 135–142.

Momber, A.W., 2003b, Cavitation damage to geomaterials in a flowing system. *J. Mater. Sci.*, Vol. 38, 747–757.

Momber, A.W., 2003c, Aggregate liberation from concrete by flow cavitation. *Int. J. Mineral Proc.*, in print.

Momber, A.W., 2003d, Rock erosion by water flow. *Int. J. Rock Mech. Min. Sci.*, in print.

Momber, A.W. and Kovacevic, R., 1994, Fundamental investigations on concrete wear by high velocity water flow. *Wear*, Vol. 177, 55–62.

Momber, A.W. and Kovacevic, R., 1998, *Principles of Abrasive Water Jet Machining*. Springer-Verlag Ltd., London.

Momber, A.W. and Nielsen, A.G., 1998, Pipeline rehabilitation by waterjetting. *Mater. Evaluation*, Vol. 37, 97–101.

Momber, A.W., Kovacevic, R. and Ye, J., 1995, The fracture of concrete due to erosive wear by high velocity water flow. *Tribol. Trans.*, Vol. 38, 686–692.

Momber, A.W., Wüstenberg, D. and Weiß, M., 2000, Entwicklung eines Verfahrens zur werkstofflichen Verwertung von Teppichproduktionsabfällen und Altteppichböden. Abschlußbericht 10831, Deutsche Bundesstiftung Umwelt, Osnabrück.

Momber, A.W., Wong, Y., Budidharma, E. and Tjo, R., 2002a, Profiling of low-carbon steel with supersonic water jets. *Wear*, Vol. 249, 853–859.

Momber, A.W., Wong, Y.C., Budidharma, E. and Tjo, R., 2002b, Hydrodynamic profiling and grit blasting of low-carbon steel. *Tribology Intern.*, Vol. 35, 271–281.

Momber, A.W., Kovacevic, R. and Mohan, R., 2002c, Fracture range detection in the hydro-abrasive erosion of concrete. *Wear*, Vol. 253, 1156–1164.

Morcillo, M., Simancas, J., 1997, Effects of soluble salts on coating life in atmospheric services. *J. Protect. Coat. & Linings*, Vol. 14, No. 9, 40-52.

Morcillo, M., Bastidas, J.M., Simanacas, J., Galvan, J.C., 1989, The effect of the abrasive work mix on the paint performance over blasted steel. *Anti Corrosion Meth. & Mater.*, Vol. 36, No. 5, 4–8.

Morel, T., 1979, Experimental study of a jet-driven Helmholtz-oscillator. *J. Fluid Engng*, Vol. 101, 838–890.

Morris, M., 2000, Update: evaluating UHP waterjetting as preparation for ballast tank coating. *Protect. Coat. Europe*, Vol. 5, No. 9, 54–59.

Mühlhan, 2001, μ-jet surface protection technology. *Protect. Coat. Europe*, Vol. 6, No. 11, 18–19, 53–54.

Nakaya, M., Nishida, N., Kitagawa, T., 1983, Development of variable delivery triple reciprocating plunger pump for water jet cutting. *Proc. 2nd U.S. Water Jet Symp.* (eds. D.A. Summers, F.F. Haston), Univ. of Missouri-Rolla, 111–118.

Nelson, D., 1996, Stripped clean. *Workboat Magazine*, Jan./Febr., 52–59.

Neusen, F.K., Alberts, D.G., Gores, T.J. and Labus, T.J., 1991, Distribution of mass in a three-phase abrasive waterjet using X-ray densitometry. *Jet Cutting Technol.* (ed. S. Stephens), Elsevier Sci. Publ., Rotterdam.

Neusen, K.F., Gores, T.J. and Labus, T.J., 1992, Measurement of particle and drop velocities in a mixed abrasive water jet using forward-scatter LDV system. *Jet Cutting Technol.* (ed. A. Lichtarowicz), Kluwer Acad. Publ., Dordrecht, 63–74.

Neusen, K.F., Gores, T.J. and Amano, R.S., 1994, Axial variation of particle and drop velocities downstream from an abrasive water jet mixing tube. *Jet Cutting Technol.* (ed. N.G. Allen), Mechanical Engng. Publ. Ltd., London, 93–103.

NSRP, 1998, Productivity study of hydroblast removal of coatings. Final Report, The National Shipbuilding Research Program, NSRP 0520 N3-96-4, US Department of the Navy.

Ochs, H.-J. and Maurmann, W., 1996, Strahl- und Beschichtungstechnik an der Ruhrtalbrücke. *Bautenschutz & Bausanierung*, Nr. 6, 17–19.

Odwazny, J., da Maia, C. and Kuljian, G., 2002, Advances in high production robotic waterjetting for the marine industry. *Protect. Coat. Europe*, Vol. 7, No. 4, 47–56.

Oertel, M., 2001, *Prandtl-Führer durch die Strömungslehre*. Viehweg, Braunschweig.

Ohnesorge, W., 1936, Die Bildung von Tropfen an Düsen und die Auflösung flüssiger Strahlen. *Zeitschrift f. angew. Math. und Mechanik*, Jg. 16, 355–358.

OSHA, 1993, Permit required confined spaces for general industry. Title 29 CFR 1910.146, Final Rule, Dept. of Labor, Jan. 14, 1993.

Palm, L. and Platz, N., 2000, Innovative Technologien zur Entlackung und Farbbeschichtung von Schiffen im Dock. *Forum ThyssenKrupp*, Nr. 1, 70–73

Pietsch, S., Kaiser, W.-D., 2002, Atmosphäre, Wasser, Erdboden – Prinzipen der Korrosionsschutzauswahl. *Der Maler und Lackiermeister*, Nr. 7, 18–21.

Platek, M., 2002, Training for confined space entry. *Protect. Coat. Europe*, Vol. 7, No. 11, 45–52.

Raghavan, C. and Olsen, J., 1989, Development of a 7,000 bar hose. *Proc. 5th Amer. Water Jet Conf.* (ed. T.J. Labus), WJTA, St Louis, 449–454.

Randall, P.M., Kranz, P.B., Sonntag, M.L. and Stadelmaier, J.E., 1998, Evaluation of needle gun and abrasive blasting technologies in bridge paint removal practices. *J. Air Waste Management Ass.*, Vol. 48, 264–270.

Raudensky, M., Horsky, J. and Telecky, L., 1999, Thermal and mechanical effect of high-pressure spraying of hot surfaces – descaling. *Proc. 3rd Int. Metallurg. Conf. Cont. Casting Dillets*, Trinec, 217–221.

Rice, R.M., 1997, Mobile full recovery waterjet stripping systems. *Proc. 9th Amer. Water Jet Conf.* (ed. M. Hashish), WJTA, St Louis, 581–587.

Richardt, W., 1998, Protecting marine newbuildings in Germany. *Protect. Coat. Europe*, Vol. 3, No. 1, 16–24.

Schikorr, W., 1986, Beitrag zum Werkstoffabtrag durch Flüssigkeitsstrahlen hoher Relativgeschwindigkeit. *Dissertation*, Univ. Hannover.

Schlatter, M., 1986, *Entgraten durch Hochdruckwasserstrahlen*. Springer-Verlag, Heidelberg.

Schmidt, P. Walzel, P., 1984, Zerstäuben von Flüssigkeiten. *Physik in unserer Zeit*, Vol. 15, 113–120.

Shi, H.H. and Dear, P., 1992, Oblique high-speed liquid-solid impact. *JSME Int. J., Ser. I*, Vol. 35, 285–295.

Shishkin, D.V., 2002, Development of icejet-based machining technology. *PhD Thesis*, NJIT, Newark, NJ.

Shishkin, D.V., Geskin, E.S. and Goldenberg, B., 2001, Development of a technology for generation of ice particles. *Proc. Int. Symp. Surface Contamination and Cleaning*, Newark.

Siebel, M.K. and Mosher, G.E., 1984, Detecting and controlling vibration. *Modern Casting*, Aug., 34–36.

Siores, E., Chen, L. and Momber, A.W., 2000, Introduction of a new precision cryogenic icejet system for processing materials. *Proc. 6th Pacific Rim Int. Conf. Water Jet Tech.* (eds. P.G. Dunn *et al.*), CMTE, 136–139.

Snyder, G., 1999, NYSDON studies chemical stripping / ice blasting process. *J. Protect. Coat. & Linings*, Vol. 16, No. 9, 53–55.

Smith, L., 2001, Safe use of ultra-high-pressure waterjetting. *J. Protect. Coat. Linings*, Vol. 18, No. 10, 35–40.

Soltz, G.C., 1991, The effects of substrate contaminants on the life of epoxy coatings submerged in sea water. *National Shipbuilding Research Program*, Task No. 3-89-2, March 1991, 1–96.

Sondermann, W., 1998, Extraction and washing contaminated soils using high pressure jet grouting technique. *Water Jet Applications in Construction Engineering* (ed. A.W. Momber), A.A. Balkema, Rotterdam, 207–216.

Springer, G.S., 1976, *Erosion by Liquid Impact*, Scripta Publishing Co., Washington DC.

SSPC-SP 12/NACE No. 5, 2002, Surface preparation and cleaning of metals by waterjetting prior to recoating. Joint Surface Preparation Standard, SSPC Publication No. 02–19.

Staskiewicz, L., 1995, Entwicklung eines Modells zur Vorhersage der Kerbtiefe beim Kerben von Bohrlöchern mit Hilfe der Hochdruckwassertechnik. *Diplomarbeit*, Inst. für Bergbaukunde II, RWTH Aachen.

Summers, D.A., 1991, Historical perspective of fluid jet technology. *Fluid Jet Technology* (ed. T.J. Labus), Water Jet Techn. Ass., St Louis, 1.1–1.21.

Summers, D.A., 1995, *Waterjetting Technology*. Chapmann & Hall, New York.

Sundaram, T.R. and Liu, H.L., 1978, On the equivalence between stationary and nonstationary modes of operation of water jets. *Proc. 4th Int. Symp. Jet Cutting Technol.* (eds. J. Clarke and H.S. Stephens), BHRA, Cranfield, F2/17-F2/30.

Swan, S.P., 1983, Economic considerations in water jet cleaning. *Proc. 2nd US Water Jet Symp.* (eds. D.A. Summers and F.F. Haston), Univ. of Rolla Press, Rolla, 433–439.

Taylor, S.A., 2000, Field removal of cold-applied tape systems from large diameter transmission lines using ultra high-pressure water jetting. *Proc. PCE Conf. and Exhibition*, Technol. Publ., Pittsburgh, 177–188.

Taylor, T.A., 1995, Surface roughening of metallic substrates by high pressure pure waterjets. *Surface Coatings Technol.*, Vol. 76–77, 95–100.

Thikomirov, R.A., Babanin, V.B., Pethukov, E.N. *et al.*, 1992, *High Pressure Jet Cutting*. ASME Press, New York.

Thiruvengadam, A., 1967, The concept of erosion strength. *ASTM STP 408*, Amer. Soc. Testing Mater., Philadelphia, 22–41.

Thomas, A.G., Field, J.E. and Woodall, D.L., 1998, Water jet removal of liquid and soft-solid coatings. *Proc. 5th Pacific Rim Int. Conf. Water Jet Technol.* (eds. M.M. Vijay), Allied Publ., Ltd., New Delhi, 212–230.

Tinklenberg, G.L., Doezema, D.M., 1998, Health concerns for workers using zinc-rich coatings. *J. Protect. Coat. & Linings*, Vol. 15, No. 5, 36–46.

Tönshoff, H.K., Kroos, F., Hartmann, M., 1995, Water peening – an advanced application of water jet technology. *Proc. 8th Amer. Water Jet Conf.* (ed. T.J. Labus), WJTA, St. Louis, 473–486.

Troesch, H.A., 1954, Die Zerstäubung von Flüssigkeiten. *Chemie-Ing.-Techn.*, Jg. 26, 311–320.

Trotter, L.E., 2001, Comparison of surface preparation using different methods. *Proc. 11th Amer. Waterjet Conf.* (ed. M. Hashish), WJTA, St Louis, 745–763.

Truchot, P., Mellinger, P., Duchamp, R., Kim, T.J. and Ocampo, R., 1991, Development of a cryogenic waterjet technique for biomaterial processing applications. *Proc. 6th Amer. Water Jet Conf.* (ed. T.J. Labus), WJTA, St Louis, 473–480.

Uhlendorf, H.-J., 2000, Korrosionsschutzmaßnahmen an Hafenanlagen in der Jade. *Hansa*, Vol. 137, Nr. 8, 75–79.

US Air Force, 1999, *Laser Paint Removal*. Final Report, Joint Depot Maintenance Activities Group, Wright-Patterson-Airbase, Ohio.

Utsumi, H., Sakoda, S., Ying, L. and Adachi, I., 1999, Experimental study in the construction joint of concrete structure using WJ technology. *Proc. Int. Symp. New Appl. Water Jet Techn.* (ed. R. Kobayashi), Ishinomaki, 163–170.

Van der Kaaden, 1994, Wet blasting studied to replace dry blasting in Netherlands shipyards. *J. Protect. Coat. Linings*, Vol. 11, No. 5, 79–86.

Vauck, W. and Müller, H., 1994, *Grundoperationen chemischer Verfahrenstechnik*. Deutscher Verlag für Grundstoffindustrie, 10. Auflage, Leipzig-Stuttgart.

VDI, 1987, Einwirkung mechanischer Schwingungen auf den Menschen – Beurteilung, *VDI-Richtlinie 2057/Blatt 3*, Mai 1987.

Veenhuizen, S.D., 2000, Operating efficiency of crankshaft drive pumps. *Proc. 6th Pacific Rim Conf. Water Jetting Technol.* (eds. P.G. Dunn *et al.*), CMTE, 249–252.

Vijay, M.M., 1998a, Power of pulsed jets. *Waterjet Applications in Construction Engineering* (ed. A.W. Momber), A.A. Balkema, Rotterdam.

Vijay, M.M., 1998b, Fluidjet technology: safety considerations. *Proc. 5th Pacific Rim Int. Conf. Water Jet Technol.* (eds. M.M. Vijay *et al.*), Allied Publ. Ltd., New Delhi, 309–320.

Vijay, M.M., Foldyna, J. and Remisz, J., 1993, Ultrasonic modulation of high-speed water jets. *Proc. Geomechanics '93* (ed. Z. Rakowski), A.A. Balkema, Rotterdam, 327–332.

Vijay, M.M., Debs, E., Paquette, N., Puchala, R.J. and Bielawski, M., 1997, Removal of coatings with low pressure pulsed water jets. *Proc. 9th Amer. Waterjet Conf.* (ed. M. Hashish), WJTA, St Louis, 563–580.

Vijay, M.M., Yan, W., Tieu, A., Bai, C. and Pecman, S., 1999, Removal of hard coatings from the interior of ships using pulsed waterjets: results of field trials. *Proc. 10th Amer. Waterjet Conf.* (ed. M. Hashish), WJTA, St Louis, Paper 53.

Volkmar, J., 1992, "Aquastrip" – an innovative paint removal technology. Presentation at the *75th AGARD Meeting*, Lindau, Germany, 7–8 October.

Wang, L.L., Field, J.E., Sun, Q. and Liu, J., 1995, Surface damage of polymethylmethacrylate by ice and nylon ball impacts. *J. Appl. Phys.*, Vol. 78, 1643–1649.

Weber, C., 1931, Zum Zerfall eines Flüssigkeitsstrahles. *Zeitschrift f. angew. Math. und Mechanik*, Jg. 11, Nr. 2, 136–154.

Weiß, M. and Momber, A.W., 1998, Carpet recycling with water jets. *Recycling Recovery Reuse '98* (ed. X. Edelmann), Genf, III.123–III.136.

Weiß, M. and Momber, A.W., 1999, Selective carpet separation with high-speed waterjets. *Proc. Int. Symp. New Appl. of Water Jet Techn.* (ed. R. Kobayashi), Ishinomaki, 227–231.

Weiß, M. and Momber, A.W., 2003, Preliminary investigations into the separation of automotive components by a hydro-erosive method. *Inst. Mechan. Engrs., J. Automobile Engng*, Vol. 217, 221–228.

Weiß, M., Wüstenberg, D., Momber, A.W., 2003, Hydro-erosive separation of plastic fibres from textile compounds. *J. Mater. Cycles and Waste Management*, Vol. 5, 84–88.

Wenzel, R.W., 1936, Resistance of solid surfaces to wetting by water. *Ind. Engng Chem.*, Vol. 28, 988–994.

Werner, M., 1991, Höchstdruckwasserstrahlen in der Bauindustrie – Einsatzmöglichkeiten und Einsatzgrenzen. Lehrgang 13809/83.130, Technische Akademie Esslingen.

Werner, M. and Kauw, V., 1991, High pressure water jet system – a new process for cleaning defective mortar joints in historic masonry. *Proc. 9th Int. Brick/Block Masonry Conf.*, Vol. 3, Berlin, 1639–1644.

Wiedemeier, J., 1981, Flüssingkeitsfreistrahlen hoher Relativgeschwindigkeit und Bruchkinetik spröder Werkstoffe. *PhD Thesis*, Univ. Hannover.

WJTA, 1994, Recommended Practices for the Use of Manually Operated High-Pressure Water Jetting Equipment. Water Jet Technology Association, St Louis, MO, USA.

Wood, B., 1996, A water-cooled, hydraulically positioned 20,000 psi lance for waterblasting inside a hot kiln. *Jetting Technology* (ed. C. Gee), Mechan. Engng. Publ. Ltd., London, 379–392.

Wright, D., Wolgamott, J. and Zink, G., 1997, A study of rotary jets for material removal. *Proc. 9th Amer. Water Jet Conf.* (ed. M. Hashish), WJTA, St Louis, 525–539.

Wright, D., Wolgamott, J. and Zink, G., 1999, Nozzle performance in rotary applications. *Proc. 10th Amer. Water Jet Conf.* (ed. M. Hashish), WJTA, St Louis, Paper 73.

Wu, S. and Kim, T.J., 1995, An application study of plain waterjet process for coating removal. *Proc. 8th Amer. Water Jet Conf.* (ed. T.J. Labus), WJTA, St Louis, 779–792.

Xue, S., Huang, W., Zhao, S. and Shi, D., 1993, Equipment and test research of high pressure water jet for rust removal. *Proc. 7th Amer. Water Jet Conf.* (ed. M. Hashish), WJTA, St Louis, 653–662.

Xue, S., Huang, W., Chen, Z., Shi, D. and Mi, W., 1996, How to formulate standards of high pressure waterjet units. *Jetting Technol.* (ed. C. Gee), Mechan. Engng. Publ., Bury St. Edmunds, 405–411.

Yanaida, K., 1974, Flow characteristics of water jets. *Proc. 2nd Int. Symp. Jet Cutting Technol.* (eds. N.G. Coles and S.J. Barrall), BHRA Fluid Engng, Cranfield, A2/19-A/2-32.

Yanaida, K. and Ohashi, A., 1980, Flow characteristics of water jets. *Proc. 5th Int. Symp. Jet Cutting Techn.* (eds. H.S. Stephens and B. Jarvis), BHRA, Cranfield, Paper A3, 33–44.

Yasui, R., Yanari, A. and Carletti, F.M., 1993, The removal of excessive resin from semiconductor leadframes with spot-shot waterjets. *Proc. 7th Amer. Water Jet Conf.* (ed. M. Hashish), WJTA, St Louis, 813–827.

Yonekura, R., Terashi, M. and Shibazaki, M. (eds.) 1996, *Grouting and Deep Mixing.* A.A. Balkema, Rotterdam.

Zublin, C.W., 1983, Water jet cleaning speeds – theoretical considerations. *Proc. 2nd US Water Jet Symp.* (eds. D.A. Summers and F.F. Haston), Univ. of Rolla, Rolla, 159–164.

Appendix

National and International Regulations on Hydroblasting

DIN EN 1829, High Pressure Cleaners – High Pressure Water Jet Machines – Safety Requirements, Draft Standard, June 1995.

Recommended Practices for the Use of Manually Operated High-Pressure Water Jetting Equipment. Water Jet Technology Association, St Louis, MO, USA, 1994.

Safety Guidelines for Water Jet Machining. Japan Industrial Safety and Health Association, Tokyo, Japan, 1992.

Code of Practice for the Use of High Pressure Water Jetting Equipment. Association of High Pressure Water Jetting Contractors, London, UK, 1993.

Handboek Hogedruk Vloeisofreiniging. Stichting Europort/Botlek Belangen, Rotterdam, Netherlands, 1987.

Betrieb von Höchstdruck-Wasserstrahl-Geräten (HWG). Richtlinie Nr. 6505, Ausgabe 7.91, Eidgenössische Koordinationskommission für Arbeitssicherheit, Luzern, Switzerland, 1991.

Unfallverhütungsvorschrift Arbeiten mit Flüssigkeitsstrahlern. BGV D15, Steinbruchs-Berufsgenossenschaft Hannover, Germany, 1999.

Bau von Höchstdruck-Wasserstrahl-Geräten (HWG). Richtlinie Nr. 6504, Ausgabe 7.91, Eidgenössische Koordinationskommission für Arbeitssicherheit, Luzern, Switzerland, 1991.

Richtlinien für Flüssigkeitsstrahler (Spritzgeräte). ZH 1/406, Hauptverband der gewerblichen Berufsgenossenschaften, St. Augustin, Germany, 1987.

SSPC-SP 12/NACE No. 5: Surface Preparation and Cleaning of Metals by Waterjetting Prior to Recoating. SSPC Publ. No. 02-19, 2002.

ISO and EN Standards on Surface Preparation and Evaluation

EN ISO 2178 Non-magnetic coatings on magnetic substrates – Measurements of coating thickness – Magnetic methods, January 1995.

DIN ISO 2360 Non-conductive coatings on non-magnetic basic metals – Measurement of coating thickness – Eddy current method, January 1995.

ISO 2409 Paints and varnishes – Cross-cut test, August 1992.

ISO 8501 Preparation of steel substrates before application of paint and related products – Visual assessment of surface cleanliness.

Part 1: Rust grades and preparation grades of uncoated steel substrates and of steel substrates after removal of previous coatings, 1988.

Informative supplement to Part 1: Representative photographic examples of the change of appearance imparted to steel when blast-cleaned with different abrasives, 1998.

Part 2: Preparation grades of previously coated steel substrates after localized removal of previous coatings, 1994.

ISO 8502 Preparation of steel substrates before application of paint and related products – Test for the assessment of substrate cleanliness.

Part 1: Field tests for soluble iron corrosion products, 1991.

Part 2: Laboratory determination of chlorides on cleaned surfaces, 1999.

Part 3: Assessment of dust on steel surfaces prepared for painting (pressure-sensitive tape method), 1999.

Part 4: Guidance on the estimation of the probability of condensation prior to paint application, 1993.

Part 5: Measurement of chloride on steel surfaces prepared for painting – Ion detector tube method, in preparation.

Part 6: Extraction of soluble contaminants for analysis – The Bresle method, 1999.

Part 7: Field method for determination of oil and grease, in preparation.

Part 8: Field method for refractometric determination of moisture, in preparation.

Part 9: Field method for the conductometric determination of water-soluble salts, 1998.

Part 10: Field method for the titrimetric determination of chloride, in preparation.

ISO 8503 Preparation of steel substrates before application of paint and related products – Surface characteristics of blast-cleaned steel substrates.

Part 1: Specifications and definitions for ISO surface profile comparators for the assessment of abrasive blast-cleaned surfaces, 1988.

Part 2: Method for the grading of surface profile of abrasive blast-cleaned steel – Comparator procedure, 1988.

Part 3: Method for the calibration of ISO surface profile comparators and for the determination of surface profile – Focussing microscope procedure, 1988.

Part 4: Method for the calibration of ISO surface profile comparators and for the determination of surface profile – Stylus instrument procedure, 1988.

ISO 8504 Preparation of steel substrates before application of paints and related products – Surface preparation methods.

Part 1: General principles, 1992.

Part 2: Abrasive blast-cleaning, 1992.

Part 3: Hand- and power-tool cleaning, 1993.

EN ISO 8785 Geometric product specifications – Surface imperfections – Tests, definitions and parameters, 1999.

ISO 4624 Paints and varnishes – Pull-of test for adhesion, 2002.

ISO 4628 Paints and varnishes – Evaluation of degradation of paint coatings – Designation of intensity, quantity and size of common types of defects.

Part 1: General principles and rating schemes, 1982.
Part 2: Designation of degree of blistering, 1982.
Part 3: Designation of degree of rusting, 1982.
Part 4: Designation of degree of cracking, 1982.
Part 5: Designation of degree of flaking, 1982.
Part 6: Rating of degree of chalking by tape method, 1990.

ISO 11124 Preparation of steel substrates before application of paints and related products – Specifications for metallic blast-cleaning abrasives.

Part 1: General introduction and classification, 1993.
Part 2: Chilled-iron grit, 1993.
Part 3: High-carbon cast steel shot and grit, 1993.
Part 4: Low-carbon cast-steel shot, 1993.

ISO 11126 Preparation of steel substrates before application of paints and related products – Specifications for non-metallic blast-cleaning abrasives.

Part 1: General introduction and classification, 1993.
Part 3: Copper refinery slag, 1993.
Part 4: Coal furnace slag, 1993.
Part 5: Nickel refinery slag, 1993.
Part 6: Iron furnace slag, 1993.
Part 7: Fused aluminium oxide.
Part 8: Olivine sand, 1993.

ISO 12944 Paints and varnishes – Corrosion protection of steel structures by protective paint systems.

Part 1: General introduction, 1998.
Part 2: Classification of environments, 1998.
Part 3: Design considerations, 1998.
Part 4: Types of surface and surface preparation, 1998.
Part 5: Protective paint systems, 1998.
Part 6: Laboratory performance test methods, 1998.
Part 7: Execution and supervision of paint works, 1998.
Part 8: Development of specifications for new work and maintenance, 1998.

EN 10238 Automatically blast-cleaned and automatically prefabrication primed structural steel products, 1996.

ISO/DIS 20340 Paints and varnishes – Performance requirements for protective paint systems for offshore and related structures, 2002.

Index

Hydroblasting
& Coating of Steel Structures

Andreas Momber

Hydroblasting is a rapidly-growing technology which is finding new uses throughout industry. It is especially important in the preparation of steel surfaces during corrosion protection and control and this book provides a succinct resource for those using, or intending to use, this technique.

Covering the basic science of hydroblasting, equipment, steel surface preparation, surface quality aspects, standards and developments, **'Hydroblasting and Coating of Steel Structures'** will doubtless become the standard work in its field.

The author has extensive experience in many aspects of hydroblasting, and this book will be an important resource for engineers, contractors, consultants and research workers in the blasting and surface preparation industry and in those many branches of engineering where steel surfaces need to be protected against corrosion.

ISBN 1 85617 395 X

ISBN 1-85617-395-X

9 781856 173957 >

ELSEVIER